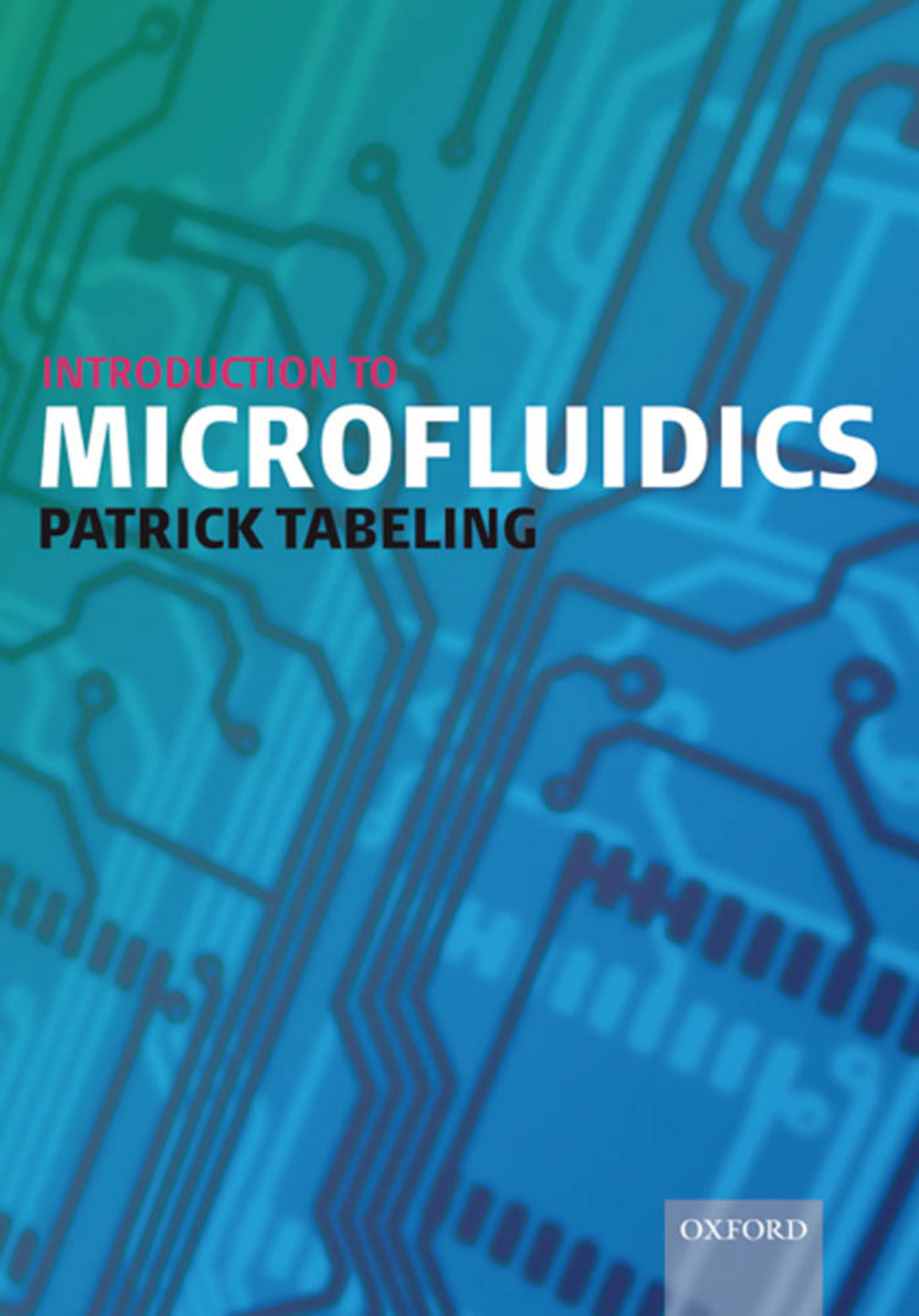
INTRODUCTION TO
MICROFLUIDICS
PATRICK TABELING
OXFORD

Introduction to Microfluidics

This page intentionally left blank

Introduction to Microfluidics

Patrick Tabeling
ESPCI, Paris

translated by

Suelin Chen
MIT, Cambridge

OXFORD
UNIVERSITY PRESS

OXFORD
UNIVERSITY PRESS
Great Clarendon Street, Oxford OX2 6DP

Oxford University Press is a department of the University of Oxford.
It furthers the University's objective of excellence in research, scholarship,
and education by publishing worldwide in

Oxford New York

Auckland Cape Town Dar es Salaam Hong Kong Karachi
Kuala Lumpur Madrid Melbourne Mexico City Nairobi
New Delhi Shanghai Taipei Toronto

With offices in

Argentina Austria Brazil Chile Czech Republic France Greece
Guatemala Hungary Italy Japan Poland Portugal Singapore
South Korea Switzerland Thailand Turkey Ukraine Vietnam

Oxford is a registered trade mark of Oxford University Press
in the UK and in certain other countries

Published in the United States
by Oxford University Press Inc., New York

First published in English 2005

British Library Cataloguing in Publication Data

Data available

Library of Congress Cataloging-in-Publication Data

Tabeling, P.
[Introduction à la microfluidique. English]
Introduction to microfluidics / Patrick Tabeling ; translated by Suelin Chen.
p. cm.
Includes bibliographical references and index.
ISBN-13: 978–0–19–856864–3 (acid-free paper)
ISBN-10: 0–19–856864–9 (acid-free paper)
1. Fluidic devices. 2. Microfluidics. 3. Microelectromechanical systems. I. Title.
TJ853.T33 2005
629.8′042—dc22

2005019679

Typeset by Newgen Imaging Systems (P) Ltd., Chennai, India

Printed in Great Britain
on acid-free paper by
Ashford Colour Press, UK

ISBN 0–19–856864–9 978–0–19–856864–3

10 9 8 7 6 5 4 3 2 1

Contents

This page intentionally left blank

Acknowledgements

This book was created from course notes written during the period 2001–2003 for DEA students in Mechanics at Jussieu, DESS students in 'Separated Environments' at Paris VI, and students at the École Polytechnique. I would like to thank all those who took the time to make remarks on all the different versions: C. Baroud, E. Brunet (brave readers of the first version), G. Degré, R. Dreyfus, J. Goulpeau, P. Joseph, L. Ménétrier, F. Okkels and H. Willaime. My thanks also go to C. Jullien for her multiple critiques, J. Bico who explained to me the subtleties of certain capillary phenomena, and A. Dodge who helped me considerably in balancing the references. I also thank A. Ajdari for his clarifying discussions on electrokinetic phenomena. I was impressed by the readings of the Belin editing team, who facilitated the elimination of a large number of mistakes. I added a chapter in the English version, dealing with thermal phenomena. I am indebted to D. Gobin for invaluable remarks on the chapter, and G. Hetsroni for his reading of this part. I was very fortunate to have Suelin Chen translating the French version. She made a number of sharp remarks that improved the presentations of the subjects. Thanks to H. Stone who pointed out interesting references I added in the English version. I am also grateful to Mado Seiffert who inspired an elegant cover and to J. Sellier for a couple of ultimate remarks. Finally, my thanks go to Pr. B. Bussel and to Dr. J.-B. Thibaut for their expert explanations on intrathecal pumps, who one day may have the fortune of being miniaturized.

Strange things at the microscale.

This page intentionally left blank

Introduction

In recent years, considerable progress has been made in the field of miniaturization. It is now effectively possible to miniaturize all kinds of systems—e.g. mechanical, fluidic, electromechanical, or thermal—down to submicrometric sizes. In the 1980s, these achievements gave rise to a new field known as MEMS (*microelectro-mechanical systems*). Later, in the 1990s, this domain became considerably diversified, with MEMS devices being fabricated for chemical, biological, and biomedical applications. These systems were employing fluid flows operating under unusual and unexplored conditions, which naturally led to the need for the creation of a new discipline—microfluidics[1]—which constitutes the central subject of this book. Microfluidics can be defined as the study of flows that are simple or complex, mono- or multiphasic, which are circulating in artificial microsystems, i.e. systems that are fabricated using new technologies[2]. This description is an engineering definition that is generally accepted and understood, so we will adopt it here.

MEMS and microfluidics

Miniaturization and MEMS gave birth to microfluidics in the 1990s and today still constitute a large portion of this young discipline. MEMS are electromechanical systems whose total size varies between 1 and 300 micrometers. Alhough these numbers are rough limits (there are actually MEMS of submicrometer size and MEMS larger than 300 micrometers), the majority of MEMS devices fabricated today have typical dimensions of this order. A famous example of a MEMS is shown in Fig. 1. This MEMS is a microgear whose size is on the order of a hundred micrometers. It is held by an actual ant who seems to be questioning the usefulness of such an object. This photo, taken by a German research group, is rather striking because it represents the intrusion of a man-made machine into the micrometric world. The entry into micrometric scales is clearly not a new feat, however. Since the invention of the optical microscope

[1] Microfluidics already existed in the 1960s, but its use was limited to developing the analogous systems of microelectronic circuits, with the electron flux being the analog to the fluid flux.

[2] The new technologies that we consider here involve several techniques, including photolithography, etching, deposition, microwetting, and microimpression, which permit the fabrication of miniaturized systems. These technologies are considered 'new' because they only first appeared in the 1970s.

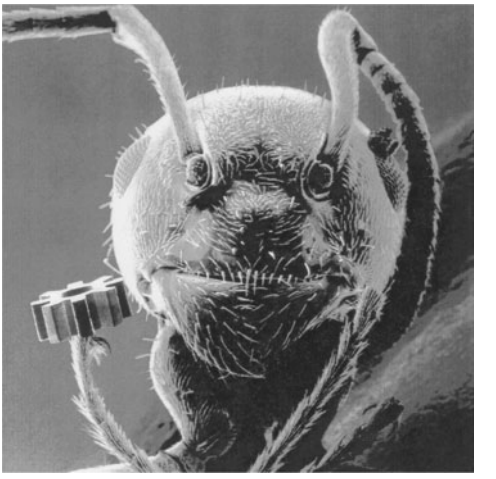

Figure 1 Ant holding a nickel micro-gear, made by LIGA technology (German for 'lithographie, galvanoformung, abformung'). This ant was metallized and placed in a vacuum in order to be photographed by electron microscopy. This image was provided by the Karlsruhe group (Germany).

in the sixteenth century, the micrometric world has been scrutinized in detail. The microscope permitted many scientific discoveries to be made, including the discoveries of protazoa, Brownian motion, and chromosomes, to cite just a few examples. However, it is far more difficult to actually *act* at a micrometric scale, which is precisely what MEMS technology allows us to do; it is thus not a far stretch to imagine that MEMS technology will lead to many technical and scientific discoveries. At the time this text was written, MEMS had essentially been created to make observations and measurements that were difficult to make using traditional methods. Some examples include the proof of the quantum nature of phonons [2], the measurement of fluid-phase chemical kinetics [3], and the characterization of the slip phenomenon in gases [4]. These are all discoveries and technical inventions that had been made possible by MEMS. In certain cases, these advances became large industrial successes such as the usage of MEMS in airbag activation (Fig. 2).

MEMS for airbags, which first appeared in the 1980s, consist of an integrated system on a silicon wafer that is just a few millimeters long, and yet are able to incorporate both electronic components and an electromechanical device capable of detecting physical impact. The detection portion is only a few hundred micrometers large and constitutes the heart of the chip. It is made of two combs, one fixed and the other mobile; the capacitance of these combs varies under the effect of an impact. As we will see in Chapter 1, the miniaturization of the capacitor element allows the creation of a highly sensitive and rapid detector. However, the industrial success of MEMS is not solely due to the improvement

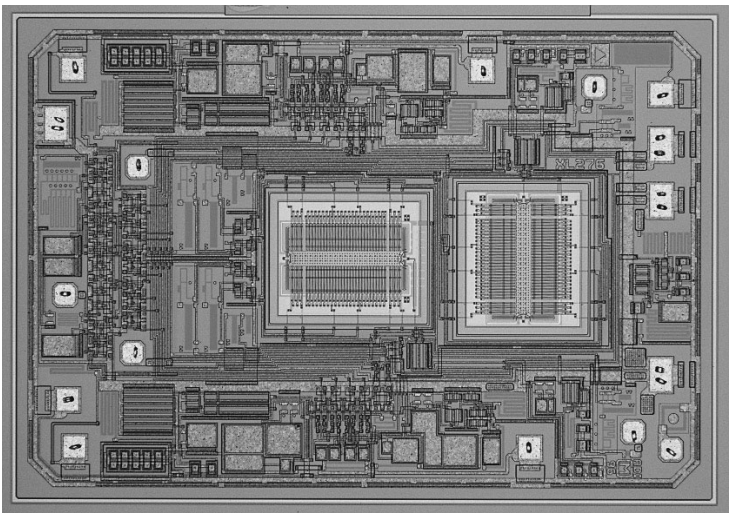

Figure 2 Device for the detection and command of airbag activation, based on MEMS technology. (Courtesy of Analog Devices, Inc. All rights reserved)

in sensor response and sensitivity, but also due to the ability to *integrate* detection, information analysis, and signal processing all on one single chip. Just as with integrated circuits, this chip can, in principle, be easily reproduced by the millions. The cost, which is so critical in the field of automobile manufacturing, becomes very advantageous as compared to traditional systems. For this reason, all modern automobiles now use MEMS for their airbags, and tens of millions of these devices are produced each year.

A second major industrial success came in the 1990s with the advent of MEMS usage for inkjet printer heads (Fig. 3).

The printer head consists of a portion microfabricated from silicon that serves as an ink reservoir, a heating element to put the fluid in motion, and a nozzle. The fluid is pushed through the nozzle due to the formation of a bubble near the heating element; this bubble is generated by the vaporization of the ink. The bubble propels the fluid towards the exterior, forming a jet that destabilizes under the action of capillary forces. Droplets created in this way have a size similar to that of the nozzle diameter, which is generally on the order of 50 μm. These droplets strike the paper, forming the basic spot. Smaller satellite droplets also exist, and form a sort of procession accompanying the principal drop (Fig. 3 right).

Today, the volume of MEMS activity is estimated to be worth between several billion and several tens of billions of dollars[3]. In the United States, there was on

[3] Due to the fluctuations of worldwide activity.

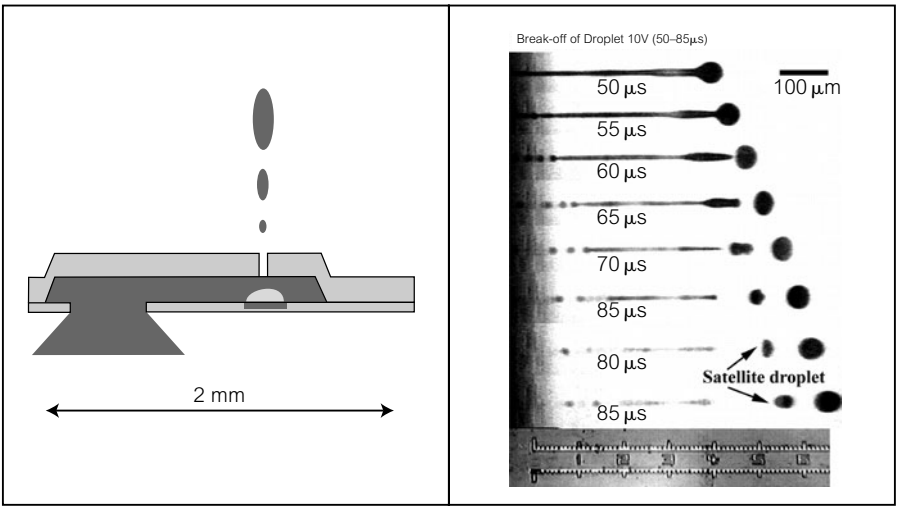

Figure 3 Figure showing a printer head of a commercial inkjet made using MEMS technology (left) and the visualization of droplets of ink projected onto a target (right). Satellite droplets, which affect the printing precision, are discernable [5].

average 1.6 MEMS per person in 2000, and this number is estimated at 4 MEMS per person now. Today, there are numerous industries involved in MEMS, as shown in Table 1, supplied by DARPA (defense)[6].

Note from the table that there are both new industries (ones that have appeared in just the last few years) as well as more traditional industries who use MEMS in a significant way in their sector of activity, or who profit from developing novel ventures by taking advantage of the potential of this young technology.

The history of the field of MEMS is an interesting one. The year 1959 is often considered to be the beginning of the history of micro- and nanotechnologies. In December of that year a visionary speech was given by Richard P. Feynman during the APS (American Physical Society) meeting at Caltech. This speech was entitled *There is plenty of room at the bottom.* The beginning of the speech went as follows:

I would like to describe a field, in which little has been done, but in which an enormous amount can be done in principle. This field is not quite the same as the others in that it will not tell us much of fundamental physics (in the sense of, "What are the strange particles?") but it is more like solid-state physics in the sense that it might tell us much of great interest about the strange phenomena that occur in complex situations. Furthermore, a point that is most important is that it would have an enormous number of technical applications.

Table 1 Companies involved in MEMS technology in the United States (table created by DARPA)

Technological field	Typical devices/ Applications	Companies	Market 2003 ($ Millions)
Inertial measurement	accelerometers, rate sensors, vibration detectors	TI,Sarcos, Boeing, ADI, EG& GIC, Sensors, AMMI, Motorola, Delco, Breed, Systron Donner, Honeywell, Allied Signals	700–1400
Microfluidics and chemical testing/processing	gene chip, lab on chip, chemical sensors, flow controllers, micronozzles, microvalves	Battelle, Samoff, Microcosm, ISSYS, Berkeley MicroInstruments, Redwood, TiN Alloy, Affymetrix, EG& GIC Sensors, Motorola, Hewlett Packard, tI, Xerox, Canon, Epson Caliper, Agilent	3000–4450
Optical MEMS (MOEMS)	displays, optical switches, adaptive optics	Tanner, SDL, GE, Samoff, Northrop-Grumman, Westinghouse, Interscience, SRI, CoraTek, Lucent, Iridigm, Silicon Light Macines, tI, optical MEMS, Honeywell	450–950
Pressure measurement	pressure sensors for automotive, medical, and industrial applications	Goodyear, Delco, Motorola, Ford, EG& GIC, Sensors, Lucas NovaSensor, Siemens, TI	1100–2150
RF technology	RF switches, filters, capacitors, inductors, antennas, phase shifters, scanned apertures	Rockwell, Hughes, ADI, Raytheon, TI, Aether	40–120
Other	actuators, microrelays, humidity sensors, data storage, strain sensors, microsatellite components	Boeing, Exponent, HP, Sarcos, Xerox, Aerospace, SRI, Hughes, AMMI, Lucas Novasensor, Sarnoff, ADI, EG& GIC Sensors, CP Clare, Sielmens, ISSYS, Honeywell, Northrop Grumman, IBM, Kionix, TRW	1230–2470

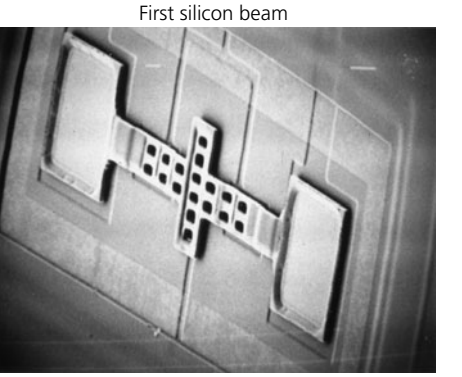

Figure 4 The first results of MEMS technology: a beam and a spiral spring. (Courtesy of Professor Richard S. Muller, Berkeley Sensor & Actuator Center, University of California, Berkeley.)

Feynman saw no physical reason why the 50 volumes of *Encyclopedia Britannica* could not be inscribed on the head of a needle. One letter would only need to consist of less than a dozen or so molecules. Confronted with the difficulty of working at micrometric scales, he suggests that we should 'train ants how to teach mites' how to construct miniaturized machines!

> How many times when you are working on something frustratingly tiny like your wife's wrist watch, have you said to yourself, 'If I could only train an ant to do this!' What I would like to suggest is the possibility of training an ant to train a mite to do this. What are the possibilities of small but movable machines? They may or may not be useful, but they surely would be fun to make.

These suggestions or predictions did not remain just as part of a fantasy world, since a few decades later, in 1995, the word 'IBM' was spelled out using only a few atoms.

The first MEMS devices were created a decade after Feynman's speech. A few examples are listed here, without an attempt to establish a rigorous chronology. The first microbeam was created in 1982, and the first microspring in 1988 (Fig. 4).

The first micromotor was created in 1989 (Fig. 5)[4]. It consists of an electrostatic motor, where the rotating electric field is generated by electrodes that have been evaporated onto a platform of polysilicon. One major difficulty in its fabrication was that of the reduction of stiction (i.e. the combined phenomena of adhesion and friction) of the rotor towards the substrate. Stiction is exacerbated by the effect of miniaturization and tends to impede the rotation of the rotor. The solution to this problem consists of reducing the surface area of the

[4] We will see in Chapter 1 that this micromotor can comprise the base element of a microturbine that converts chemical energy to electrical energy. It is also interesting to note that microgears, fabricated using MEMS technology, are often used today in clock making.

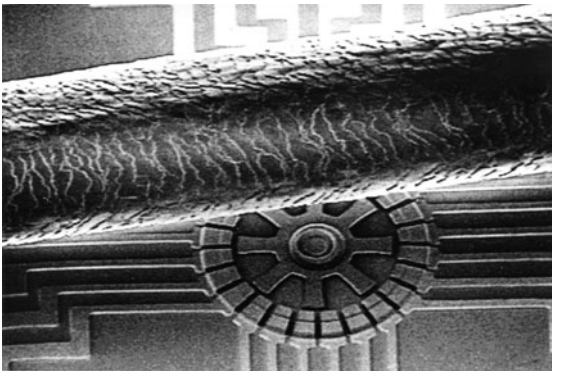

Figure 5 The first micromotor, made at UC Berkeley by Tai and Muller in 1989. This motor has been placed next to a human hair whose diameter is on the order of 200 μm. (Courtesy of Professor Richard S. Muller, Berkeley Sensor & Actuator Center, University of California, Berkeley.)

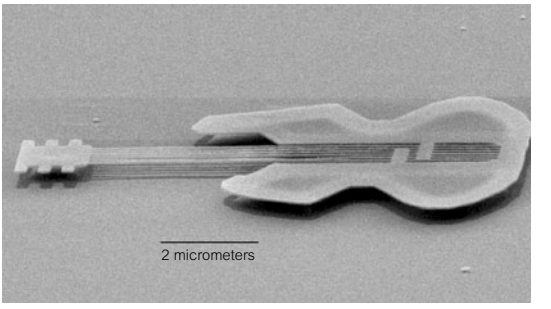

Figure 6 A microguitar with nanostrings 30 nm in diameter, made at Cornell by the group of H.G. Craighead. If this guitar could be played, it would produce a sound in the domain of MHz, which would require a particularly sharp ear to hear.

rotor/substrate contact, which obviously makes microfabrication of this machine more difficult.

Other examples of MEMS are presented below. A microgear, a pair of microtweezers, a micro-electrovibrator, a system of inclinable mirrors that permit communication between the ground and an airborne microengine [8], and an astonishing microguitar possessing nanostrings that vibrate at a frequency of MHz, Fig. 6. Not all of these objects are necessarily practical, but they allow for exploration into a field of miniaturization where new concepts can be developed. The invention of new microsystems has been the center of activities of laboratories involved in MEMS in the 1990s. Today, a sort of maturation in the domain of MEMS prevails, resulting in less time being spent on creating new systems and more time being spent on investigating concrete applications.

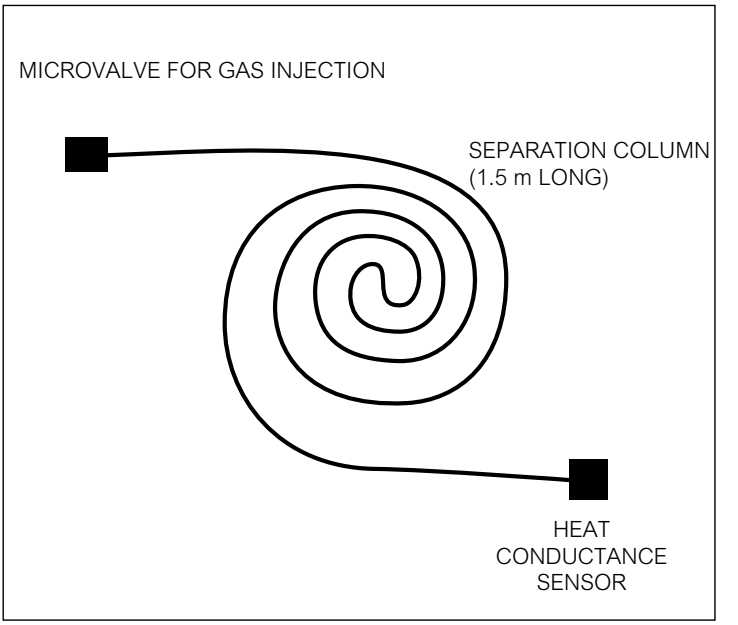

Figure 7 Diagram of miniaturized gas chromatography, created by Terray in 1975 [9].

The birth of microfluidics

We now concentrate on microfluidics. In the period when silicon-based MEMS began to take off, there were no technical obstacles in making simple microfluidic systems [11]. Thus, the first miniaturized gas chromatography system was created around 1975 [9,10].

This remarkable device circulated gas through microcanals etched in silicon. The system consisted of miniaturized electromagnetic injection as well as miniaturized thermal detection, all contained on a single chip just a few centimeters wide. This achievement was an isolated one, most likely because the separation-science community was not ready to develop silicon technologies for its own needs [12]. It was only after 1991 that the advantages of miniaturization were thrust into the spotlight, particularly for its application to chromatography [13], and then all sorts of microfluidic systems began to be fabricated. Appearing approximately chronologically were electrophoretic separation systems, [14–16], electro-osmotic pumping systems [17], diffusive separation systems [18], micromixers [19–22], DNA amplifiers [23–28], cytometers [29–31], and chemical microreactors [32, 33], to cite just a few examples.

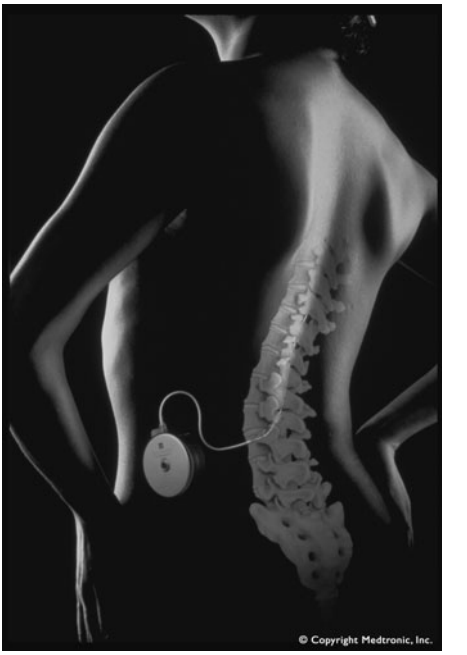

Figure 8 Patients that have spinal cord lesions can now be healed effectively thanks to the injection of a product into the cereberospinal fluid. The efficacy of this mode of injection is far greater than by oral means. The company Medtronic has commercialized these injection pumps, which are generally implanted below the abdomen and connected to the zone to be treated using a 500 μm diameter catheter, which the neurosurgeon must manipulate with great dexterity. There are also implanted pumps for the injection of insulin into the liver for the treatment of diabetes.

During the same period of time, microfluidics was being used to tackle fundamental physical questions. For example, the first experiments involving the stretching of DNA, carried out by Chu *et al.* [34] in 1993, used a microfluidic system to control the viscous stretching force applied to the molecule; for the first time, it was possible to conduct a detailed study of the different configurations of the stretched molecule. This experiment founded a new domain of fundamental research: the study of the single molecule.

One of the amazing creations of microfluidics includes micropumps (Fig. 9). Many tricky problems arise when constructing a mechanical micropump: for example, miniaturized valves have a tendency to stick irreversibly to the substrate, making it necessary to minimize the contact surface area (as was necessary for the miniaturized motor). The micropump of the company Debiotech, schematically represented in Fig. 9, overcame this problem elegantly. This pump is destined for implantation in patients needing continuous injection of a product. Currently, insulin injection pumps in the liver and Bactofen pumps in the spinal cord are not easy to implant, particularly in children. As compared with traditional technologies, this micropump reduces its scale by an order of magnitude (Fig. 8), an important improvement from the surgeon's point of view as well as a significant gain in comfort for the patient.

The first microfluidic product commercialized on a large scale was the inkjet printer head described above (Fig. 10). Today, tens of millions of inkjet

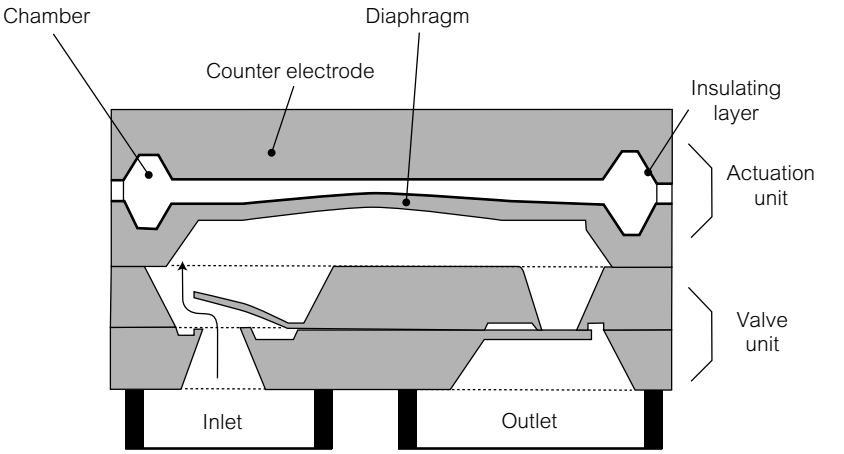

Figure 9 The future is moving towards the miniaturization of intrathecal pumps. The miniaturized pump is just a few millimeters in size, which corresponds to an improvement of two orders of magnitude over current intrathecal pumps.

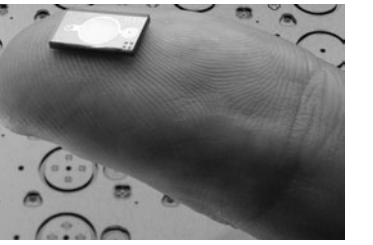

Figure 10 The Debiotech micropump can be held on the fingertip like a postage stamp.

printers use MEMS and billions of documents are written and read thanks to microfluidics. By parallelizing ejection heads, droplet dispensers can also be constructed. In this case, the destination of these droplets is not sheets of paper, but plates containing wells used for chemical or biological analyses.

Droplet dispensers at this time constitute a substantial part of commercial activity in the field of microfluidics [7]. Currently, chips are produced by the millions for chemistry and biology. These chips allow massive numbers of tests to be run in parallel, allowing large amounts of data to be delivered that aid in the precise characterization of a product. Today, this kind of technology is crucial in the search for new types of medical treatments. Microfluidic systems do not normally use moving parts (the micropump of the company Debiotech represents a rare counterexample) and this constitutes a significant simplification with respect to non-microfluidic MEMS. Consequently, it has become possible in microfluidic systems to turn to simpler technologies, ones that are faster and less expensive than silicon technology. We are generally referring to 'soft' technology, based on elastomers such as PDMS (polydimethylsiloxane) or on plastic materials, which comprise a large portion of the field today. We will return to these subjects

in Chapter 6. Due to the absence of moving parts and the relative ease and accessibility of many of these technologies, it has become possible to integrate several elements on the same chip and to create lab-on-a-chip devices. The idea of constructing microfactories from MEMS often came up in the 1980s, but the difficulties involved in actually fabricating working devices using silicon technology made this dream unattainable. For microfluidic MEMS and related technologies that have no moving parts, the integration of different components has since opened up a wide range of possibilities.

Microfluidics and lab-on-a-chip devices

The rapid expansion of the field of microfluidics seems to be driven in part by the possibility of integration. The ultimate goal is to be able to detect biological molecules, and transport, mix and characterize a raw sample, all with one device. In traditional genomic analyses, it was necessary to purify and amplify a DNA fragment prior to analysis. This pre-treatment required complex labor and highlights the advantage of being able to integrate all these procedures on one chip to make it possible to directly analyse a raw sample, such as a drop of blood or a piece of gruyere cheese. Achieving this would require miniaturizing systems such as cytometers, separators, and bioreactors, and then connecting them together. The domain of integrated analysis systems has been designated as μTAS (*micro-total analysis systems*) [35], or also 'lab-on-a-chip' systems. The two terms are essentially synonymous. Lab-on-a-chip devices or μTAS delineate an abundant field that includes analysers of air and water quality, diagnostics of illnesses, and devices that replace the many functions of the nose, the tongue, etc. The economic possibilities of this field have been estimated at tens of billions of dollars per year.

Today, these possibilities have ceased to become just a dream. Already, in 1994, a group of researchers succeeded in fabricating a chip integrating three different functions: the mixing of reactants, enzymatic reaction, and separation [36]. Four years later, one single device capable of titrating aqueous solutes and then performing the mixing, amplification, enzymatic digestion, electrophoretic separation, and detection was published in the journal *Science* [37]. During the last few years researchers have come up with all sorts of solutions to improve and simplify the manipulation of fluids on-chip. There is still an enormous amount of progress to be made in this domain, which is precisely one of the tasks allocated to microfluidics.

In the meantime, lab-on-a-chip devices accomplishing a small number of functions have already been commercialized. For example, the company Biosite

Figure 11 Biosite chip. A droplet of blood is placed in an opening on the chip. This drop is pulled towards the microfilter and the microseparator (in the direction of the arrow) by capillarity. The results of the analysis are given after data is analysed on a microcomputer. In just 15 min, this diagnostic can determine whether or not a heart attack has taken place.

Figure 12 This chip, commercialized by Agilent Technologies, is a few centimeters long, and permits the identification of specific genetic sequences in a 1-μl sample of roughly purified DNA. This process takes place in just 10 min.

has commercialized systems that can take a drop of blood from a patient and transport it by capillary force across a filter, analyse the blood in a functionalized microcanal, and then diagnose whether or not the patient had suffered a heart attack. The principle of the test is founded on the detection of three myocardial proteins that are produced in abnormal quantities once a heart attack has taken place. This system is shown in Figs. 11 and 12.

This system is not completely integrated because a computer is required to analyse data produced by the chip, although the data-acquisition system itself is portable. In this case, the interest of miniaturization is not just to allow for portability, but also the rapidity of achieving results[5]. For the Biosite chip, a

[5] Note that in this case, the reduction of diagnostic time is not only related to the physical phenomena in play. It is also due to the reduction of necessary human involvement, since physico-chemical processes are almost completely integrated.

Figure 13 Agilent 2100 Bioanalyzer. The Agilent chip in the preceding figure is small in size, but it still requires a non-miniaturized computer environment to analyse the acquired data.

diagnosis is given in 15 min, while traditional systems need several hours. Not knowing the true nature of a patient's condition, doctors needing to make quick decisions sometimes end up treating non-existent cardiac problems. Furthermore, patients can be unnecessarily alarmed by a false diagnosis, believing they have a fatal condition when in fact the problem may be much less serious.

It is worthwhile to mention other commercialized systems that are precursors of the lab-on-a-chip systems of the future. Figure 12 represents a remarkable miniaturized system commercialized by Agilent. Among other functions, this system can perform genotyping, i.e. the identification of an object (a virus for example) from characteristic sequences of genes. It is not necessary to sequence the whole genome of a strand of DNA, but just to identify fragments. The chip is made of a network of gel-filled microcanals, and uses a powerful separation technique known as CEC (*capillary electro-chromatography*). This chip can also idenfity RNA and proteins.

Just as for the Biosite system, integration is not complete; the device must be used in tandem with a system for data analysis, as shown in Fig. 13[6].

Microfluidics and chemical engineering

Another problem in microfluidics is that of miniaturization of processes for chemical engineering. We will see in Chapter 1 that miniaturization favors heat

[6] This fact can sometimes lead to a discussion of whether it is more appropriate to call these systems 'chip-in-a-laboratory' instead of 'laboratory-on-a-chip.' Clearly, there remains much progress to be made for the complete miniaturization of a chain of analysis.

Figure 14 Can a refinery be miniaturized? The problem of production volume would require massive parallelization of lab-on-a-chip systems for chemical engineering (© J. Walker/S.P.L./Cosmos).

exchange, and allows the control of strongly endo- or exothermic reactions that can be difficult to manage in traditional chemical engineering systems. By improving control, selectivity is also improved (by avoiding the formation of unwanted chemical species). Emerging from all this came the idea of the miniaturization of chemical factories, as shown in Fig. 14.

It is not clear whether it is possible to miniaturize the factory shown in Fig. 14. The obvious problem that arises is whether there would be sufficient production volume[7]: can enough volume be produced using a miniaturized system? Is it possible to displace a mountain with a small spoon? One possible idea would be to multiply the system using massive parallelism, an approach known as *numbering up*. It is undoubtedly necessary to rethink modes of production in this domain so that it can best profit from the advantages of miniaturization, especially to break down units of production or install them near the users. The latter would present many advantages, such as the reduction of transport and the reduction of chemical-contamination risks. The appeal of microsystems for chemical engineering has been perceived at least since 1996, as cited by several references [38, 39]. Today, microsystems are seen as an important source of innovation; international conferences organized on this subject, such as the IMRET series, have seen a strong vitality in research activity on the theme of miniaturization. A recent review of these subjects is given in [40].

[7] A related issue in the domains of biology and analytical chemistry is how to obtain a large amount of data by parallelizing many miniaturized analysis units. These systems are called *high-throughput* devices.

Astonishing microfluidic systems in nature

The framework in which we have placed ourselves—that of 'systems made by man'—is obviously restrictive. Nature produces astonishing micrometric and nanometric systems that have impressive characteristics, and these include the controlled circulation of fluids. We mention the tree as an example, where a hydrodynamic problem involving these types of scales appears: how can a tree bring water and nutrients to the leaves? Nature found an amazing solution using a complex network of capillaries (Fig. 15).

Tens of thousands of leaves are nourished by a capillary network containing hundreds of thousands of microcanals of diameters between a hundred micrometers (in the trunk) and several tens of nanometers (in the leaf). Despite the complexity of the network, the supply of sap is homogeneous[8]. To understand the hydrodynamics of this system, it is necessary to consider the *deformability* of the canals (the ability of the capillaries to deform under the effect

Figure 15 This tree possesses a complex network of capillaries that allows it to supply water homogeneously to the tens of thousands of leaves that it carries on its branches. This system also involves flows in micro- and submicrometric-sized canals (© Packwood/OSF/Bios).

[8] It is interesting to note that the pressure drops that develop in the network are significant (several tens of bars); implying that the sap is subjected to negative pressures.

Figure 16 One of the silk glands of a *nephila clavipes* (photo graciously provided by J. Bico, M.I.T.).

of pressure), the considerable significance of capillary effects (which originate from the drainage of fluid), and the role of redundancy (if one capillary dies, another takes its place). A second example of how nature extraordinarily handles complex micrometric flows appears in the spider web. To spin its sticky trap, the spider produces a long silken thread a few dozen micrometers in diameter, and despite its slenderness this thread has exceptional mechanical properties. The silken thread is the result of a protein that is synthesized in a gland mixed with a solution. This system is shown for the spider *nephila clavipes* in Fig. 16.

We will describe in Chapter 3 microfluidic reactors where chemical reactions take place under well-controlled conditions. However, these man-made systems are still far from being able to compete with this animal.

It would be easy to continue listing examples of microfluidic systems from nature. However, despite the many interesting characteristics of these systems, this text will be limited to mono- and polyphasic fluid flows, and the associated transport phenomena, of microsystems *made by man*. This 'engineering' definition is simplified but generally accepted.

Different aspects of microfluidics

There are several different aspects of the field of microfluidics. The first major set of questions involve issues of microplumbing, i.e. how to circulate fluids in microsystems. It is necessary to resolve problems of fluid outlets, valves, and tubes, which, in macrometric systems, are taken care of by a plumber. These

issues most notably involve:

• **Fluidic interconnects.** These accomplish the coupling between two microfluidic systems, or between a microfluidic system and the exterior world. It is desirable that the linkage is made in a simple, standardized way, without leaks, similar to how two electronic circuits are connected. Multiple fluidic interconnect systems have been conceived in research laboratories, but they are rarely useful industrially. It would be useful to have a simple and universal interconnect available, but such an interconnect does not yet exist. This difficulty presents an obstacle to integration;

• **Pumps and valves.** Control elements such as valves and pumps, when made using silicon technology, are complicated to fabricate and then difficult to integrate onto lab-on-a-chip systems. However, the use of 'soft' technologies based on elastomers offer elegant possibilites for valves and pumps that we will describe in more detail in Chapter 6. The question of the choice of material and how this choice relates to the possibilites of microfabricating control elements is still an open problem today in the field of microfluidics;

• **Fluid injection.** The injection of fluids is a practical difficulty that does not always have a simple solution, especially when the sample is very small and is not amplifiable (for example, proteins extracted from a single cell). The sample can be diluted in a large volume so that it can be manipulated more easily, but this creates a series of difficulties, including the need for sensitive instrumentation. The injection of minute quantities of fluid remains an open problem in the management of fluid volumes.

These microplumbing problems are subtle, and are systematically examined during microfluidic conferences, but they are not all that make up microfluidics! There are also situations involving physical or physico-chemical phenomena in unusual contexts that cannot be attributed to microplumbing problems; for example, the situation of gas flowing in microcanals, where ordinary hydrodynamic boundary conditions no longer apply. Also, the intensification of the coupling between the flow and the electric field at the micrometric scale gives rise to novel methods for the movement of fluids that are impossible to apply in the macrometric world. In addition to this, there exists the possibility of using microfluidics to manipulate rapid chemical kinetics, an achievement that is generally outside the range of ordinary systems. Another aspect of microfluidics involves the idea of building complex integrated systems whose functioning is qualitatively different from those based on more modest integration. This text will use several examples to show that microfluidics goes far beyond difficulties related just to microplumbing.

Possibilities offered by nanofluidics

To manipulate objects of nanometric size in solutions, one may think of eventually developing 'nanofluidics', i.e. the field involving the study of flows in nanometer-sized systems. This topic currently includes the activity of several research groups interested in the flow of fluids in submicrometric-sized canals [41–42], the implementation of nanojets [21, 43], and the confinement of objects of a submicrometric scale. Nanofluidics can undoubtedly contribute to the field of physics of the single molecule, as well as to mesoscopic physics (i.e. studies involving scales intermediate between micro- and macroscopic). To illustrate this aspect of nanofluidics, it is worthwile to look at a few suggestions offered by Fujita [44] that are pertinent to this field:

– confining molecules produced by a cell or an enzyme in a nanometric space for detection purposes,
– following the rapid kinetics of chemical reactions,
– characterizing the activity of individual molecules,
– intensifying and analysing the role of surfaces in a catalytic reaction,
– applying local or intense electric or magnetic fields that can control chemical reactions,
– manipulating molecules directly and physically,
– labelling molecules and following their conformational changes during a chemical reaction,
– constructing hybrid systems by assembling biomolecules in NEMS (*nano-electromechanical systems*).

At this time, the domain of nanofluidics is still largely unexplored; it is acceptable to think that a growing effort will develop in the future on this subject.

Specialized publications

Microfluidics is a young science, and as a consequence of this (at the time of the writing of this book), there are not a large number of works and reviews written on the subject. We mention that the first text on microfluidics can be considered to be '*Microflows*' [4], which appeared in 2002. This book most notably dealt with the phenomena of slip, the modelling of flows, and electrokinetics. A more

recent book is 'Fundamental and Application of Microfluidics', by N.T. Nguyen and S. Wereley [46], which uncovers a broader part of the subject. There are also collections of papers, edited as books: 'Lab on a Chip', edited by E. Oosterbroek and A. Van den Berg [45], Microfluidique, edited by S. Colin [47], and the MEMS Handbook by G. el Had *et al.* [48]. In addition, a journal on this topic, entitled 'Micro and NanoFluidics', appeared in 2003. Reviews on the research carried out in the field of microfluidics also exist: we cite Ho and Tai [49] on control[9], Gad el Hak [50] on the control of rarefied gases, Giordano and Cheng [41], Tabeling [51], Stone and Kim [52] on physical aspects, Beebe *et al.* [53] on the physics and biomedical applications, Sanders and Verpoorte [54, 55] on biochemical analysis, Lichtenberg *et al.* [56] on sample pre-treatment, the review prepared by the group of A. Manz [12, 57] on μTAS, and a recent review by Ajdari *et al.* [58] on the hydrodynamic aspects of microfluidics. In general, research articles in microfluidics are dispersed in journals such as *Analytical Chemistry*, *Physical Review Letters*, *Physics of Fluids*, *Sensors and Actuators*, *Journal of Chromatography*, *Electrophoresis*, *Nature*, *Science*, *Applied Physics Letters* and *Lab on a Chip*; the *Proceedings* of conferences such as μTAS, and, to a lesser extent, *MEMS* and *Transducers* are also an important source of information on the research efforts in the field. Courses on microfluidics are currently dispersed in notes that can sometimes be found on the Internet. We also refer to microfludic courses proposed during international conferences, or organized on a regular basis [59].

Organization of the text

This text consists of seven chapters.

– In the first chapter, entitled 'The physics of miniaturization', consequences of the miniaturization of the 'ordinary' world are described from a physical point of view. Miniaturization often leads to the disturbance of force equilibria: volumetric forces such as gravity cease to prevail in the micrometric world. Instead, this world tends to be dominated by surface forces like capillarity. This fact leads to situations that are sometimes surprising, and go

[9] The problem of flow control involves finding activation methods that allow the influence of a flow to limit or heighten unstable modes, reduce or augment turbulence, etc. In this context, MEMS are particularly useful, because they allow one to act at the center of a flow from where vortices originate. For example, the group of C.M. Ho showed that it is possible to maneuver a Delta airplane without a mobile centerboard, instead controlling it by activating hundreds of MEMS. These MEMS are placed in a line along the edge of the wings; these microsystems act on the formation of spiral vortices, which play an important role in the lift force developed by the wing [49].

against physical intuition. The consequences of these surface forces are often cleverly exploited by nature, for example by small insects. Miniaturization also gives more importance to phenomena that are negligible in the macrometric world[10]: one example is the mean free path of gases, often neglected in ordinary hydrodynamics, but which must be explicitly taken into account in microfluidic flows.

– The second chapter tackles microfluidics itself, and low Reynolds number flows (the regime defining microhydrodynamics) are presented. The effects of solid/liquid and solid/gas slip are also discussed. Then, capillary phenomena in the microfluidics of droplets and bubbles are detailed. Also, the role of surfactants in miniaturized systems, including the production of emulsions, is studied.
– In the third chapter the phenomena of diffusion, dispersion, mixing, adsorption, and separation are described. Taking the importance of chromatographic questions in microfluidics into account, this text proposes an introduction to separation techniques with several examples of miniaturized separation systems. Other basic notions on chemical kinetics in the context of microsystems are also given.
– The fourth chapter describes the electrohydrodynamics of microsystems; electrophoresis and electro-osmosis, two extremely important phenomena for understanding lab-on-a-chip devices, are discussed in detail. Dielectrophoretic effects allowing the micromanipulation of neutral particles are also presented.
– The fifth chapter is dedicated to heat exchanges in microfluidic systems: after a discussion of the limits of macroscopic approach, the equations governing velocity and heat fluxes are introduced, and some basic solutions relevant to microfluidics are derived. The results obtained in this part are applied to the particular problem of temperature control in the next generation of microprocessors.
– In the sixth chapter, microfabrication methods are introduced. Today, it is difficult to tell which technologies will dominate in the coming years. Currently, microfabrication technologies include a diversity of technological approaches. In this spirit, silicon technology is described in this chapter; a substantial portion of the chapter is also dedicated to soft technologies based on elastomers and also plastic MEMS, accounting for their ever-growing importance.

[10] The term macrometric will often be used in this book. The term designates the range of scales above the dimensions of MEMS.

– Finally, the seventh chapter gives a few examples of the products and devices of microfluidics, interconnects, valves, and pumps.

Perspectives on microfluidics

Today, we expect a lot from microfluidics: we hope that the complete control of the flows at micrometric scales will allow the construction of highly complex microsystems, where fluids can circulate in a controlled manner, performing a large number of tasks in a maze of microcanals[11]. This is the dream of integrated systems of the future, whose capabilities are difficult to imagine, just as fifty years ago it was difficult to imagine the level of performance of computers today. Living systems provide a sort of perspective on the level of complexity that could be attained in artificial systems. We tend to consider today that the path leading to such complexity is partly obstructed by problems of flow control; the definitive solutions to these problems could very well be provided by microfluidics. The field of microfluidics is abundant; all sorts of solutions, elegant or crude, fragile or robust, simple or sophisticated, are brought to the problem of fluid management in microsystems. This book does not intend to be exhaustive, as the number of microfluidic achievements are in the thousands. Thus, the title of the book *Introduction to Microfluidics* is appropriate. We hope that while reading, the reader will acquire a frame of reference as well as pertinent knowledge that will enable the reader to tackle a large number of situations involving fluid flows through miniaturized systems, which in essence defines the field of microfluidics.

References

[1] Forschungszentrum Karlsruhe GmbH Technik und Umwelt, Projekt Mikrosystemtechnik (PMT).

[2] K. Schwab, J. Arlett, J. Worlock, M. Roukes, *Physica* **E9**, 60 (2001); K. Schwabe, E. Henriksen, J. Worlock, M. Roukes, *Lett. Nature*, **404**, 974 (2000).

[3] A. Pabit, S. Hagen, *Biophys. Journal*, **83**, 2872 (2002).

[4] G. Karniadakis, A. Beskok, *Micro Flows*, Springer Verlag 2002.

[5] F. Tseng, C.-J. Kim, C.-M. Ho, *ASME Int. Mechanical Engineering Congress and Exposition*, Anaheim, November 1988, pp. 89–95.

[11] Microfluidics was declared in 2001 to be one of ten technologies capable of 'changing the world' (according to [60]).

[6] This group consists of 22 companies involved in the field of MEMS, essentially in the United States. The numbers were released in its annual report (made in 2001).

[7] The company Yole, based in Lyon, carries out analyses on the industrial situation of domains such as MEMS and microfluidics. The evaluations mentioned in this text are taken from a recent report (see www.yole.com).

[8] The project SMARTDUST, directed by the University of Berkeley, consists of creating microrobots equipped with mirrors allowing communication with the ground.

[9] S. Terry, PhD, Stanford University (1975).

[10] S. Terry, J.H. Jerman, J. Angell, *IEEE Trans. Electron. Devices*, **ED-26**, 1880 (1979).

[11] M. Madou, *Fundamentals of Microfabrication*, CRC Press (2000).

[12] D. Reyes, D. Iossifidis, P-A. Auroux, A. Manz, *Anal. Chem.*, **74**, 2623 (2002).

[13] A. Manz, N. Graber, H. Widmer, *Sens. Actuators*, **B1**, 244 (1990).

[14] A. Manz, D. Harrison, E. Verpoorte, J. Fettinger, A. Pausus, H. Ludi, H. Widmer, *J. Chromat.*, **593**, 253 (1992).

[15] D. Harrison, K. Fluri, K. Seiler, Z. Fan, C. Effenhauser, A. Manz, *Science*, **261**, 895 (1993).

[16] S. Jacobson, R. Hergenroder, L. Koutny, R. Warmack, J. Ramsey, *Anal. Chem*, **66**, 1107 (1994).

[17] D. Harrison, A. Manz, P. Glavina, *Transducers*, **917**, 92 (1991).

[18] B. Weigl, P. Yager, *Science*, **283**, 346 (1998).

[19] D. Evans, D. Liepmann, A.P. Pisano, *Proceedings of MEMS 97*, Nagoya, Japan, 96 (1997).

[20] S. Bohm, K. Greiner, S. Schlautmann, S. de Vries, A. Van der Berg, *Proc. μTAS*, 25 (2001).

[21] J. Knight, A. Vishwanath, J. Brody, R. Austin, *Phys. Rev. Lett.*, **80**, 3866 (1998).

[22] A. Bertsch, S. Heimgartner, P. Cousseau, P. Renaud, *Proc. MEMS 2001*, Interlaken, 507 (2001).

[23] P. Wilding, M. Schoffner, L. Kricka, *J. Clin. Chem.*, **40**, 1815 (1994).

[24] A. Chaudhari, T. Wounderberg, M. Albin, K. Goodson, *Micro ElectroMechanical Systems*, **7**, 918 (1998).

[25] M. Northrup, B. Benett, D. Hadley, P. Lander, S. Lehew, J. Richards, P. Stratton, *Anal. Chem*, **70**, 918 (1998).

[26] J. Daniel, S. Millington, D. Moore, C. Lowe, D. Leslie, M. Lee, M. Pearce, *Sens. Actuators*, A 81 (1998).

[27] R. Oda, M. Strausbauch, A. Huhmer, N. Borson, S. Jurrens, J. Craighead, P. Wettstein, B. Eckloff, B. Kline, J. Landers, *Anal. Chem.*, **70**, 4361 (1998).

[28] M. Kopp, A. De Mello, A. Manz, *Science*, **280**, 1046 (1998).

[29] E. Altendorf, Zebert, M. Holl, A. Vannelli, C. Wu, C. Schulte, *Proc. μTAS*, 73 (1998).

[30] P. Renaud, U. Seger, S. Gawad, *Proc. Nanotech 2002*, Montreux (2002).

[31] A.Y. Fu, C. Spence, G.H. Arnold, S.R. Quake, *Nature Biotechnol.*, **17**, 1109 (1999).

[32] J. Eijkel, A. Prak, S. Cowen, D. Craston, A. Manz, *J. Chromat. A*, **815**, 265 (1998).

[33] A. Kalmholz, B. Weighl, B. Finlayson, P. Yager, *Anal. Chem*, **23**, 71 (1999).

[34] In the 1990s, S. Chu made the first observations of the conformation of strands of elongated DNA at the intersection of two microcanals. One reference is Smith, D., Chu, S., *Science*, **281**, 1335 (1998).

[35] This word is now frequently used. The series of conferences μTAS is today one of the most important international conferences in the field of microfluidics.

[36] S. Jacobson, R. Hergenroder, A. Moore, J. Ramsey, *Anal. Chem*, **66**, 4127 (1994).

[37] M. Burns, B. Johnson, S. Brahmasandra, K. Handique, J. Webster, M. Krishnan, T. Sammarco, P. Man, D. Jones, D. Heldsinger, C. Mastrangelo, D. Burke, *Science*, **282**, 484 (1998).

[38] R. Srinivasan, I. Hsing, P. Berger, K. Jensen, S. Firebaugh, M. Schmidt, M. Harold, J. Lerou, J. Ryley, *AIChE J.*, **43**, 11 (1997).

[39] W. Ehrfeld, V. Hessel, H. Mobius, T. Richter, K. Russow, *Dechema*, **132**, 1 (1996).

[40] W. Ehrfeld, V. Hessel, H. Lowe, *Microreactors*, Wiley-VCH, Weinheim (2000).

[41] N. Giordano, J.T. Cheng, *J. Phys: Condens Matter*, **13**, R271 (2001).

[42] Jacobson, Alarie, Ramsey, *Proc.* μ*TAS*, 608 (2002).

[43] R. Ohigashi, K. Tsuchiya, Y. Mita, H. Fujita, *Proc. MEMS2001*, Interlaken, Suisse, 389 (2001).

[44] H. Fujita, *Proc.* μ*TAS2002*, Nara (Japan), 912 (2002).

[45] Lab on a Chip, (ed.) E. Ooserbroek, A. Van den Berg, Elsevier (2004).

[46] N.T Nguyen, S. Wereley, Fundamental and Applications of Microfluidics, Artech House (2003).

[47] Microfluidique, Traité Egem, Hermès (2004) S. Colin editor.

[48] The MEMS Handbook, Gad el Hak (ed.), (2nd edition 2005), CRC Press.

[49] C.M. Ho, Y. Tai, *Ann. Rev. Fluid. Mech*, **30**, 579 (1998).

[50] M. Gad El Hak, The Fluid Mechanics of Microdevices, *Journal of Fluid Engineering*, **121**, 5 (1999).

[51] P. Tabeling, *Proc XIV Annual Fluid Mechanical Conference* (2001).

[52] H. Stone, S. Kim, *AiChE Journal*, **41**, 1250 (2001).

[53] D. Beebe, G. Mensing, G. Walker, *Ann. Rev. Biomed. Eng.*, **4**, 261 (2002).

[54] G. Sanders, A. Manz, *Trends Anal. Chem.*, **19**, 364 (2000).

[55] E. Verpoorte, *Electrophoresis*, **23**, 677 (2002).

[56] J. Lichtenberg, N. de Rooif, E. Verpoorte, *Talanta*, **56**, 233 (2002).

[57] P.A. Auroux, D. Iossifids, D. Reyes, A. Manz, *Anal. Chem.*, **74**, 2637 (2002).

[58] H.A. Stone, A.D. Stroock, A. Ajdari, *Ann. Rev. Fluid. Mech.*, **36**, 381 (2004).

[59] One example is FSRM (Swiss Foundation for Research and Microtechnique).

[60] B. Weigl, K. Hedine, *American Biotechnology Laboratory*, January, **28** (2002).

ONE

Physics at the micrometric scale

1.1 Introduction

The title of this chapter, 'Physics at the micrometric scale', may seem surprising: for the physics of the systems we are discussing, it seems as if the micrometer is not inherently be a scale at which anything out of the ordinary should happen. For example, in simple liquids, molecule sizes, intermolecular distances, and correlation lengths are on the order of a *nanometer* and are thus actually much smaller than the dimensions of an ordinary microsystem. A cubic micrometer of tetradecane contains around 10^{12} atoms, a number sufficiently large to disregard the identity of the atoms, neglect thermodynamic fluctuations, and adopt without hesitation a macrometric approach. In the same way, for interfaces, the ranges of most intermolecular forces are no larger than 30 nm, a length scale that is extremely small with respect to the size of micrometric systems. In these systems, the spatial distribution of interfacial forces can be neglected without concern, and can generally be considered purely superficial, just as in macroscopic systems. Thus, one may question the necessity of dedicating an entire chapter to physics at the micrometric scale, since there does not seem to be any distinguishable differences from ordinary macroscopic physics.

However, this point of view is extreme. There are, in fact, several significant situations in microsystems where the macroscopic description must be amended, or even simply abandoned. This is indeed the case for gas flows in microcanals, whose boundary conditions include an expression for the mean free path of the gas, a quantity that is logically absent from the system of equations governing ordinary hydrodynamics. This is also the case for large molecules such as DNA or high molecular weight proteins, which must often be treated individually once they are introduced into a microsystem. Yet another example is thermal noise, which does not play an explicit role in ordinary problems of hydrodynamic

instability, but which controls the destabilization of ultraminiaturized jets. There is thus a whole collection of situations where microscopic phenomena directly intervene in the physics of systems of micrometric size, and these situations are worthy of analysis. As a final point, in many of these cases, the micrometer and nanometer are both present in the same microsystem. Furthermore, microfluidic systems equipped with nanometric detection or control elements will undoubtedly be developed in the future, thus conjugating the two scales. Extreme miniaturization will probably bring us to scales on the order of a hundred nanometers, a world intermediate between the microscopic and the nanoscopic; all these remarks justify the foray we will make in this chapter into the nanometric world.

Another question highlighted in this chapter is that of the disruption in microsystems of the equilibria of forces dominating at macroscopic scales. For example, in our 'ordinary' world, we are accustomed to the omnipresence and importance of gravitational forces. This chapter will show that at micrometric scales, gravitational forces become negligible, and the equilibria that take their place are often instead dominated by surface forces such as capillarity, wetting and adhesion. Surprising physical phenomena sometimes result, and we are forced to rationalize in a counterintuitive world. In practice, it is necessary to first determine the new equilibria that will appear in microsystems in order to know whether it will be advantageous to miniaturize. This chapter will try to accomplish precisely this goal, and will present several methods that will allow for the anticipation, without elaborate calculation, of the nature of the new equilibria dominating miniaturized systems.

In this chapter, we will first present a few elementary ideas on the sizes of different objects and the ranges of the principal intermolecular forces.

We will then analyse in the second part of this chapter the consequences of reducing the size of the system, i.e. miniaturizing, in several different situations. We accomplish this by determining the scaling laws governing the physical quantities in a given system. Nature provides us with astonishing examples of scaling laws that are not only heeded, but actually exploited by evolution.

In the third section of the chapter, we will analyse specific situations, where electrostatic, electromagnetic, mechanical, thermal, and chemical systems play a role (the hydrodynamics of microsystems is discussed in Chapter 2). The reader will note that it is often advantageous to work with miniaturized devices rather than devices operating at macrometric scales. This fact undoubtedly justifies the big expectations we have today for the field of microsystems[1].

[1] In the field of MEMS, the macrometric scale is sometimes referred to as the 'macroscopic scale'. To avoid confusion, we will not use this terminology here.

1.2 Ranges of forces of microscopic origin

1.2.1 Ranges of forces between molecules

■ **The ranges of forces between small molecules in a vacuum do not exceed a few nanometers**

We consider here the forces existing between two simple non-polar molecules, i.e. those whose barycenters of positive and negative charges overlap. Examples of non-polar molecules include the molecules of helium, nitrogen, and oxygen. When placed in a vacuum, these forces are made up of two contributions.

– The first contribution is a force of quantum-mechanical origin that can be either attractive or repulsive. In the attractive case, the force gives rise to the formation of a covalent bond. The force in the repulsive case is known as hard-sphere repulsion, and it assures the interpenetrability of atoms.
– The second contribution is from Van der Waals attraction. This term has a physical origin that can be outlined in the following manner: at a given instant, each molecule forms a dipole that deforms the electronic cloud of a neighboring molecule. When the forces generated in such a system are calculated, an attractive force is systematically produced. This polarization of a nearby molecule is known as an induced dipole-induced dipole interaction. Over the course of time, molecules and their electron clouds can fluctuate in position and in orientation, but the attractive effect always remains.

For hard-sphere repulsion, the interaction between two molecules can be described by the 'Lennard–Jones potential' $V(r)$. This potential has the following form:

$$V(r) = 4\epsilon \left(\left(\frac{\sigma}{r} \right)^{12} - \left(\frac{\sigma}{r} \right)^{6} \right), \tag{1.1}$$

where ϵ and σ are the two parameters characterizing the interaction. This potential is shown in Fig. 1.1, for helium. The parameters ϵ and σ obviously depend on which molecules are present. For example, for helium, we have the following values: $\sigma = 2.58$ Å and $\epsilon/k = 10.22$ K (here ϵ is expressed, after dividing by the Boltzmann constant k, in absolute degrees).

The force between two molecules is the opposite of the gradient of the Lennard–Jones potential. We have the following expression:

$$F(r) = -\frac{\mathrm{d}V}{\mathrm{d}r} = 24\epsilon \left(2 \left(\frac{\sigma^{12}}{r^{13}} \right) - \left(\frac{\sigma^{6}}{r^{7}} \right) \right).$$

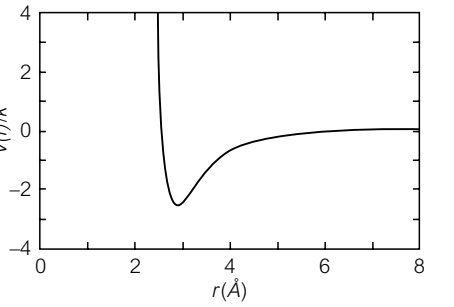

Figure 1.1 Representation of the Lennard–Jones potential for a helium molecule. The equilibrium radius, corresponding to the minimum of the potential, is 2.9 Å.

At 'large' distances, this force decreases with the inverse of the distance to the seventh power. Taking actual numerical values into account, the range of Van der Waals forces for two simple molecules can be estimated to be no more than a few nanometers. In the context of micrometric systems, these forces can thus be considered to be localized, or acting on an area of zero size, similar to an idealized point.

The above considerations apply to non-polar molecules, but once the barycenters of positive and negative charges in the molecule no longer overlap and become distinct from one another, a permanent internal dipolar moment appears and the molecule becomes polar. Water and carbon dioxide are examples of polar molecules. In these situations, there is always a hard-sphere repulsion (that has the same form as in the non-polar case) and a Van der Waals attraction. However, due to the polar character of the molecules, the attraction term includes supplementary contributions: the first is due to a permanent dipole-induced dipole interaction, and the second has a statistical origin. These terms are described thoroughly in the text of Israelachvili [1], and their presentation goes beyond the scope of this book. The important result is that these contributions decrease with $1/r^7$. We have reached the important conclusion that the Lennard–Jones potential can represent not only interactions between neutral molecules, but also those existing between isolated polar molecules in a vacuum. In the end, regardless of whether the molecule is polar, we can consider in all cases that the forces that are present do not exceed a few nanometers.

■ Two small molecules placed in a solvent interact in multiple ways, but over a distance of no more than a few nanometers

When two molecules are placed in a solvent—a common situation in biology and chemistry—it is obviously necessary to consider the solvent itself as a third participant in the interactions. Numerous phenomena are generated in this situation, profoundly modifying the situation described in the preceding section.

A few of these phenomena are described here, but the reader can refer to the work of Israelachvili [1] for a more complete presentation of this subject.

– When placed in a solvent such as water, an ionic crystal (e.g. salt) dissolves, and forms a collection of independent ions. The ions locally produce an electric field that tends to collect counter-ions, or the polar heads of the opposite charge, thus forming a complex and structuring the nearby environment. The charges grouped around the ion screen the electric field. Forces associated with these complexes are called hydration forces when the solvent is water.
– For certain solvents such as water, hydrogen bonds can form. A hydrogen bond is an electrostatic bond relating two electronegative ions by means of a hydrogen atom. These bonds have considerable importance in biology: dissolved in an aqueous phase, many proteins adopt a conformation determined by this type of bonding[2].

Medium-sized molecules, when placed in a solvent, interact locally with their environment

Medium-sized molecules, which have a radius of gyration (defined later) of a few nanometers, include small globular proteins and DNA fragments. Placing them in a solvent will cause the appearance of new phenomena. These phenomena are related to two factors: forces now result from the contribution of a large number of different elements, and the molecule does not have a fixed shape: it can modify its conformation as a function of its environment. This subject is vast, and only a few essentials will be given here to give a basic idea of the range of available interactions.

– When placed in an aqueous solvent, a molecule can sometimes be subjected to forces that are 'hydrophobic'. One example is a hydrophobic protein that folds on itself to minimize the contact area with the aqueous environment in which it is immersed. A 'hydrophobic' force is associated with such a conformation change, and this force is obviously not a part of the Lennard–Jones potential described previously. In the same vein, there are 'hydrophilic' forces that work to expose hydrophilic parts of the molecule to the solvent.
– Medium-sized molecules can adopt a substantial number of different conformations. We can thus legitimately introduce an entropy of conformation that the system spontaneously tries to maximize. As in all thermodynamic

[2] Hydrogen bonding is also the origin of the exceptional properties of water. If there was no such thing as hydrogen bonding, water would be gaseous at ambient temperature, ice would not float on liquid water, and most of the oceans in the world would be frozen.

systems, a force can be associated with this entropy, and this force must be taken into account in the total balance of the forces present.

Despite the large variety of different situations, it seems that in all cases the ranges of forces for simple molecules involve distances that do not exceed a few nanometers. For more complex molecules of decananometric size, we can consider that the distances involved are comparable to their own size, and are thus still on a completely submicrometric scale. The case of large molecules (e.g. DNA, large proteins), whose characteristic lengths become comparable to the size of the microsystem itself, will be analysed later.

1.2.2 Ranges of intermolecular forces between surfaces

We have examined the ranges of forces acting between two molecules, be they polar or non-polar, isolated or placed in a solvent, simple or moderately complex. In this context, the ranges of forces extend no farther than a few nanometers. However, molecules can come together to form a surface and develop interaction forces with a neighboring surface. We will see that this cumulative effect results in a large augmentation of force range. It is thus important to analyse these situations, and to study at what scale in a microsystem will it become necessary to explicitly take into account the spatial structure of intermolecular forces near interfaces.

Intermolecular forces between surfaces can be measured using the surface force apparatus (SFA)

Today we have a large amount of information available on the origin and the microscopic structure of forces appearing between surfaces, in a vacuum or in the presence of liquid. The major part of the work carried out on this subject arose during the 1980s [1]. Many laboratories benefited from a remarkable device called 'the force apparatus' that allowed the approach of stages with a precision on the order of just a few angstroms [2–4], and to measure the corresponding forces with great precision. One such device is shown in Fig. 1.2.

The stage on the device is displaced in an extremely precise manner, thanks to a system of springs with varying stiffnesses, which act as a displacement divider. The space between the stages is generally measured by Fabry–Pérot interferometry [3, 4]. Information obtained using this device is presented in the form of a force–displacement curve.

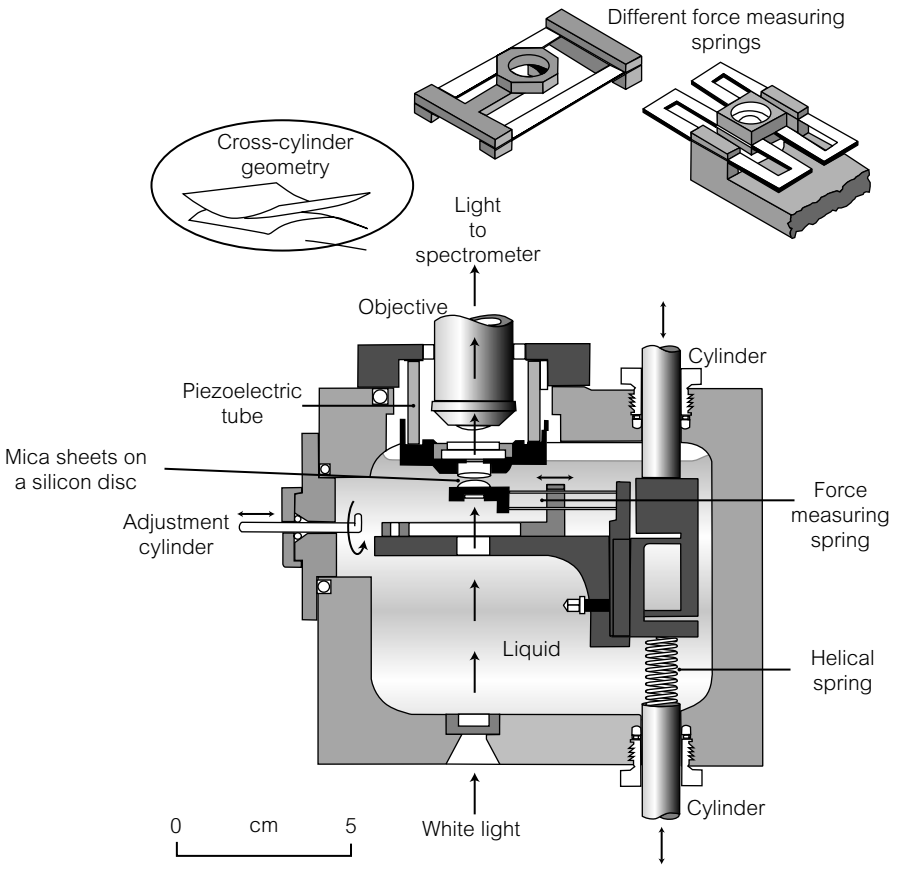

Figure 1.2 Diagram of a surface force apparatus that allowed, in the 1980s, the measurement of intermolecular forces existing near interfaces (see details in text) [1].

Classification of forces of interaction between surfaces

Of the forces of interaction between surfaces, there are those forces that act between molecules, and others that are more specifically related to the fact that we are dealing with surfaces. We conclude this section with the following list.

• **Forces of quantum origin.** These forces were introduced above in the section describing interactions between two neutral molecules. Their range is on the order of the angstrom, just as for two molecules.

• **Van der Waals forces.** We saw that the Van der Waals force varies as $1/r^7$ for molecules (where r is the distance between two molecules); this calculation shows that this same force varies as $1/r^5$ for plane–molecule systems, and as $1/r^3$ for plane–plane systems. The Van der Waals attraction force between two planes

is thus written by the following formula:

$$F = -\frac{A}{6\pi r^3},$$

where A is the Hamaker constant[3]. A typical value of this constant for hydrocarbon surfaces is 5×10^{-20} J. As we will see in Chapter 3, it is generally preferable in interface problems to work in terms of energy rather than force. We thus define the energy of interaction between two planes by the quantity:

$$E = -\frac{A}{12\pi D_0^2},$$

where D_0 is the equilibrium distance between two planes, i.e. the distance where repulsive quantum forces equal the attractive Van der Waals forces. This energy is the energy of adhesion between two planes. It is written:

$$E = -\frac{A}{12\pi D_0^2} = -2\gamma,$$

where γ is the surface tension. An energy of 2γ is necessary to separate two planes bound by Van der Waals adhesion.

The spatial dependence of the intensity of Van der Waals forces was not experimentally verified in plane–plane systems, but in sphere–sphere or sphere–plane systems. For a sphere–sphere system, the calculation shows that the Van der Waals force decreases as $1/D^2$ (instead of $1/D^3$). This evolution is clearly confirmed by the experimental curve in Fig. 1.3, obtained for two surfaces of mica. This curve also shows that the range of Van der Waals forces is on the order of 10 nm.

• **Electrostatic forces.** When a dielectric is immersed in an electrolyte, a surface charge almost always spontaneously appears. For example, a plate of glass immersed in aqueous solution becomes negatively charged[4]. The origin of this phenomenon comes from the fact that the silane terminals Si–O–H localized on the glass surface lose hydrogen ions in the presence of the aqueous solution; this protonation leaves Si–O^- terminals on the surface, thus causing the

[3] It is instructive here to mention Lifschitz theory, which is applicable in the situation of two surfaces composed of non-polar molecules, separated by a vacuum [5]. This theory leads to the following formula for the Hamaker constant:

$$A = \frac{3}{4}kT\frac{\epsilon_1 - \epsilon_2}{\epsilon_1 + \epsilon_2} + \frac{3I}{16\sqrt{2}}\frac{(n_1^2 - n_2^2)^2}{(n_1^2 + n_2^2)^{3/2}},$$

an expression in which k is the Boltzmann constant, T is the absolute temperature, ϵ_1 and ϵ_2 are the dielectric constants for the environment in question, n_1 and n_2 are the optical indices, and I is their ionization potential.

[4] If the pH of the solution is greater than 4.

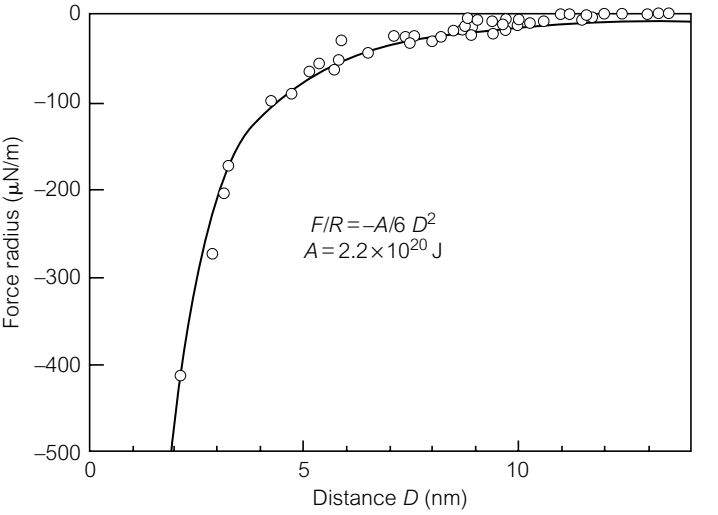

Figure 1.3 Measurement of the force between two crossed mica cylinders of radius $R \approx 1$ cm, in water. To interpret these measurements, it is necessary to note that two crossed cylinders exert attractive Van der Waals forces that are inversely proportional to the square of their distance (while forces between two planes are proportional to the cube of the distance between them). After [1].

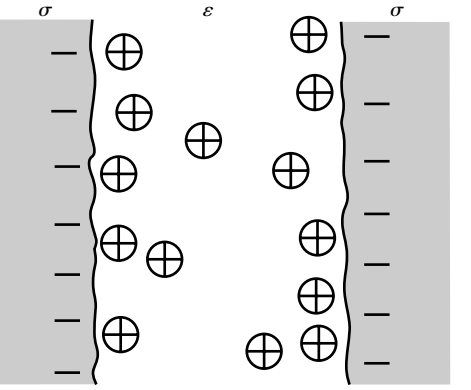

Figure 1.4 Diagram showing the formation of charged layers in the fluid and in the solid, leading to the generation of electrostatic forces. The mechanism is the following: the surfaces, when exposed to the solvent, are spontaneously charged; the counter-ions tend to migrate towards the charged surfaces, under the effect of Coulomb forces, forming a Debye–Huckel double layer.

glass exposed to aqueous solution to become negatively charged. To illustrate, the electric potential associated with these charges, for a pH of 7, is on the order of −100 mV. These processes are described in detail in the text of Cabane and Hénon [6].

These surface charges are equilibrated in the fluid by a double layer of counter-ions, as shown in Fig. 1.4.

The first layer is a molecular film of counter-ions, and is fixed at the level of the solid/liquid interface under the effect of attractive forces acting between the charged solid surfaces. This first layer is called the 'Stern layer'. It is associated with the solid by an electrostatic interaction. The second layer is not connected to the crystalline network (ordered or disordered) of the solid: it is diffuse. Its structure results from a statistical equilibrium between thermal agitation (which tends to homogenize the charge distribution) and electric forces (which tend to displace charges of the same sign towards the surface, thus creating a default in the homogeneity). The characteristics of this layer are obtained using statistical physics, worked out for the first time by Debye and Huckel. The order of magnitude of the thickness of the double layer, designated by λ (the Debye–Huckel length) is given by the following expression:

$$\lambda_D = \sqrt{\frac{D\epsilon}{\sigma}},$$

where σ is the electrical conductivity, ϵ the dielectric permittivity, and D the diffusion coefficient of the ions of the double layer. To illustrate, we can note that the double layer is a dozen nanometers thick for an ionic solution of 1 mM of salt. As λ increases proportionally with the inverse of the square root of the conductivity of the solution, it can in principle achieve high values. However, practically speaking, since it is very difficult to limit the dissolution of ions that is inevitably present on the surfaces containing the liquid, the thickness of double layers does not exceed about a hundred nanometers. This double layer is the origin of electrostatic forces, which had been measured in force machines. Figure 1.5 shows one measurement of such forces, between two mica cylinders.

The force of the double layer decreases exponentially, as the theory predicts. Figure 1.5 also indicates that the ranges of the forces of the double layer can attain several tens of nanometers.

• **Solvation forces.** When a simple liquid or a polymer melt is confined between two surfaces separated by a few nanometers, the liquid tends to structure itself, as shown in Fig. 1.6.

As the confinement increases, at some point only a few molecular layers remain between the two planes. We can imagine that the forces of interaction between the two planes will depend on this structuration effect. This type of experiment was able to show that the force is an oscillating function of the distance. The spatial period is on the order of the intermolecular distance of the liquid, and the amplitude of the associated force only decreases beyond a distance on the order of 10 nm. This force is called the solvation force.

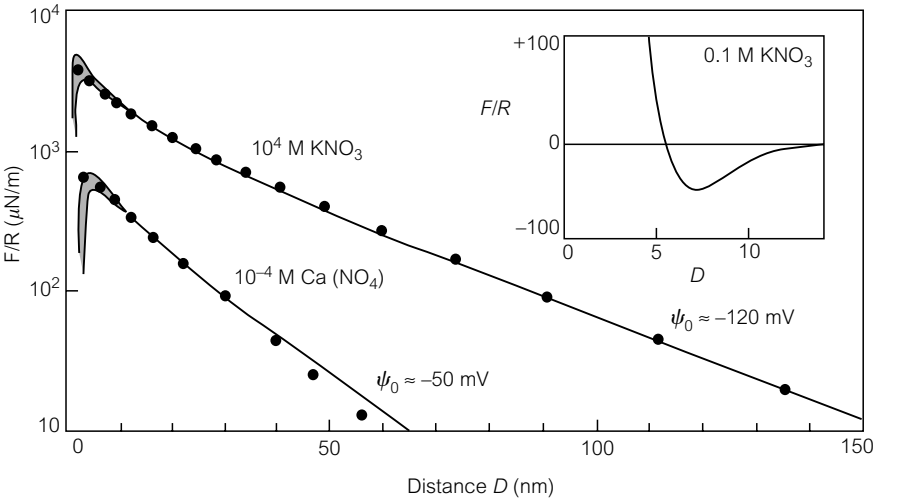

Figure 1.5 Measurement of force between two crossed mica cylinders of $R \approx 1$ cm in electrolytes. The forces of the double layer decrease exponentially with distance, and can extend over several tens of nanometers. The solutions used for this experiment are KNO_3, and $CaNO_3$ for the upper and lower curve, respectively. The continuous lines are obtained from the 'DLVO' theory, after [1].

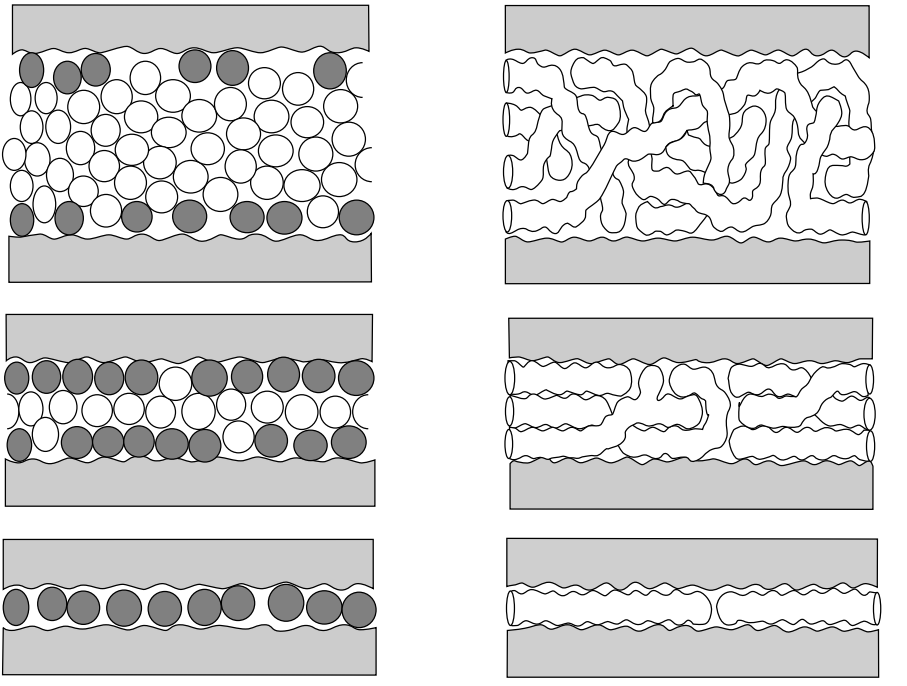

Figure 1.6 Diagram showing how a crystalline surface can affect the structure of a liquid near the liquid/solid interface, in two situations: a simple liquid (left) and a polymer melt (right). From top to bottom, the confinement increases until the system reaches a situation where one single molecular layer can insert itself between the solid surfaces.

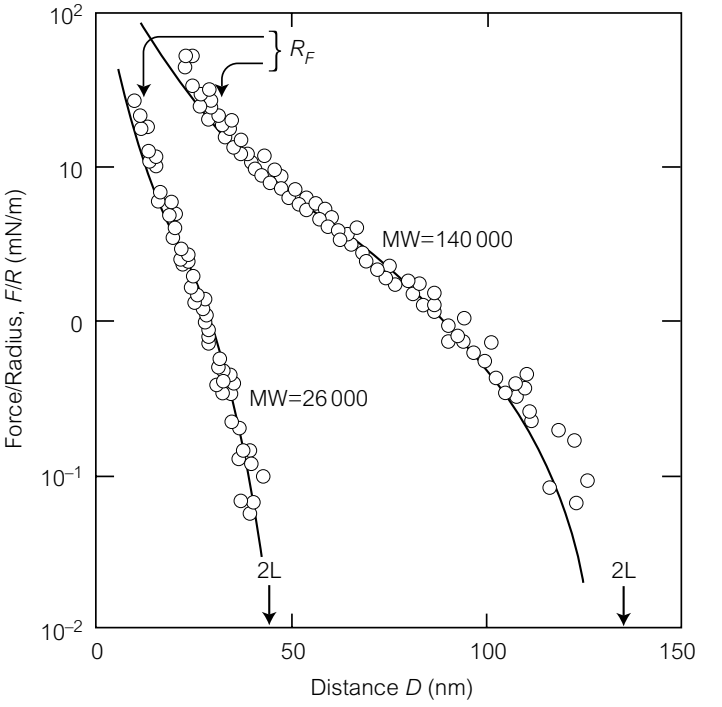

Figure 1.7 Forces between two surfaces of mica functionalized by layers of polystyrene [7]. Two situations are represented here, corresponding to two different molecular weights (MW) of polystyrene. The continuous lines represent the theory of Alexander de Gennes.

• **Forces related to fluctuations.** Other forces play a part in the specific case where surfaces are functionalized (i.e. covered by one or several molecular layers adsorbed to the surface, modifiying its physicochemical properties). The curve in Fig. 1.7 shows one case where the surface of mica is functionalized by the adsorption of polystyrene molecules. In this case, there exists a repulsion effect between the two surfaces that extends over several tens of nanometers. To understand the origin of this effect intuitively, it is necessary to consider that the molecules functionalizing the surface are not rigidly bonded to the surface; their positions fluctuate considerably, and these fluctuations make the layer seem much thicker than it actually is.

• **In conclusion**, the range of interactions between planes is much larger than interactions between two molecules. In practice, this range does not go beyond 100 nm. In terms of 'standard' microsytsems (i.e. systems a few tens of micrometers in size), intermolecular forces can be considered to be localized, i.e. applied to regions of zero thickness. These systems could be treated by methods analogous to those used in macroscopic systems. In particular, it will be

logical to introduce the idea of 'capillarity', which we will develop in Chapter 2. In ultraminiaturized systems, which have tranverse dimensions less than a hundred or so nanometers, we expect that effects directly related to the spatial extension of Van der Waals forces will appear at the extension of the double layer. We enter here into the domain of nanofluidics, which we have mentioned several times in this text. By way of example, we can refer to an experiment carried out in a nanocanal that allowed the indirect characterization of the internal structure of the double layer [8]. There still has not been experimental proof the spatial structure of Van der Waals forces in an ultraminiaturized microsystem. As we mentioned above, experimental systems have allowed the successful analysis of intermolecular forces acting between surfaces using force apparatuses, and these can be classified as 'traditional' mechanical systems.

1.3 Microscopic scales intervening in liquids and gases

Scales involved in gas and simple liquid systems are as follows:

– The sizes of molecules are usually defined by the distance at which the Lennard–Jones potential, given by the relation (1.1), is at a minimum. This value is the equilibrium radius of the pair of molecules in interaction. This quantity is (see equation (1.1)):

$$r_e = 2^{1/6}\sigma.$$

For simple molecules, these values are on the order of a few angstroms.

– A second important scale is the average distance between molecules. A relation often used is that relating the density n and the average intermolecular distance d:

$$d = n^{1/3}.$$

We know that for a liquid, the size of the molecule is comparable to the intermolecular distance, while for a gas, the former is much smaller than the latter.

– For gases, the fundamental scale necessary to establish dynamical properties is neither r_e nor d, but the mean free path λ. This scale is defined as the average

distance travelled by a molecule between two successive collisions. The kinetic theory of gases allows the following expression to be established:

$$\lambda = \frac{1}{\sqrt{2}\pi n a^2} = \frac{kT}{\sqrt{2}\pi p a^2},$$

where n is the density (the number of molecules per unit volume), T is the temperature, k is the Boltzmann constant, p is the pressure, and a the size of the molecule.

What is the order of magnitude of a mean free path for air?

We can estimate this value from the preceding formulas: Avogadro's law stipulates that all gases contain the same number of molecules per unit volume; at ordinary pressure, and at a temperature of 273 K, this number is 2.69×10^{19} cm^{-3}. For air, assuming that the size of the molecule is on the order of 3 Å, we obtain a mean free path of around 60 nm. However, in practice the determination of the mean free path is made from viscosity measurements given by the kinetic theory of gases.

We thus obtain a list of values of the mean free path for different gases [9][5], shown in the table below.

Gas	λ (nm)
Air	61
Nitrogen	60
Argon	64
Helium	177

It seems that under normal conditions, the mean free path is a (small) fraction of a micrometer. It is obvious that this scale must be explicitly considered once the dimensions of the microcanals are on the order of magnitude of a micrometer. We will analyse the hydrodynamic consequences of this in the following chapter.

[5] For reasons that are not well understood, the values of the mean free path of gases vary from one publication to another by about 10%. The values shown in the table have been taken from [9]. They are consistent with known values of gas viscosities.

1.4 Micromanipulation of molecules and cells in microsystems

1.4.1 Introduction

Microsystems allow for the micromanipulation of macromolecules, such as DNA, individually. The first experiment involving controlled stretching of a molecule of individual DNA was carried out at the intersection of two microcanals etched in silicon [10]. After the success of this experiment, other experimental setups based on more traditional techniques allowed the study of the elasticity of DNA with excellent precision, and the analysis of phenomena such as the coiling of the molecule under a variety of conditions [12].

Microsystems also permit the micromanipulation of biological cells. At this time, many experiments have shown that it is possible to trap, carry out transfection, electroporate, and lyse cells individually, and in a controlled manner in microsystems [13–15]. This type of manipulation is not new in the domain of biophysics. However, the fact remains that microsystems allow integration and parallelism, which open up promising possibilites in fields like biology.

In this section, we give some general information on the size of objects contributing to distinctive experimental studies carried out in microsystems, and we will then mention a few specific studies performed on the subject.

1.4.2 Generalizations on the sizes of macromolecules

Macromolecules are molecules containing a large number (between a few thousand and millions) of atoms: they include proteins, DNA, and polymers. Figure 1.8 represents three molecules of biological interest, developing the idea of the differences in size between ordinary molecules and large macromolecules.

Depending on their crystallographic structure, the solvent in which they are immersed, or the temperature, macromolecules can adopt different shapes: helices, globules, sheets, stretched structures, etc.[6].

[6] The form of macromolecules is characterized by their structure. Generally, four levels of structure are distinguishable: primary, secondary, tertiary, and quaternary. The primary structure of a protein is the sequence of amino acid residues making up the polypeptide chain. The secondary structure characterizes the spatial arrangement of the base units of the chain (for example, in the form of a helix or a sheet). The tertiary structure corresponds to the overall form of the macromolecule (globular, stretched-out, etc.) and the quaternary structure comes into play when the macromolecule itself forms several types of molecular assemblies.

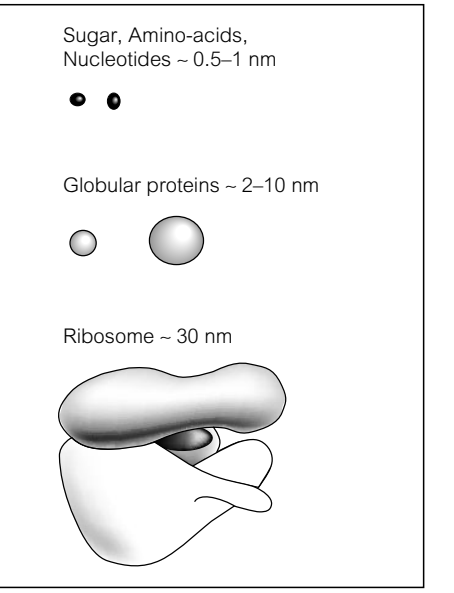

Figure 1.8 Figure showing three molecules of different sizes: the largest molecules here are enzymes, which typically have sizes (more precisely, radii of gyration, in a non-denatured conformation) on the order of a few tens of nanometers. The smallest are simple molecules, whose sizes are on the order of a few angstroms. The small globular proteins have a size of a few nanometers.

Figure 1.9 Fluorescent signature of a partially extended 16-lambda DNA. The contour length is 336 μm. (Courtesy of Professor Steve Chu, Physics Department, Stanford University.)

Figures 1.9 and 1.10 show two macromolecules, one stretched out, and the other in a folded form.

Three geometric measurements are important to know:

– The contour length R_c is the length of the macromolecule measured along its backbone. For a polymer made up of N monomers, each separated by a distance l, we have:

$$R_c = Nl.$$

– the radius of gyration R_g, which for a macromolecule shaped around a frame represents the average distance between the extremities of that frame, while the molecule is in a folded form. We have the following relation, obtained by comparing the position of each atom along the frame to a Brownian step:

$$R_g \sim N^{1/2},$$

where N is the number of atoms making up the molecule;

– the persistence length, which characterizes the correlation length measured along the frame of the molecule.

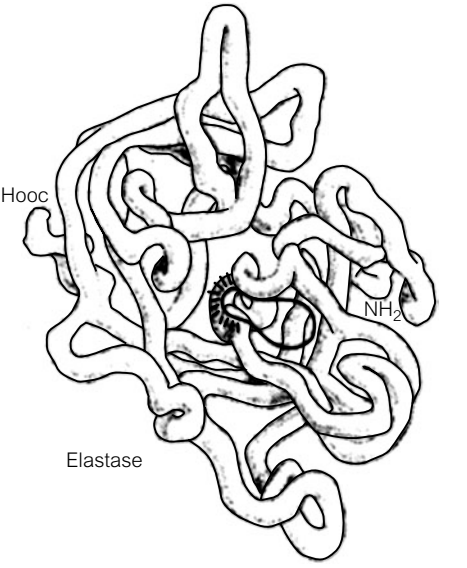

Figure 1.10 Representation of the protein elastase.

The table below gives a few orders of magnitude for DNA.

Molecule	Contour length	Radius of gyration
DNA of a human chromosome	5 cm	1 μm
DNA of the bacteria *E. Coli*	1.5 mm	100 nm

We see that the scales associated with DNA are not far from the sizes of micrometric systems. It is thus possible, in principle, to individually micromanipulate these molecules in microsystems. In such a context, we leave macroscopic hypotheses behind. The physics involved in these systems is often referred to as 'the physics of the single object'.

1.4.3 **Sizes of some objects significant in biology**

Macromolecules can assemble themselves to form molecular structures, and nature has obviously produced an immeasurable variety of them. Considering the large extent of this subject, only the animal cell will be described here, because the animal cell includes several molecular structures. The dimensions of these complex assemblies seem to satisfy the conditions for individual micromanipulation in the framework of microsystems. The size of an animal cell is between 10 and 30 μm. A diagram of the principal cellular elements is shown in Fig. 1.11.

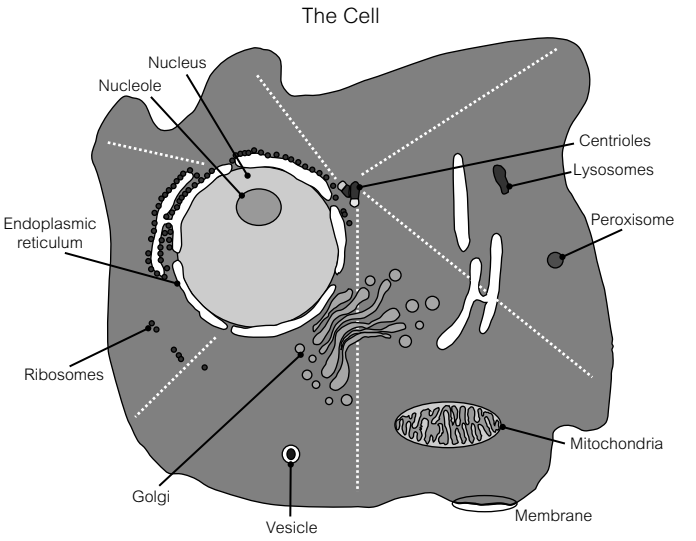

Figure 1.11 Diagram of a cell, with its major structures.

The cell is made up of several different elements:

– a nucleus of size between 3 and 10 μm. The nucleus itself is a complex object that contains, among other elements, DNA folded into the form of a chromosome. Chromosomes are objects of micrometric size;
– mitochondria, which are nucleated cells of micrometric size. Mitochondria have the cellular function of supplying energy to the cell[7];
– the endoplasmic reticulum, a collection of vesicles across which proteins are fabricated and transported. The vesicles of the reticulum are micrometric objects;
– the cytoskeleton, containing actin, tubulin, and intermediate filaments. These objects are between 10 and 30 nm in diameter, and a few micrometer in length. They ensure the mechanical cohesion of the cell;
– the cellular membrane, which has a thickness of a few tens of nanometers.

The table below presents the size of different types of cells, cellular elements, or different objects of biological significance.

[7] Mitochondria are reservoirs of ADP (acid diphosphate); the transformation of ADP to ATP (acid triphosphate), outside the mitonchondria, supplies the cell with energy.

Element	Size
Amino acid	0.8 nm
Diameter of a DNA helix	2 nm
Globular protein	4 nm
Thickness of a cellular membrane	10 nm
Diameter of a microtubule	25 nm
Large virus	100 nm
Lysosome	200 nm
Prokaryote	1–10 μm
Bacteria *E. Coli*	2 μm
Mitochondria	3 μm
Eukaryote	10–30 μm
Amoeba	90 μm
Frog oocyte	2 mm

We thus see that, in principle, the sizes of these objects lend themselves well to experimental study in microsystems. The following section will discuss a few of these experiments on DNA and the cell, which were studied individually.

1.4.4 Experiments on the micromanipulation of DNA and cells in microsystems

There exist several physical experiments carried out on DNA or biological cells using microsystems. In the vast majority of cases, these experiments are devised to offer an alternative to biological protocols, which most often treat large populations of objects (eventually polydisperse), and not isolated objects.

However, the experiment of Chu [16] is an important exception. Chu was the first to study an individual strand of DNA in a microsystem. The motivation for the experiment was a physical study of the dynamics of the molecule. In such an experiment, one end of the molecule is fixed onto a bead, and the bead is placed at the intersection of microcanals made by etching in silicon (Fig. 1.12)(these fabrication techniques will be described in Chapter 6). Figure 1.13 represents a series of photographs showing the evolution of the fluorescent signature of the DNA of a flexible bacteriophage λ. This DNA has a contour length of 22 μm, and is put under the influence of shear[8]. This type of image shows the considerable richness of the conformational dynamics of a long molecule placed in a fluid flow[9].

[8] The setup is different from that of Fig. 1.12.

[9] Among other things, these observations are useful for the problem of the reduction of hydrodynamic drag in the presence of polymers.

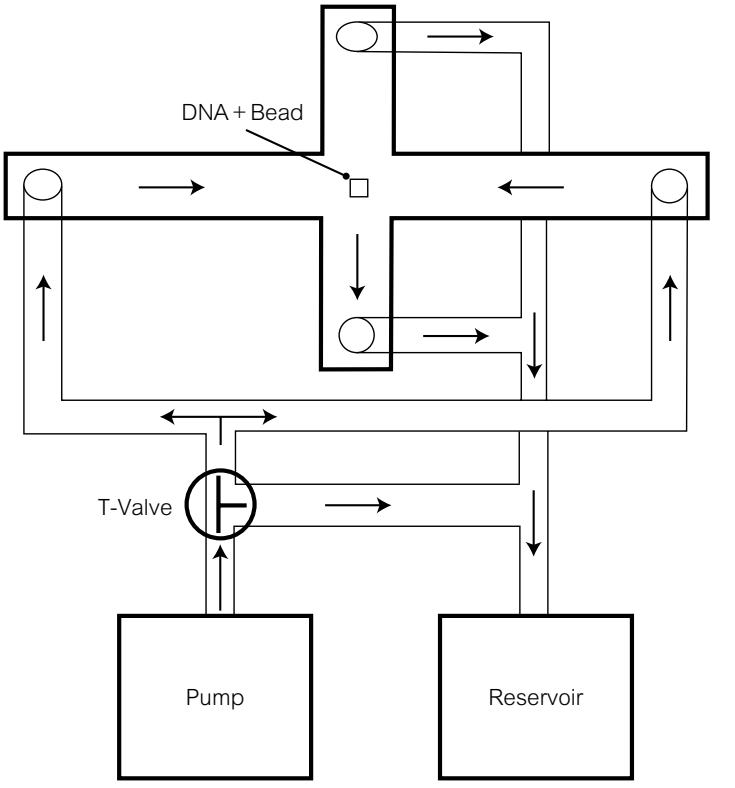

Figure 1.12 Experimental setup allowing for the study of dynamic stretching phenomena on an individual DNA molecule.

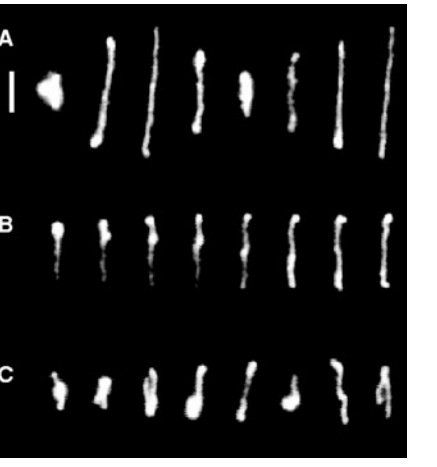

Figure 1.13 Different conformations of a DNA molecule placed in a field of pure shear, characterized by a rate of shear of 1 s^{-1}, in a viscous solution of sucrose (photo published with the permission of D.E. Smith et al., *Sciences*, 283, 1999. (Copyright 2003. American Association for the Advancement of Science).

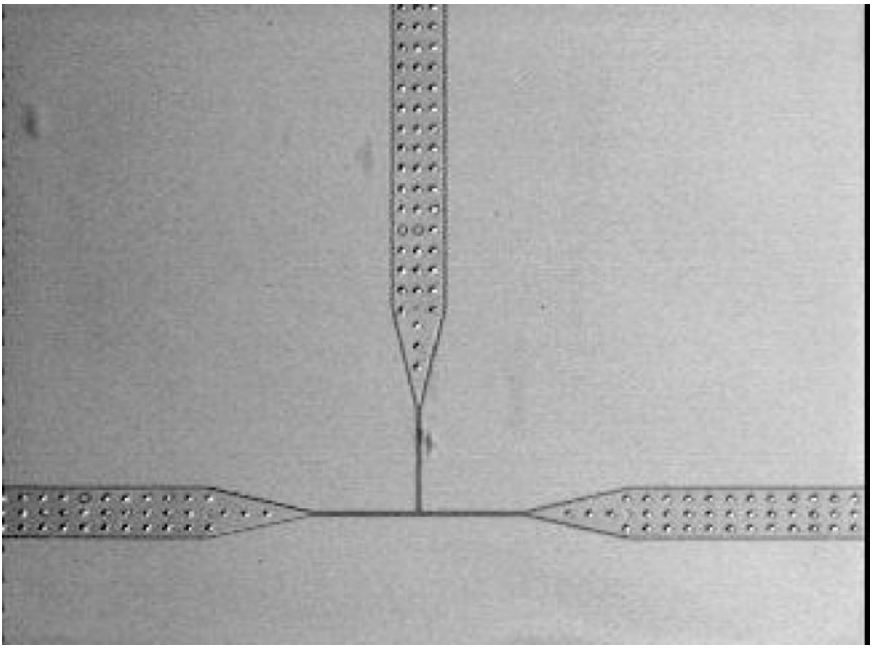

Figure 1.14 Microcytometer sorting cells one by one. Canals have a height of 3 μm; far from the intersection, they are 100 μm wide; at the intersection, their width is reduced to 5 μm; these canals were made of PDMS (see Chapter 6). The circles appearing in the microcanals are pillars preventing the collapse of the PDMS. This system is also used for sorting DNA molecules [22].

As for the micromanipulation of biological cells, there are several experimental setups that allow several elementary operations to be carried out, including lysis, transfection, characterization, etc. [14, 17, 18].

Figure 1.14 shows an example of microcytometry, which allows the measurement and sorting of cells, one by one. The proof of principle experiment was performed on *E. Coli* cells labelled with fluorescent genes (GDP)[10]; this system was later integrated [19]. Other microcytometers acting on the individual cell itself have been created [15, 20].

Systems of cellular micromanipulation will likely continue to develop in the future. Being capable of acting at the cellular level effectively provides original solutions to problems that were difficult to solve by traditional methods. Other motivations based on biological considerations emphasize the interest in acting at the level of the individual cell: in the field of neurology, the fact that the proteome[11] differs from one cell to another, and that the cells cannot be cultured, necessitates the use of the single-cell approach.

[10] In a slightly different system from that shown in Fig. 1.14.
[11] The proteome is a collection of proteins of a given system.

1.5 The physics of miniaturization

1.5.1 Introduction

In the preceding pages, we analysed scales involved in several micro/mesoscopic phenomena. Here, physical phenomena are no longer considered alone, but in relation with others. The objective of this section is to determine where equilibrium points are situated (mechanical or otherwise) in micrometric systems, and how the equilibrium is transformed when decimetric-sized systems (designated as 'macrometric' or 'ordinary' systems) are miniaturized.

1.5.2 Scaling laws for a few physical quantities

To analyse the equilibria prevailing in miniaturized systems, it is useful to introduce the idea of the scaling law . A 'scaling law' signifies: the law of the variation of physical quantities with the size l of the system or the object in question. Table 1.1 presents such laws for a few physical quantities. Here, the scale l can be understood in two ways:

- the object is isotropic (having the same dimensions, by order of magnitude, in the three spatial dimensions). Here, the scale simply represents the order of magnitude of the size of the object;
- the object is anisotropic. For example, a microcanal is anisotropic as its length is generally larger that its width and height. In this case, the quantity l must be understood to be a scale controling all dimensions of the system; when l decreases (length, height, etc.), all the dimensions of the system also decrease while maintaining constant aspect ratios.

We comment here on Table 1.1. It is clear that for certain quantities, the scaling law is obvious. This is the case for mass and volume, where we have the law:

$$M \sim V \sim l^3,$$

where M is the mass and V the volume of an object of size l. An analogous commentary can be made on distance and time. However, in the majority of cases, the relation between the quantity under consideration and the scale of the system implicates other physical quantities. There are two possibilities:

- the physical quantities that intervene in the scaling law are constants. This is the case for Van der Waals forces (per unit surface) between two planar interfaces,

Table 1.1 Scaling laws for different physical quantities

Quantity	Scaling law
Intermolecular Van der Waals force	l^{-7}
Density of Van der Waals force between interfaces	l^{-3}
Time	l^{0}
Capillary force	l^{1}
Distance	l^{1}
Flow velocity	l^{1}
Thermal power transferred by conduction	l^{1}
Electrostatic force	l^{2}
Diffusion time	l^{2}
Volume	l^{3}
Mass	l^{3}
Force of gravity	l^{3}
Magnetic force with an exterior field	l^{3}
Magnetic force without an exterior field	l^{4}
Electrical motive power	l^{3}
Centrifugal force	l^{4}

whose expression is:

$$F_{\mathrm{V}} = -\frac{A}{6\pi l^3},$$

where A is the Hamaker constant, already introduced in this chapter. We also obtain for the density of Van der Waals force the obvious relation:

$$F_{\mathrm{V}} \sim l^{-3},$$

as Table 1.1 indicates;

– physical quantities appearing in the scaling law eventually depend on the scale. This is the case for electrostatic forces, where besides the size of the system, the electric field and the dielectric constant of the surroundings intervene. We have the following expression for the electrostatic force F_{e}:

$$F_{\mathrm{e}} \sim \epsilon E^2 l^2,$$

where ϵ is the dielectric constant of the environment in question and E is the electric field in the system[12]. To reach the expression shown in Table 1.1, the electric field must be assumed to be fixed. In this case, one tries to estimate the maximum forces that miniaturized electrostatic systems can develop.

[12] We will justify the expression used here later.

These forces are also assumed to function near the electric field break-off point, which is treated as a constant. A similar hypothesis is made for electromagnetic forces, where the current density producing the magnetic field is considered fixed.

We comment on the exponent of the flow velocity, which is equal to 1: we assume here that the pressure difference causing fluid motion in a canal is fixed. Everywhere else, we place ourselves in a 'microfluidic' context, where the flow regime is laminar. Applying Stokes' law, we obtain in terms of order of magnitude:

$$U \sim \frac{b^2 \Delta P}{\mu L},$$

where μ is the fluid viscosity, ΔP is the pressure difference applied along the canal, L the canal length, and b its transverse dimension. From the standpoint of scaling laws, we thus have at fixed pressure difference: $U \sim l$. Thus, we arrive at the conclusion that in a typical microfluidic flow situation (a fluid circulating through a microcanal at a fixed pressure difference), the exponent associated with the velocity is equal to one. This does not imply that the exponent associated with the velocity of an object is equal to one in all cases. Such an assumption would indeed be incorrect: one counterexample can be found in the maximum velocities of animals, which are largely independent of their size.

After making these considerations, the general rule of thumb is the following: when two forces are present, it is the force associated with the weaker exponent that becomes dominant in miniaturized systems. Thus, we begin to understand that the equilibria we are used to in the macrometric world can be disrupted at the micrometric scale. For example, when the exponent of the forces of gravity is compared to that of capillary forces, one can conclude, or very nearly so (we will return to this in section 5.5) that the forces of gravity are negligible with respect to capillary forces. This situation is the inverse of the situation in the macrometric world. We will later present a few illustrations of this concept using examples drawn from nature.

1.5.3 The Π theorem

It is useful to review here the theorem of the product, called the 'Π theorem', which allows the reduction of the effective number of variables of a system, and the prediction of the consequences of miniaturization. We will not give a demonstration of this theorem; the reader can find this in most works of fluid

mechanics (see, for example, reference [23]). A classical presentation involves the definition of matrices and the determination of their row by calculating the number of variables without independent dimension. We present the result in a more compact but equivalent form:

$$A = f(a_1, a_2, \ldots, a_n)$$

in a system of units consisting of k independent units, this law can be shown to be written:

$$\Pi = g(\pi_1, \pi_2, \ldots \pi_{n-k}),$$

where the πs are the dimensionless products formed from the initial quantities. We now only have a relation between $n - k + 1$ (instead of $n + 1$) variables, which can often represent a considerable simplification with respect to the initial law. This theorem has numerous applications, notably in fluid mechanics and thermal physics. It allows the determination of the effect of scaling changes by the analysis of the evolution of dimensionless numbers governing the problem. We study an example of the simple utilization of this theorem in the context of microsystems. How do fluid flows behave in miniaturized systems, for incompressible Newtonian fluids? If the Π theorem is used to respond to this question, the local velocity u (assumed to be stationary) must be written as functions of the following parameters:

$$\boldsymbol{u} = f(\boldsymbol{x}, l, \Delta P, \mu, \rho),$$

where $\boldsymbol{x}$ is the spatial coordinate, l is the characteristic scale of the system, ΔP is the pressure difference causing the flow, μ is the viscosity and ρ is the volumetric mass of the fluid. We also here have $k = 3$ amd $n = 5$. We deduce that we can form $n+1-k = 3$ independent dimensionless numbers, which we have chosen to equal:

$$\frac{\boldsymbol{x}}{l}, \quad \frac{\boldsymbol{u}}{U} \quad \text{and} \quad \frac{Ul}{\nu},$$

where U is a velocity equal to $\Delta Pl/\mu$, and $\nu = \mu/\rho$ is the kinematic viscosity. The product Ul/ν is known as the Reynolds number *Re*. Thus, the preceding relation can be written in the form: $\boldsymbol{u}/U = f(Re, \boldsymbol{x}/l)$. We thus have a much simpler expression than the initial expression. In Chapter 2, we will demonstrate numerous consequences that result from such a formulation.

1.5.4 The system of units describing small quantities

Volumes are associated with an exponent equal to 3, which is rather high. From the centimeter to the micrometer, volumes decrease by 12 orders of magnitude. In this context, it is useful to know some expressions used in the world of microsystems for describing extremely small quantities. We thus have the following table:

Name	Power
milli	10^{-3}
micro	10^{-6}
nano	10^{-9}
pico	10^{-12}
femto	10^{-15}
atto	10^{-18}
zepto	10^{-21}
yocto	10^{-24}

These small units are frequently used, a few examples of which are presented below. Volumes contained in microfluidic systems commonly range from about 10 to a few hundred nanoliters. A biological cell as we saw above is typically a sphere 10 μm in diameter, enclosing a volume of 4 pL. Reference [24] reaches a detection threshold of 15 amole (i.e. 15 atto-mole) by coupling a microfluidic system to a mass spectrometer. A recent study [25] showed that it is possible to detect the presence of a zeptomole of DNA by means of a miniaturized electrochemical method. The expressions 'atto' and 'zepto' are actually frequently used in the field of microsystems.

1.5.5 A few consequences of scaling laws in nature

We examine a few consequences of scaling laws in nature for plants and animals, scaling laws whose importance has already been presented by Galileo [26]. Scaling effects were discussed in detail more than a century ago by Sir D'Arcy Thomson, in a text [27] that even today remains an important reference. In the present day, these questions are still discussed: for example, the performances of giant extinct animals are still being investigated. What is the maximum velocity of the tyrannosaurus in the film 'Jurassic Park'? Did this animal run at 20 m/s, the speed of a jeep (as in the film), or did it only attain a speed of 11 m/s in its best moments (a result suggested by numerical simulation [21])? Here, we simplify the situations considerably, and only mention results that are both well accepted (at least along their main points) and also pertinent to orders of

magnitude. We take the example of small animals: they receive energy per unit time, coming from the food they eat, proportional to their weight (this pertains not only specifically to small animals, but to all animals). We thus have an input of chemical energy per unit time, which is equal to:

$$Q_{\mathrm{N}} \sim l^3.$$

These animals transfer heat towards the outside, according to a law that can be established assuming that the transfer is made through a layer of thickness δ and surface area S. The amount of heat evacuated per unit time Q by the animal is thus:

$$Q = \frac{kS}{\delta}\Delta T,$$

where k is the conductivity of the surroundings and ΔT is the temperature difference between the body of the animal and the exterior. Considering that the surface S and the thickness δ vary as l^2 and l, respectively, we obtain the following scaling law for Q:

$$Q \sim l.$$

We also see that the smaller the organism, the more difficult it is to compensate for thermal losses by eating food, and thus the more difficult it is to maintain its internal temperature at a level substantially different from the exterior temperature[13]. We can see that for animals, there exists a lower limit to size beyond which thermal equilibrium cannot be assured. This limit is represented by the pygmy shrew, whose size is of a few centimeters (Fig. 1.15). Like some mythological victim of torture, this animal must permanently eat to maintain its internal temperature at a fixed level in order to survive. These scaling effects on thermal fluxes also explain why small insects can only survive by being cold-blooded (they are 'poïkilotherms'), at a non-imposed temperature.

Another example: at small scales, capillary forces dominate gravitational forces. This is what is indicated in Table 1.1. In effect, after taking the relevant exponents into account, it is easy to see that capillary forces clearly dominate gravitational forces in systems of small size. Capillary forces are associated with an exponent equal to 1, while gravitational forces are associated with an exponent equal to +3. One important consequence of the predominance of capillary effects on weight is that it is possible to walk on water thanks to wetting forces. In the case of walking on water, the foot of the insect is subjected to hydrophobic

[13] On the other hand, large animals have a difficult time getting rid of their thermal energy. The whale uses its blood circulation to transfer heat towards the exterior. When hunters killed a whale, its circulation stopped, the exchange of heat ceased, causing the internal tissues to cook. Hunters valued the meat of the whale cooked in this way.

Figure 1.15 This figure shows an ordinary shrew, which is 9 cm long and weighs a few grams. This animal ingests its own weight in insects, worms, and spiders on a daily basis. The pygmy shrew is even smaller, and must ingest food even more quickly to survive. The predator of the shrew is the weasel, who, because of its size, has more leisure time before meals. © Laurent Thouzeau/Bios.

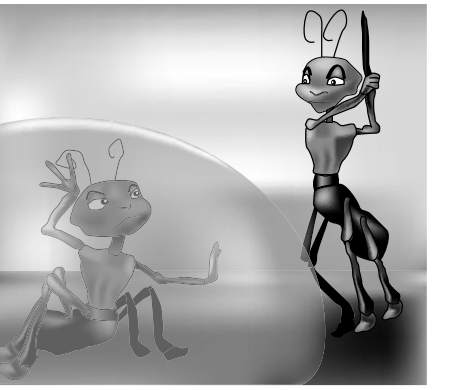

Figure 1.16 This drawing, inspired by a famous animated drawing, represents the significant effort it would take for an ant to free a comrade imprisoned in a bubble. At the scale of an ant, capillary forces are very significant with respect to the muscular forces the animal can exert. After [11].

forces maintaining it partially out of water. The effect of gravity, which tends to immerse the foot, is easily compensated for. In the same vein, we can see that it is not difficult for insects to climb up walls.

As emphasized by Kim [11], if we lived in a submillimetric world, the principal phenomenon that would concern us would be capillarity and not gravity or inertia. We would fear getting stuck to the surface of liquids, but we would not risk being hurt by an impact. At this scale, we would undoubtedly have invented (if our intelligence was still intact) numerous machines driven by surface tension. It would seem natural that in our microworld, automobile accidents would not be caused by collisions, but by drops of water abandoned in the road.

Capillary forces dominate gravitational forces at this scale, and even more easily dominate centrifugal forces (see Table 1.1). The scaling law for centrifugual forces is obtained by the following logic: we consider an object of size l and

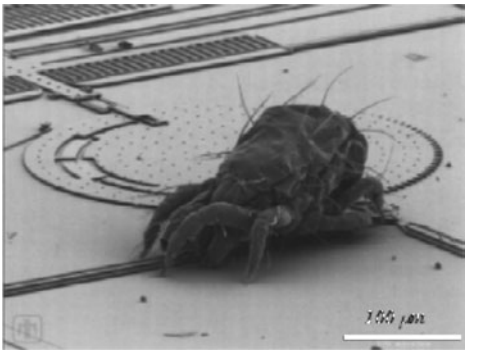

Figure 1.17 A mite from New Mexico placed on a micromotor (see the site of Sandia National Laboratories www.sandia.com). The film on the site shows the rotating motor does not eject the mite from the rotor, despite high rotation velocities. The mite's impressive performance can be explained by the scaling laws we are discussing here.

density ρ, placed on a micromotor rotating at a velocity of Ω. In these conditions, the centrifugal force is:

$$F_c \sim \rho \Omega^2 l^4.$$

It is thus not difficult for an insect such as the one shown in Fig. 1.17 to use the adhesion forces proportional to l^2 to cling to the motor. To fabricate the micromotor, this scaling law will allow the development of considerable velocities of rotation without risk of breaking rotating pieces.

We now look into the question of jumping heights of animals. Usually if one considers that muscular force increases proportionally with the square of the size of the animal. The argument is the following: a force is a stress times an area, and the maximum stress the muscle can develop depends on its constituents not on its size. The muscular energy necessary to make a movement of amplitude l is thus proportional to l^3. This quantity must be compared with the potential energy of the jump E_p, which has a value:

$$E_p \sim mgH \sim l^3 H.$$

Comparing the two energies, the height of the jump H is deduced to be on the order of l^0. The height attained is thus independent of the size of the animal. We can thus conclude that, in terms of scaling laws, the flea jumps just as high as the elephant[14].

[14] In passing, we can note that as the muscular force is proportional to l^2, it follows that the ant can only break a water bubble with difficulty. The force that it must exert to counteract capillary forces is on the order of l.

We conclude with the running of animals and the tyrannosaurus problem. The expression for the velocity $v = l/\tau$ of an animal that runs by displacing its feet at an amplitude l over a period of time τ. We assume that the feet function at a frequency near the resonance frequency of the biomechanical system made up of the foot and the knee. We thus have $\tau \sim 1/l$, which implies $v \sim l^0$. Thus, animals all run at about the same speed. This law is verified by orders of magnitude: for a mouse, a man, an elephant and a tyrannosaurus, the maximum attainable speeds are all on the order of ten or so meters per second. The controversy over the speed of tyrannosaurus, and those of other large prehistoric animals, does not have a bearing on orders of magnitude. The controversy is over whether this animal can actually run as fast as a jeep, or if it cannot even surpass the speed of a man. Here, it is necessary to take into account the structure of the joints, the flux involved in supplying the muscles, etc., a subject that we will not deal with here. We thus show several examples illustrating how physical laws governing small insects are different from those governing the macrometric world due to the fact that the force equilibria are different. As a final point we note that scaling laws can also involve exponents that are not fractions: the surface area of exchange of certain important organs involved in metabolism such as the lungs and the intestines have a fractal structure.

1.5.6 **Range of applications of scaling laws**

We have reasoned here using exponents without discussing in detail the physical laws in play. This approach has the advantage of being simple and direct, but at times it leads to conclusions that cannot be applied to microsystems, since the range of scales is shifted with respect to their size. The purpose of this section is to highlight this issue. We consider the problem of mixing in microsystems, and more specifically, the question of knowing whether the agitation of fluids can result in the reduction of mixing time in a microfluidic system. According to Table 1.1, we would expect that in microsystems, diffusion phenomena are much faster than hydrodynamic transport phenomena. A typical hydrodynamic transport time is:

$$\tau_a \sim \frac{l}{U} \sim l^0,$$

where, as has been the case throughout this chapter, l is the characteristic scale, and U is a typical speed. The molecular diffusion time is expressed as:

$$\tau_d \sim \frac{l^2}{D} \sim l^2,$$

where D is the diffusion coefficient. For miniaturized systems, and if we work things out using only exponents, we expect to have $\tau_a \gg \tau_d$ because the exponent for the transport time is equal to zero, while the exponent associated with diffusion time is equal to two. Given that the effect of molecular diffusion is to mix, we could conclude that in microsystems it is useless to agitate the fluid in order to accelerate the mixing process. However, in practice, such a conclusion would be extreme once actual numerical values are considered. Examine the more complete expressions for the two preceding characteristic times. Their ratio is a dimensionless number, the Peclet number:

$$Pe = \frac{\tau_d}{\tau_a} = \frac{Ul}{D}.$$

To illustrate its significance, we consider the case of fluorescein mixed with water in a volume of 100 μm, flowing at a rate of 30 μm/s. In such a situation, the Peclet number is: $Pe \approx 10$. This elevated value suggests that diffusion phenomena are acting much more slowly than hydrodynamic transport phenomena, a result contrary to that suggested by only examining the exponents of the terms. For mixing, we can see that the conditions under which a reduction in scale is sensible are those given by $Pe < 1$; in the previous example, this would necessitate a reduction of the volume dimensions by an order of magnitude in order to satisfy this criteria. Thus, in several situations, it is important to rationalize using physical laws in their more detailed form to ensure that the effect of miniaturization is significant within the range of dimensions on the order of ten or a hundred micrometers, which are the scales normally used in microsystems.

1.6 Miniaturization of electrostatic systems

1.6.1 Dielectric breakdown is retarded in miniaturized systems

The phenomenon of sparks between two electrodes originates from the fact that, when subjected to an intense electric field, gas molecules situated between two electrodes are ionized, thus forming a plasma. Ionization is propagated little by little by a cascade phenomenon: in such a process, a large number of electrons are liberated, and an intense electric current can circulate between the two electrodes. This current is accompanied by a luminous emission that gives rise to the phenomenon of the electric arc. In air, under normal conditions, the breakdown electric field strength is on the order of 30 kV/cm, which is generally considered to be a reference value.

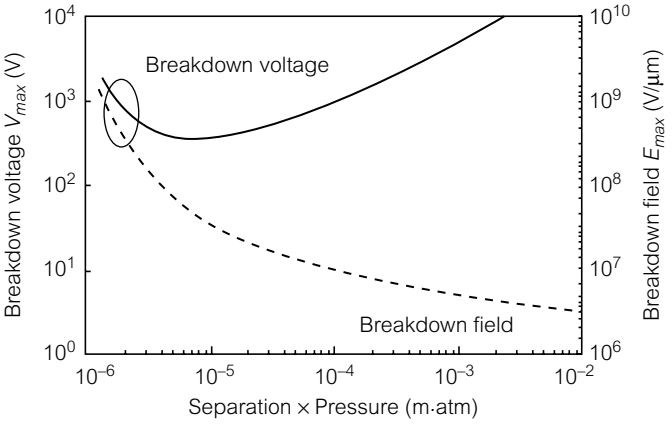

Figure 1.18 'Paschen curve': evolution of the potential difference and electric field strength of dielectric breakdown for a parallel-plate capacitor as a function of the product pressure × distance between electrodes; the curve is obtained in air.

In miniaturized systems, it is remarkable that much higher electric fields can be produced without the generation of an electric arc. This phenomenon is due to an effect of rarefaction that we will mention again in Chapter 2 under another form, pertaining to gas flows in microcanals. This effect is well represented by the Paschen curve, depicted in Fig. 1.18.

The Paschen curve represents the dielectric breakdown voltage between two electrodes, measured in air. This curve is shown along with the electric field, and is traced as a function of the pressure–distance product. We see that at large values of pressure × distance, the breakdown electric field strength E_d is:

$$E_d = 30\ \text{kV/cm}.$$

The curve shows that at small values of this product, the breakdown electric field strength increases significantly. This phenomenon is related to the fact that at small values of the pressure × distance product, the mean free path of the gas is on the order of the size of the system[15]. When the mean free path becomes comparable to the distance between electrodes, the majority of molecular collisions tend to take place between the gas and the surface, and not within the gas itself. This situation inhibits the formation of the cascade process and consequently makes it more difficult for an electric discharge to form in the gas.

[15] Under normal conditions in air, the mean free path is 61 nm. This value, much smaller than distances appearing on the figure, is nonetheless sufficiently high to induce a change of regime.

1.6.2 **Miniaturization of capacitors**

Many systems use miniaturized parallel-plate capacitors. We will consider this type of device as a prototype to establish the scaling laws involved in electrostatics. The electrostatic energy W_e stored by a parallel-plate capacitor is written:

$$W_e = \frac{1}{2}CV^2 = \frac{\epsilon_0 SV^2}{2d},$$

where C is the capacitance, S is the surface area of the plates, ϵ_0 is the dielectric constant, V is the voltage applied on the edges of the capacitor, and d the distance between plates. The forces used to displace one of the plates result in a gradient of this energy. For example, a displacement normal to the plane of the capacitor necessitates a force equal to:

$$F = -\frac{\delta W_e}{\delta z} = \frac{\epsilon_0 SV^2}{2d^2} \sim \epsilon_0 E^2 l^2$$

(z being an axis perpendicular to a plate), where E is the electric field created in the capacitor. In terms of scaling laws, and considering that the electric field strength is comparable to the breakdown field strength[16], we find that the energy varies as l^3, and the force as l^2. We have at our disposal an estimation of the *maximum* forces that can release an electrostatic system of a given size. This force could be compared to that which supplies, for example, the coupling of a current and a magnetic field. It seems in all cases that electrostatic forces are dominant over gravitational forces and inertia (which vary as l^3); there is thus no difficulty in exerting rapid accelerations in microsystems with the aid of electric fields. Such systems could promisingly be used as accelerometers (their weak inertia allows for the detection of sudden impacts, such as those involving automobiles).

1.6.3 **An electrostatic microactuator**

The possibility of creating elevated electric fields has led to the creation of a large number of electrostatic actuators. Figure 1.19 shows a simplified actuator, detailed in reference [28].

Here we have a beam and a base subjected to an electrostatic potential, thus forming the two plates of a capacitor. $f(x)$ is designated as the density of electrostatic attraction force (per unit surface) evaluated at the position x.

[16] Taking the preceding paragraph into account, it would be good to include a discussion on the phenomenon of the inhibition of electric breakdown in microsystems, though we do not introduce this aspect here.

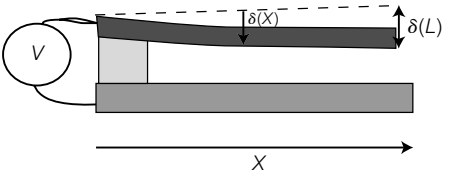

Figure 1.19 A cantilever beam, where the beam and the substrate are conductive. The beam is subjected to an electrical potential difference V, creating an actuator.

The expression of the density of force $f(x)$ can be obtained from the electrostatic force, given in section 1.6.2. We obtain:

$$f(x) = \frac{\epsilon_0}{2}\left(\frac{V}{d-\delta(x)}\right)^2,$$

where V is the applied voltage, ϵ_0 is the dielectric constant of the vacuum, d is the distance between the beam and the plate for $x = 0$, and $\delta(x)$ the deflection of the beam at the abscissa x (Fig. 1.19).

This force produces a deflection $\delta(x)$, which is controlled by a local elastic equilibrium, given by the relation:

$$\mathrm{d}\delta(x) = \frac{x^2}{6EI}(3L - x)wf(x)\mathrm{d}x$$

where E is the Young's modulus of the beam, I is its moment of inertia, L is its length and w is its width. We recall the expression of the moment of inertia of a beam of width w and thickness h:

$$I = \frac{1}{12}wh^3.$$

To determine the deflection at the end of the beam, one must integrate this equation. The profile of the beam is governed by the equation:

$$\delta(x) \approx \left(\frac{x}{L}\right)\delta(L).$$

This permits the determination of the relation between the total force F applied on the beam, and its relative maximum deflection given by:

$$\Delta = \delta(L)/d.$$

The calculation gives, in the limit of small deflections:

$$F = \frac{\epsilon_0 wL^4V^2}{2EId^3} \approx \frac{4\Delta}{3}.$$

In terms of scaling laws, we see that the relative deflection Δ is expressed as:

$$\Delta \sim \frac{V^2}{l^2},$$

which shows that it is possible to obtain significant displacements by miniaturizing while maintaining a fixed potential difference (assuming that the breakdown field is not surpassed). This possibility, illustrated in the case of an extremely simple electrostatic actuator, is actually used in a large number of MEMS.

1.6.4 **The electrostatic micromotor**

The electrostatic micromotor is an example of a sophisticated and remarkable electrostatic actuator. An electrostatic micromotor made using MEMS technology is represented in Fig. 1.20a, and a diagram of its operating principle is shown in Fig. 1.20b.

The force produced by such a motor is:

$$F = -\frac{V^2}{2R}\frac{\partial C}{\partial \theta},$$

where R is the radius of the rotor, V is the applied voltage, C is the capacitance of the rotor/stator and θ is the angular variable. The arrows in Fig. 1.20 indicate that the stator produced a rotating field. The shaded areas of the rotor represent an inhomogeneity of the dielectric constant of the materials making up the rotor. The principle of how this motor functions lies in the fact that the rotor will try to align the region with the strongest dielectric constant with the regions with the strongest electric field. Since the field is rotating, the rotor will tend to follow the maxima of the field, and will thus begin to turn. To analyse the functioning of the motor, the forces in play must be averaged along the angular coordinate, taking into account the fact that the electrostatic field produced by

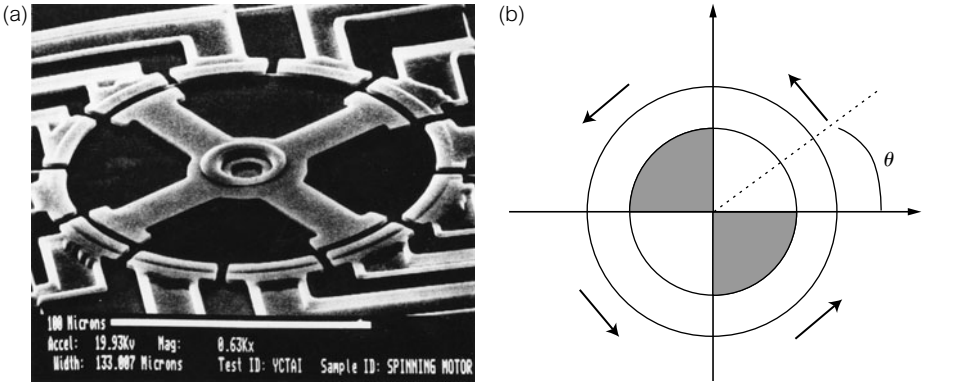

Figure 1.20 (a) First micromotor created in 1988 by Fan *et al*. [29]. The rotor has a diameter of 200 μm. (b) Diagram of the operating principle of an electrostatic motor. (photo courtesy of Richard S. Muller)

the stator is a rotating field. We will not perform this analysis, which is necessary for a more detailed comprehension of the system; we will instead reduce the calculation considerably by using scaling laws[17]. Using these scaling laws, the force is proportional to l^2, while the couple supplied by such a motor is proportional to l^3. Practically speaking, couples are produced on the order of nano- or piconewtonmeters, powers on the order of the microwatt, for thousands or tens of thousands turns per minute. Generally speaking, it is advantageous to envisage rapid rotations in order to produce significant power. Impressive devices are currently being created, including ones that function at several million turns per minute. One example is the turbine recently developed at MIT [30]. The objective here is to fabricate a millimetric microturbine that functions at 2.4 million turns/minute and produces 20 W with a yield of a few tens of per cent. A turbine like this, when put into rotation by combustion gases, would allow the conversion of chemical energy into mechanical and electric energy. We return here to the theme of miniaturization of energy sources, an extremely important subject in the field of MEMS.

1.7 **Miniaturization of electromagnetic systems**

We consider two conducting loops separated by a distance l, through which a current I passes (see Fig. 1.21).

Here, we assume that the cross-section of the wire carrying the electric current has a size comparable by order of magnitude to the diameter of the microcoil producing the magnetic field. This hypothesis can seem astonishing for a system of macrometric size: normally, the electromagnetic coils have cross-sections of

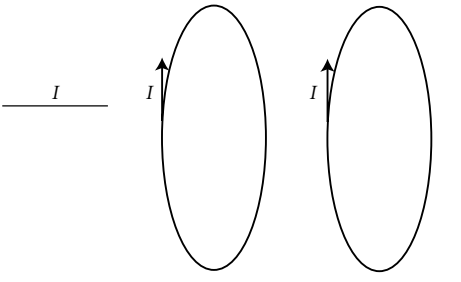

Figure 1.21 Diagram representing two conducting loops of characteristic size I, through which a current I passes, separated by a distance $O(l)$, i.e. a length on the order of l.

[17] This constitutes both the strength and the weakness of rationales based only on using orders of magnitude.

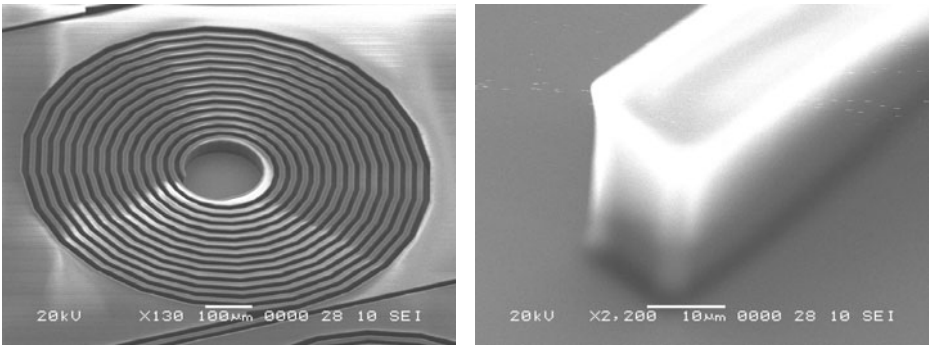

Figure 1.22 Microcoil created by the group of Fujita [31]. The figure on the right shows a conducting cross-section forming the microcoil.

wire that are much smaller than the diameter of the coil. This hypothesis is natural, however, for the microcoils created using microfabrication techniques presented in Chapter 6. An example is given in Fig. 1.22.

Thus, the magnetic field B produced by N turns is:

$$B \sim N\mu_0 jl$$

(this expression can be obtained in a variety of ways, for example by using Ampere's theorem). Here j is the current density, which we will consider to be fixed. We also deduce from this that the magnetic energy is:

$$E_{\mathrm{m}} \sim \frac{B^2}{\mu_0} l^3 \sim j^2 l^5.$$

These expressions show that it is difficult to produce elevated magnetic fields by miniaturizing standard electromagnetic elements, such as the coils. For a system with a size of 100 µm the maximum magnetic field that can be reasonably produced (without excessive heating) is on the order of 100 mT, which in a large number of situations would be considered to be a weak level of induction. This is a difficulty hampering the development of miniaturized electromagnetism for microsystems. For the forces between coils, we have:

$$F \sim jBl^3 \sim j^2 l^4.$$

We obtain the exponent from the scaling law table presented above. Consider also the case of a coil immersed in a fixed magnetic field, produced for example by a system of decimetric size. In this case, we determine the force applied on the coil using the law of Laplace

$$F \sim IBl \sim jBl^3,$$

where B is the magnetic field assumed to be constant. We see here that the force varies as l^3 if one performs the analysis at a fixed current density. In all cases, whether using a magnetic field produced locally or from the exterior, the exponents of the electromagnetic forces are higher than those associated with electrostatic forces[18].

To illustrate these calculations, we proceed to a comparison between electrostatic and electromagnetic microactuators. We recall the expression for electrostatic forces for a parallel-plate capacitor:

$$F \sim \epsilon_0 E^2 l^2,$$

where E is the breakdown electric field. For an electric field of 30 kV/cm and a device of 10 μm, we obtain:

$$F \sim 10 \text{ nN}.$$

For an electromagnetic system containing N coils in series, we have the following order of magnitude for the force:

$$F \sim \mu_0 N j^2 l^4.$$

Taking $N = 100$ coils, $j = 10^7$ A/m^2 and $l = 10$ μm, we obtain the following order of magnitude for the force exerted between two microcoils:

$$F \sim 100 \text{ pN}.$$

We verify, as would have been predicted using scaling law rationale, that the force produced by the microcoils is far less than that produced by a capacitor device. At which scale do electrostatic forces become dominant with respect to electromagnetic forces? We consider two 'prototypic' situations chosen arbitrarily: the case of the parallel-plate capacitor and that of mutually coupled coils. Re-examining the expressions established above, the scale that we find is on the order of a few hundred micrometers. More generally, we allow that ten or so micrometers correspond to the physical limit beyond which electrostatic forces begin to dominate over electromagnetic forces for optimized devices (which we have not considered here). Reference [28] presents a detailed discussion on this subject.

[18] We note that, in principle, it is possible to augment the current density in conductors, by maintaining (as we will see later) intense thermal exchanges in miniaturized systems. This possibility has not resulted in a definite answer, and the discussion is still open [28].

1.8 Miniaturization of mechanical systems

1.8.1 Microbeams resonate at elevated frequencies

A cantilever beam possesses a resonance frequency determined by the following relation:

$$f \approx \frac{hc}{2\pi L^2},$$

where h is the thickness of the beam, L is its length, and c is the speed of sound in the beam. This expression is obtained by resolving the elasticity equation. In terms of scaling laws, we have the relation $f \sim l^{-1}$. This law can be directly obtained by noting that an acoustic wave associated with the mechanical resonance has a wavelength on the order of the size of the object. We thus have the relation:

$$f \sim \frac{c}{l},$$

which corresponds to the expression deduced from the preceding formula.

The scaling law obtained here shows that the resonance frequency of a mechanical system increases as the size of the system diminishes. This characteristic is used to make resonators used in the domain of radiofrequency. Figure 1.23 shows an example of one particular setup for a miniaturized resonator, and Fig. 1.24 presents a recent creation obtained using MEMS technology [32].

In terms of orders of magnitude, we have for silicon:

$$c \approx 7470 \text{ m/s}.$$

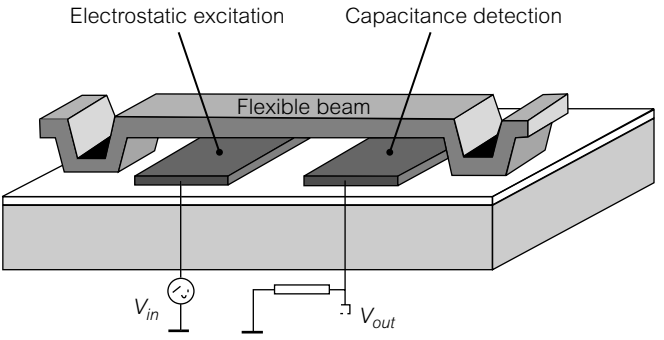

Figure 1.23 Diagram showing a mechanical resonator energized by an electric field. The material used for this mechanical resonator must be piezoelectric.

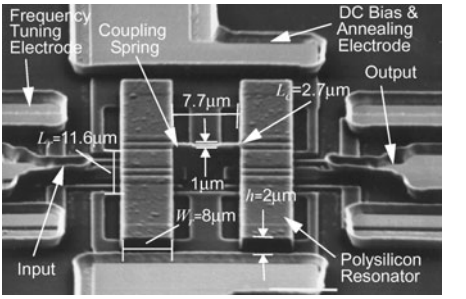

Figure 1.24 A resonator functioning at 75 MHz, made with silicon at the University of Michigan [32].

Thus, for a beam 1 μm thick and 3 μm long, the formula given above leads to:

$$f \approx 100 \text{ MHz}.$$

Such a value is well suited for the field of radiofrequency.

We recall the definition of a quality factor, generally denoted as Q, for a system similar to a dampened oscillator. Such a system is governed by the following differential equation:

$$m\frac{d^2x}{dt^2} - b\frac{dx}{dt} - kx = 0,$$

where m is the mass of the spring, b is the attenuation coefficient, and k is the spring constant. For this type of system, the quality factor is:

$$Q = \omega_0 \frac{m}{b},$$

where ω_0 is the resonance frequency defined by:

$$\omega_0 = \sqrt{\frac{k}{m}}.$$

The quality factor characterizes the shape of the resonance curve. The form of such a curve is effectively given by the expression:

$$a(w) = \frac{1}{\sqrt{\left(1 - \frac{\omega^2}{\omega_0^2}\right)^2 - \frac{\omega^2}{Q^2\omega_0^2}}}.$$

The width of the resonance curve is thus directly related to the value Q: this width (calculated at mid-height, i.e. for a value of $a(\omega)$ equal to $\frac{1}{2}$), is in effect on the order of the inverse of Q. Thus, the higher the Q, the smaller the resonance. The factor that limits Q is, in this presentation, the friction represented by the coefficient b.

In the case of the vibrating beam, an equation analogous to the dampened oscillator can be established. In this case, the variable x is the maximum deflection of the beam, the damping factor b is proportional to the viscosity of the surrounding fluid, and the spring constant k is a function of the Young's modulus of the material and the geometrical characteristics of the beam.

For a cantilever beam, the quality factor (for regimes of non-rarefied gas) is estimated by the expression [28]:

$$Q = \frac{\sqrt{E\rho}wh^2}{24\nu L^2},$$

where ν is the kinematic viscosity of the gas and E is the Young's modulus of the material forming the beam. This law is not very favorable when the quality factor decreases with the scale. However, in practice, quality factors of ordinary microresonators can attain elevated values (on the order of 1000). The law obviously encourages operation in a vacuum, where the highest quality factors are obtained (between 10^4 and 10^5).

1.8.2 Thermal noise limits the quality factor of microresonators

It is instructive to calculate, for a cantilever beam, the displacement induced by thermal noise. This calculation provides a good example of a phenomenon of insignificant amplitude in systems of decimetric size; yet the importance of this phenomenon becomes considerable in miniaturized systems.

At thermodynamic equilibrium, elastic energy balances thermal (according to the equipartition theorem). We thus have:

$$\frac{1}{2}k < \delta^2 > = \frac{1}{2}k_B T,$$

where δ is the displacement of the beam, k is the constant recalling the mechanical system (that we again compare to a spring), k_B is the Boltzmann constant, and T is the temperature. We then show that this equation leads to the following expression for the 'thermal' displacement δ:

$$\delta \approx \sqrt{\frac{2k_B TL^3}{Ewh^3}},$$

where E is Young's modulus, L is the length, h is the thickness and w is the width of the beam. In terms of scaling laws, we thus have the following relation:

$$\delta \sim l^{-1/2}$$

which shows that the more we miniaturize, the larger the thermal displacement. From a numerical point of view, the thermal displacement for a silicon beam of 1 μm is on the order of a picometer. This is a very small displacement, but it is enough to limit achieving high quality factors for microresonators.

1.9 Miniaturization of thermal systems

Heat transfers by conduction are governed by the Fourier equation, which is written:

$$q = -K\nabla T,$$

where K is the thermal conductivity of the medium, T is the local temperature, and q is the heat flux, i.e. the quantity of heat traversing a surface element per unit surface (the units of q are thus energy per unit time and surface). The flux density varies as the inverse of the scale, at a fixed temperature difference. A typical situation is a bar thermally isolated on the sides, and whose ends are in contact with two thermostats that impose a temperature difference $\Delta T = T_2 - T_1$ (Fig. 1.25). Under these conditions, the heat flux going through such a bar is written:

$$Q = \frac{KS\Delta T}{l},$$

where S is the cross-sectional area of the bar, and l is its length. The following scaling law comes from this:

$$Q \sim Kl\Delta T,$$

which governs the heat flux. This law corresponds to the law shown in the general scaling law table, with the assumption that the temperature difference is fixed.

We now suppose that there exists in the bar sources of volumetric heat: we cite for example a Joule heating effect (if the bar is a conductor of electricity, and subjected to an electromagnetic field), or heating from a chemical origin (if the bar is the site of exothermic reactions). In both these cases, we can consider that the heat produced by a volumetric source is:

$$Q_v \sim l^3,$$

which represents an exponent much higher than that associated with heat evacuated by conduction. We can thus conclude that volumetric heat sources can be easily thermalized in miniaturized systems. One example of a microexchanger currently on the market is shown in Fig. 1.26.

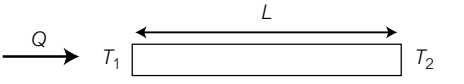

Figure 1.25 Diagram representing a bar carrying a heat flux Q, with notations used in the text.

Figure 1.26 Microexchangers on chip, commercialized by the company Ehrfeld Microtechnik. Their size is comparable to a euro.

It is interesting to consider this from a dynamic point of view: the heat flux (stored or dissipated) associated with a temporal variation of temperature $\mathrm{d}T$ and a time $\mathrm{d}t$, is governed by the following relation:

$$q = \rho C_{\mathrm{p}} \frac{\mathrm{d}T}{\mathrm{d}t},$$

where ρ is the volumetric mass, C_{p} is the specific heat at constant pressure, and t is the time. Thus the order of magnitude of the time constant of thermalization associated with an object of dimension l is written:

$$\tau \sim \frac{\rho C_{\mathrm{p}}}{K} l^2 \sim \frac{l^2}{\kappa},$$

where κ is the thermal diffusivity of the environment under consideration. Consistent with the preceding remarks this expression shows that miniaturization considerably accelerates the return to thermal equilibrium of the bulk subjected to a sharp temperature change. In other words, miniaturization radically reduces the significance of the phenomena of thermal inertia. The preceding logic shows that exo- or endothermic chemical reactions can in principle be finely thermalized in microsystems. This characteristic is very useful for chemical engineering. In general, temperature exchangers currently used by industrial reactors tend to develop unwanted parasite reactions. These reactions limit the 'selectivity' of the

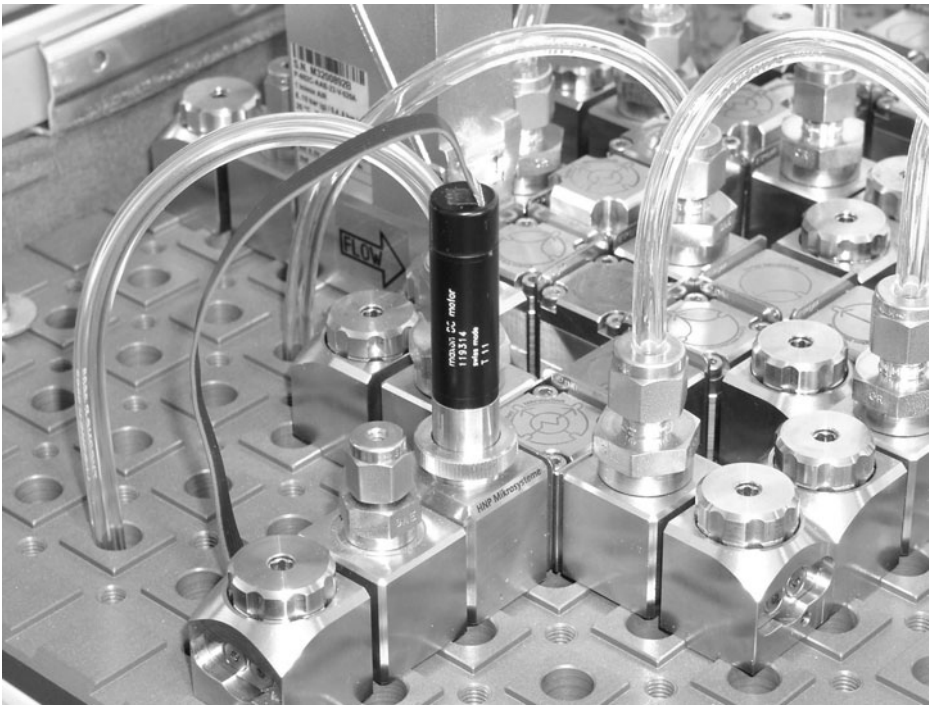

Figure 1.27 Microreactors commercialized by the company Ehrfeld Microtechnik. In the photo, they are assembled with other elements (microexchangers, microfilters, etc.) in such a way as to create a chemical microfactory. The side of an Ehrfeld cube has a measurement of about 2 cm. This system is more a matter of mini-space rather than microfluidics.

process. There are also reactions, impossible to use industrially, that can inherently control thermal conditions. For these types of systems, miniaturization offers a source of important improvements. Companies such as Ehrfeld have proposed the building of microreactors that can complete chemical engineering processes (Fig. 1.27).

1.10 Miniaturization of systems for chemical analysis

In the following chapters we will describe several physico-chemical transformations that take place in laboratories on chip. Here, we mention two physical problems in miniaturized systems of analysis that can present themselves during sampling, detection, and post-treatment.

1.10.1 **Microdroplets evaporate rapidly**

Microsystems are often closed systems, communicating with the exterior world indirectly via sensors and microfluidic connections. We can imagine inserting access to the outside world in different places in these systems. These could be, for example, a microcanal used to transport chemical reactants that is connected to chambers open to the exterior. When such a system is created, different problems arise. Evaporation of liquid is one of these problems. The evaporation of a drop of diameter d at time t is governed by the 'D^2 law' which reads:

$$d^2 = d_0^2 - \beta t$$

in which d_0 is the initial diameter, and β is independent of the drop size. The time τ it takes for the drop to disappear is thus:

$$\tau = \frac{d_0^2}{\beta} \sim l^2$$

Miniaturization thus favors rapid evaporation of droplets, and this phenomenon must be taken into account when droplets form in microsystems, whether or not they are destined for chemical use.

1.10.2 **Is there even a molecule in the chamber?**

One question poses itself for components present in weak concentrations in a given sample: is there a sufficient number of molecules to transfer into the analysis microchamber for detection? We calculate a few orders of magnitude: the volume containing an isolated molecule is given by:

$$v = \frac{1}{CN_A},$$

where C is the concentration of the chemical species in consideration and N_A is Avogadro's number. Thus, for a chamber with a side of 10 μm, the minimum concentration providing one molecule per analysis chamber is on the order of 10^{-12} mol/L. It is not certain that such a level is reached when the component to be analysed is presented in trace form. The problem is presented differently for DNA, because it is possible to use an amplification step (PCR) before analysis in a microsystem. For other molecules, amplification is not generally possible, and it is often necessary to apply a concentration step before detection. Here we come across many methods well known in the field of chromatography.

References

[1] J. Israelachvili, *Intermolecular and Surfaces Forces*, Academic Press, 2nd edn, 1991.

[2] J. Israelachvili, *Chemtracts-Anal Phy. Chem.*, **1**, 1 (1989).

[3] D. Tabor, *J. Colloid Interf. Sci*, **58**, 2 (1977).

[4] C. Tabor, R. Winterton, *Proc. R. Soc. Lond. A*, **312**, 435 (1969).

[5] E.M. Lifschitz, *Soviet Phys. JETP (Eng. Transl.)*, **2**, 73 (1956).

[6] B. Cabane and S. Hénon, *Liquides. Solutions, Dispersions, Émulsions, Gels*, Belin, 2003.

[7] H. Taunton, C. Toprakciaglu, L. Fetters, J. Klein, *Macromolecules*, **23**, 571 (1990).

[8] Jacobson, Alarie, Ramsey, *Proc. μTAS*, 608 (2002).

[9] G. Karniadakis, A. Beskok, *Micro Flows*, Springer Verlag, 2002.

[10] In the 1990s, S. Chu made the first observations of the conformation of strands of elongated DNA at the intersection of two microcanals. One more recent reference is Smith, D., Chu, S., *Science*, **281**, 1335 (1998).

[11] C.J. Kim, *Proc. Symp. Micromachining and Microfabrication*, **4177**, Sant-Khandurina, R. Foote, J. Ramsey, *Anal. Chem.*, **70**, 158 (1998).

[12] N. Crisona, T. Strick, D. Bensimon, V. Croquette, N. Cozarelli, *Gene Dev.*, **14**, 22, 2881 (2000).

[13] C. Li, D. Harrison, *Anal. Chem.*, **69**, 1564 (1997).

[14] F. Morin, M. Denoual, L. Griscom, B. LePioufle, J. Fujita, E. Tamiya, *Proc. μTAS*, 515 (2002).

[15] P. Renaud, U. Seger, S. Gawad, *Proc. Nanotech 2002*, Montreux (2002).

[16] D. Smith, H. Babcock, S. Chu, *Science*, **283**, 1724 (1999).

[17] S. Lee, Y. Tai, *Sens. Actuators*, **73**, 74 (1999).

[18] T. Lehnert, R. Netzer, U. Bischoff, M. Gijs, *Proc. Nanotech 2002*, Montreux (2002).

[19] A.Y. Fu, H.P. Chou, C. Spence, G.H. Arnold, S.R. Quake, *Anal. Chem.*, **74**, 2451, (2002).

[20] E. Altendorf, Zebert, M. Holl, A. Vannelli, C. Wu, C. Schulte, *Proc. μTAS*, 73 (1998).

[21] J.R. Hutchinson, M. Garcia, *Lett. Nature*, **415**, 1018 (2002).

[22] A.Y. Fu, C. Spence, G.H. Arnold, S.R. Quake, *Nature Biotechnol.*, **17**, 1109 (1999).

[23] E. Guyon, J.P. Hulin, L. Petit, *Hydrodynamique Physique*, CNRS Edition, 2nd edn, 2001.

[24] Q. Wang, A. Desai, Y. Tai, L. Licklider, T. Lee, *Proc. MEMS* Orlando, 523 (1999).

[25] T. Wang, S. Masset, C.M. Ho, *Proc. MEMS 2001*, Interlaken, 431 (2001).

[26] Galileo Galilei, *Dialogue Concerning Two New Sciences*, 1638.

[27] D'Arcy Thompson, *On Growth and Form*, revised version, Camb. Univ. Press (1942).

[28] G. Kovacs, *Micromachined Transducers*, WCB, McGraw Hill, 1998.

[29] L.C. Fan, Y.C. Tai, R.S. Muller, *IEEE Trans. Electron. Devices*, **ED-35**, 6, 724 (1988).

[30] C.M. Spadaccini, X. Zhang, C.P. Cadou, N. Miki, I.A. Waitz, *Proc. MEMS 2002*, 228–232 (2002).

[31] L. Houlet, G. Reyne, T. Iizuka, T. Bourarina, E. Dufour-Gergam, H. Fujita, SPIE International Symposium on Microelectronics and Micro-Electromechanical Systems, Adelaide (Australia), **4592**, 17–19, December 2001.

[32] A-C. Wang, J.R. Clark, C.T.-C. Nguyen, *Digest of Technical Papers*, 10th International Conference on Solid-State Sensors and Actuators, Sendai (Japan), June 1999.

TWO

Hydrodynamics of microfluidic systems

2.1 Introduction

Circulating a fluid through a canal only a few micrometers wide, transporting a 10-micrometers long droplet with the aid of a liquid, and using shear to deform a bubble 100 micrometers in diameter are all situations frequently encountered in the domain of microfluidics. Many of these systems present unique problems in hydrodynamics due to the significant role of surfaces, the presence of Brownian motion, and more generally, the unusual force balances, analogous to those discussed in the previous chapter.

In this chapter we tackle the subject of hydrodynamics in micrometric systems, and we are essentially interested in the correlation between the definition of microfluidics given in the introduction and the actual man-made Newtonian systems. The phenomena of transport and electrokinetics, which are also a part of this field, will be examined in the following chapters.

This chapter is organized in the following manner.

- We will first present the equations of hydrodynamics in the specific context of microsystems, where, as we have seen before, certain 'microscopic' scales can start to compete with the size of the system.
- Secondly, we will concentrate on microhydrodynamics, i.e. hydrodynamics at small Reynolds numbers.
- Thirdly, we will tackle systems operating at moderate Reynolds numbers, which is the case for certain microsystems.
- Then, we will present capillary and wetting phenomena both with and without surfactants. This section will justify the importance of the surface-to-volume ratio in microsystems.

– Lastly, we will tackle diphasic systems, which will be used in the future to control the formation of droplets and emulsions.

This chapter does not deal with non-Newtonian fluids. Although these fluids could be significant for some microsystems [1], at this point in time, their usage is scarce in the domain of microfluidics.

2.2 Hypotheses of hydrodynamics

2.2.1 The notion of the fluid particle

Hydrodynamics are governed by equations obtained using hypotheses that are important to remember in the framework of this book. A few useful references include the classic work of Batchelor *An Introduction to Fluid Dynamics* [2], the work of Guyon *et al.*, *Hydrodynamique Physique* [3], as well as the review by Gad-el-Hak entitled *The Fluid Mechanics of Micro Devices* [4]. The first fundamental hypothesis is that of the continuum, illustrated in Fig. 2.1, borrowed from the work of Batchelor [2].

At small scales spatial fluctuations in density take place due to the molecular structure of the fluid; while at the scale of the system, density can evolve with respect to the spatial co-ordinates, the presence of temperature variations, or the presence of inhomogeneities in the system. We are thus led to define a 'fluid particle' associated with a 'mesoscopic' scale, which is located on the plateau of the preceding figure. If such a plateau exists, it becomes possible to establish

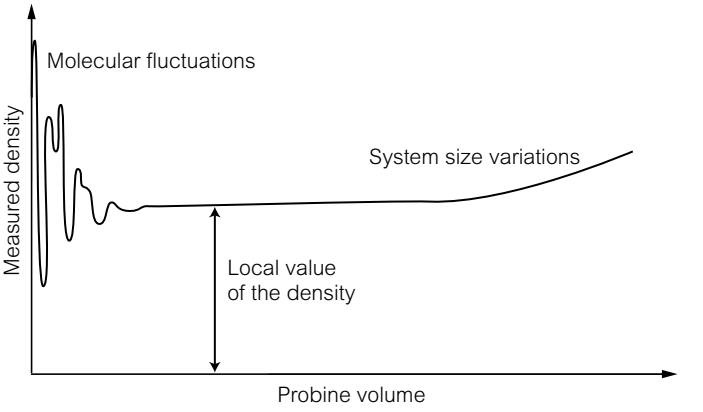

Figure 2.1 Curve schematically representing the variation of the instantaneous density of the fluid particle with respect to its volume. Figure extracted from the text of Batchelor [2].

equations of fluid flow assuming a continuous medium; in addition to this, the obtained equations will have a local character.

It is in this manner that the 'ordinary' hydrodynamic equations are obtained.

How is the fluid particle of a liquid defined? For this material state, the fluid particle is a volume containing a large number of molecules. For the simple liquids presented in the preceding chapter, such as alkanes, one can consider the fluid particle to have a size of a few nanometers. The fluid particle in this case will thus typically be much smaller than a microcanal, and the fundamental hypothesis of hydrodynamics that we are discussing here can be applied without difficulty. For nanocanals with a tranverse dimension of just a few tens of nanometers, this situation obviously must be re-examined. In this case we enter into the domain of nanofluids, a field that even today is only marginally explored. If the liquid is a polymer melt, the situation becomes more complex, and the reader can refer to the abundant literature for more information. We will not discuss this particular case, which would necessitate significant detail.

For a gas, the mean free path is the best estimate of an interaction length scale. Thus, the fluid particle of a gas is a volume incorporating a large number of mean free paths[1]. It is useful to recall the formula giving the expression for the mean free path λ for a gas:

$$\lambda = \frac{1}{\sqrt{2}\pi n a^2} = \frac{kT}{\sqrt{2}\pi p a^2},$$

where n is the density (the number of molecules per unit volume), T is the temperature, k is the Boltzmann constant, p is the pressure and a is the size of the molecule.

We noted in Chapter 1 that the mean free paths of gases are on the order of 100 nm, a length only 10 times smaller than the micrometer: thus, the fluid particle of the gas must have a size comparable to the size of the microsystem. This kind of situation is not new in physics. Gas flows whose mean free paths are comparable (by order of magnitude) to the size of the system are frequently studied: this is the domain of rarified gases, situations where the pressure is so weak that the mean free path becomes very large (see the preceding formula). There are well-established results in this area that will be referenced in this chapter.

[1] For gases, Batchelor suggests using a volume of 10 μm cubed, enclosing 3×10^{10} molecules at atmospheric pressure. However, it is clear that in the framework of this particular text, such a suggestion must be reconsidered.

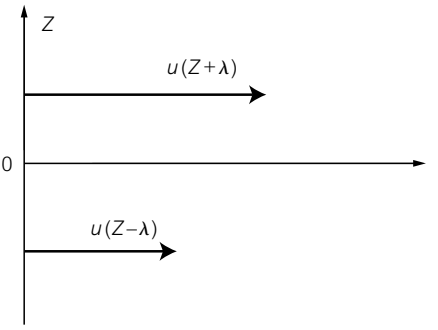

Figure 2.2 Figure representing two streamlines in a gas, separated by two mean free paths, and moving at two different velocities.

2.2.2 **The notion of viscosity**

For gases, one physical representation of viscosity is that of two trucks filled with sacks of coal, circulating around at slightly different velocities. The drivers continually exchange sacks between the two trucks. Due to the exchange of momentum, the two trucks will have a tendency to adopt identical speeds, just as if they exerted a 'friction' force on one another. Such is the physical interpretation of viscous forces in gases. The kinetic theory of gases permits an estimation of viscosity. To perform the calculation, we consider two layers of gas separated by two mean free paths, as diagrammed in Fig. 2.2.

A particle situated on line $z = 0$ travels a distance λ before experiencing a collision. Once the particle has travelled $z = \lambda$, it collides and exchanges momentum with a neighboring particle, thus modifying its velocity. On average, the particle emitted from the line $z = 0$ will tend to speed up when displaced towards the more rapid layers, and to slow down when displaced towards the slower layers. Calculating the difference in impulse flux between layers located at $z - \lambda$ and $z + \lambda$, the estimation of the tangential stress for a three-dimensional system can be obtained from the environment, on the plane $z = 0$:

$$\tau = \frac{1}{6}\rho u_{\text{therm}}(u(z+\lambda) - u(z-\lambda)),$$

where ρ is the gas density and u_{therm} is the thermal agitation velocity. This stress is equal to the viscous stress:

$$\tau = \mu \frac{\partial u}{\partial z}.$$

Using a Taylor series expansion, we finally obtain the coefficient of viscosity μ, which is given by the relation:

$$\mu = \frac{1}{3}\rho u_{\text{therm}} l.$$

This is the expression for the viscosity of gases, which comes out of Maxwell's kinetic theory. Although this expression is not rigorous, it has been well verified experimentally. Under normal conditions, the order of magnitude of viscosities of gases is around 0.15 cm^2/s.

For liquids, the situation is entirely different. Liquids possess the effect of having a certain crystalline order over short distances (smaller than a nanometer) while still remaining disordered over large distances. Molecules must cross an energy barrier to leave from the 'cage' formed by their immediate neighbors, and exchange momentum with a fluid layer moving at a different velocity. The calculation leads to the following form for the viscosity of simple liquids:

$$\mu = A \exp\left(\frac{E}{kT}\right),$$

where A is a constant and E is energy. This reasoning assumes that the idea of viscosity only applies to liquids confined in systems whose size is many times the size of the intermolecular distance, i.e. many times the size of about a nanometer.

Measurements made by Israelachvili [5] on simple liquids showed that the apparent viscosity of a film is equal to the intrinsic viscosity of the liquid once the film has achieved a thickness greater than a dozen molecular layers ($\sim$5 nm); beyond this thickness, the apparent viscosity grows by several orders of magnitudes. The fact that a statistical concept could be applied just as well to systems only containing a moderate number of molecules may seem surprising. Nevertheless, from a practical standpoint these experiments provide useful information for microfluidics: they show that the values in viscosity tables for simple liquids are applicable in micrometric systems. However, these values must be re-examined for canals of only a few dozen nanometers wide. We find here another 'nanofluidic' problem, one that has not yet been thoroughly examined at the time this text was written. From a continuum mechanics standpoint, viscosity is a 'constitutive' parameter relating the mechanical stress tensor to the velocity gradient tensor. The corresponding law is known as 'Stokes' Law,' which defines Newtonian fluids. We thus have as the tensor relation [3]:

$$\sigma'_{ij} = \mu\left(2e_{ij} - \frac{2}{3}\delta_{ij}e_{mm}\right) + \zeta\,\delta_{ij}e_{mm},$$

where σ' is the viscous stress tensor, e_{ij} is the velocity gradient tensor, and δ_{ij} is the Kronecker symbol. The expression of the tensor e_{ij} is written:

$$e_{ij} = \frac{1}{2}\left(\frac{\partial u_j}{\partial x_i} + \frac{\partial u_i}{\partial x_j}\right),$$

where u_i is the velocity component along i and x_i is the corresponding co-ordinate. In the preceding expression, μ is the dynamic viscosity, and ζ is the *second viscosity* or the *volumetric viscosity*. This term disappears from the equations of motion in the case of incompressible fluids, and we will neglect them in the rest of the book.

2.2.3 **Hydrodynamics equations**

The hydrodynamics equations are worked out at length in many works of fluid mechanics. We can again refer here to the work of Batchelor [2]. Here, we will present these equations succinctly.

Assuming the fluid particle is much smaller than the size of the system, and applying the fundamental relation of the dynamics of the material point, we obtain the following equations for fluid motion:

$$\rho \frac{Du_i}{Dt} = F_i + \frac{\partial \sigma_{ij}}{\partial x_j},$$

where ρ is the density, u_i is the velocity component along i, and F_i is the external force component along i unit volume. In this equation, the operator D/Dt is the material derivative, whose expression is written:

$$\frac{D}{Dt} = \frac{\partial}{\partial t} + u_j \frac{\partial}{\partial x_j},$$

where, using Einstein's notation, there is a summation for each repeated index. The preceding equation must be completed by the conservation of mass equation that is written:

$$\frac{D\rho}{Dt} + \rho \frac{\partial u_i}{\partial x_i} = 0.$$

It is now necessary to write a constitutive law between the stresses and the velocity gradients. An important class of fluids are the Newtonian fluids, for whom, as we saw above, the stress tensor is linearly related to the deformation tensor according to Stokes' Law. We thus obtain, for the particular case of Newtonian fluids, the Navier–Stokes equation:

$$\rho \frac{Du_i}{Dt} = F_i - \frac{\partial p}{\partial x_i} + \mu \frac{\partial^2 u_i}{\partial x_j^2},$$

where μ is the dynamic viscosity of the fluid. A more compact form of the Navier–Stokes equation is often used:

$$\frac{D\boldsymbol{u}}{Dt} = -\frac{1}{\rho}\nabla p + \nu\Delta\boldsymbol{u} + \frac{1}{\rho}\boldsymbol{F},$$

where $\nu = \mu/\rho$ is the kinematic viscosity and $\boldsymbol{F}$ is the external force per unit volume. In the same notation, the conservation of mass equation can be written:

$$\frac{D\rho}{Dt} + \rho \operatorname{div} \boldsymbol{u} = 0.$$

It is necessary to note that in 'ordinary' hydrodynamics, the incompressibility hypothesis is often considered to be justified when the velocity of the fluid is much lower than the speed of sound. The speed of sound is on the order of a thousand meters per second, and we are accustomed to considering liquids to be 'intrinsically' incompressible. However, the criterion of incompressibility is actually rather subtle, and only using the Mach number (i.e. the ratio of fluid velocity over sound velocity) to determine compressibility can lead to erroneous conclusions for microfluidics. It is necessary to understand that viscous effects can compel pressure and density to vary substantially in a microsystem, which would make it necessary to treat the flow as compressible, even in the case of liquids. Such a situation is illustrated by the 'bottleneck' effect.

2.2.4 **Reynolds numbers in microsystems**

As we have seen in Chapter 1, the usage of the Π theorem shows that stationary, incompressible flows that are characterized by one single spatial scale l are controlled by a single dimensionless number: the Reynolds number. Its expression is:

$$Re = \frac{Ul}{\nu},$$

where U is the characteristic velocity of the fluid and ν is its kinematic viscosity. What is the value of the Reynolds number in microfluidic systems? In such systems, typical fluid velocities do not exceed a centimeter per second and widths of canals are on the order of tens of micrometers; it follows that, in general, Reynolds numbers in microfluidic systems do not exceed 10^{-1}. As we saw in Chapter 1, we can consider that for scaling laws in a large number of situations, the velocity U satisfies the following law: $U \sim l$. This law is obtained by analysing the flow of a low Reynolds number incompressible Newtonian fluid along a microcanal characterized by the scale l. In such a configuration, the velocity of

the fluid is estimated by the following relation:

$$U \sim \frac{\Delta P l}{\mu},$$

where ΔP is the pressure difference needed to put the fluid in motion. In practice, flow in many microfluidic systems is produced by placing the inlet at higher pressure, or by moving the piston of a syringe. Regardless of how the pressure difference is obtained, the pressure differences ΔP in this situation are on the order of one bar or a fraction of a bar. This value is comparable to that of non-miniaturized systems; it thus seems justified by order of magnitude to treat ΔP as a constant. We thus obtain the following result for such microsystems: the velocity is proportional to the scale:

$$Re \sim l^2.$$

Thus, miniaturization tends to favor low Reynolds numbers. If the fluid motion is produced by an integrated pump, ΔP can no longer be considered independent of scale. However, pressure differences within the system are generally inferior to those produced by external sources. In all cases, whether the pump is external or integrated, the Reynolds number is typically low in microsystems. This is what we could call the low Reynolds number 'rule' for microfluidic systems.

This rule applies well for most of the microfluidic systems of practical interest, though there are exceptions: for example, microheat exchangers with submillimetric channels destined to function at high speeds, or microjets strongly propelled across a micro-orifice develop moderately large Reynolds numbers. As will be seen in Chapter 5, large Reynolds numbers are necessary for microheat exchangers to transfer substantial amounts of heat. In such systems, the driving pump must deliver high pressure drops, and the small Reynolds number rule mentioned above does not apply.

One astonishing effect of compressibility: the bottleneck effect

THE BOTTLENECK EFFECT FOR RIGID SYSTEMS

The bottleneck effect appears in the situation where a piston in a chamber connected to a capillary abruptly puts a fluid in motion (see Fig. 2.3). We consider here the case where the capillary is a microcanal with a rectangular cross-section.

Initially the piston is stationary; it is then abruptly set into motion at a fixed velocity U. The direction of the flow is along x, and the origin $x = 0$ represents the initial position of the piston. The flow in the piston chamber is assumed to be uniform in the plane of the

(Continued)

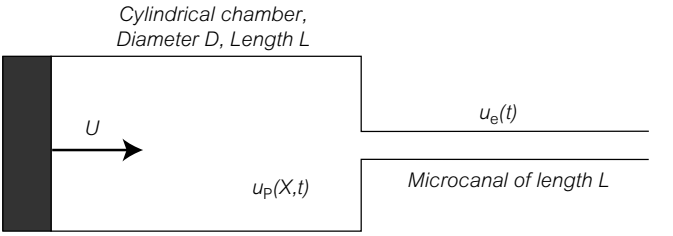

Figure 2.3 Diagram showing the geometry of the bottleneck effect, which is discussed below.

cross-section. Under these conditions, the equations governing the problem are written:

$$\frac{\partial \rho}{\partial t} + \frac{\partial (\rho u_P)}{\partial x} = 0,$$

$$\rho \frac{Du_P}{Dt} = -\frac{\partial p}{\partial x} + \mu \frac{\partial^2 u_P}{\partial x^2},$$

where ρ is the fluid density, μ is its viscocity, u_P is the velocity in the chamber, t is time and p is pressure. Note that we have assumed the fluid to be compressible, even though the velocities themselves are very low with respect to the velocity of sound propagation. Taking compressibility into account is critical for the effect that we are discussing. The compressibility of the fluid can be characterized by the following relation, for liquids:

$$\frac{\partial p}{\partial \rho} = \frac{E}{\rho},$$

where E is Young's modulus. In the Navier–Stokes equation, the inertial term can be neglected at very low Reynolds numbers[2], and we have the following approximation:

$$\frac{\partial p}{\partial x} \approx \mu \frac{\partial^2 u_P}{\partial x^2}.$$

This equation, when integrated and combined with the continuity equation and Young's relation, leads to:

$$p + \frac{\mu}{E} \frac{\partial p}{\partial t} = F(t),$$

where $F(t)$ is a function of time. By orders of magnitude, the time constant μ/E is, for normal fluids like water, on the order of 10^{-12} s. This time constant is extremely rapid with respect to

[2] The Reynolds number can be defined here as UL/ν, where L is the length of the chamber. In the system we are describing, L is on the order of a centimeter and the advance of the piston is very slow, which imply that the Reynolds number can be considered to be very low. In the following sections, it will be evident that when the Reynolds number is low, the inertial terms can, in general, be neglected. We frame our problem within this approximation to perform the calculation.

(Continued)
the evolution of the phenomena described here. We can thus neglect it, and write: $p \approx F(t)$. Thus, pressure and density are uniform in the chamber of the piston. It follows that we can integrate the continuity equation, and obtain:

$$u_P(x,t) = -\frac{1}{\rho}\frac{d\rho}{dt}(x - Ut) + U = -\frac{1}{E}\frac{dp}{dt}(x - Ut) + U.$$

Thus, the velocity of the fluid decreases linearly with the coordinate x in the chamber. The junction with the microcanal takes place at $x = L$. We consider here that the microcanal or the capillary of length l has a rectangular cross-section with width w and height b. At the level of the chamber–microcanal junction, we write the conservation of flow:

$$u_P(L,t) = \frac{4wb}{\pi D^2}u_C(t),$$

where D is the diameter of the chamber. In the capillary, we have the following relation, valid for a slender canal, where the width w is much larger than the height b:

$$u_C(t) \approx \frac{b^2}{12l\mu}p$$

because we have considered here, for the sake of simplification, that the pressure is zero at the exit of the microcanal. These relations can be rearranged into the form of a differential equation:

$$(1 - \alpha t)\frac{dp}{dt} + \frac{p}{\tau} = \frac{UE}{L},$$

where α is equal to U/L, and τ is a time constant whose expression is:

$$\tau = \frac{3\pi l\mu D^2 L}{Ewb^3}.$$

Assuming the product αt is much smaller than 1 (the piston is still far from reaching the end of the chamber), we have the following solution:

$$p(t) \approx p_{inf}(1 - e^{-t/\tau}).$$

Thus, equilibrium is achieved once the time τ, defined above, has been reached. Since τ varies with the inverse of the height of the microcanal to the third power, it is possible that in these microsystems, this time is important. To illustrate, this characteristic time is on the order of several tens of seconds for water pushed down a microcanal that is 1 micrometer high, 100 μm wide and 2 cm long; however, this time would be on the order of hours if this same type of microcanal had a height of 100 nm. It is thus necessary to take the characteristic time into

(Continued)
account when examining flows in ultraminiaturized systems. It is possible to be free of this constant by working at constant pressure, and not at constant velocity or flux; from this standpoint, it is advisable to use pressure sources to put fluids in motion in microcanals rather than to use syringes[3].

THE CASE OF A DEFORMABLE SYSTEM

A transitory effect analogous to the effect discussed above frequently appears in microfluidic systems. This effect causes the degree of elasticity of the tubes making up the microfluidic circuit to become significant. To illustrate this effect, we assume that the chamber of the preceding figure is deformable, and neglect the compressibility of the fluid (we assume E to be infinite). The equations governing the problem are as follows:

$$2\frac{\rho}{D}\frac{\mathrm{d}D}{\mathrm{d}t} + \rho\frac{\partial u_{\mathrm{P}}}{\partial x} = 0,$$

$$\frac{\partial p}{\partial x} \approx 0.$$

We assume here that the diameter D of the chamber varies as a function of time since the system is deformable. A constitutive relation is necessary to complete the equations. We have at our disposal a relation obtained from an elastic deformation calculation, whose form is:

$$\frac{\delta D}{D} = \frac{1}{K}\delta p,$$

where K is a constant that depends on the Young's modulus of the material making up the tube. From this we deduce a differential equation for p, involving a time constant τ' equal to:

$$\tau' = \frac{6\pi l \mu D^2 L}{K w b^3}.$$

In practice, for plastic tubes, this time constant is longer than the one mentioned here. The fluid–structure coupling typically leads to time constants of several hours for canals having a transverse dimension on the order of a micrometer (while the preceding time constant is on the order of minutes) for plastic tubes in which the epoxy glues are exposed to liquid. This situation is illustrated in Fig. 2.4, where data has been obtained for a canal 1.4 μm wide.

It is thus to our general advantage to replace flexible tubes with rigid tubes, and to avoid glues possessing a substantial elasticity when in contact with a liquid. As in the preceding section, it is always possible in principle to avoid this kind of transitory phenomenon by working at constant pressure (and not at constant flow rate).

[3] The bottleneck effect is well known in the domain of chromatography; one can consult, for example, reference [6].

(Continued)

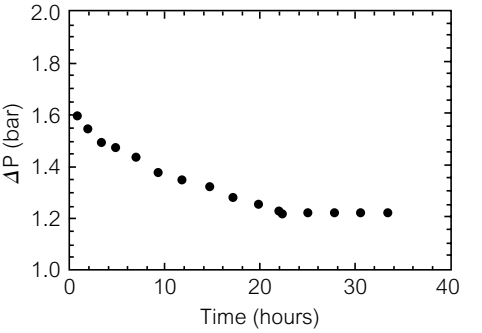

Figure 2.4 Evolution of the pressure drop over time for a flow of hexadecane, carried out in a microcanal 1.4 μm wide [7]. Here, we have greatly reduced the flow rate in the syringe supplying the system from 10 to 3 nl/min. The required duration of time to reach the final state is several hours. This experiment emphasizes the importance of elastic effects in systems of micro- or submicrometric size.

2.3 Hydrodynamics of gases in microsystems

2.3.1 The different regimes of gas flows

We saw in the preceding section that in the context of microsystems, it is not certain that the size of a fluid particle is always insignificant with respect to the system in consideration. To characterize this situation, we introduce a dimensionless number equal to the ratio of the mean free path λ over the characteristic size l of the system. This number is known as the Knudsen number [8], and is defined by the relation:

$$Kn = \frac{\lambda}{l}.$$

The 'ordinary' hydrodynamic equations are applicable at small Knudsen numbers. In practice, three regimes can be defined, which are well detailed in studies such as [9].

- For Knudsen numbers smaller than 0.01, the flow is described by the Navier–Stokes equations.
- For Knudsen numbers between 0.01 and 0.3, we are in the 'slip' regime. The Navier–Stokes equations can be applied to the flow, but at the surface, the gas 'slips': these last molecular layers have a velocity different from that of the

surface. Thus, in this regime, only the boundary conditions must be modified. We will analyse this case in detail later.

– For Knudsen numbers between 0.3 and 10, the 'intermediate' regime can be applied, where the effects of the rarefication of volume start to become significant. In this case, the Navier–Stokes equations must be amended[4].
– Finally, for Knudsen numbers greater than 10, the system is in the regime known as 'rarefied' gases. The Navier–Stokes equations must be abandoned, and the gas must be described by the Boltzmann equations.

It is not rare to find microsystems in the slip regime. In fact, once the canal through which the gas circulates becomes micro- or submicrometric-sized, we easily obtain, under normal conditions, Knudsen number values between 0.01 and 0.3.

2.3.2 **Analysis of slip regimes for gases**

We consider here in detail the case of gas flows in microcanals, which have Knudsen numbers between 0.01 and 0.3, the regime known as the 'slip' regime. In such conditions, we already mentioned that the hydrodynamic equations can be applied, but that the boundary conditions must be changed. Specifically, the gas can 'slip' along the surface. The condition of null velocity at the level of the surface (for a stationary surface) must be replaced by the following boundary condition:

$$u = C\lambda \left(\frac{\partial u}{\partial z} \right),$$

where u is the velocity parallel to the surface, C is a coefficient and z the direction normal to the surface.

The physics involved in the establishment of this boundary condition was explained by Maxwell [10], and is described in detail in the work [9]. We will consider the case where the gas particles reflect randomly off the solid surface, with an angle of reflection not correlated to the incidence angle, and an equipartition of the angles of reflection: this mode of reflection is called 'diffuse.' In such a situation, it is not obvious to determine *without calculating* the velocity at the surface; in particular, there is no reason a priori to consider that it is zero. In fact, the balance of the momentum flux, analogous to that leading to the determination of the viscosity, shows that molecules *must slip* along the surface.

[4] This fact gives rise to the Burnett equations, generally unsolvable even in extremely simple systems.

This balance leads to the following relation:

$$\frac{1}{6}\rho u_{\text{therm}} u(\lambda) = \mu \frac{\partial u}{\partial z},$$

where u_{therm} is the thermal velocity and $u(\lambda)$ is the velocity of the fluid estimated at a distance λ from the surface. Using a Taylor series expansion and using the expression for viscosity given by the formula:

$$\mu = \frac{1}{3}\rho\lambda u_{\text{therm}},$$

we finally find the following boundary condition at the surface $z = 0$:

$$u = \lambda \left(\frac{\partial u}{\partial z}\right).$$

Diffuse reflection thus corresponds to the particular value $C = 1$. In the case where the only part undergoing a diffuse reflection is at the surface (the other parts reflect specularly, i.e with their incident angle equal to their reflection angle), the coefficient C introduced above is no longer 1. We show that the parameter C is written:

$$C = \frac{2 - \sigma}{\sigma},$$

where σ is the 'accommodation' coefficient, representing the proportion of particles diffusing onto the surface. The limit discussed previously (completely diffuse reflection) corresponds to σ=1. All values of σ between 0 and 1 are inherently possible, which implies that C can vary between 1 and infinity. When C is larger than 1, one can consider that with respect to the purely diffuse case, there is an effect of overslippage. If all molecules specularly reflect, or when σ is equal to zero, C will be infinite. In this particular case, the boundary condition is written:

$$\frac{\partial u}{\partial z} = 0.$$

We would have here a 'free' boundary condition, and the surface would have the behavior of a free surface. The fluid would slip in this case, freely, in the microcanal, without causing a pressure drop. The parameter σ obviously depends on the gas/surface couple, and particularly the nature of the interface. Measurements of σ made in a vacuum or using spectroscopic methods have clearly shown it to be easily smaller than one [11]. In the case of flows in microsystems, typical values of σ for helium/silicon or nitrogen/silicon interfaces lie between 0.8 and 1 [9, 12–14].

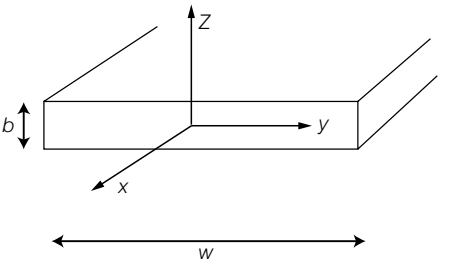

Figure 2.5 Representation of the canal, with corresponding notations.

When the boundary condition is written in a general form, it seems that a rigorous calculation of flow is rather complicated: it is necessary to take into account the fact that the pressure varies along the length of the flow, implying that the flow must be treated three-dimensionally. We will not discuss such a theory in the framework of this book, but will use a simplified theory valid at small Reynolds numbers and for systems only slowly varying along the length of the flow. We consider a canal with a rectangular cross-section, represented in Fig. 2.5.

We assume a small Knudsen number. We also assume that the magnitudes of the values (density, pressure) vary slowly along the length of the canal. We limit ourselves to small Reynolds numbers, allowing us to neglect inertial terms. Finally, we assume that the flow does not vary along the direction $0y$, as shown in Fig. 2.5. At a given position x in the canal, we have the following relation between the local volumetric flux $q(x)$ and the local pressure gradient $G(x)$:

$$q(x) = \frac{Gb^3 w}{12\mu},$$

with

$$G = -\frac{\partial p}{\partial x}.$$

In these expressions, μ is the viscosity, w is the width of the canal, and b is its height. This relation is obtained by resolving the equations of motion at a given position x. The mass flux Q_{m} is conserved along the length of the canal. We can thus write the following relation:

$$Q_{\mathrm{m}} = \rho q(x) = \rho \frac{Gb^3 w}{12\mu}(1 + 6CKn(x)),$$

with $Kn(x)$ defined as:

$$Kn(x) = Kn\frac{P_{\mathrm{m}}}{p(x)},$$

where Kn (in short) represents the average Knudsen number evaluated with the average pressure P_m, defined by:

$$P_m = \frac{1}{2}(p_I + p_O),$$

where p_I is the entry pressure and p_O is the exit pressure.

Now, applying the perfect gas law, we have:

$$\rho = \frac{p}{RT},$$

where R is the universal gas constant, and T is the absolute temperature. Regrouping the equations, we obtain the relation:

$$\frac{1}{2}\frac{\partial p^2}{\partial x} = -\frac{12\mu Q_m RT}{wb^3(1 + 6CKn(x))},$$

Integrating, we obtain:

$$Q_m = \frac{\Delta P P_m w b^3}{12\mu RTL}(1 + 6CKn),$$

where, as before, P_m is the average pressure in the canal and ΔP the charge loss, that is, the difference between pressure at the entrance and the exit of the canal. Here, the Knudsen number Kn is, we recall, calculated at the average pressure existing along the canal. A dimensionless quantity facilitating the discussion of the importance of slip is the slip coefficient S, defined by the expression:

$$S = \frac{12 Q_v \mu p(L) L}{\Delta P P_m w b^3}$$

where Q_v is the volumetric flux at the exit of the canal. The calculation carried out here shows that such a coefficient satisfies the following equation:

$$S = 1 + 6CKn.$$

In determining S experimentally, there is the possiblity of measuring the parameter C, and thus the accommodation coefficient σ. The evolution of S as a function of the Knudsen number, measured for helium, is shown in Fig. 2.6.

If there was no slip, we would have $S = 1$. The curve of Fig. 2.6 shows that slip exists, and that if neglected, it would create a considerable amount of error in the pressure-flux relation. These last few years, curves analogous to the one in Fig. 2.6 were obtained in different laboratories [12–15]; research is currently being conducted to determine how to relate these measurements to the Boltzmann equation in domains both within and outside of the slip regime [9].

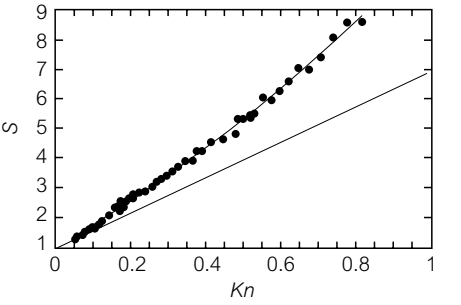

Figure 2.6 Evolution of slip coefficient S as a function of the Knudsen number, for a canal with a rectangular cross-section 1.14 μm high and 200 μm wide [14]. The continuous line shows what is given by a calculation assuming $\sigma = 1$. We deduce from this curve the estimation of $\sigma \approx 0.93$.

2.4 Flow of liquids with slip at the surface

2.4.1 The physics of slip for simple liquids

The important effects of slip have recently been proved between ordinary fluids (like hexadecane) and an atomically smooth surface (like mica) that has been made non-wettable with a deposition of a molecular layer [16, 17]. For ordinary liquids, these observations are surprising for the following reasons: one could argue that a molecule of liquid close to the surface is subjected to attractive Van der Waals forces exerted by the surface itself (see Chapter 1). These forces tend to trap the molecule at a molecular site[5]. For a molecule of size a, this force is:

$$F_v \sim \epsilon a,$$

where ϵ is the interfacial energy (per unit area) involved in this interaction. Moreover, in the presence of a flow along the surface, the molecule is subjected to the action of hydrodynamic stress, which tends to take the molecule far from the site. This force is written:

$$F_v \sim \mu a^2 \gamma,$$

where γ is the shear stress at the surface that is induced by the flow. When these two effects are set equal to each other, we obtain the following condition for the detachment of the molecule:

$$\gamma_c = \frac{\epsilon}{\mu a}.$$

For a fluid subjected to a shear higher than γ_c, we can wait for slip to occur. The orders of magnitude of γ_c are, for a plastic/water interface, around 10^{10} Hz.

[5] A molecular site is necessary for this argument to apply. If the surface was perfectly smooth, there would be no reason at all for the molecule to be trapped in a particular place.

These considerations correspond with results obtained from numerical simulations, which indicate that the critical shear γ_c, beyond which a substantial slip effect appears is given by the expression [18–19]:

$$\gamma_c = \frac{1}{\tau},$$

where τ is a molecular time. This time has a physical origin analogous to those discussed previously. The numerical simulation in fact leads to values on the order of 10^{13} s^{-1} for γ_c.

The experiments of references [16, 17] show that substantial slip phenomena appear for shear much less than γ_c. To discuss this point, it is convenient to reason in terms of the slip length.

This magnitude is defined using the boundary conditions at the surface, written in the form:

$$u = L_s \left(\frac{\partial u}{\partial z} \right),$$

L_s is known as the Navier length, and is the first expression in this condition. This relation has the same form as the relation for gas, but it is less physically justified. Much smaller than γ_c, the preceding rationale suggests that slip lengths are at best on the order of the nanometer. However, the experiments of references [16, 17] show otherwise, that slip lengths can attain lengths of 1 μm[6].

This situation led De Gennes [20] to analyse the following possibility: the slip phenomenon may result from the spontaneous formation of a gaseous underlayer that lubricates the flow[7]. In this theory, under conditions where the fluid does not wet the solid bubbles of gas nucleate in a way that minimizes the surface energy of the system. These bubbles are then stretched into the form of a film by the flow. This gaseous film is represented schematically in Fig. 2.7.

We can envision the presence of a gaseous layer giving rise to the slip effect, rather like an ice skater sliding on the ice due to the formation of an intermediary phase between the ice skate and the solid. De Gennes [20] calculated the corresponding Navier length by using a moderate Knudsen number in the gas. The resulting estimate is written:

$$L_s \sim \frac{\nu}{u_{\text{therm}}},$$

[6] We in fact know very little about L_s. It is not at all impossible that a dependence on shear exists, which would suggest that L_s is not constant for a given liquid/solid interface. This type of situation has been most notably alluded to by the experiments of Zhu and Granick [17].

[7] As mentioned in a recent review by E. Lauga, M. Brenner and H. Stone, a similar hypothesis was made by Boehneke [38] to interpret measurements on slip phenomena, showing differences between degassed and non degassed liquids.

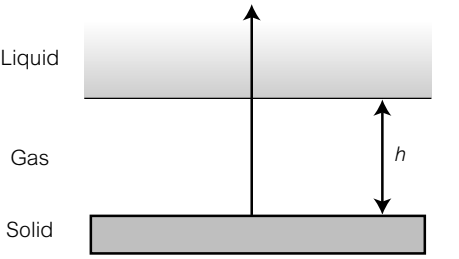

Figure 2.7 Interpretation discussed by De Gennes [20]. A nanometric film of gas forms and causes the slip effect associated with Navier lengths much higher than the liquid correlation lengths. The liquid slips at the surface, rather like an ice skater, owing to the presence of an intermediary phase.

where u_{therm} is the thermal velocity in the gas, i.e. roughly the velocity of sound. Taking for air $\nu = 0.15$ cm^2/s and $u_{\text{therm}} = 300$ m/s, the slip lengths are calculated to be on the order of a few micrometers, which may explain some of the obtained experimental values. This theory still needs to be confirmed experimentally (in a more direct manner), and it has already motivated a great deal of research[8].

2.4.2 **Hydrodynamics of liquid flows with slip**

We now analyse the consequences of the existence of slip, and place ourselves in the framework of the boundary conditions described above:

$$u = L_s \left(\frac{\partial u}{\partial z} \right).$$

The calculation is carried out in the same way for gas. We assume a flat Poiseuille flow is established in such a way that u only depends on the distance to the surface (described by a co-ordinate z, with the origin of the axes situated on the axis of symmetry of the canal) (Fig. 2.5). From this the expression of the velocity profile can be determined to be:

$$u(z) = \frac{L_s G b}{2\mu} - \frac{G}{2\mu} \left(z^2 - \frac{b^2}{4} \right),$$

where, as before, G is the pressure gradient and μ is the viscosity of the fluid. We thus have a Poiseuille profile, but with the surface situated at the position:

$$z = \pm \sqrt{\frac{b^2}{4} + L_s b},$$

[8] In practice, fluids are most often placed in the presence of rough surfaces. At this point in time, there are paradoxical results concerning the role of roughness with respect to slip. Results obtained by Zhu and Granick [21] suggest that whatever the wavelength of the ridges on the surface, roughness inhibits slip once it exceeds about 6 nm. However, numerical simulations by [22] suggest that roughness can, on the contrary, increase the slip effect by favoring nucleation of pockets of gas or formation of dewetting zones in crevices. These questions are presently the subject of an intense research effort. For a recent review, see, for instance, reference [39].

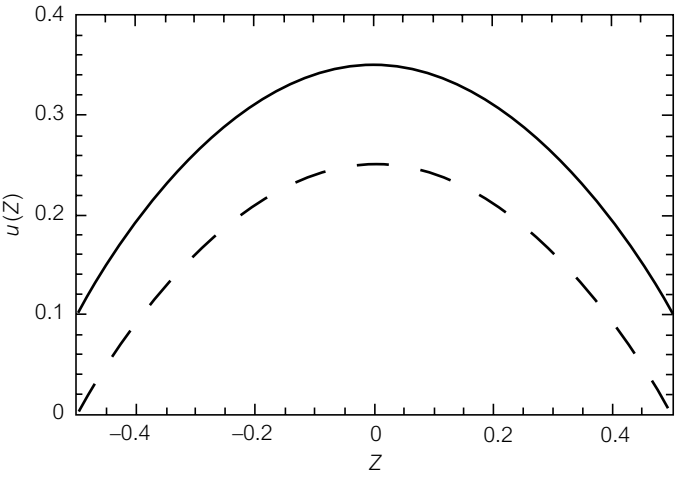

Figure 2.8 Two velocity profiles, with (straight line) and without (dashed line) slip. In the case with slip, the Navier length is taken to be equal to $b/10$, or a tenth of the canal width.

instead of $\pm b/2$ in the absence of slip. When the width b is much larger than L_s, one may use the approximate formula:

$$z = \pm\left(\frac{b}{2} + L_s\right).$$

In the context of this approximation, and only in this case, we can consider the surface to be displaced by a distance L_s towards the exterior; this approximation is used to define the slip length. The velocity profiles with and without slip are represented in Fig. 2.8.

We thus note that the profile with slip is simply the displacement of the same profile without slip. The pressure drop ΔP produced along a canal by a flow with slip is easily calculated:

$$\Delta P = \frac{2\mu LQ}{wb^2(L_s + b/6)}.$$

The phenomenon of slip brings about a reduction of charge loss. It is not difficult to imagine that if the fluid slips, the charge losses will be reduced for a given flow rate with respect to the non-slip case. This property can be useful for the extreme miniaturization of microfluidic circuits (leading to nanofluidics). At the time of writing of this text, has there been any experimental proof of slip effects in microsystems? Well, the actual number of experiments is not very large; the first experiments 'proving' the slip effect [23] are in fact controversial. Nevertheless, [24] proposes some convincing arguments. In recent work, the speed of a flow of water is measured very close to the surface (down to 450 nm) in a microcanal.

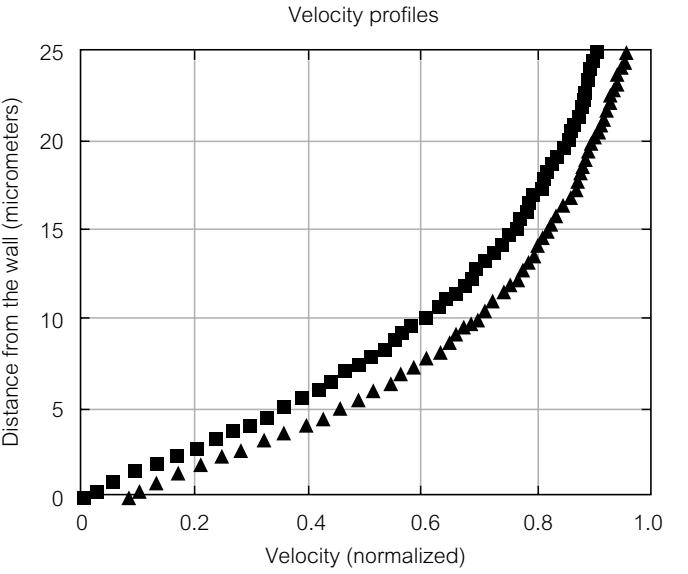

Figure 2.9 Two velocity profiles measured by the technique μPIV.

The measurements of Fig. 2.9 show the existence of slip when the surface is treated to be hydrophobic. The velocity profile is substantially displaced with respect to an 'ordinary' Poiseuille profile (observed in the hydrophilic case). The slip lengths obtained in such an experiment are on the order of several hundred nanometers.

A large reduction in the pressure drop by the slip effect seemed to have been recently proved by Giordano and Cheng [25] in nanocanals of 30 to 500 nm etched in silicon. However, these authors used hexadecane, which wets silicon, while in all other cases where slip has been observed, the surface has not been wettable by the liquid. Many questions on this subject remain open.

2.5 **Microhydrodynamics**

2.5.1 **Generalizations**

We have seen in Section 2.2.4 that a large number of microfluidic systems operate at low Reynolds numbers. The field of studying flows at small Reynolds numbers is known as *microhydrodynamics*. This domain is well established in fluid mechanics, and we will review here some of the essential results. The flows of

incompressible Newtonian fluids at small Reynolds numbers are governed by the Stokes equation:

$$\rho F_i - \frac{\partial p}{\partial x_i} + \mu \frac{\partial^2 u_i}{\partial x_j^2} = 0,$$

where, we recall, u_i is the component of velocity along the i axis, p is the pressure, and F_i is the ith component of the external volumetric force. A more compact form of the Stokes equation is written:

$$-\frac{1}{\rho}\nabla p + \nu \Delta \boldsymbol{u} + \frac{1}{\rho}\boldsymbol{F} = 0.$$

To obtain the Stokes equation, we consider the two inertial terms to be negligible with respect to the viscous term when the Reynolds number is small. In effect:

- the first term, written in index notation, is $\rho u_j(\partial u_j/\partial x_j)$. Its order of magnitude is $\rho U^2/l$, where U is a typical velocity and l is the scale of the characteristic variation of the velocity. This term must be compared to the viscous term, which is on the order of $\mu U/l^2$; the ratio of the first to the second term is precisely $Re \ll 1$;
- the second component involved in the inertial force is the acceleration term $\rho(\partial u_i/\partial t)$, which has an order of magnitude of $\rho U/\tau$, where τ is the characteristic time of the variation of velocity. One can imagine situations where the characteristic time of the velocity is very small, and in this case, it is not certain that the acceleration term can be neglected with respect to the viscous term. Here, we place ourselves in the context where the characteristic times of the flow variations are not much smaller than the turn over time l/U, which constitutes the 'natural' time of the flow. In this case, we use a method of analysis analogous to before to find that the ratio of the acceleration term and the viscous term is also on the order of the Reynolds number.

Ultimately, the inertial term of the Navier–Stokes equation given for the ith component by the expression $\rho(Du_i/Dt)$, can be neglected. In the absence of free surfaces or interfaces, the flows governed by the Stokes equation possess remarkable properties: linearity, reversibility, uniqueness of solution, reciprocity, and the existence of a minimum of dissipation.

- **Linearity**: the Stokes equations are linear in velocity. This property permits the superposition of the elementary solutions of the equation to determine a given flow.

- **Reversibility**: changing t to $-t$ does not modify the equations. Similarly, changing u to $-u$ on the boundaries of the flow reverses the velocity throughout the flow.
- **Minimum of dissipation**: the flow resulting from the solution to the Stokes equation minimizes the kinetic energy dissipation with respect to the kinetically admissible fields, which are compatible with the boundary conditions.
- **Uniqueness**: the solution to the Stokes equation is unique, and thus there cannot be bifurcations of solutions, which would permit, for example, hydrodynamic instabilities to appear (again, in the absence of free surfaces).
- **Reciprocity**: two solutions associated with different boundary conditions are related by an integral.

Reversibility is illustrated in the context of microfluidics in Fig. 2.10. The geometry of the microcanal, curved in a special manner, is that of the 'Tesla valve' (1920). This valve is made up of a series of hydrodynamic circuits of curved geometry, one unit of which is shown in Fig. 2.10. At high Reynolds numbers, the direction of circulation matters, because the shape and position of vortices of separation of the boundary layers differ depending on the direction of flow. At low Reynolds numbers, however, the reversibility of the Stokes equation makes the two directions of circulation equivalent. This characteristic is illustrated by the experiment shown in Fig. 2.10, Carried out in a microsystem where the geometry of the streamlines is independent of the direction of flow[9].

The reversibility at low Reynolds numbers has important practical consequences for the field of microfluidics. For example, this signifies that at very low Reynolds numbers, it is not possible to fabricate a fluid 'diode', which would present a weak resistance to flow in one direction, and a high resistance in the other direction. For such a diode to function, it would be necessary to work at moderate or high Reynolds numbers, which is difficult to achieve in microsystems.

2.5.2 Flows in canals with rectangular cross-sections

It is instructive here to determine the expression for a low Reynolds number, unidirectional flow in the case where the aspect ratio of the cross-section of the canal is arbitrary, as shown in Fig. 2.11.

[9] We note that in this case, the Reynolds number, calculated for the height of the canal b, is on the order of ten, which is relatively high. The Reynolds number for estimating the ratio of inertial forces to viscous forces must by defined differently here. Redefined, this number becomes smaller than one under the chosen experimental conditions.

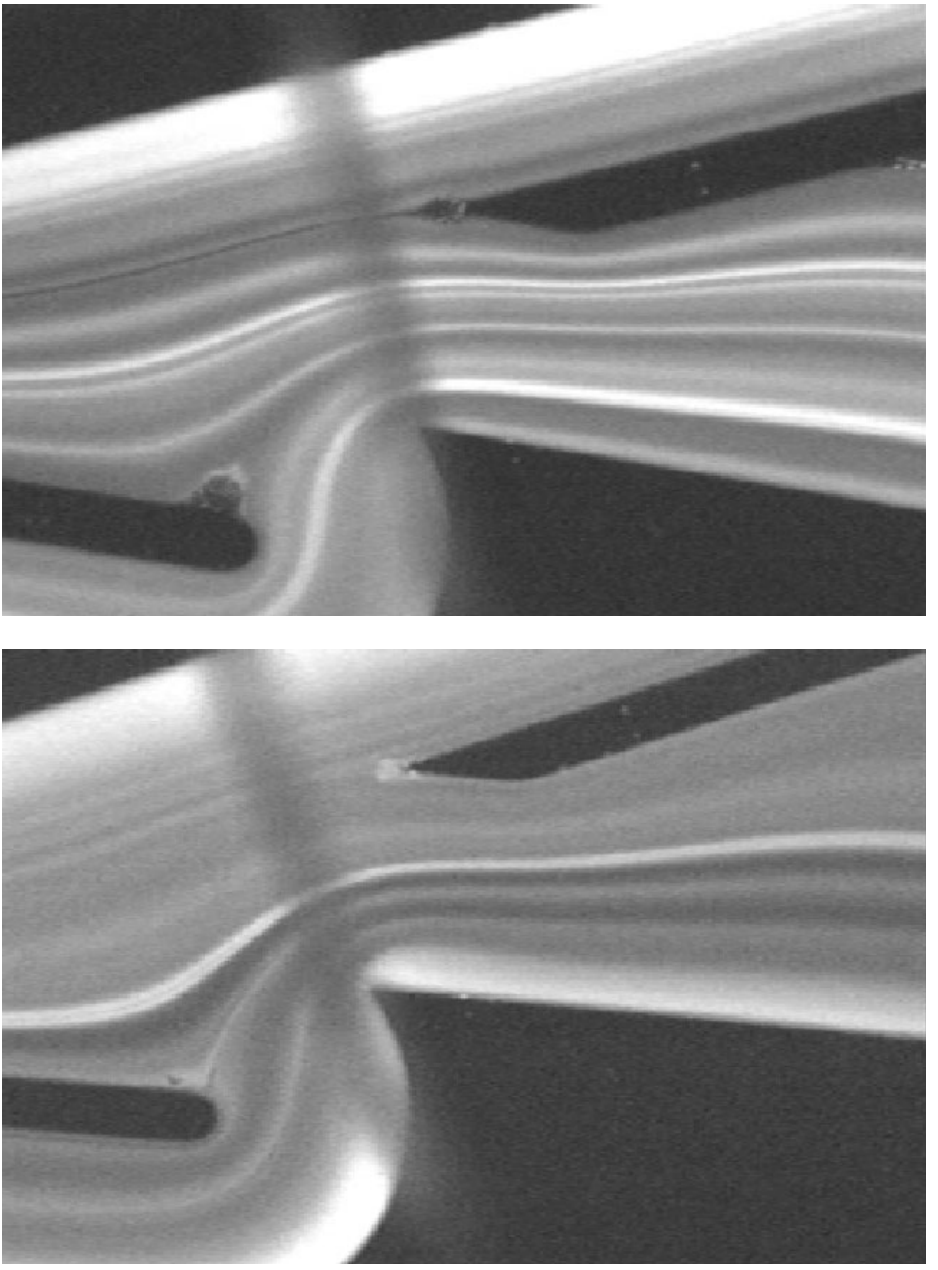

Figure 2.10 Flow through a microsystem with a Tesla geometry; the flow rate is 600 μl/min, the height of the canal is 20 μm, and its width is 200 μm on average. In the top photo, the flow is going from left to right, and in the bottom photo, the flow is going from right to left (courtesy of O. Stern and P. Tabeling (2001); experiment carried out at the MMN laboratory (microfluidics, MEMS, and nanostructures)) in Paris.

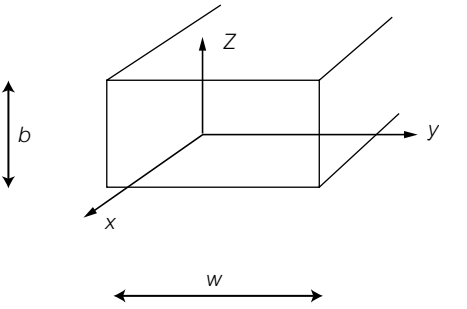

Figure 2.11 Cross-section of the canal in question.

Such situations are common in practice. The equation to solve is:

$$\Delta u = -\frac{G}{\mu},$$

where Δ is the bidimensional Laplacian operator, defined using the variables y and z. The boundary conditions are:

$$y = \pm\frac{w}{2}, \quad u = 0 \quad \text{and} \quad z = \pm\frac{b}{2}, \quad u = 0.$$

The problem is one of the Poisson equation (if the second term was zero, it would be a Laplace equation problem), with 'Dirichlet' boundary conditions. Several methods exist to solve it. Here we choose to use a Fourier series expansion. We carry out the Fourier series expansion along one of the two dimensions y or z of the plane. We thus obtain the expression of the velocity $u(y, z)$ (by calculating along y):

$$u(y,z) = \frac{4G}{\mu w}\sum_{n=1}^{\infty}\frac{(-1)^{n+1}}{\beta_n^3}\left(1 - \frac{ch\beta_n z}{ch\beta_n \frac{b}{2}}\right)\cos\beta_n y,$$

where β_n is defined by:

$$\beta_n = (2n-1)\frac{\pi}{w}.$$

It follows that the volumetric flux Q, defined by:

$$Q = \int_{-w/2}^{w/2}\int_{-b/2}^{b/2} u(y,z)\mathrm{d}y\mathrm{d}z,$$

satisfies the following relation:

$$Q = \frac{8Gb}{\mu w}\sum_{n=1}^{\infty}\frac{1}{\beta_n^4}\left(1 - \frac{2}{\beta_n b}th\beta_n\frac{b}{2}\right).$$

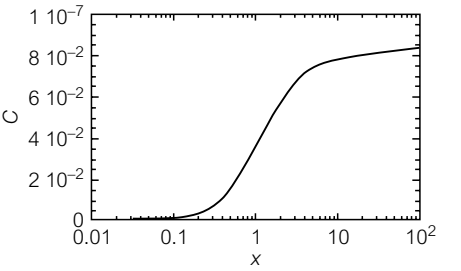

Figure 2.12 Evolution of friction factor C (defined in the text), for a canal characterized by an aspect ratio of $\chi = w/b$.

A close estimate (up to about 10%) of the flux, valid for $b \leq w$, is established from this expression, which is useful to know [26]:

$$Q \approx \frac{wb^3 G}{12\mu}\left(1 - \frac{6 \times 2^5 b}{\pi^5 w}\right).$$

The coefficient C relating the flux Q to the pressure gradient G, is defined by:

$$Q = C\frac{Gb^3 w}{\mu}.$$

Its variations as a function of the aspect ratio $\chi = w/b$[10] are shown in Fig. 2.12, for χ varying between 1 and 100.

It seems that once the aspect ratio w/b is larger than 10, one easily finds with no surprise the asymptotic value 1/12, which corresponds to the limit of the planar Poiseuille. Symmetrically, in the case where w/b is very small, the evolution of the factor $C(\chi)$ is as follows:

$$C(\chi) \approx \frac{\chi^2}{12}.$$

2.5.3 **Flows in Hele–Shaw cells**

A situation important to consider in the domain of microfluidics is that of Hele–Shaw flows. A Hele–Shaw flow is produced between two parallel plates separated by a distance b that is much smaller than the scale of the variation of the velocity field in a plane parallel to the plates: this flow is assumed to be

[10] There is no reason to distinguish between w and b in this problem. Thus, the formula relating the flow rate to the pressure drop along the microcanal may seem surprising, since it does not explicitly cause such a symmetry to appear. It is the factor C that restores the non-symmetry of the formula. From a practical standpoint, one must often analyse sharply curved canals, for which the preceding formula is useful to consider.

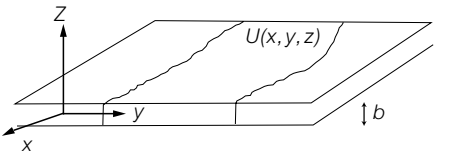

Figure 2.13 Geometry of Hele–Shaw flows, with the corresponding definition of the adapted system of co-ordinates.

operating at very low Reynolds numbers. The representative situation of these flows is schematicized in Fig. 2.13.

The flow goes along the (x, y) plane (parallel to the plates), and the component normal to the plane of the plates is considered to be zero. Along the z direction, the velocity $U(x, y, z)$ can be written:

$$\boldsymbol{U}(x, y, z) = \frac{3}{2}\left(1 - \frac{4z^2}{b^2}\right)\boldsymbol{V}(x, y),$$

where $\boldsymbol{V}$ is a vector possessing two components in the planes x and y, which are functions of x and y. This relation is obtained from the equations of motion, in the limits of the Stokes approximation. They are valid in the center of the Hele–Shaw canal (far from the surfaces parallel to the axis Oz). Inserting this expression into the Stokes equation, and averaging along the direction z, we obtain the following relation:

$$\boldsymbol{V}(x, y) = -\frac{b^2}{12\mu}\nabla P,$$

where P is the pressure and, as in the rest of this chapter, μ is the dynamic viscosity. This relation is often known as the 'Law of Darcy'. Such a law shows that in Hele–Shaw flows, the velocity field is derived from a potential proportional to the pressure. One can immediately deduce:

$$\omega = (\mathbf{rot}\ \boldsymbol{V})_z = 0.$$

The vorticity associated with V is thus null everywhere. There cannot be vortices in Hele–Shaw flows. This implies that the flow structures of Fig. 2.14 cannot be observed in a Hele–Shaw cell. Then, applying the conservation of mass, we obtain the following relation:

$$\Delta P = 0,$$

showing that pressure is a harmonic function. These properties characterize Hele–Shaw flows, and in many cases allow the determination of their structure in a precise and simple manner.

Flows in rectangular cavities

In the limit of the Stokes approximation, it is useful to know the different two-dimensional forms of flow existing for rectangular cavities positioned along a flow. The calculations are based on analysis and on numerical simulations, and are rather complicated, so we do not discuss them here. The shapes of the streamlines of these flows are shown in Fig. 2.14:

Thus, when the aspect ratio of a cavity increases, a growing number of vortices forms in the cavity. This is not a situation of boundary-layer separation (in fact, there is no boundary layer in this case, since the Reynolds number is very small), but is an issue of the solutions of the equations of motion governed by the Stokes equation. If the geometry was confined in the direction normal to the plane of Fig. 2.14, a Hele–Shaw situation would result. In this case, there would not be vortices in the cavity, because the velocity would be derived from a potential.

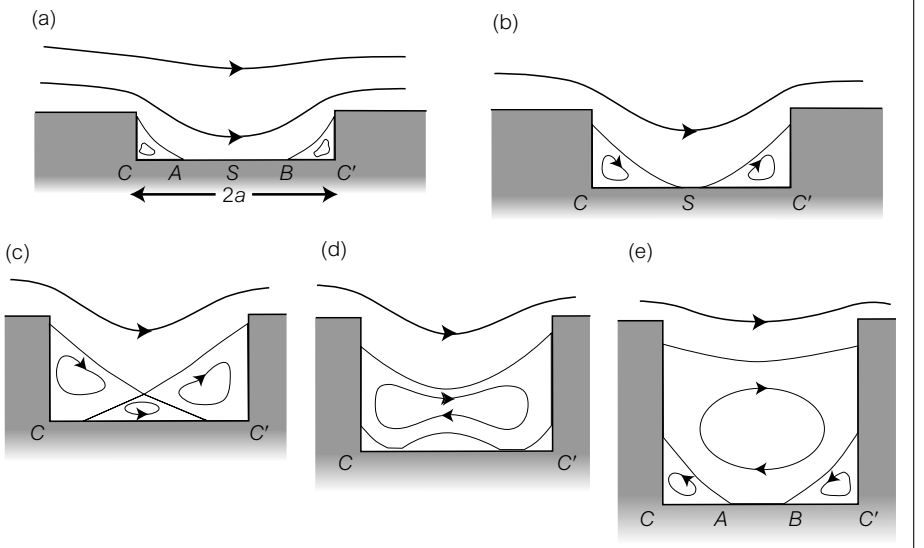

Figure 2.14 Different flow structures through cavities at small Reynolds numbers. Here, the system is invariant along the direction normal to the plane of the figure. We note that vortices can appear in the cavity. It is necessary to emphasize that they are not related to the existence of boundary layer separation, which only appears at large Reynolds numbers, as we will see a little later.

2.5.4 **The notion of hydrodynamic resistance**

Microfluidic circuits are often rather complex, and it is useful to review the idea of hydrodynamic resistance to determine what the flows will be in each branch of

a given circuit. The notion of hydrodynamic resistance R of a canal is introduced using the relation:

$$\Delta P = RQ_{\mathrm{m}},$$

where ΔP is the pressure difference along the canal, and Q_{m} is the mass flux through the canal. An analogy can be made with electronic circuits: the pressure corresponds to an electric voltage, and the flux corresponds to the current intensity. This analogy is robust at very low Reynolds numbers. It relies on the following reasoning, valid in the Stokes approximation (which, we repeat, involves very small Reynolds numbers): we consider a unidirectional, incompressible, steady flow along a canal that is invariant along the direction x and only depends on y and z, which represent the co-ordinates transverse to the flow. By projecting the Stokes equation along y and z, one can demonstrate that the pressure P only depends on x. The projection along x then shows that P must have the form:

$$P = -Gx + \mathrm{Cst},$$

where G is given by the relation:

$$G = \frac{\Delta P}{L},$$

where ΔP is the pressure drop along a length L of the canal, in the direction of flow, i.e. the difference between the pressure upstream and the pressure downstream. ΔP is thus a positive quantity. We now consider the projection along x of the Stokes equation:

$$G + \mu \Delta u = 0,$$

where u is the x-component of velocity. This equation, associated with the boundary conditions along the surface, allows the velocity field to be solved as:

$$u = \frac{G}{\mu} f(y, z),$$

where f is a function that only depends on y and z, and on the specific shape of the cross-section of the canal. What is important here is that f does not depend on any parameter other than those characterizing the geometry of the cross-section of the canal (for example, the aspect ratio for a rectangular section). Integrating along y and z, we obtain:

$$Q_{\mathrm{m}} = K' \frac{G}{\nu},$$

where K' is a geometric constant that depends on the shape of the canal's cross-section. The expression for the pressure drop associated with a fluid flow in a

canal of length L and cross-sectional area S, traversed by flow rate Q_m, can be deduced:

$$\Delta P = K\nu \frac{L}{S} Q_m,$$

where $K = 1/K'$ is a dimensional factor. For a planar Poiseuille flow between two plates separated by a distance b and of width w (with $b \ll w$), the coefficient K is:

$$K = \frac{12}{b^2}.$$

The preceding expression can be rewritten in the form:

$$\Delta P = RQ_m,$$

where R is the hydrodynamic resistance we are looking for. For the preceding case of a planar Poiseuille flow, we thus have:

$$R = \frac{12\nu L}{b^2 S}.$$

This expression evokes the equation for electrical resistance; here, the resistivity is replaced by the factor $12\nu/b^2$. The units of hydrodynamic resistance are $m^{-1}s^{-1}$ (this set of units does not have a particular name). The above relation shows that the hydrodynamic resistance increases considerably as the scale diminishes. It is instructive to note that in the most general case where the rectangular cross-section has any given aspect ratio, we have:

$$R = \frac{\nu L}{C(\chi) b^3 w},$$

where, as we have seen above, w is the width of the canal, χ is the aspect ratio w/b, and $C(\chi)$ is the function represented in Fig. 2.12.

All these relations indicate an analogy between pressure and electrical voltage on the one hand, and flow rate and electrical current intensity on the other. It is possible to show that there are laws for nodes and branches, just as in electrokinetics. For a node, the sum of the flow rates cancel each other out. For a branch, we have the equivalent of a Kirchoff law. It follows that hydrodynamic circuits can be treated as electronic circuits. For example, two resistances R_1 and R_2 placed in series are equivalent to a reistance $R_1 + R_2$, and two resistances in

parallel are equivalent to a resistance whose expression is:

$$R_{//} = \frac{R_1 R_2}{R_1 + R_2}.$$

All these analogies are extremely useful when dealing with microfluidic circuits with several branches, which can often be the case.

To conclude, it is necessary to point out certain limitations. In the Stokes approximation, the velocity is not derived directly from a potential itself, while in electrokinetics, the density of electric current is proportional to the local electrical field, which is derived from a potential. The local equations are thus not equivalent between electrokinetics and Stokes flows in microcanals. The analogy carries over to global quantities. It is also necessary to emphasize that the analogy is only valid for Stokes regimes. Once the Reynolds number becomes much larger than 1, and non-linearities of the Navier–Stokes equation cease to be negligible, the analogy that we have established here is no longer true. Finally, we have assumed that the canals are invariant along the direction of flow. It is possible to extend the idea of resistance to geometries that change slowly along x, but we do not do that here.

2.5.5 **The notion of hydrodynamic capacitance**

In the same way as for resistance, the notion of hydrodynamic capacitance of an element can be introduced with the relation:

$$Q_{\mathrm{m}} = C\frac{\mathrm{d}\Delta P}{\mathrm{d}t},$$

where Q_{m} is the mass flux through the element, C is its capacitance, and ΔP is the pressure drop along the element in question. The idea of hydrodynamic capacitance is pertinent when deformable elements, such as the control membranes of mechanical microvalves, are used in a microfluidic circuit. The units of hydrodynamic capacitance are ms^2, which do not have a specific name. To illustrate, we consider a closed, undeformable canal of volume V, containing a compressible fluid whose density $\rho(t)$ varies with time. From the density variations of this 'fluid' element, a mass flux Q_{m} appears, which is given by the expression:

$$Q_{\mathrm{m}} = V\frac{\mathrm{d}\rho}{\mathrm{d}t}.$$

The density variations are related to pressure variations using the relation $\Delta P = \kappa^{-1}\delta\rho/\rho$, where κ is the compressibility of the fluid. From this we deduce the

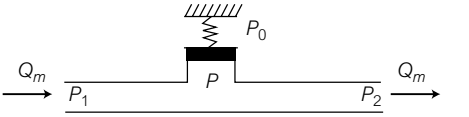

Figure 2.15 Flow in a microcanal, along which a deformable membrane can be schematicized by a piston/spring system.

expression of hydrodynamic capacitance in this particular case:

$$C = \kappa m_0,$$

where m_0 is the mass of the fluid in the element.

We now consider the case where the fluid is incompressible, but the canal is deformable. A membrane was introduced into the system, as shown in Fig. 2.15.

The flow goes along the microcanal under the effect of an imposed pressure difference $\Delta P = P_1 - P_2$, where P_1 and P_2 are the pressures at the entrance and exit of the canal, respectively. The membrane is schematicized by a piston/spring system. It is possible to show that in this system, the flow rate is related to the pressure drop by the following expression:

$$Q_{\mathrm{m}} = R\Delta P + C\frac{\Delta P}{\mathrm{d}t},$$

where R is the hydrodynamic resistance of the canal and C is its capacitance, given by the expression:

$$C = \frac{2\rho}{k},$$

where k is the spring constant (the measure of spring stiffness). This type of calculation is useful because it allows, for example, the determination of the response time constant of a valve inserted in a microfluidic circuit. In the case that we consider here, the time constant is RC.

2.6 **Microfluidics involving inertial effects**

2.6.1 **Generalities**

We have noted that, due to scaling laws, the Reynolds number is inherently small in microsystems, and as a consequence, the equations governing these flows are the Stokes equations. However, it is necessary to qualify this line of thought. In microsystems, there are flows associated with moderate Reynolds numbers on the order of several tens. As previously stated, this is the case for microflows dedicated to extract the heat generated by microprocessors, a subject

that we will present in Chapter 5: in order to obtain efficient heat transfer, these exchangers must operate at moderately high Reynolds numbers. Moderate Reynolds numbers are also involved in inkjet printers, which were presented at the beginning of the book. In this device, velocities are on the order of several meters per second, for jet diameters on the order of 100 μm. The Reynolds number is thus:

$$Re = \frac{Ul}{\nu} \sim 100.$$

This Reynolds number is not high enough to produce hydrodynamic instabilities, but it is too high to be able to apply the Stokes approximation. In other cases, divergent systems have been made to function at sufficiently high Reynolds numbers to induce effects of irreversibility. These situations are closer to minifluidics than microfluidics. Nevertheless, they are not rare, particularly in the field of chemical engineering. The domain of moderate Reynolds numbers groups together phenomena often difficult to describe precisely, because they are not asymptotic and are thus difficult to simplify. Here, we will be satisfied to mention just one important phenomenon occurring at moderate Reynolds numbers: the origin of irreversibility in microsystems. It is an issue of the phenomenon of boundary layer separation. We will then give an example of a recently commercialized microsystem that is based on inertial effects.

2.6.2 **The phenomenon of boundary-layer separation**

We will not review here the characteristics of laminar boundary layers that one can find in several works on hydrodynamics (for example, in [27]). We assume here that a laminar boundary layer is established along a surface in the presence of a hydrodynamic flux (see Fig. 2.16). This situation could be, for example, the flow along the walls of a convergent or divergent microcanal. We can thus distinguish two situations considered as 'favorable' or 'unfavorable' for separation. The favorable case is roughly sketched in Fig. 2.16.

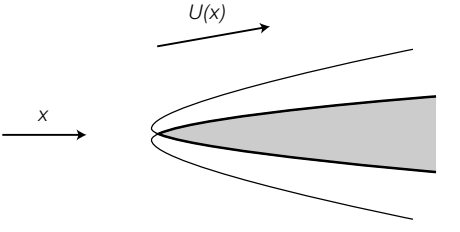

Figure 2.16 The case of a convergent flow is favorable for the attachment of the boundary layer.

Here we have the following two conditions:

$$\frac{\mathrm{d}U}{\mathrm{d}x} > 0 \quad \text{and} \quad \frac{\mathrm{d}P}{\mathrm{d}x} < 0,$$

where $U(x)$ represents the flow external to the boundary layer, at the abscissa x, and $P(x)$ is the corresponding pressure; we assume here that the component of the flow is essentially along x. The flow $U(x)$ increases along x by means of conservation of flux, and Bernoulli's theorem shows that the pressure decreases (we note here that the usage of the theorem implies a moderate or high Reynolds number). The boundary layer thus experiences a pressure field that favors a flow near the surface, in the direction of the principal flow. In this configuration, there is no formation of a 'counterflow', and this case is known as 'favorable'.

The unfavorable case is shown in Fig. 2.17, corresponding to a flow in a divergent canal.

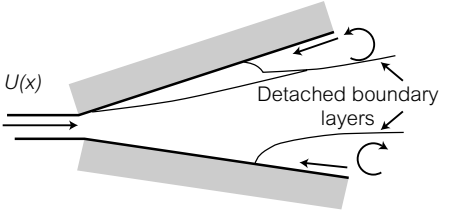

Figure 2.17 The case of a divergent flow, which is unfavorable for the attachment of a boundary layer.

In this case, the velocity $U(x)$ decreases, implying (due to the Bernoulli theorem) that the pressure increases along the flow. There is thus the possibility of inducing a counterflow in the boundary layer, and zones of recirculation can be observed along the surface. The formation of a recirculation zone corresponds to the phenomenon of boundary-layer separation. The point of separation of the boundary layer is unstable, which is why the appearance of separation generally corresponds with the appearance of turbulence in the boundary layer. This turbulence induces hydrodynamic losses, which accentuate the difference between the 'favorable' case and the 'unfavorable' case.

The separation phenomenon can intervene in microsystems functioning at moderate Reynolds numbers with complex geometries. This fact is exploited by some micropumps [28, 29]: the principle consists of pushing fluid alternately in two opposing directions, through divergent canals in one direction and convergent canals in the other. When the fluid circulates in the divergent canals, separation of the boundary layer is produced, and there is substantial charge loss. In the other direction, the canal is convergent, and circulation of the fluid is facilitated. In this way it is possible to favor, on average, a flux in one given direction, which is the basic functioning principle of these devices[11].

[11] However, the majority of micropumps used in the domain of microfludics do not function using this principle.

Microfluidics using centrifugal forces

An elegant concept, developed by the company Gyros, consists of etching microfluidic circuits onto a CD, and using centrifugual forces to move fluids through microcanals [30]. Even though the scaling laws associated with inertial terms are generally unfavorable in microsystems, the high rotation speeds allow the development of appreciable centrifugal forces, permitting the controlled movement, at low speeds, of fluids. The rotation speeds used here are on the order of 3000 turns per minute. The principle of the functioning of such a system is represented in Fig. 2.18.

In the figure, we see a dispenser supplying fluid to a rotating disk. The details of these canals and etched reservoirs in the disk are shown in Fig. 2.19. Each reservoir is successively filled using an incremental augmentation of the rotation speed of the disk.

The following equation defines a 'centrifugal valve':

$$f = \rho v \Omega^2 R \geq f_{\text{capillary}},$$

where Ω is the rotation velocity, v is the volume of the fluid element in consideration, R is the radial position of the valve, and $f_{\text{capillary}}$ is the capillary force, or the wetting forces (see the following section) acting on the fluid element. This inequality compares capillary forces, which retain the fluid meniscus in a restriction, with the centrigual forces, which put the fluid into motion towards the periphery of the disk. The valve is open if centrifugal forces are higher than the capillary forces, which is expressed by the inequality above. The capillary force can be controlled by adjusting the dimensions of the canal connecting the two reservoirs, or the properties of the surfaces exposed to the fluid. The thinner the canal, the larger the forces keeping the liquid on the disk must be. By altering the rotation speed, it is possible to make a fluid volume migrate towards the growing radii to fill new reservoirs or reactors.

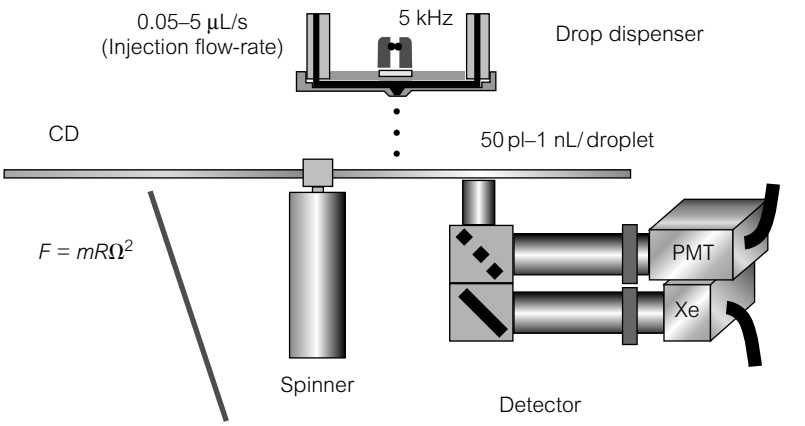

Figure 2.18 Microfluidic system using centrifugal forces to put fluids into motion, developed by the company Gyros.

(Continued)

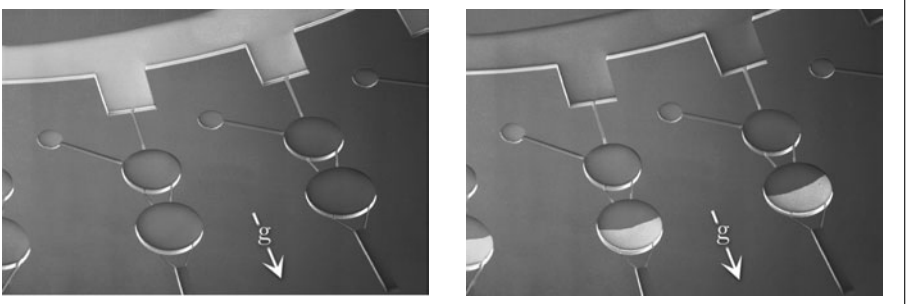

Figure 2.19 Detail of a microfluidic system using centrifugal forces, showing a valve that is essentially a cavity that holds the fluid by means of wetting forces at small rotation speeds, and frees the fluid at higher rotation speeds (© Gyros).

Thus, centrifugal microfluidics elegantly resolves the delicate problem of pumps and valves, despite the handicap of the unfavorable scaling laws. It is of course possible, on the same CD, to etch a large number of canals, and to carry out multiple operations in parallel (the number of canals is on the order of 400 for certain commercialized systems). This type of device could be useful for combinatorial chemistry, a field that uses massive parallelism of chemical reactions.

2.7 Interface phenomena: a few ideas about capillarity

2.7.1 Introduction

We saw in the first chapter that the surface-to-volume ratio is much higher (by several orders of magnitude) in microsystems than in decimetric systems. This implies that interfaces will play a more important role in microsystems than in systems of a more 'ordinary' size. We will briefly present here phenomena occuring at interfaces, so that we may have at our disposal a few ideas that will be useful for the analysis of experimental situations often encountered in microsystems.

2.7.2 Surface energy and capillarity

As shown in Chapter 1, all interfaces are associated with a surface density energy represented by E or γ, and whose units in the S.I. system are joules/m^2. This quantity is known as the interfacial tension or 'surface energy'. The (total) energy

of an interface is given by this tension or surface energy multiplied by the area of the interface in question. The physical origin of surface energy was presented in the previous chapter. It is related to the intermolecular interactions existing between surfaces. We recall that the Van der Waals forces for two interfaces in a vacuum are attractive, and it is necessary to expend some energy to separate two interfaces that are initially in contact. Reviewing the expression for this situation a vacuum:

$$E = \frac{A}{12\pi D_0^2} = 2\gamma,$$

where A is the Hamaker constant and D_0 is a microscopic length scale. It is necessary to provide energy equal to 2γ to separate the two planes bound by Van der Waals adhesion.

Another way to introduce surface energy is to consider that the molecules making up the interface are subjected to a specific environment—an 'interphase' that differentiates them from molecules 'buried' in the liquid or solid bulk volume. The surface energy is thus naturally introduced, attesting to the presence of a thin layer of molecules at the interface, which are expected to have a unique behavior. The surface energy obviously depends on the nature of the solids or liquids forming the interface. The higher the cohesion of the solids or liquids forming the interface, the higher the surface energy of the formed interface will be. One such development is contained within the Hamaker constant, whose theoretical expression, obtained in the specific case presented by Lifschitz, was given in the preceding chapter [5]. To cite an example, metals, bonded by metallic bonds (resembling covalent bonds), are associated with high-energy surfaces; Van der Waals solids (e.g. teflon, plastic), whose internal cohesion is assured by Van der Waals forces (much weaker than covalent bonds), develop interfaces with weak energies. The surface energy for a metal/air interface is on the order of 500 mJ/m^2 and for an oil/air or teflon/air interface, the surface energy is on the order of 20 mJ/m^2.

All these conclusions assume that we are working at scales much larger than the range of intermolecular forces appearing at interfaces. As we emphasized in Chapter 1, this hypothesis is well verified in ordinary microfluidic systems. However, this hypothesis must be reconsidered for canals of sizes smaller than 100 nm.

2.7.3 **Laplace's Law**

Laplace's Law demonstrates that in order to maintain a curved interface in mechanical equilibrium, it is necessary to exert a higher pressure on the interface,

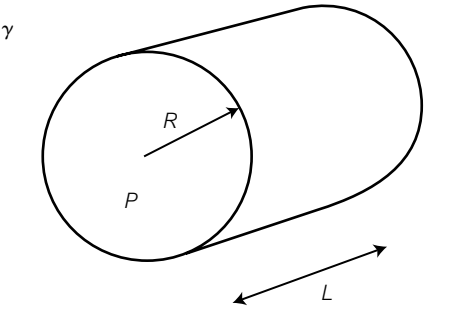

Figure 2.20 Geometry used for the derivation of the Laplace's Law.

rather as if it had to be maintained by blowing. We consider a cylinder of radius R that forms an interface between two media (Fig. 2.20).

This interface is associated with an energy:

$$E_S = 2\gamma\pi RL,$$

where γ is the surface tension. We assume that the interior of the cylinder has a pressure P, and the exterior is in a vacuum (at zero pressure). The associated internal energy required to maintain such a pressure is written:

$$E_V = \pi R^2 LP.$$

We look to find the mechanical equilibrium conditions of such a system, and we do this by imposing a variation δR of the radius of the cylinder. If the system is at equilibrium, the corresponding energy variations will be equal. We thus have:

$$\delta E_S = \delta E_V.$$

This implies

$$P = \frac{\gamma}{R},$$

which is Laplace's Law for a cylindrical interface. For a three-dimensional interface, it is necessary to introduce the two radii of principal curvature, designated as R_1 and R_2. We thus obtain:

$$P = \gamma\left(\frac{1}{R_1} + \frac{1}{R_2}\right).$$

2.7.4 **Wetting**

Wetting comes into play at three interfaces, connected by a contact line (Fig. 2.21). The geometry of the setup is infinitely long (contact lines have an infinite length), and is invariant along the direction normal to the plane of the figure.

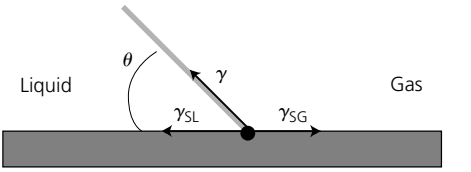

Figure 2.21 Diagram showing a solid–liquid–gas contact line, for which Young's relation is applied.

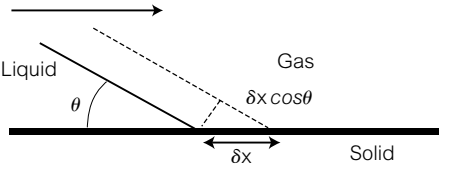

Figure 2.22 Solid–liquid–gas contact line, subjected to an infintessimal displacement δx.

We again use reasoning based on the concept of surface energy. We have here three interfaces: solid/gas, liquid/solid and liquid/air. Between each of these interfaces there is an associated surface energy γ_{SG}, γ_{SL} and γ, respectively. A fundamental parameter is the spreading coefficient S, which is defined by:

$$S = \gamma_{SG} - \gamma_{SL} - \gamma.$$

The system above is in mechanical equilibrium if the resultant of the forces is zero at the contact line. In the opposite case, the contact line either advances or recedes. To express this mechanical equilibrium, we calculate the variation in energy produced by a displacement of the contact line along a direction parallel to the plane δx (Fig. 2.22).

Calculating the work δW necessary to displace the line, we obtain:

$$\delta W = (\gamma_{SG} - \gamma_{SL})\delta x - \gamma \cos\theta \delta x.$$

This work must equal zero at equilibrium. In this way we obtain Young's relation, which is written:

$$\gamma_{SG} - \gamma_{SL} = \gamma \cos\theta,$$

or:

$$\cos\theta = \frac{S}{\gamma} + 1.$$

We see that if the spreading coefficient S is positive or less than -2γ, there cannot be mechanical equilibrium. For positive S, the system forms a film completely covering the solid. This is the case for a system involving a liquid such as oil on

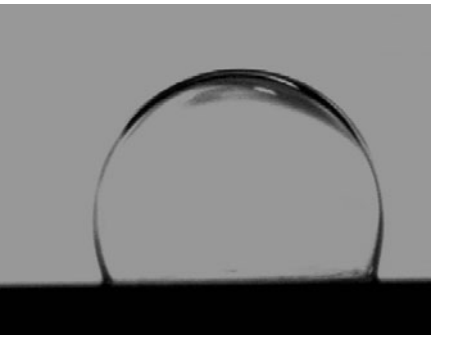

Figure 2.23 Partial wetting: Droplet of tetradecane in water, on a surface of silicon. (Photo taken by Rémi Dreyfus).

a high-energy surface, and the situation is known as total wetting. For

$$S \leq -2\gamma$$

the liquid adopts a shape that minimizes contact with the solid. This is a non-wetting situation. Between these two extremes, there is a 'partial' wetting situation, which involves a contact angle determined by Young's relation. One example is given in Fig. 2.23.

A verification of the Young–Dupré relation for solid-liquid-gas systems was made by Chaudhury and Whitesides at the beginning of the 1990s [31]. The test was based on the JKR test [32]. A solid bead is placed on a plane of the same material, and a stress is applied on the bead in a direction normal to the plane, pressing the bead into the plane. The determination of the contact zone (which is possible for soft solids like teflon) can be related to the surface energy γ_{SV}, in the case where the test is carried out in the presence of gas. In the case where the system is immersed in a liquid, we obtain γ_{SL}. The determination of these physical quantities, associated to that of γ, show that the Young–Dupré relation can be applied remarkably well to soft solids.

2.7.5 **Capillary effects with surfactants**

2.7.5.1 Introduction

Capillary phenomena are very sensitive to impurities. For example, pure water has a water/air surface tension on the order of 70 mJ/m, while ordinary tap water has a surface tension of no more than 40 mJ/m. The difference between the two values is due to the presence of a thin layer of impurities that alters the energetic properties of the water surface. This empirical observation indicates that there are molecules that prefer to reside at interfaces rather than staying immersed in

the liquid. These molecules are called surfactants. Decades ago, synthetic chemistry produced a vast collection of surfactant molecules. Surfactants encompass a vast and rich domain that is still developing, and possesses an extensive literature. This field has given rise to a considerable number of applications in the industries of food, cosmetics, oil, etc. To cite a spectacular example mentioned in the text of De Gennes *et al.* [33], the daily extraction of tons of ore rely on the subtle effects induced by the presence of surfactants. In liquid systems, surfactants allow small droplets to be formed, giving rise to emulsions. It is usually impossible to create an emulsion without the use of surfactants. The objective of this section is to give a few ideas on surfactants, which play an important role in systems where capillary effects prevail (this is the case for microsystems in the presence of interfaces). We will present certain static and dynamic effects, which will allow us to better understand the behavior of diphasic systems in microfluidics, a theme recently undertaken by several research groups.

2.7.5.2 What is a surfactant?

A surfactant is a molecule made of two parts, each part having a different affinity: the hydrophilic part 'likes' water (energetically speaking), and the hydrophobic part does not like water. These molecules are known as amphiphilic, because they like simultaneously being in one phase and out of that same phase. Three examples of surfactants are shown in Fig. 2.24 [33].

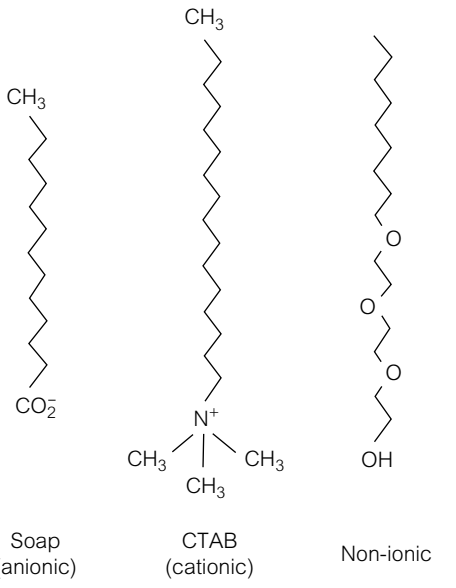

Figure 2.24 Three surfactants.

For the vast majority of cases, the hydrophilic part of the surfactant is an ion forming the 'polar head', and the hydrophobic part is one (or several) aliphatic chains $CH_3(CH_2)_n$ forming a hydrophobic 'tail'[12]. The hydrophobicity of the aliphatic chains comes from the fact that they force water molecules to organize themselves locally in a way that is entropically unfavorable. Thus, for a water-soluble surfactant, the general rule is: the tails try to avoid water, and the heads try to stay in water. It is this type of behavior that has led to the term 'frustrated couple' being used to describe the actions of these molecules [33].

When a water-soluble surfactant is placed in an aqueous environment, it will find that the most energetically favorable state is to populate the interfaces, with its head in the water and its tail out of the water. In these conditions, due to the action of the hydrophilic head, and sometimes due to the hydrophobic tail, the molecule significantly reduces the interfacial energy of the system. We see here the role the surfactant plays in the determination of the interfacial tension.

The preceding description may lead us to think that the surfactant is found primarily at the interfaces, and that its concentration in the bulk is zero. However, in reality, thermal agitation tends to homogenize concentrations, and thus oppose the formation of high concentration gradients, which would be present if all surfactant molecules were concentrated at the interface. Thus, there exists a statistical equilibrium between the molecules localized at the interface and those in the bulk, and this equilibrium is calculable from the chemical potentials of the molecules in question [27]. In general, we must consider that the surfactant is present both in the bulk and at the interfaces.

2.7.5.3 Classification of surfactants

Due to the fact that the surfactant is present both in the bulk and on the surface, it is natural to introduce a partition coefficient k with the relation (for the case of an oil-water system):

$$k = \frac{c_o}{c_W},$$

where c_o and c_W are the equilibrium concentrations of the surfactant in oil and in water, respectively. For water surfactants that are soluble in water and not oil, the partition coefficient is very small, and the converse is also true. To characterize a surfactant, we use a scale proposed by Griffin, the HLB (*hydrophilic lipophilic balance*). For oil-water systems, this quantity is defined in the following manner:

$$HLB = 7 + \alpha \log(k),$$

[12] Figure 2.24 does not overlook the third case, where the head is replaced by a hydrophilic chain made up of water-soluble units; while this molecule is also amphiphilic, it is non-ionic as well.

where α is a scaling constant. The table below illustrates the different possibilities.

HLB	System
1, 5–3	Antifoamers
3–6	Water/oil emulsions
7–9	Foams, wetting agents
8–18	Oil/water emulsions
13–15	Detergents
15–20	Solubilizers of organic products

We thus note the variety of uses for surfactants. We are interested here in oil/water emulsions, that is, systems where the HLB is between 8 and 18, according to the proposed classification[13].

2.7.5.4 Micelles

When the concentration of surfactant is raised, the system tends to form micelles, a type of structure shown in Fig. 2.25.

One can see that this structure is energetically favorable: micelles allow the aliphatic tails to be protected from the aqueous environment, only exposing the polar heads. It is necessary to conjugate this structure with thermal agitation, which tends to disperse molecules in solution in a homogeneous manner. As in the preceding paragraph, the notion of thermodynamic equilibrium will have to be introduced. We observe that micelles will appear above a critical concentration of amphiphilic molecules, called the CMC (critical micellar concentration). For concentrations below the CMC, molecules are present in the bulk individually, and for concentrations above the CMC, micelles appear and are in equilibrium

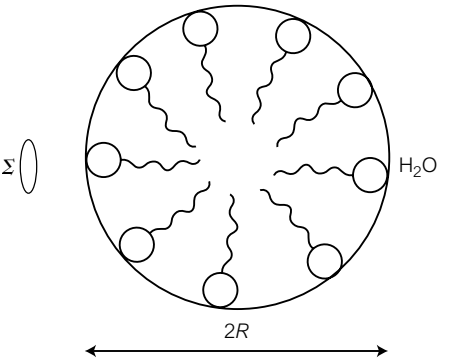

Figure 2.25 Diagram of a steric micelle: the hydrophobic tails are in the middle and protected from the aqueous phase.

[13] Note that the classification of these situations using the HLB are approximate, and that these values vary depending on the authors.

with both molecules at the interface and molecules in solution. These micelles are aggregates that are typically made up of about a hundred molecules. The micellar structure is often used, for example, to obtain microemulsions (we will discuss these later). Micelles are also the basis for microbeads, often made from polystyrene, which are today used for medical tests and have many uses in chemistry and biology in general.

2.7.5.5 The influence of a surfactant on the interfacial tension

A typical curve showing the evolution of the water oil interfacial tension as a function of the surfactant concentration is presented in Fig. 2.26.

The interfacial tension seems to decrease as the surfactant concentration increases. When C_S augments, the interface is increasingly covered by the amphiphilic molecules, causing the interfacial energy to decrease. This process continues until the interface is saturated, i.e. when $C_S = C_{sat}$; After this value is reached, the interfacial tension continues to decrease, but much more slowly. This behavior can be explained using chemical potentials. Saturation is reached once the CMC is attained. In this situation, the bulk concentration and surface concentration of isolated amphiphilic molecules is saturated. Only the number of micelles increases, without any effect on the energy of the system. The system thus no longer evolves, and the interfacial tension saturates at its lowest level.

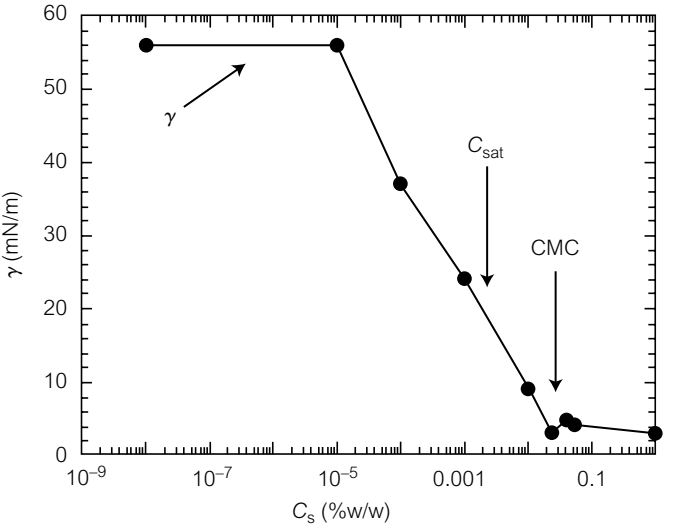

Figure 2.26 Evolution of the water/hexadecane interfacial tension as a function of the surfact concentration C_S. The concentration axis has units of %w/w (w for weight), which is a percentage, by mass, of solute in solvent. Here the surfactant used was DTOS (a surfactant that is soluble in oil, less soluble in water). Taken from [34].

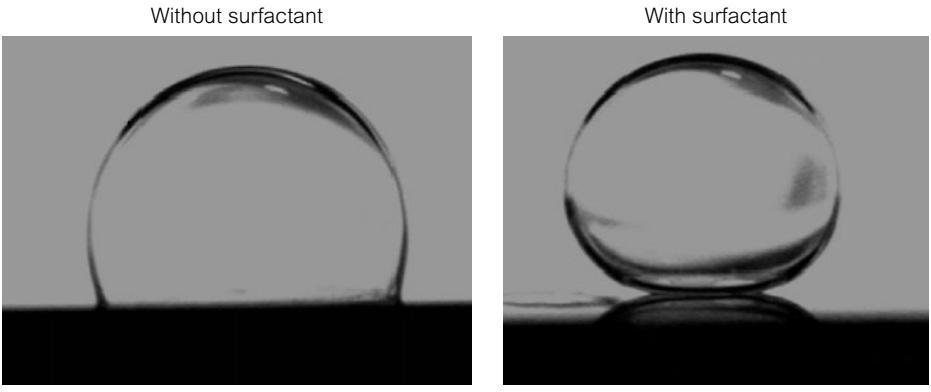

Figure 2.27 The effect of detergence in a water-tetradecane system. On increasing the concentration of surfactant (SPAN 80), the system goes from a partial wetting regime to a total wetting regime of tetradecane on the substrate. The water droplet thus tends to detach itself from the substrate.

To obtain weak interfacial tensions, it is advisable to work at concentrations less than the CMC.

2.7.5.6 The effect of detergence

What effect does a surfactant have on the contact angle? This effect is important in general and can even be spectacular. This characteristic is illustrated by the effect of detergence, one that laundry detergents exploit for cleaning clothes, for example (Fig. 2.27).

The photo on the left represents a droplet of pure water in tetradecane, without surfactant. We have here a situation of partial wetting. At the right, we have added the surfactant SPAN 80 (with a concentration on the order of 3×10^{-2} % w/w[14]). The effect of the surfactant is significant: we go from a partial-wetting situation to a total-wetting situation[15]. Just a little hydrodynamic flow is enough to detach the droplet of water from the surface and be carried along by the current. This phenomenon is, in fact, a consequence of the Young–Dupré relation, which is written:

$$\gamma_{SW} - \gamma_{SO} = \gamma_{WO}\cos\theta,$$

where the symbols S, W, O signify solid, water, and oil respectively, and θ is the contact angle formed between the solid and water. Adding the surfactant, as we have emphasized before, considerably diminishes the interfacial tensions γ_{SO} and γ_{WO}; the term γ_{SW} also diminishes, but proportionally less, because

[14] % w/w percentage, by mass, of the solute in the solvent.

[15] Here, it is the tetradecane that, due to the action of the surfactant, becomes wettable with respect to the surface.

the surfactant that was used was less soluble in water. When the surfactant concentration increases, the Young–Dupré relation shows that the term $\cos\theta$ increases until it reaches its maximum value 1. When this value is attained, the contact angle is zero. Beyond this value, it is no longer possible to define an equilibrium angle. The system is divided into three parts: solid, water, and liquid, without a triple line. This situation corresponds to the figure on the right, where the droplet detached from the solid (which would happen if gravity did not maintain the droplet on the solid surface). Laundry detergents use the detergent effect to their advantage: the droplet in this situation is an oil stain initially adsorbed onto a piece of clothing. The surfactant transforms the stain to a drop, then the hydrodynamic fluctuations or currents of the washing machine detach these droplets from the clothing.

2.7.5.7 A few notions on emulsions

We will later see that it is tempting to want to form emulsions, benefiting from the excellent control of fluid flows made possible by miniaturization. What is an emulsion? A liquid/liquid emulsion is a system formed by the dispersion of small droplets of one liquid in another. Mayonnaise[16], which is a dense dispersion of small drops of oil in vinegar, and cosmetic cremes, are two examples of emulsions. To form small droplets, it is necessary to work with weak interfacial energies (otherwise capillary effects, which favor the formation of large drops, destabilize the emulsion by causing droplets to coalesce); in practice, it is necessary to use surfactants to form an emulsion. Depending on the relative concentrations, different types of emulsions can be distinguished: simple emulsions, emulsion-gels, biliquid foams. We also introduce a classification according to the size of the droplets: macro-emulsions are systems made up of droplets larger than a micrometer (e.g. milk), and micro-emulsions are made from submicrometric micelles. Macro-emulsions are in a metastable state, and are destined to undergo a separation of phases (for milk, this leads to the spontaneous formation of cream). Phase separation is energetically favorable because it minimizes, at a fixed volume, the area of contact between phases. Micro-emulsions are stable, because micelles do not gain energy by coalescing[17]. Thus, there is an important difference between macro- and micro-emulsions.

[16] In mayonnaise, egg yolk combined with vinegar initially form an emulsion of lipids in an acidic aqueous phase. When oil is added, the lipid drops swell. It is not necessary to add too much oil, as this could cause the emulsion to coalesce, because there would no longer be enough lipids to preserve oil/vinegar interfaces.

[17] The interfacial energy for a micelle is not simply proportional to its area. There is another expression that also takes the effects of elasticity into account, effects that are absent at ordinary interfaces. For this reason the system can no longer be considered to evolve spontaneously towards a reduction of exposed area, and thus towards coalescence.

2.7.5.8 Miniaturization impedes the action of surfactants

What happens to the action of surfactants when a liquid-liquid system like water-oil is miniaturized? This question is not necessarily novel: emulsions themselves, by transforming macrometric volumes into small droplets, impose a sort of miniaturization on the system. Considering that surfactants play a critical role

Displacement of the contact line

What happens when a drop is in motion on a plane? This question is important when one wishes to transport solutes not in microcanals, but in individual droplets [35]. We give here information on the principal elements of the problem. It has been established that the drop advances with a 'caterpillar-track' motion [36]. In the frame of reference of the drop, the recirculation movement resembles a caterpillar track (Fig. 2.28).

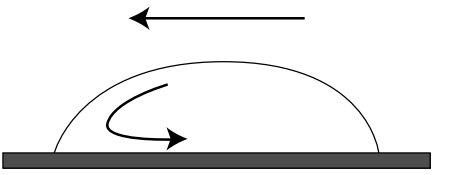

Figure 2.28 Diagram showing the movement of a drop along a plane, with a 'caterpillar-track' internal movement.

One difficulty exists with the contact line: there is a problem of a possible discontinuity of the velocity, which would induce infinite stresses. One solution is that it has been shown that for wetting fluids, a precursor film a few nanometers thick appears more rapidly than the droplet, thus eliminating this singularity, or postponing it to the front of this microscopic film. For partially wetting fluids, the singularity remains, and the possibility of an infinite stress exists. As De Gennes mentions in [37], one could think that *even Hercules would be unable to submerge a rock in a basin.* In effect, to immerse a rock in a non-wetting fluid, it is necessary to displace a triple line and thus compensate for a singularity in the stress. However, viscous stresses created by such a singularity have been shown to have a logarithmic dependence on their distance from the surface. Introducing a microscopic cutoff scale, these stresses remain at levels compatible with experimental evidence. A second fundamental observation is that of the hysteresis of the contact angle: even for very small displacements, there exists a difference between the advancing and receding contact angles of the drop. This difference is due to heterogeneities of the surface energy, or due to the roughness of the substrate. We thus define the advancing contact angle to be θ_a, and the receding contact angle to be θ_r as the velocity goes to zero. This difference between the advancing and receding angles, which exists at a quasi-null velocity, proves the effect of hysteresis for a contact-angle. It is thus necessary, when taking contact-angle measurements, to state whether the drop has reached an equilibrium stationary state by advancing or receding.

in these systems, we could think that the same would be true for microsystems. However, there is a scaling effect that generally tends to reduce the action of surfactants in microsystems. This scaling effect, which also exists in emulsions, can be introduced using a water-oil system with a given concentration C_0 (by volume) of surfactant. We assume that the surfactant is insoluble in oil so that it is only found in the water phase. As explained above, surfactant molecules repartition in the bulk and at the interfaces. We thus have the relation:

$$C_0 = C_V + C_S \frac{S}{V},$$

where C_V and C_S are the surfactant concentrations in the bulk and on the surface, respectively, S is the area of surfaces exposed to water, and V is the volume of water. We thus have, by order of magnitude, the following equality:

$$C_S \sim l(C_0 - C_V),$$

where l is the scale of the system. This relation implies:

$$C_S < lC_0.$$

Thus, when one miniaturizes at a fixed C_0, the surfactant concentration at the surface tends to diminish. There are fewer and fewer surfactant molecules at the interfaces, and their action is thus reduced. Since miniaturization can reduce l by several orders of magnitude, it is expected that this effect is not negligible. This scaling effect, which essentially comes from the fact that we are dealing with a fixed volumetric concentration, is well known in the field of emulsions (high concentrations of surfactant are always used to avoid the depletion of surfactants at interfaces). We will see a consequence of this effect in diphasic flows in microsystems.

2.7.6 **Membrane interfaces**

It is important to report that there are forms of energy other than those described above. These forms are important to consider when dealing with objects such as biological membranes. For example, it is crucial that the elasticity of a biological membrane be taken into account, which would obviously mean modifying the surface-energy expression described in this section. Note that it is no longer possible to consider the surface energy to be constant at the interface. One

example of a relation decribing an interface that is elastic but lacking in capillarity is as follows:

$$E = \frac{1}{2} K A_0 \left(\frac{A - A_0}{A_0} \right)^2,$$

where K is a modulus of elasticity, A is the area of the interface, and A_0 the resting area, i.e. the area in the absence of deformation. This form of energy is typically involved in mechanical equilibria of biological membranes [40]. One consequence of this equation is that the equilibrium shape of an isolated vesicle (i.e. a membrane with a spherical topology) is not necessarily a sphere. An example of this is the red blood cell, whose equilibrium shape under standard conditions is a disk. We will not expand further on this vast subject.

2.7.7 A ubiquitous phenomenon of capillary instability: the Rayleigh–Plateau instability

Images of the inkjet printer presented in the introduction of this book (Fig. 3) show that a column of liquid spontaneously creates droplets. This is due to an omnipresent instability in microfluidics: the Rayleigh–Plateau instability. This instability is best explained energetically. We consider the total capillary energy of a column of fluid that has a fixed volume V. This energy is:

$$E_C = 2\pi RL\gamma = \frac{2\pi V\gamma}{R}.$$

We now consider the energy associated with a collection of N drops of radius R' of the same volume:

$$E = 4\pi R^2 N\gamma = \frac{3\gamma V}{R}.$$

We thus see that the drops with radii

$$R' \geq \frac{3}{2\pi} R,$$

become more energetically favorable than the column. An instability is thus developed, and the column 'prefers' to form a string of drops, which can be useful for printing and encapsulating. A rigorous calculation shows that the column is destabilized for perturbations of wavelength:

$$\lambda \geq 2\pi R.$$

The most unstable wavelength is thus equal to $2\pi R\sqrt{2}$. The radius R' associated with the drops is more precisely estimated by the relation:

$$\frac{R'}{R} = \left(\frac{3\pi}{\sqrt{2}}\right)^{1/3} \quad \text{implying} \quad R' \approx 1.85R.$$

To conclude, we show that the instability calculation also provides the length L of the column above which drops will appear:

$$L = U\left(\frac{8\rho R^3}{\gamma}\right)^{1/2},$$

where U is the velocity of the jet, and λ the instability wavelength.

2.7.8 **The breaking up of a nanojet**

What happens when the jet becomes nanometric, that is to say, possessing a diameter on the order of a few to a few tens of nanometers? There have not yet been any experiments investigating this subject, but numerical simulations based on molecular dynamics have been carried out. In these simulations, the trajectories of the fluid particles are calculated one by one, assuming in general that they are evolving in a Lennard–Jones potential (introduced at the beginning of this chapter). The analysis of these simulations [41] shows that at the nanometer scale, thermal noise is responsible for the breaking up of the jet. A fundamental magnitude in this type of problem is the scale allowing the comparison of the thermal energy (given by kT), and the energy per unit liquid/gas interface (assuming that the liquid jet is in a gas), given by γ. The following length scale can thus be defined:

$$l_B = \sqrt{\frac{kT}{\gamma}}.$$

A typical value of l_B for the oil air interface is 4 nanometers. For jets much larger than just a few nanometers, the Rayleigh instability dominates, while for jets on the order of tens of nanometers, Brownian motion 'mixes' the interface in the surrounding fluid, as if it were acting on miscible fluids. Obviously, experimental studies must be carried out to confirm that this type of situation is physically observable.

2.8 Microfluidics of drops and bubbles

2.8.1 Introduction

As we have emphasized in preceding sections, capillary forces play an important role in miniaturized systems. This characteristic can be a hindrance: one example is the appearance of interfering bubbles in microcanals during the initial filling with liquid. Due to the predominance of anchoring capillary forces over viscous shear forces, it is difficult to get rid of the bubbles using fluid flow alone. Certain laboratories have tried to use capillary forces in a constructive manner, and this has given rise to the 'microfluidics of drops also called digital microfluidics'. The object of this field is to transport and transform fluid samples in a controlled manner, not in canals, but in drops. In this context, the pumping of fluids becomes a problem of drop displacement, and the mixing problem becomes an issue of mixing within drops. The domain of drop microfluidics was still in its infancy when this book was written, but will likely be strongly developed in the future.

2.8.2 Gradients of roughness or chemical properties on surfaces

One way to move a liquid drop placed on a surface is to adjust the gradient of energetic properties of the surface exposed to the liquid. This can be done by depositing molecular layers or by varying the surface roughness. In both cases, the mechanism for motion is the same; this mechanism is depicted in Fig. 2.29.

The Young–Dupré relation describes the different contact angles at the left and the right of the foot of the drop. In the case shown in Fig. 2.29, the curve of the drop is larger on the right half than on the left half. Pressure differences within the drop result. Since we are in a liquid, fluid motion will occur from higher to lower pressure; thus, in the case shown in Fig. 2.29, fluid moves from the right to the left. As a result, the drop will advance towards the left, i.e. to the side where the curvature is smaller and the contact angle is smaller. If the moving drop of water has a hydrophilic and a hydrophobic part, the water will leak from

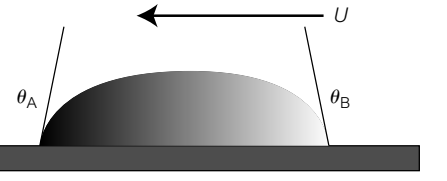

Figure 2.29 Difference between the contact angles of two sides of a drop produced by a gradient in the roughness of a surface or a gradient in the surface chemistry. Due to the different radii of curvature, the drop will move to the side where the contact angle is smaller.

the hydrophobic regions to be redirected towards the hydrophilic regions. This is understandable in terms of the end goal to minimize the energy of the system.

2.8.3 **The phenomenon of electrowetting**

When the base of a drop is subjected to an electric field, the contact angle varies with respect to the situation where the electric field is zero. This phenomenon is called electrowetting. It is governed by the law of Lippman–Young, which is written:

$$\cos\theta = \cos\theta_0 + \frac{1}{2\gamma} CV^2,$$

where θ is the contact angle, θ_0 is the same angle in the absence of an electric field, C is a capacitance and V is the difference in electrostatic potential. This relation shows that by applying a different electric field on the right and left parts of a drop, it becomes possible to displace the drop. This principle was used to make a fluid micromotor (Fig. 2.30) and a complex system where drops circulate along a network (Fig. 2.31).

We refer the reader to references [42] and [35] for more detail on these devices.

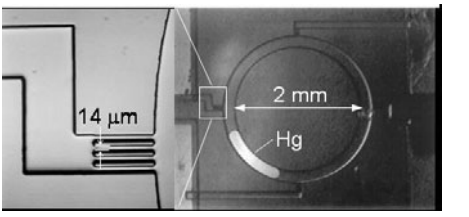

Figure 2.30 Liquid micromotor, where a volume of mercury (shown in white) is put into circular motion in a ring; here, a rotating electric field acts on the coupling angles of the fluid/substrate volume, and leads to its displacement. On the left side of the figure, a detail of the circuit producing the electric field in the ring is shown [42].

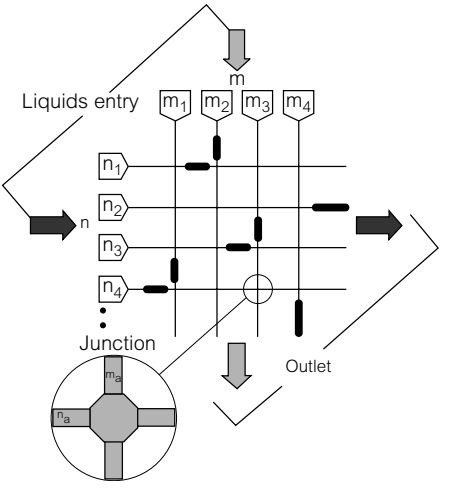

Figure 2.31 Network of canals along which a drop circulates under the effect of electrowetting forces [35].

2.9 Diphasic flows, emulsions in microsystems

2.9.1 Introduction

In many cases, it is beneficial to circulate two immiscible phases in the same microfluidic system. One example is that of microexchangers, which ensure the cooling of integrated circuits [44]. Along the exchanger, the liquid is heated up, then subjected to a phase transition to gas. There are thus two immiscible phases flowing in a microcanal. Another example is that of emulsions [45, 46]. It seems desirable to take advantage of the absence of inertial instabilities in miniaturized systems to produce liquid-liquid drops in a well-controlled manner. This method is comparable to methods allowing the production of well-calibrated liquid–gas droplets in inkjet printers and microdroplet dispensers. Currently, researchers are trying to develop this type of approach to produce emulsions. We will see that the physics of liquid-liquid systems are more complex than that of ink jets in air. This is undoubtedly why there are not more commercialized miniaturized emulsion systems. The production of liquid structures in microsystems is still being worked out. Before introducing miniaturized systems, it will help to recall that for macrometric hydrodynamics, diphasic flows are not a *terra incognita.* Multiphasic systems have in fact been studied to a great extent these last few decades (see, for example, [43]). Motivations for this have been principally industrial, particularly in the oil and nuclear industries. The behavior of diphasic flows is in general very complex: interfaces adopt elaborate forms, and classification of regimes can sometimes lead to inextricable phase diagrams, where many regimes are mixed-up. An example of this situation can be seen in a vertical water-gas flow for a canal of decimetric size, taken from [43] and shown in Fig. 2.32a.

Several different regimes can be identified, known as: 'bubble, slug or plug, annular, churn, wispy annular.' The parameters controlling these regimes are the flow rates, the characteristics of the two fluids, and the diameter of the canal. The diagram of Fig. 2.32 illustrates these observed regimes.

In the figure, U_L and U_G are the values of the flow rates of the liquid and the gas, divided by the cross-section of the canal (these quantities are known as 'superficial velocities'). We see that the parameters shown in the diagram are inertial parameters, and will probably not be relevant for microsystems. We may anticipate here that the morphologies of flow in microsystems will be very different from those shown in Fig. 2.32, as the physical parameters in play are completely different.

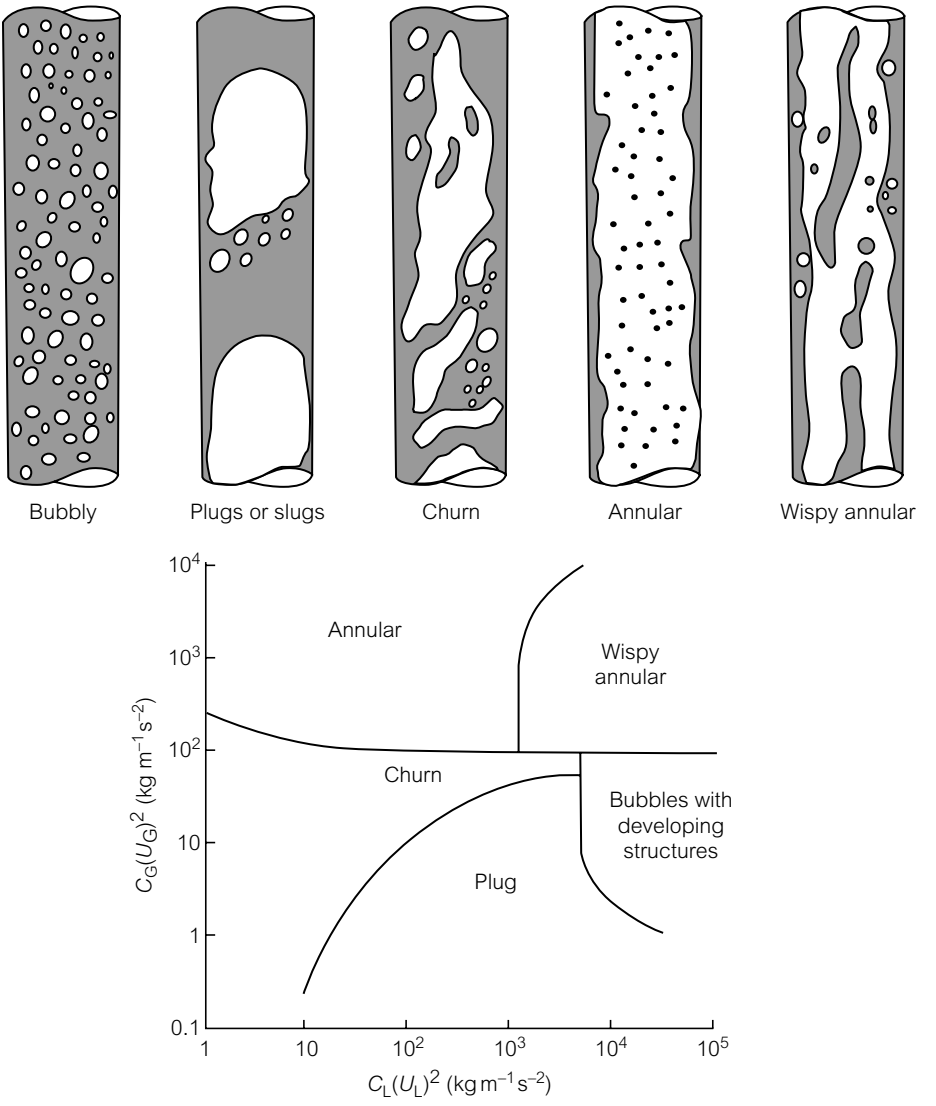

Figure 2.32 Regimes obtained in a vertical canal of decimetric size, through which there is a flux of water and air. [43].

Diphasic flows in microsystems

This domain is still not well documented. Some experimental results obtained from [34] will be described here. In a microsystem, gravity can be neglected, and the dominant phenomena are those related to viscous stresses and to capillarity. We examine the corresponding scaling laws. Take a bubble of size l, subjected to a flow U in a microcanal. The force exerted

(Continued)
by such a flow on a bubble is, by order of magnitude:

$$F \sim \mu l U.$$

Capillary forces or wetting are involved in this problem and are, by order of magnitude:

$$F_C \sim \gamma l.$$

The competition between these two types of forces will be denoted by a dimensionless number defined as:

$$Ca = \frac{\mu U}{\gamma}.$$

This is the capillary number that we have already mentioned. According to scaling laws, we saw in Chapter 1 that the velocity varies proportionally to l. We thus have the following estimation:

$$Ca \sim l.$$

We can thus generally consider that in microsystems, the capillary number is small, which signifies that capillary effects tend to dominate over viscous effects. This estimation is acceptable for liquid–gas systems (giving rise to inkjet printers). However, miniaturized liquid–liquid systems have until now used the addition of surfactants to favor, as we will see, the appearance of well-defined structures (such as spherical drops). The consequence of this is a reduction of the interfacial tension γ, and thus an augmentation of the capillary number. Thus, in experiments that are actually carried out in water-oil systems, the capillary number must be considered to vary between 10^{-3} and 10^{-1}. Laws governing capillary effects are not always applicable in these microfluidic systems: both cases (whether or not capillary effects are dominant) must be considered. We can thus anticipate the following behavior.

- At small capillary numbers, capillarity dominates, and bubbles and drops will be spherical, or will have a shape imposed by the conditions of interaction with the surface. We will have a static situation: the flow plays a role, but this role is mostly kinematic, and it must accommodate itself to the constraining morphologies imposed by capillarity. One possible situation could be, for example, a spherical drop being carried, without deformation, by a fluid flux.
- As for moderate capillary numbers, structures will be subjected to deformations induced by the viscous forces. The flow affects the morphologies, tending to align the interfaces along streamlines. In this case, we expect simple interface morphologies if the flow itself has a simple structure.

(Continued)

These general conditions were able to be demonstrated in the experiments of reference [34] (Fig. 2.33). The fluids used are tetradecane and water, both with and without the surfactant Span 80. The fluids were made to flow in a canal 25 μm deep and 200 μm wide that was etched in glass and covered with a silicon wafer (see Chapter 6). In the case where the surfactant is present (with a concentration much higher than the CMC), well-defined morphologies are obtained (see Fig. 2.34: isolated flattened drops, pairs of drops, necklaces

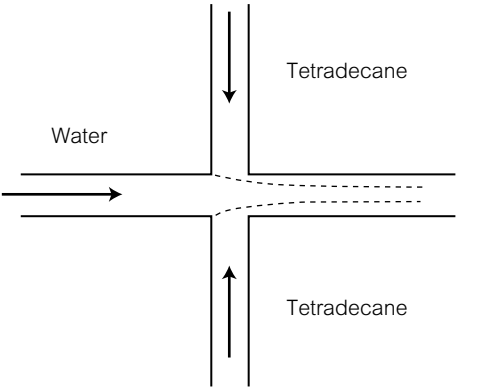

Figure 2.33 Diagram of the experiment of [34]: water is injected at the center, tetradecane at the sides, and the fluids are collected in a principal microcanal.

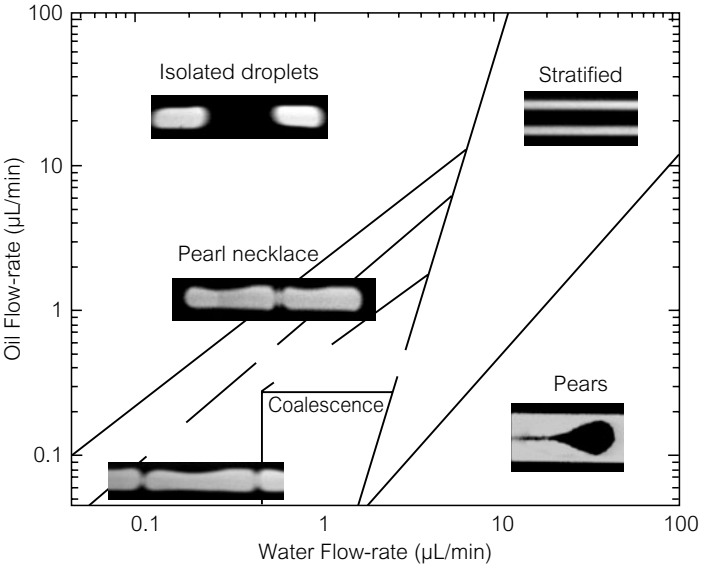

Figure 2.34 Different regimes observed in a microcanal 20 μm deep and 200 μm wide, for tetradecane-water systems, with a surfactant (Span 80) whose concentration is over the CMC [34].

(Continued)

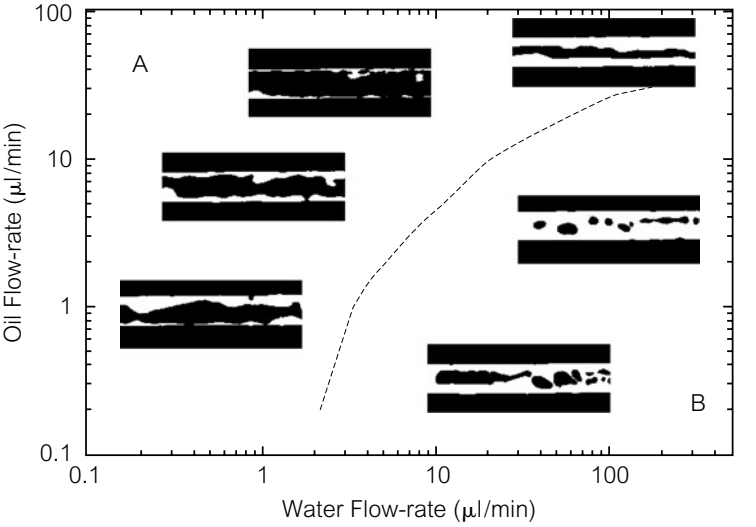

Figure 2.35 Disordered regimes observed in a microcanal, 200 μm wide, 20 μm high, for tetradecane-water systems, without surfactants (From [34]).

of drops, stratified regimes, pears, etc., We can analyse the evolution of the morphologies in the diagram by introducing the capillary number (which favors stratified regimes) and the volumetric fraction of water (whose increase favors the aggregation of drops).

All the preceding regimes were obtainable due to the presence of a surfactant, which favors the emergence of well-defined structures that can be transported without contacting the surface, as if lubricated by the other phase. In the absence of surfactant, very different morphologies are obtained (Fig. 2.35).

In this case, wetting is partial, and contact lines develop. Regimes are governed by the movement of the contact lines along the surface. The experiment shows that the lines are trapped on the surface on fixed sites (probably due to the inevitable presence of impurities). The flow produced is therefore meandering, unshaped, and unsuitable for forming well-defined structures.

The experiment thus confimed that miniaturization tends to oppose the action of surfactants due to the scaling effects explained above. For water-oil flows in microsystems, this signifies that it will be difficult to obtain liquid/liquid drops of nanometric size: in effect, the more one miniaturizes, the more partial the wetting and the more disordered the regimes become, such as those that are shown in Fig. 2.35; it thus becomes more difficult to form drops. These phenomena are very different from those taking place in macrometric systems. It is obviously necessary to take them into account any effort dedicated to producing well-controlled morphologies.

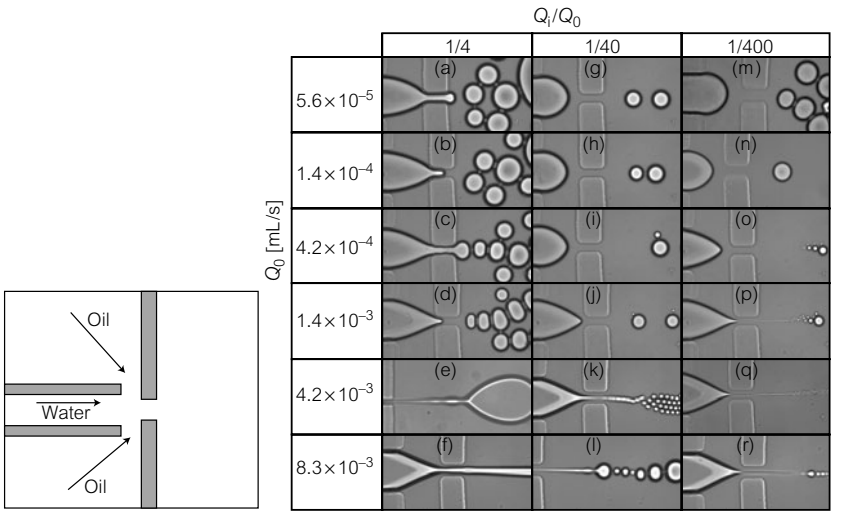

Figure 2.36 Different regimes produced by the experiment of [48].

2.9.2 **Emulsions in microsystems**

A number of groups have recently tried to create emulsions in microfluidic systems [45–46]. The experiment of Thorsen *et al.* [47] proved that interesting structures, such as intertwined droplets, can be the basis for forming an emulsion. This experiment was carried out in PDMS microcanals using 'soft lithography', which will be described in Chapter 6. The fluids used here are tetradecane and water, with an important addition of surfactant, for reasons described previously. The research team of [48] demonstrated the richness of the variety of emulsion regimes. Some of these are depicted in Fig. 2.36. PDMS is also used in this case for the fabrication of microstructures. Injection is symmetric, with water (labelled with fluorescein) being injected in the center, and oil at the sides. Polydisperse drops a few dozen micrometers in diameter are formed. Here as well, we have the formation of a macro-emulsion. The patterns produced by the instability phenomena are often remarkable: for example, Anna *et al.* [48] were able to obtain 'crystals' of droplets.

These experiments undoubtedly constitute a departure point for the development of systems that may, in the future, allow for the creation of 'tailor-made' emulsions.

References

[1] A. Groissman, V. Steinberg, *Nature*, **410**, 905 (2001).

[2] G. Batchelor, *An Introduction to Fluid Dynamics*, Cambridge University Press.

[3] E. Guyon, J.P. Hulin, L. Petit, *Hydrodynamique Physique*, CNRS Edition, 2nd edn, 2001.
[4] M. Gad-El-Hak, 'The Fluid Mechanics of Microdevices[a], *J. Fluid Eng.*, **121**, 5 (1999).
[5] Israelachvilii, *J. Colloid Interface Sci.*, **110**, 263 (1986).
[6] M. Martin, G. Blu, G. Guiochon, *J. Chromat.*, **72**, 399 (1975).
[7] M. Cecillon, P. Tabeling, Experiment carried out at the MMN laboratory (2001).
[8] M. Knudsen, *Annal. Phys.*, **28**, 75, 130 (1909).
[9] G. Karniadakis, A. Beskok, *Micro Flows*, Springer Verlag (2002).
[10] Maxwell, *Phil. Trans. Roy Society*, I, **17**, 231 (1879).
[11] S. Schaaf, in *Modern Developments in Gas Dynamics*, W. Loh (ed.), Plenum Press, 235 (1969).
[12] E. Arkilic, K. Breuer, M. Schmidt, *J. Fluid. Mech*, **437**, 29 (2001).
[13] C. Aubert, S.Colin, *Microscale Therm. Eng.*, **5**, 1, 41 (2001).
[14] J. Maurer, P. Joseph, H. Willaime, P. Tabeling, *Phys. Fluids*, **15** (9), 2613 (2003).
[15] Li, Xinxin, W.Y. Lee., M. Wong, Y. Zohar, *Sens. Actuators*, **83**, 277 (2000).
[16] L. Leger, H. Hervet, R. Pit, *Phys. Rev. Lett.*, **85**, 980 (2000).
[17] Y. Zhu, S. Granick, *Phys. Rev. Lett.*, **87**,9, (2001).
[18] P. Thompson, S. Troian, *Nature*, **389**, 360 (1997).
[19] P.A. Thomson, S.M. Troian, *Phys. Rev. Lett.*, **63**, 766 (1997).
[20] P.G. De Gennes, *Langmuir*, **18**, 3413 (2002).
[21] Y. Zhu, S. Granick *Phys. Rev. Lett.*, **88**, 10 (2002).
[22] C. Cottin-Bizone, J.L. Barrat, L. Bocquet, E. Charlaix, *Nature Mater.*, **2**, 237 (2003).
[23] J. Pfhaler, C. Harley, H. Bau, J. Zemel, *ASME*, **32**, 49 (1991).
[24] D. Tretheway, C. Meinhart, *Lett. Phys Fluids*, **14**, 3, L9 (2002).
[25] N. Giordano, J.T. Cheng, *J. Phys: Condens. Matter*, **13**, R271 (2001).
[26] H.A. Stone, A.D. Stroock, A. Ajdari, *Ann. Rev. Fluid. Mech.*, **36**, 381 (2004).
[27] Landau-Lifschitz, *Mécanique Statistique*, Mir, 1967.
[28] Y. Lee, T. Kang, Y. Cho, *Proc. IEEE*, 403 (2000).
[29] S. Bendid, O. Francais, P. Tabeling, H. Willaime, *Proc. 12th Micromechanics Eur. Work. MME2001*, 16–18th Sept., 23 (2001).
[30] M. Madou, *Fundamentals of Microfabrication*, CRC Press (2000).
[31] M.K. Chaudury, G.M. Whitesides, *Langmuir*, **7**, 1013 (1991).
[32] K.L. Johnson, K. Kerdall, A.D. Roberts, *Proc. Roy. Soc. Lond.*, **A324**, 301 (1971).
[33] P.G. De Gennes, F. Brochard, D. Quéré, *Gouttes, Bulles, Perles Ondes*, Edition Belin, 2002.
[34] R. Dreyfus, P. Tabeling, H. Willaime, *Phys. Rev. Lett.*, **90**, 14 (2003).
[35] J. Lee, H. Moon, J. Fowler, T. Schoellhammer, C.-J. Kim, *Sens. Actuators*, **A95**, 259 (2002).
[36] E. Dussan V, *Annual Rev. Fluid. Mech.*, **11**, 371 (1979).
[37] P.G. De Gennes, *Rev. Mod. Phys.*, **57**, 827 (1985).
[38] U. Boehnke, T. Remmler, H. Motschmann, S. Wurlitzer, J. Hauwede, Th. M. Fischer, *J. Colloid Int. Sci.*, **211**, 243 (1999).
[39] E. Lauga, M. Brenner, H. Stone, to appear in *Handbook on Experimental Fluid Dynamics*, Springer (2005).
[40] One example out of numerous contributions, W. Helfrich, *Z. Naturforsch.*, **29**c, 510 (1974).

[41] J. Eggers, *arXiv:physics/02011001* v1, 2 January 2002.

[42] J. Lee, C.-J. Kim, *J. Microelectromech. Systems*, **9**, 171 (2000).

[43] G. Hetsroni, *Handbook on Multiphase Flows*, Clarendon Press (1980).

[44] L. Zhang, J.M. Ko, K.K. Goodson, J.G. Santiago, T.W. Kenny, *J. of MEMS*, **11**, 1 (2002).

[45] S. Sugiura, M. Nakajima, S. Iwamoto, S. Seki, *Langmuir*, **17**, 5562 (2001).

[46] P.B. Umbanhowar, V. Prasad, D.A. Weitz, *Langmuir*, **16**, 347 (2002).

[47] T. Thorsen, R. Roberts, F. Arnold, S. Quake, *Phys. Rev. Lett*, **86**, 4163 (2001).

[48] S. Anna, N. Bontoux, H. Stone, *Appl. Phys. Lett.*, **82**, 4163 (2003).

THREE

Diffusion, mixing, and separation in microsystems

3.1 Introduction

In lab-on-a-chip or 'μTAS' systems, it is often necessary to mix reactants. For example, in biology, in order to identify proteins in an unknown sample, proteins are fragmented by mixing them with enzymes. Proteins can then be characterized using mass spectrometry analysis of the resulting fragments. This method is the 'modern' method of protein identification[1], and the corresponding field is known as proteomics[2]. In both miniaturized and non-miniaturized analytical chemistry, the identification of a component generally depends on the analysis of chemical transformations carried out in a reactor where the reactants are supposed to be mixed. How is it possible to mix in a microsystem, where, as we saw in the preceding chapter, the Reynolds number is so small that hydrodynamic instabilities and turbulence are practically non-existent? This is the problem of mixing in miniaturized systems, and, more generally, in all chemical microreactors. We attempt to answer these questions, and this leads us to present several ideas on chemical kinetics, the process of diffusion, and dispersion phenomena. Another topic developed in this chapter is that of adsorption. The phenomenon of adsorption involves the trapping of objects (molecules or particles) on surfaces. In microsystems, the surface-to-volume ratio is high, implying that surfaces play an important role. If the surfaces of a miniaturized system happen to be very adsorbant with respect to the transported molecules, these surfaces could possibly prevent the transport of these molecules through the microcanals. On the other hand, adsorption is also

[1] The 'traditional' method is based on 2-D gels, which consists of the decomposition of proteins on a gel according to their isoelectric point and their molecular mass. This method was first proposed in 1975 by O'Farrell [1].

[2] Microfluidics has been called upon to make methodological progress in proteomics.

the fundamental mechanism on which many powerful separation techniques in analytical chemistry are based. In particular, the domain of chromatography has advanced significantly over the last thirty years, and today allows the separation of one single sample into hundreds of components. At the time this book was written, large efforts were being made to miniaturize chromatographic systems. In the 'μTAS' literature, dozens of articles on this subject are published each year. We will thus present in this chapter the general phenomena related to adsorption, as well as the most common chromatographic techniques. We will also mention a few recent studies seeking to miniaturize separation systems, using either well-known designs or completely novel concepts[3].

3.2 The microscopic origin of diffusion processes

3.2.1 Brownian motion

Brownian motion was discovered in 1827 by a Scottish botanist named Robert Brown[4]. By using a microscope, Brown showed for the first time the erratic character of the movement of pollen grains on the surface of water. He suggested that the origin of this phenomenon was related to the existence of numerous collisions between pollen grains and water molecules. The theory of Brownian motion and of molecular diffusion was worked out much later, at the start of the twentieth century, from the work of Langevin, Smoluchowshi and Einstein [4].

One-dimensional Brownian motion is often shown as a walker on a line, taking steps of length $\pm l$ in a random manner, rather like a drunkard (Fig. 3.1).

A Brownian walker like this occupies a position $X(N)$ from the origin that is equal to the sum of the N steps that it has made:

$$X(N) = \sum_{1}^{N} l_i,$$

where l_i is a random variable that can take two values: $+l$ or $-l$. To determine the squared value of the displacement of the walker, the following quantity must be calculated:

$$X^2(N) = \sum_{1}^{N} l_i^2 = N < l^2 >.$$

[3] A well-documented review of this field can be provided by [2, 3].

[4] Although in reality, credit for the discovery should probably be given to Dutch doctor Jan Ingenhousz, who in 1785 noticed the erratic movement of charcoal powder on the surface of an alcoholic solution.

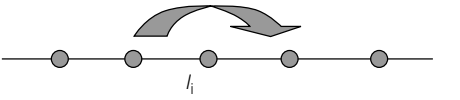

Figure 3.1 Brownian walker along a line. The walker takes random steps of length l from left to right.

As N can be taken to be proportional to time t, we have the following relation:

$$X^2(N) \sim Dt,$$

where D is a diffusion coefficient . Although a Brownian walker makes larger and larger excursions as time goes on, it remains, on average, at its initial position. A collection of walkers would generate a spot in two dimensions that would expand in time according to the preceding law. This law corresponds to the spreading of a spot in a fluid at rest, a situation that we will describe in Section 4.1 with the help of the evolution equations and directly using statistical averages. Nevertheless, from the Brownian model it is possible to obtain the appearance of the distribution of walkers within such a spot. It is a matter of a fundamental statistical result: the 'Central Limit Theorem.' This theorem stipulates that at long times, the distribution of the number of walkers in space is Gaussian. For a spot of dye in a fluid, this signifies that the concentration field is a Gaussian function of the spatial coordinates, a result confirmed by the diffusion equation.

Normal and anomalous diffusion

The concept of 'anomalous' diffusion can be introduced by generalizing the Brownian model discussed previously. We assume that the walker makes a step of length l with a probability $p(l)$. To determine the variance of the displacement $X(N)$, we must calculate the following quantity:

$$X^2(N) = \sum_1^N p(l_i) l_i^2.$$

It is thus necessary to differentiate between two situations:

- the distribution $p(l)$ is narrow: in this case, we can show that as N goes to infinity, the variance tends to be proportional to N, and we find the properties of the ordinary Brownian diffusion process. This situation is known as 'normal' diffusion;
- the distribution $p(l)$ is wide (for example, it decreases slowly with the argument l). In this case, it is no longer possible to establish that at large values of N, $X^2(N)$ and N are proportional to each other. Once this proportionality is lost, we are no longer in the regime of ordinary diffusion, and the corresponding process is known as 'anomalous diffusion.'

(Continued)
The notion of anomalous diffusion comes into play once statistical pathologies appear in the process defining the displacement of the walkers. This point can be clarified by reasoning in a continuum, that is to say by replacing the sums with integrals. Thus, the average of X, evaluated at large values of N, is rewritten in the following form:

$$\langle X \rangle = \int_0^\infty X\, p(X) \mathrm{d}X, \tag{3.1}$$

where $p(X)$ is the probability density function (pdf) associated with the quantity X. To discuss the different cases we assume that $p(X)$ has the following form:

$$p(X) \sim X^{-(1+\mu)}$$

at large values of X, we see that the integral (3.1) only converges if μ is greater than 1. If, on the other hand, μ is less than 1, the integral diverges, and it is no longer possible to define the ensemble average. We are dealing with an anomalous diffusion process in this case. These algebraic distributions are known as the Levy distributions. What do we do in this situation? It is necessary to reason with finite times. We define $X_{\max}$ as the maximum value of X in the period of time that we are considering, i.e. times between 0 and $T_{\max}$. $X_{\max}$, which increases indefinitely with time, represents the most intense event during a given period of time. Using this quantity, we can write for a Levy distribution:

$$\langle X \rangle = \int_0^{T\,\max} X\, p(X) \mathrm{d}X \sim X_{\max}^{(1-\mu)}. \tag{3.2}$$

Thus, in this case the ensemble average is controlled by the most intense event of the distribution. This very specific situation references the 'physics of rare events,' where the statistical averages of an entire process are controlled by one single event: the most intense event. In physics, anomalous diffusion processes are actually common: they are involved in the physics of polymers, in the phenomena of hydrodynamic dispersion, and in diffusion in non-Newtonian systems. Anomalous diffusion is also an important concept in the domain of transport phenomena in fluids.

3.2.2 **The Stokes–Einstein law**

The Brownian walker models the diffusion of molecules evolving in a free environment, where the only relevant events are collisions at localized sites. One way we use this model is to understand the process of diffusion of one gas in another. However, when the 'diffusers' (small particles, molecules, etc.) find themselves immersed in a dense phase (for example a liquid of viscosity μ), the problem must be formulated differently in order for the role of the dense phase to appear explicitly (as intuition may suggest). In this case, the diffusers can be described as satisfying a stochastic equation known as the Langevin equation.

This equation has the following form:

$$\frac{\mathrm{d}u}{\mathrm{d}t} - \beta u = f(t),$$

where u is one of the three velocity components of the diffuser, and β is a friction coefficient representing the friction exercised by the fluid on the particle. The Langevin equation expresses mechanical equilibrium for a particle immersed in a fluid and subject to the effects of friction forces, its own inertia, and stochastic forcing (translating into the presence of collisions), which is all contained in the function $f(t)$. The factor β representing the friction of the liquid acting on the diffusers is written:

$$\beta = 6\pi R\mu/m,$$

where R is the radius of the diffuser (assumed to be spherical), μ is the viscosity of the fluid, and m is the mass of the diffusing particle. $f(t)$ is a stochastic function (i.e. random with respect to time), defined by its moments. This equation models the succession of collisions experienced by the diffuser in the fluid, which is the cause of its displacement. Since the collisions are very brief and are not correlated with each other, it is natural to use for $f(t)$ a delta-correlation function in time:

$$\langle f(t)f(t')\rangle = A\delta(t - t'),$$

where δ is the Dirac distribution, and A is a constant that will be determined later. We will use this property of 'delta correlation in time' to determine the statistics of the movement of the particle. After integrating the Langevin equation, we obtain the following result:

$$u(t) = u_0 \mathrm{e}^{-\beta t} + \mathrm{e}^{-\beta t} \int_0^t \mathrm{e}^{\beta t'} f(t')\mathrm{d}t'. \tag{3.3}$$

The order of magnitude of the time constant β^{-1} is 10^{-8} s for a particle of 1 μm immersed in water. This time may seem short and it would be tempting to immediately take the limit of long times in the expression of $u(t)$, which would lead to the elimination of the first term of the right-hand side of equation (3.3). However, in reality, when carrying through the calculation it is very important to conserve such a term.

The variance of the displacement $x(t)$ of the particle is calculated in the following manner (this calculation is taken from Taylor [5]):

$$\frac{\mathrm{d}x^2}{\mathrm{d}t} = 2x(t)u(t) = 2\int_0^t u(t)u(t')\mathrm{d}t'.$$

Taking the ensemble averages of each term of this relation, we find:

$$\frac{\mathrm{d}\langle x^2\rangle}{\mathrm{d}t} = 2\langle u^2\rangle \int_0^t R(\tau)\mathrm{d}\tau, \tag{3.4}$$

where $\langle u^2\rangle$ is the variance of the velocity of the particle, and $R(\tau)$ is the correlation coefficient, which is defined as:

$$R(\tau) = \frac{\langle u(0)u(\tau)\rangle}{\langle u^2\rangle}.$$

This relation is obtained by manipulating integrals and using the fact that the correlation of the velocities does not depend on the times t and t' themselves, but on the difference $t - t'$ (we assume that the description of the system is independent of the choice of the origin of time). Re-examining the solution of the Langevin equation (3.3), we obtain (noting that the function $f(t)$ is delta-correlated with time, and that all correlations of the type $\langle f(t)f(t')\rangle$ are thus zero):

$$R(\tau) = \mathrm{e}^{-\beta\tau}.$$

After that, substituting this expression into (3.4), we have for times much larger than β^{-1}:

$$\langle x^2(t)\rangle = 2Dt.$$

The particle follows a Brownian-type motion, with a coefficient of diffusion D given by:

$$D = \frac{\langle u^2\rangle}{\beta}.$$

To arrive at the Stokes–Einstein relation, it is necessary to note that $\langle u^2\rangle$ is subjected to the energy equipartition theorem. It is thus:

$$\frac{1}{2}m\langle u^2\rangle = \frac{1}{2}kT.$$

We arrive at the formula of Stokes–Einstein [4]:

$$D = \frac{kT}{6\pi R\mu}.$$

This expression is important to remember. It allows the estimation, often more accurate than 30%, of a large number of diffusion coefficients based on the size of the diffusing molecule. For example, for the diffusion of oxygen in water, taking 1.73 Å as the radius of the oxygen molecule, the law of Stokes–Einstein gives a value of 1.3×10^{-5} cm^2/s, at 25 °C [6]. This value is only 30% lower

than the measured value, and thus the order of magnitude is well estimated. The formula of Stokes–Einstein becomes imprecise in highly concentrated solutions and in non-Newtonian fluids, such as polymers.

3.3 Advection-diffusion equation and its properties

3.3.1 Fick's Law

We have explained in detail the motion of isolated walkers. Now, we will consider a group of diffusers that is characterized by a mass concentration $C(\boldsymbol{x}, t)$ defined by the relation:

$$C(\boldsymbol{x}, t) = \frac{\delta m}{\delta V},$$

where δm is the mass of the collection of diffusers that are contained in δV at the point $\boldsymbol{x}$ and at time t (Fig. 3.2).

It is also necessary to define the flux by:

$$J = \frac{\delta m}{\delta t \delta A},$$

where δA is the surface element through which the flux passes. A fundamental law relating the flux to the gradients is Fick's law. This law is expressed with the following relation:

$$J = -D\nabla C,$$

where D is the diffusivity, or the coefficient of diffusion, that can be massive, molecular, or chemical. This law can be obtained by considering the movement of a collection of Brownian walkers. Fick's law is thus justified, in principle, in dilute systems. However, in practice, the domain of the validity of Fick's law can

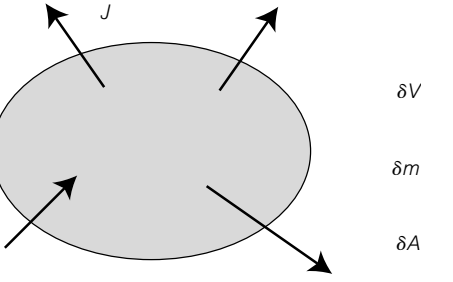

Figure 3.2 Representation of an elementary volume crossed by a material flux.

be considered to be very large, to the point that it would not be necessary to introduce the notion of a 'non-Fickian' system in the way that 'non-Newtonian' systems were mentioned in the preceding chapter.

The units of the diffusion coefficient are m^2/s, and it is instructive to note that dimensionally, both D and the kinematic viscosity ν have the same units. Both cases involve a coefficient characterizing the transport of a quantity, giving rise to a 'flux.' It is thus logical to find the same units for these two fundamental physical parameters. For gases, we have the following estimation:

$$D \approx \frac{1}{3}\lambda u,$$

where λ is the mean free path and u the speed of thermal agitation. This relation agrees with measurements of D, which give a value of about 0.15 cm^2/s for gases under normal conditions. For liquids, D is much weaker because we are dealing with a dense phase, and the viscosity of the surrounding fluid must be taken into account as it slows down the displacement of molecules. Several values for molecules diffusing in water at 20 °C [6] are shown in the table below:

Solute	D (cm^2/s)
water	10^{-5}
fluorescein	3×10^{-6}
sucrose	4.6×10^{-10}
myosin	1.2×10^{-11}

It is interesting to note that those values are well predicted by the Stokes–Einstein equation, which we rewrite here:

$$D = \frac{kT}{6\pi R\mu}.$$

In general, the orders of magnitude of the coefficients of diffusion for simple liquids (such as water in water or alcohol in water), are on the order of 10^{-6} to 10^{-5} cm^2/s. The small diffusion coefficients for sucrose and myosin are due to the large size of these molecules: large molecules have difficulty displacing themselves, since they are more susceptible to viscous friction forces of the liquid environment. The correlation of the diffusion coefficient with size can also be seen in the Stokes–Einstein relation.

3.3.2 **Advection-diffusion equation**

The advection-diffusion equation formalizes the law of conservation of mass for an elementary volume such as the one shown in Fig. 3.2. To find this equation, we write that the rate of variation of the mass of such an element results from

the diffusion flux, governed by Fick's law, crossing the surface bounding this volume[5]. We thus obtain the advection-diffusion equation:

$$\frac{DC}{Dt} = \frac{\partial C}{\partial t} + \boldsymbol{u}\nabla C = D\Delta C + s(\boldsymbol{x}, t)$$

where $\boldsymbol{u}$ is the velocity field in which the 'dye' is immersed and $s(\boldsymbol{x}, t)$ is a source (or a sink, depending on its sign). There are two important cases: if $\boldsymbol{u}$ is zero, we are dealing with pure diffusion. If $\boldsymbol{u}$ is not zero, we were dealing with advection-diffusion or dispersion phenomena. We now discuss a few properties of the advection-diffusion equation.

– In the absence of a source, and in the case where $D = 0$, the advection-diffusion equation is simplified and we obtain:

$$\frac{DC}{Dt} = 0.$$

Thus, the local concentration $C(\boldsymbol{x}, t)$ is conserved along the trajectories of the fluid particles. This important property is applicable at 'short' times, i.e. during an interval of time where diffusion has not yet acted. For example, in the succession of photos in Fig. 3.3 (where a fluorescent spot was placed in a turbulent flow [7]), we can consider that in the first two images, the characteristic extension of the spot remains such that the associated diffusion times are much longer than the experiment time. Thus, for such a period of time, diffusion can be neglected, and everything takes place as if $C(\boldsymbol{x}, t)$ is conserved along the trajectories of the fluid particles. This property is lost in the following photos, where the spot has reorganized into thin striations: in this case, the diffusion times have become comparable to the experiment time.

– Returning to a more general case (where D is not zero), we define a quantity analogous to energy by the expression:

$$\Theta = \int C^2 \mathrm{d}x\mathrm{d}y\mathrm{d}z,$$

where the integral is taken over the whole volume occupied by the fluid. This quantity is called the variance of the concentration. In the absence of a source or a sink, and in the case where the boundaries of the fluid volume are impermeable to the tracer in question, we can validate the following relation:

$$\frac{\partial \Theta}{\partial t} = -D \int (\nabla C)^2 \mathrm{d}x\mathrm{d}y\mathrm{d}z.$$

[5] We assume, for the simplification of calculation, that the diffusion coefficient D is a constant.

This exact relation demonstrates that the variance can only decrease over the course of time. The geometric interpretation is that the spots of tracer of course tend to spread (and not to condense). If D was negative, this would be an antidiffusion problem, and the spots would contract in on themselves instead of spreading.

– We can also define the following quantity:

$$\chi = \int (\nabla C)^2 \mathrm{d}x\mathrm{d}y\mathrm{d}z,$$

where, as previously, the integral is carried out over the volume occupied by the fluid. This quantity gives a measurement of the concentration gradients. The important thing to remember is that unlike the variance, concentration gradients can grow with time. This increase in gradients is inevitably produced in a turbulent regime, and is one of the profound, spectacular and astonishing actions of turbulence. In an ordinary turbulent macromixer, the flow reorganizes the field of the tracer, dye, or reactant, and induces an augmentation of concentration gradients. According to Fick's law, this imposes a considerable increase in the transfers between initially unmixed regions. This process is illustrated in Fig. 3.3, where a spot of fluorscein forms fine filaments under the effect of turbulence.

In this case, the increase in the concentration gradients is due to the formation of thin filaments. In this type of experiment, mixing is completed in just a few seconds, while in the absence of turbulence, several days of waiting would be necessary for the mix to be completed. In microsystems, the low Reynolds numbers of the flows make it no longer possible to depend on turbulence for mixing. We will later see a few solutions that have been proposed to deal with this problem.

3.3.3 Order of magnitude of the Peclet number in microsystems

One extremely important dimensionless number in advection-diffusion problems is the Peclet number. It is defined:

$$Pe = \frac{Ul}{D},$$

where U is a characteristic flow velocity, l is the size of the system, and, as we saw above, D is the diffusion coefficient. This number, equivalent to the Reynolds number, measures the relative importance of advection with respect to diffusion. The order of magnitude of the advection terms is $U\delta C/l$ (where δC is a typical

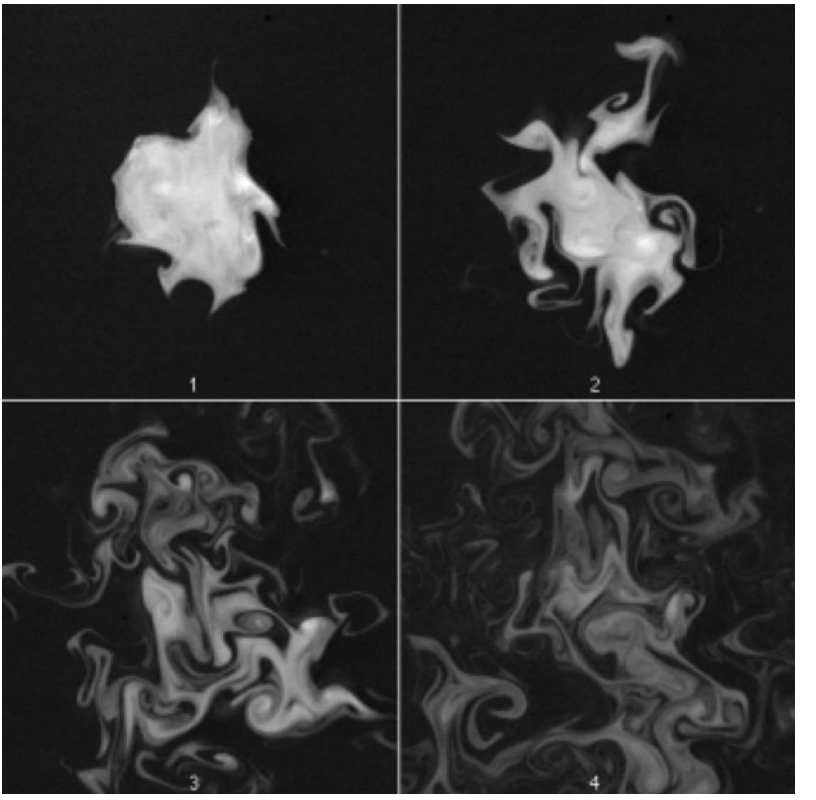

Figure 3.3 Evolution of a spot of fluorescein immersed in a turbulent bidimensional flow, in a thin fluid layer. In this experiment, the Reynolds number is on the order of several thousand, and a turbulent regime is established. The spot spreads in a few seconds; during this first phase of spreading, the variance of the concentration of tracer decreases on average (because the spot spreads), while the gradients increase over the course of time (eventually the gradients decrease, once molecular diffusion begins to act) [7].

variation of the concentration over a distance l), and the order of magnitude of the diffusion terms is $D\delta C/l^2$. The Peclet number represents the ratio of the first term to the second. Thus, the higher the Peclet number, the more the influence of the flow dominates over molecular diffusion. In terms of scaling laws, we can again use the table in Chapter 1 to determine the following relation for the Peclet number:

$$Pe \sim l^2.$$

This again assumes that we work at a fixed pressure difference between the ordinary world and the miniaturized world, a common situation in the domain of microfluidics. We thus have a Peclet number that varies as l^2. We could conclude from this that in microsystems, only diffusion matters, and the

advection terms become negligible—a situation that is in a way analogous to microhydrodynamics. This would imply, for example, that in microsystems, it is useless to stir two fluids to mix them. However, these conclusions would be erroneous: in fact, as we have emphasized in Chapter 1, it is sometimes necessary to perform detailed calculations before coming to a definitive conclusion. It seems that in practice, diffusion coefficients D are low, notably in liquids: as we mentioned above, D is typically on the order of 10^{-5} cm^2/s for simple liquids. Thus, with velocities on the order of 1 mm/s, in a canal 100 μm high, the Peclet number is on the order of 100. We could obviously envision a situation where the Peclet number is small: if we consider a canal a micrometer high, with the same liquid flowing through at 10 μm/s, the Peclet number is 10^{-2}. It is important to note that neither of these two situations are exceptional in the domain of microfluidics. Thus, in microsystems, there is not a characteristic order of magnitude for the Peclet number.

3.4 Analysis of some diffusion phenomena

3.4.1 A fundamental problem of diffusion: the spreading of a spot in a resting fluid

We consider a spot of tracer, assumed to be initially very small, and calculate the spreading of such a spot in a resting fluid. We assume the problem to be unidimensional, where the spatial coordinate is x. The initial conditions are:

$$\text{at} \quad t = 0, C = C_0 \delta(x),$$

where $\delta(x)$ is the Dirac function[6]. With these initial conditions, we find by solving the advection-diffusion equation (reduced in this specific case to a diffusion equation) the following solution for $t > 0$:

$$C(x,t) = \frac{C_0}{\sqrt{4\pi Dt}} \exp\left(-\frac{x^2}{4Dt}\right).$$

It is useful to remember that the size of the spot l can be given by the standard deviation of the distribution associated with the Gaussian function. From this we have the estimation:

$$l \approx 2\sqrt{Dt}.$$

[6] We recall that the Dirac function is a generalized function that is zero everywhere except at the origin, where it has a value of infinity. The integral of the Dirac function is equal to one.

The spot spreads proportionally with the square root of time. This result can be obtained in several different ways: from the solution, we try to find how a line of isoconcentration evolves with time . This result can also be derived via dimensional reasoning: we assume in this case that the general form of the law of spreading of a spot is written:

$$l = f(D, t).$$

After applying the Π theorem, we obtain the result we were seeking, undoubtedly the most important of all results in diffusion.

3.4.2 **Diffusion of a concentration front**

Here, we consider the problem of spreading of a front separating two regions: one untouched, and the other occupied by a tracer with the diffusion coefficient D and initially having a uniform concentration C_0. Just as with the problem of the spot, we are limited here to a unidimensional geometry. The initial condition is thus:

$$\text{at } t = 0, \quad C(x, 0) = C_0 \quad \text{for} \quad x \leq 0, \quad \text{and} \quad C = 0 \quad \text{for} \quad x \geq 0.$$

The exact solution of this problem is calculated by noting that the Dirac function is the derivative of the 'echelon' function of Heaviside (which uses the initial condition of the problem that we consider here). We obtain the following solution for the problem of the spreading of the front:

$$C(x, t) = \frac{1}{2} C_0 \left(1 - \text{erf}\left(\frac{x}{2\sqrt{Dt}}\right)\right),$$

where erf is the error function, which is defined by:

$$\text{erf}(z) = \frac{2}{\sqrt{\pi}} \int_0^z \exp(-v^2) \mathrm{d}v.$$

Here, the thickness δ of the front is given by the 'width' of the error function that we define (also with a certain looseness) using the relation:

$$\delta = 2\sqrt{Dt}.$$

The front thus spreads proportionally with the square root of time.

3.4.3 **Measurement of a diffusion coefficient in a microsystem**

Microsystems represent an interesting context for the measurement of diffusion coefficients in liquid phase: taking the relatively small diffusion coefficients

in liquids into account, a parasite flow, even a very slow one, can disrupt the measurement. Operating in a microsystem, parasite flows are reduced to a very low level, since these flows are produced, for example, by defects in thermal homogeneity. In this mindset, references [9, 10] have proposed the implementation of a measuring method in a T-shaped microsystem, represented schematically in Fig. 3.4. Fluids are injected into the arms of the T and circulate side-by-side in the principal canal. Along this canal, solutes are transported by the hydrodynamic flux, and build up a diffusive zone in the shape of an angular sector that opens up gradually along the flow. A theoretical analysis of the concentration field $C(x, y)$ at the interior of the diffusive zone shows that it must have the following

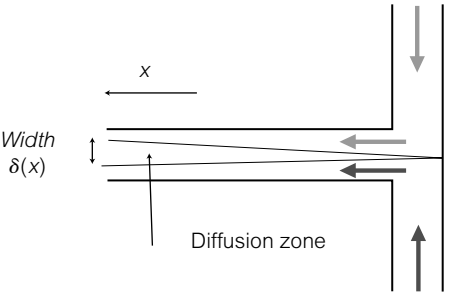

Figure 3.4 Basic principle of the experiment of diffusion in a microcanal, allowing the measurement of diffusion coefficients [8].

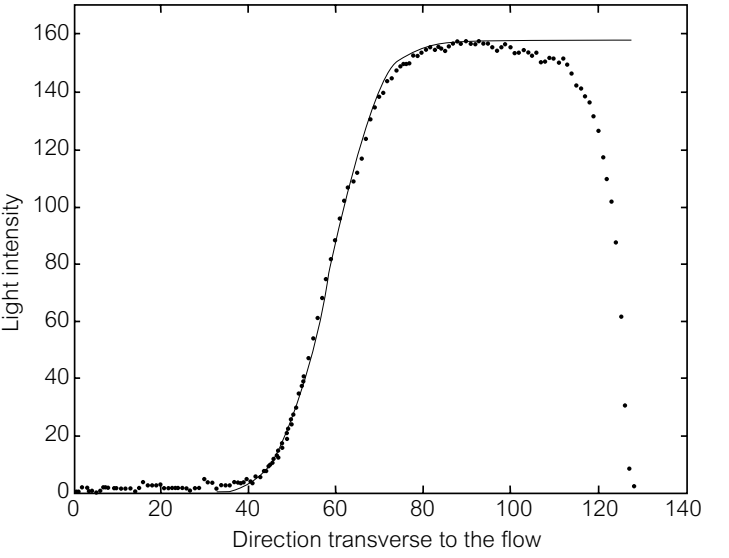

Figure 3.5 Curve showing the agreement between theory and experiment for the diffusion of a grade in concentration in a T-shaped microsystem.

expression:

$$C(x,y) = \frac{1}{2} C_0 \left(1 - \operatorname{erf} \frac{y\sqrt{U}}{2\sqrt{Dx}}\right),$$

where x is the co-ordinate along the flow, y is the transverse coordinate of the flow, U is the average velocity in the principal canal, and D is the diffusion coefficient we are looking for. Figure 3.5 shows that this theoretical formula correlates well with experimental measurements. The comparison of the theory and the experiment, with D as the free parameter, leads to a measurement of D.

3.5 Analysis of dispersion phenomena

3.5.1 Dispersion of a dye in a stretching field

We have analysed several processes of pure diffusion, and now we turn to the study of hydrodynamic dispersion. Here, we analyse a basic phenomenon: the filamentation and reorientation of a field of tracer by hydrodynamic stretching. This basic process takes place in all micromixers using a flow to reduce the mixing time. We consider a flow of pure straining field, defined by:

$$U = (\alpha x, -\alpha y), \quad \alpha > 0.$$

Initially, we have:

$$t = 0, \quad C(x) = A_0 \sin \boldsymbol{M} \cdot \boldsymbol{x},$$

where C is the concentration field of a tracer, C_0 is a constant, and $\boldsymbol{M}$ a given vector with components (M_1, M_2). $\boldsymbol{M}$ is the 'wave vector' characterizing the initial conditions, that is to say the initial shape of the spot. This initial condition represents a series of bands of dye of thickness $1/M$ (by order of magnitude), oriented perpendicularly to the vector $\boldsymbol{M}$, which are abruptly immersed in a field of pure straining. The choice of this initial condition facilitates the analytical resolution of the problem. By solving the advection-diffusion equation, we obtain the following solution:

$$C(x,t) = A(t) \sin \boldsymbol{m}(t) \cdot \boldsymbol{x},$$

where $\mathbf{m}(t)$ is a vector that depends on time. The solution (which is explained in [11] and not detailed here) shows that this factor tends to align itself along the axis Oy over the course of time, as per an exponential process; on the other hand,

its amplitude grows exponentially with time. Thus, the spot tends to align itself with the axis Oy while simultaneously forming thinner and thinner filaments. At times that are long with respect to the characteristic stretching time $1/\alpha$, the thickness $l(t)$ of these filaments (by order of magnitude) is:

$$l(t) \sim 1/m(t) = 1/M_1 \exp(-\alpha t),$$

where $m(t) = |\boldsymbol{m}(t)|$.

The process of filamentation is represented schematically in Fig. 3.6, and involves a time domain during which diffusion has not yet acted. If we wait for long times, filamentation continues, but molecular diffusivity will begin to have an effect. This 'diffusive' or 'dissipative' characteristic time is given by order of magnitude by $1/\alpha$; beyond this time, the amplitude $A(t)$ of the concentration field weakens; this process of the decline in amplitude is dramatic since the calculation leads to an exponential of an exponential! To conclude, in this problem the mixing time of the spots of dye with the surrounding fluid is on the order of $1/\alpha$. At high Peclet numbers, this time is much shorter than the time for pure diffusion, which would be given by l^2/D.

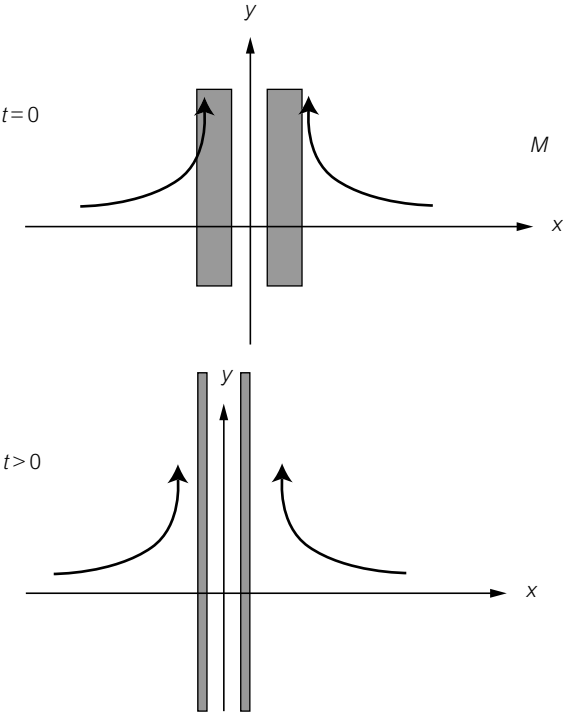

Figure 3.6 Evolution of a band of dye subjected to a pure straining velocity field, in two dimensions.

3.5.2 **Taylor–Aris dispersion in microcanals**

We now consider an important phenomenon: the process of Taylor–Aris dispersion, often known as 'Taylor dispersion' [12]. This phenomenon consists of the dispersion of a passive tracer along a stationary flow in a canal with a small transverse dimension (such as a capillary, or a microcanal). We consider the advection-diffusion equation in the case where the flow takes place along the axis Ox between two planes separated by b, with a velocity profile that is dependent on the transverse coordinate z only (Fig. 3.7).

Let $\boldsymbol{U}(z)$ be such a flow. The advection-diffusion equation is written:

$$\frac{DC}{Dt} = \frac{\partial C}{\partial t} + \boldsymbol{U}(z)\frac{\partial C}{\partial x} = D\Delta C,$$

where the concentration C is a function of $C(x, z, t)$. The Taylor–Aris approximation consists of assuming that the canal has a transverse dimension so small that the tracer is nearly homogeneous, at all times, for a given cross-section of the canal. This hypothesis permits the replacement of quantity $C(x, z, t)$ by its spatial average along z, notated by $\bar{C}(x, t)$. At all times, the gradients of C along z must be left as they are. This hypothesis is made in the limit of long times, in the sense that the times considered are much larger than the diffusion time in the cross-section of the canal, which is on the order of b^2/D.

We do not perform the calculation, which is rather long, in this text; we will, however, demonstrate its structure. The key equation allowing the resolution of the problem is written:

$$\frac{DC}{Dt} = \frac{\partial \bar{C}}{\partial t} + U(z)\frac{\partial \bar{C}}{\partial x'} \approx D\frac{\partial^2 C}{\partial z^2}.$$

This equation can be integrated, since $\bar{C}(x, t)$ does not depend on the coordinate z. After integration and derivation, the equation governing the spreading of the spot is written, in the frame of reference of the center of mass of the spot:

$$\frac{\partial \bar{C}}{\partial t} = D_{\text{eff}}\frac{\partial^2 \bar{C}}{\partial x'^2},$$

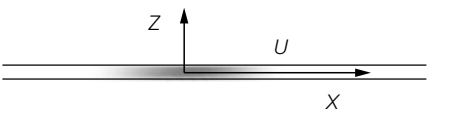

Figure 3.7 Geometry of the Taylor–Aris problem that we consider here. The flow is produced along the axis Ox between two planes separated by b with a velocity profile that only depends on the transverse coordinate z.

with

$$D_{\text{eff}} = D\left(1 + \beta\left(\frac{Ub}{D}\right)^2\right),$$

where β is a coefficient that depends on the shape of the cross-section of the canal. In the case that we will consider here (a canal confined between two parallel planes), we have:

$$\beta = \frac{1}{210},$$

a result that would have undoubtedly been difficult to anticipate intuitively[7]. It is instructive to note that for a capillary with circular cross-section, we have:

$$\beta = \frac{1}{48}.$$

We thus have here an effective diffusion coefficient that at high velocities increases proportionally with the square of the velocity of the flow. All this occurs as though the spot was spreading much faster in the direction of the flow than if molecular diffusion had been the only mechanism in play. This is the result obtained by Taylor–Aris. We can note that within the limits designated by Taylor and Aris, the particle had the time to explore the whole cross-section of the canal, because the scales of the times considered were much slower than the diffusion time in the cross-section. In this process, the particle randomly visits different streamlines characterized by distinct velocities, which tends to take it far from its original position. We can see that the particle is thus rapidly dispersed along the canal. The calculation of Taylor–Aris [12] does not describe what happens at short times, that is to say at times shorter than b^2/D. At these short times, the dye follows the streamlines; it is stretched out linearly with time until diffusion acts to homogenize the cross-section. We will later see an illustration of this process. An expression given by Taylor [12] approximates the effective diffusion and allows the description of several orders of magnitude:

$$D_{\text{eff}} \sim Pe^2 D,$$

where *Pe* is the Peclet number, already introduced here: Ub/D. This formula is acceptable at high Peclet numbers. In practice, in the context of microsystems, the Peclet number can attain values between 0.1 and 100. For the highest values, diffusion along the flow can be increased by several orders of magnitude with respect to molecular diffusion. This amplification of the coefficient has been used

[7] Another non-intuitive characteristic: the boundary of the infinite parallel plane is not reached in a canal with a rectangular cross-section, with the aspect ratio b/w (where w is the width of the canal) going towards zero. For rectangular canals, the existence of velocity gradients near *all* surfaces must be taken into accout, regardless of their aspect ratio. This paradox is highlighted in [13].

in the context of microsystems to make micromixers. We will see an example of this in Section 7.3.

3.6 Notions on chaos and chaotic mixing

3.6.1 Definitions and virtues of chaotic regimes

The idea of chaos deserves a thorough treatment that would take us well beyond an introductory presentation of microfluidics. Many works have been written on the subject, including [14–16]. We will thus only highlight a few general ideas on the subject.

One central concept involved in chaotic regimes is that of the dynamical system. In the context that interests us, i.e. in the context of chaotic mixing, the relevant dynamical system is that which relates the fluid velocity $\boldsymbol{u}(\boldsymbol{x}, t)$ to the position $\boldsymbol{x}(t)$ of the dye particle (that we here identify to be the fluid particle, neglecting the action of molecular diffusion). We have:

$$\frac{\mathrm{d}\boldsymbol{x}}{\mathrm{d}t} = \boldsymbol{u}(\boldsymbol{x}, t). \tag{3.5}$$

These equations thus define a system of equations that we call a 'dynamical system'. These systems have been studied for decades, and there exist very powerful theorems restricting the solutions. In general, the solutions of the system (3.5) can be seen as trajectories of the particle with coordinate $X(t)$ in physical space, with the frame of reference being the system of coordinates (X, Y, Z). A solution is considered chaotic if it possesses the property of 'sensitivity to initial conditions'; in other words, if two particles situated on neighboring trajectories diverge (on average) at an exponential rate. This situation is represented schematically in Fig. 3.8.

It is useful to elaborate on the idea of sensitivity to initial conditions, because it is an important concept for chaotic systems. We consider a point X placed on a trajectory at time t_0 that we choose as the origin of time. We designate by $X + \boldsymbol{\delta}x$ the vector located at a point near X, always for $t = 0$. Over the course of time, the two points evolve on neighboring trajectories. Depending on the orientation of the vector $\boldsymbol{\delta}x$, the two points may or may not move away from one another. In a chaotic system, a direction i must exist along which the two points separate exponentially from one another. In these simplest cases, we can write:

$$\delta x_i(t) \approx \delta x_0 \mathrm{e}^{\sigma_i t},$$

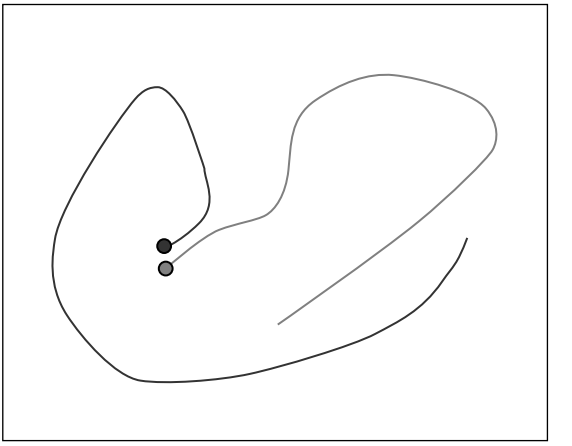

Figure 3.8 Evolution of a pair of particles, initially very near one another, within a chaotic system. When the system is chaotic, the particles separate themselves exponentially.

where δx_i is the component of the separation vector along i, σ_i is a positive parameter and δx_0 a small parameter[8]. From the preceding formula, we deduce a rate of local divergence along the direction i by the expression:

$$\sigma_i = \frac{1}{t} \log \left(\frac{\delta x_i(t)}{\delta x_0} \right).$$

We can repeat this analysis along the trajectory $X(t)$ and come up with a collection of parameters σ_i that depend on the position $X(t)$ on the trajectory. If there exists a direction on which the exponent is, on average, positive, the system is chaotic. The corresponding value is known as the Lyapunov number or exponent along the direction i. The Lyapunov number corresponds to the direction along which the rate of divergence is maximal. For simplification, we can thus say that a system is chaotic if, on average, its trajectories separate from one another at an exponential rate.

Sensitivity to initial conditions results from this property: an initial separation between two close initial conditions will be exponentially amplified (if it corresponds to a direction in which the Lyapunov number is positive). The system is thus very sensitive to the small details characterizing initial conditons. For physical systems, the property of sensitivity to initial conditions implies that perturbations of the trajectory relating to thermal noise are also amplified. This results in the fact that although chaotic systems are governed by deterministic

[8] The determination of the direction or directions i, and thus that of the parameter σ_i, is made by diagonalizing the tangent matrix to the trajectory at the point $X(0)$ [14]. We will not perform this calculation here, and will simply rationalize as if there was one single direction of divergence.

equations, they rapidly decorrelate from these equations with time. What is the magnitude of the Lyapunov number? In a chaotic mixer, the typical order of magnitude of this number is the inverse of the turnaround time, i.e. the characteristic length over the characteristic speed of mixing, whose exact value depends on the flow being used.

There is an equivalent way to define chaos. We show that chaotic systems develop an infinite succession of folds and stretching on their material lines in phase space, a process that one can associate with the presence of a 'horseshoe' map. One schematization of a horseshoe map is the baker's transformation, that the artisan carries out when making mille-feuilles pastry (Fig. 3.9).

Initially, we have a rectangle. We stretch it, fold it, stretch it again, fold it again, etc. This transformation, which conserves areas, leads to the formation of extremely thin striations, and is representative of a chaotic process.

We will now show that these two definitions of chaos are equivalent. Intuitively this makes sense: if the trajectories diverge, this implies that in the direction of divergence, the lengths of the material lines grow exponentially. In a closed system (which is within the framework of the theorems mentioned here), the material line must be subjected to folding in order to remain confined in the system. We are thus led to understand that the exponential divergence of the trajectories forces the material lines to stretch and fold themselves, rather like the baker's transformation (Fig. 3.9): in the baker's transformation, at each stretching, the distance between the points along the length of the stretching direction is multiplied by 2. There is thus clearly an exponential divergence of separation. Over the course of the evolution of a chaotic system, there is thus a tendency to fill in the flow with very convoluted material lines. This naturally leads to the formation of patterns such as those shown in Fig. 3.10. One consequence of the stretching of material lines is the exponential growth of the exchange surface between a spot initially placed in a flow and the surrounding fluid. This effect intensifies diffusive exchanges between the dye and the fluid, thus rendering chaotic mixing quite effective.

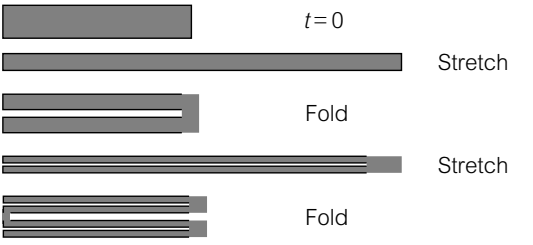

Figure 3.9 Baker's transformation: we stretch the dough, we fold it over, we strech, we fold, etc.

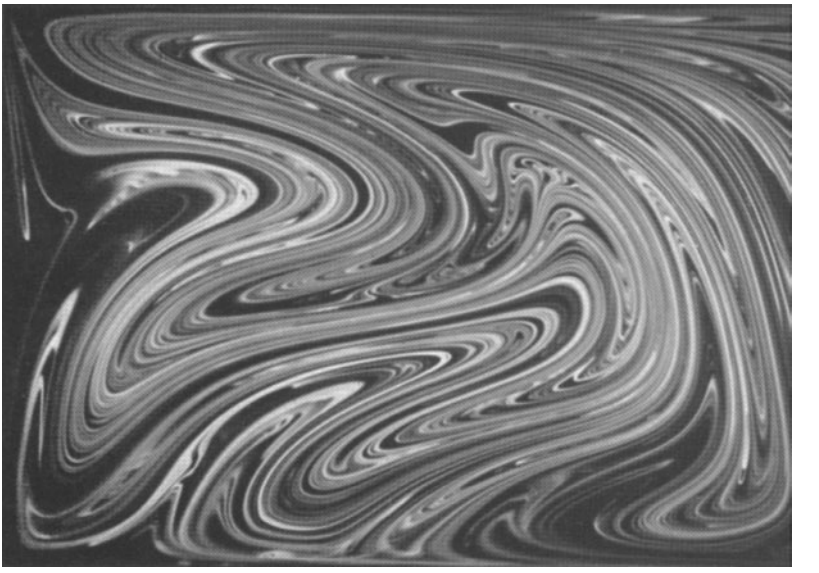

Figure 3.10 Chaotic mixer showing the structure of a field of dye (in white), which produces several folds and stretching due to the oscillatory movement of one of the surfaces of the mixer (after [15]). © Courtesy of Professor M. Ottino, Northwestern University.

3.6.2 **Conditions for obtaining a chaotic regime**

Is it possible to know a priori whether a system is chaotic? On this point, there are several robust theorems [14–16]. For a dynamical system, confined as 'autonomous' (that is to say, with coefficients independent of time), we show that it is not possible to have chaos in two dimensions. Thus, for the dynamical system defined by equation (3.5), if the velocity field is two-dimensional and stationary, it cannot have a chaotic trajectory. Two trajectories will remain, on average, near one another, and in the case of an incompressible fluid, we can be convinced by geometric reasoning that this situation is not favorable for mixing.

To obtain chaotic trajectories, it is necessary to 'gain a dimension.' We achieve this in two ways:

– We can get away from the plane by considering stationary *three*-dimensional flows. At the time this text was written, there was not yet a mixer of this type, although attempts have been made to create one.
– We can work with non-autonomous bidimensional systems, i.e. systems whose velocity depends on time. In effect, we assume that the two dimensions in space are x and y. If we introduce a third variable z defined by:

$$\frac{\mathrm{d}z}{\mathrm{d}t} = 1,$$

and if we formally replace the time t with the variable z in other equations, we obtain a new autonomous system, but this time in three dimensions. This is the type of method that is used in chaotic micromixers that we will present here.

It is important to understand that in the systems we discuss here, the trajectories are chaotic while the flow that is formed is not. There is thus a qualitative difference between the movement of the fluid particles and the dynamical characteristics of the velocity field. Clearly, if the flow was itself chaotic (i.e. if a representative point in the velocity field placed in a co-ordinate system (u_x, u_y, u_z) developed a chaotic trajectory) the trajectories of the fluid particles would also be chaotic. However, it is not a necessary condition and we do not consider such a situation here. This striking distinction between the velocity field and the trajectories of the fluid particles is, although counterintuitive, fundamental. To conclude this brief presentation, we note that the solutions to questions in the field of chaos are traditionally obtained, for confined systems, in the absence of chemical reactions. The area of open flows, or those of non-conservative systems, was only recently undertaken in a theoretical manner. Microsystems could likely provide new experimental situations for the study of these subjects.

3.7 Mixing in microsystems: a few examples

3.7.1 Diffusion is often too slow in microsystems

Mixing time

As we have seen in Chapter 2, the Reynolds number is small in microsystems, implying that hydrodynamic instabilities do not develop. Microfluidic flows can thus be neither chaotic nor turbulent. How is it then possible to mix reactants in a microreactor without turbulence? One *'laisser-faire'* solution is to let mixing occur simply by using molecular diffusion. As we have seen throughout this chapter, the diffusion mixing time is on the order of l^2/D (where D is the diffusion coefficient); miniaturization can thus be expected to lead to small diffusive mixing times. The table below helps clarify this point:

System	Mixing time
Dye in water, in a glass of 10 cm	10^5 s
Dye in water, in a microsystem of 1 μm	10^{-3} s
Dye in water, in a microsystem of 100 μm	10 s
Enzymes and proteins in a microreactor of 100 μm	1000 s

This table indicates that mixing is rapid in micrometric-sized systems for small molecules such as water. In this case, we can use the 'laisser-faire' molecular diffusion approach to achieve mixing. For large molecules and reactors of sizes more realistic for lab-on-a-chip systems, the diffusion mixing time is on the order of a thousand seconds. If, for example, many reactions must be carried out on a single chip for the analysis of a sample, these orders of magnitude may pose a problem. In this type of situation, it thus seems necessary to mix actively, that is to say by manipulating the hydrodynamics of the system. We thus comprehend the problem of mixing in microsystems.

At the time this text was written, about 20 or so micromixers had already been invented. The underlying principles for these micromixers are diverse. Some mixers function at moderate Reynolds numbers and attempt to encourage the appearance of instabilities, separation of boundary layers, and recirculations induced by centrifugal forces, all of which are conducive to mixing[9] (see, for example, [18, 19]). These systems function in a way that is conceptually analogous to macrometric systems. We will not describe them here; instead we will concentrate on micromixers at small Reynolds numbers.

Micromixers at $Re \ll 1$

There are two types of micromixers at small Reynolds numbers.

- The first type is not chaotic. In this case, the 'work' of molecular diffusion is facilitated by diminishing the size of the system, or by exploiting the Taylor–Aris dispersion to increase the effective diffusion along the flow.
- The second type uses chaos to mix. In this case, chaos of the trajectories is generated by exploiting the fact that the base flow is non-stationary in a purely bidimensional or pseudo-tridimensional context. The first chaotic mixer was proposed at the University of Berkeley [45], and there are now three or four mixers of this type.

We note that it is not enough to perturb a flow to promote mixing. This point is illustrated in Fig. 3.11.

Here we have a flow going through a canal in which a line of obstacles has been placed, rather like a miniaturized bumper pool table. Due to the property of reversibility of flows at small Reynolds numbers, the streamlines will be the same at the entrance and exit of the canal. There is no wake or recirculation after the pillars. Since the pillars induce a shear on the flow, there will be a Taylor–Aris

[9] We highlight an elegant mixer (that we will not describe in detail) that uses the viscoelasticity of polymers added to the fluid to develop hydrodynamic instabilities even at small Reynolds numbers [17].

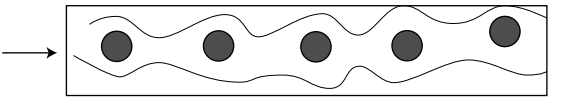

Figure 3.11 This device does not mix fluid particles located on different streamlines.

dispersion effect in the flow direction.[10] The flow will not contribute anything to the mixing of the tracers normal to the streamlines. We can conclude that such a system, although likely to be effective at high Reynolds numbers due to the turbulence induced by the pillars, will not be effective for achieving mixing in microsystems, particularly in directions normal to the streamlines.

3.7.2 **Micromixer based on size reduction**

One mixing idea is to reduce the size of the system in order to diminish the diffusive mixing time. Figure 3.12 shows a simplified example of such a device.

Two fluids A and B enter a T-shaped intersection. Beyond the T, the cross-section of the collecting canal is reduced. We assume that this canal, in the reduced portion, has a rectangular cross-section of height b and width w. The diffusive mixing time in the reduced cross-section is given by the relation:

$$\tau \sim \frac{w^2}{D}.$$

The length of the canal necessary for mixing is estimated by assuming that the two fluids are carried at a velocity of Q/wb in the reduced section, where Q is the total flux. Thus, the length necessary to achieve mixing is written:

$$L \sim \frac{Qw}{bD}.$$

At fixed height, the length of mixing decreases with the width w; this observation justifies the advantage of diminishing w in order to obtain mixing in a shorter time, and over a shorter distance. However, L can in practice be elevated, particularly at high speeds. This mixer functions within a defined range of speeds.

Knight *et al.* [20] created a remarkable system where, by using hydrodynamic focusing, the size of a liquid beam can be reduced to just a few tens of nanometers. This allows the mixing time within the beam to be on the order of just ten or so microseconds. This system is shown in Fig. 3.13.

[10] The effect, however, will be weak, because, if we neglect molecular diffusion, it averages out to zero.

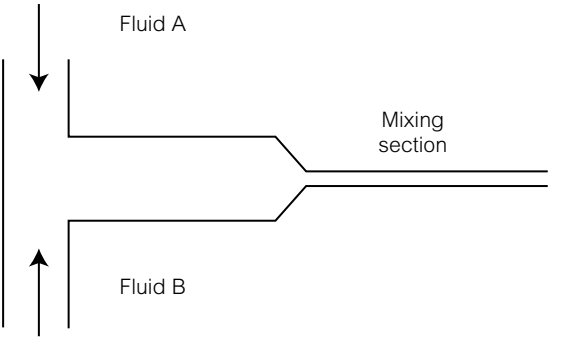

Figure 3.12 T-shaped diffusor, forcing fluids to mix by diffusion in a constriction of the microcanal.

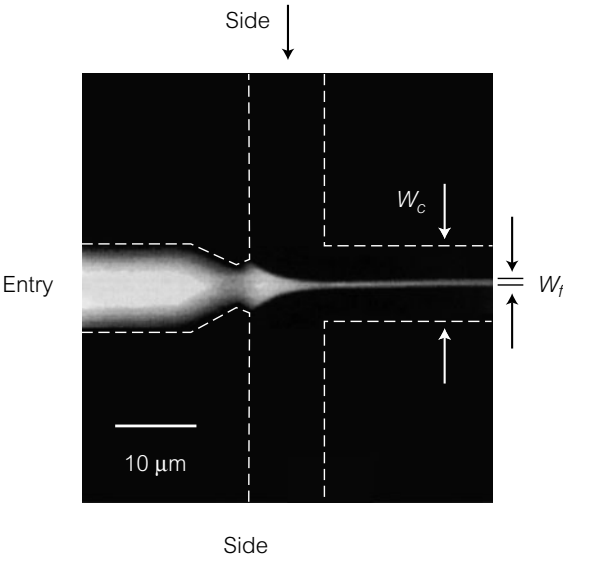

Figure 3.13 Geometry of a hydrodynamic focusing element allowing for reduction of the size of planar jets as well as for rapid mixing transverse to the jet (photo from Prof. Robert H. Austin, Princeton University).

The size of the planar jet formed in the collection canal is controlled by the ratio of the flow rates coming out of the three canals transporting the fluids to the intersection. Working with very high (several hundred) flow ratios, Knight *et al.* [20] showed that it is possible to form fluid layers with widths around 30 nanometers. The mixing time within a layer is on the order of ten or so μs. The characteristic times involved in such a system were determined using a known reaction of fluorescence quenching. The inverse of this type of system can be used to study such a reaction [21]. We return to the subject of chemical microreactors in the following section, which is dedicated to phenomena that couple dispersion and chemical kinetics.

The domains in which these mixers are operational increase when working with a large number of microcanals in parallel. One remarkable example is presented in Fig. 3.14.

3.7.3 **Ring-shaped micromixer**

Scherer and Quake [22] developed a circular micromixer based on the action of a velocity gradient; the gradient assures rapid mixing along streamlines of two spots A and B (Fig. 3.15). This system is a peristaltic pump that drives a flow around a ring.

The resulting flow is a Poiseuille-shaped flow, and the flow is developed in canals of small transverse dimension (with respect to their length). There are

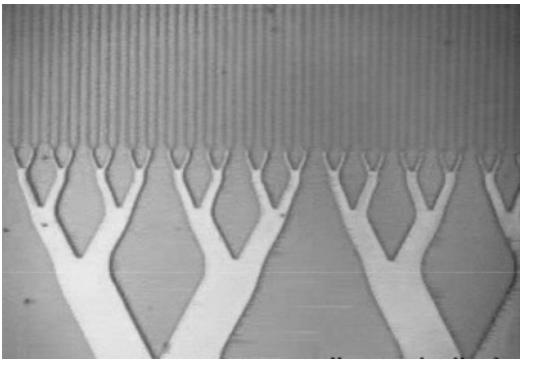

Figure 3.14 Diffusor in which the cross-section of the principal canal was divided into a large number of canals of smaller cross-sections.

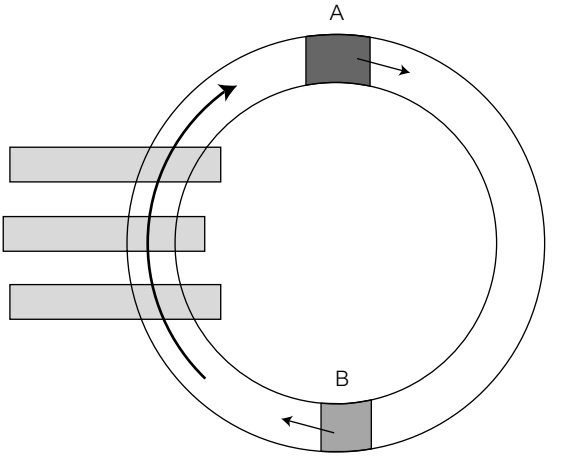

Figure 3.15 Micromixer based on Taylor–Aris dispersion, operating along the streamlines. The three rectangles at the left represent a peristaltic micropump, described in detail in Chapter 6.

two possible estimations of the mixing time, according to the modified Peclet number defined by[11]:

$$Pe_g = \frac{Ub^2}{LD}.$$

(1) For large values of Pe_g, the tracer is carried along the streamlines without having time to homogenize in the cross-section. In this case, the spots of dye A and B of Fig. 3.15 are stretched and folded, until molecular diffusion starts to homogenize the system. This process is linear with time (which differentiates it from chaotic mixing). The mixing time can be estimated by the expression:

$$t_M \sim \left(\frac{b^2L^2}{U^2D}\right)^{1/3} \sim t_R\left(\frac{t_d}{t_R}\right)^{1/3},$$

where U is the speed of rotation of the fluids, L is the circumference of the ring, b is the height of the canal, and D is the diffusion coefficient. We define here $t_R = L/U$ as the typical rotation time in the ring, and $t_d = l^2/D$ as the diffusion times in the cross-section of the ring. This formula shows that in order to mix, it is necessary to have the number of turns equal to $(t_d/t_R)^{1/3}$.

(2) For large values of Pe_g, the tracer is homogeneous at all times in the cross-section of the ring, and the system is thus in a Taylor–Aris configuration as discussed above. The effective diffusion along the flow is thus much higher (if the Peclet number calculated for the transverse dimension of the canal is large) than for plain molecular diffusion. We have:

$$D_{eff} \sim \left(\frac{Ub}{D}\right)^2 D \sim Pe^2 D,$$

where Pe is expressed as:

$$Pe = \frac{Ub}{D}.$$

When Pe is large, the two spots A and B represented in Fig. 3.15 can be mixed according to time t_M defined as:

$$t_M \sim \frac{L^2}{D_{eff}} \sim \frac{DL^2}{U^2b^2} \sim t_R\frac{t_R}{t_d}.$$

This expression shows that it is necessary for the system to make t_R/t_d turns to mix spots A and B.

[11] This non-published calculation was the result of a discussion with A. Ajdari.

In practice, the system used in [22] operates in the first regime mentioned above, and thorough mixing is achieved after just a few rotations. It is important to note that the structure of the ring-shaped mixer could be advantageous for miniaturized chemical analyses, where samples have a given size but not a fixed permanent flow rate.

3.7.4 **The cross-shaped chaotic micromixer**

Figure 3.16 shows a micromixer that functions using the development of chaotic regimes at 'finite times' [23]. This mixer consists of a principal canal, along which a stationary flow is imposed. This canal intersects adjacent canals, along which a non-stationary flow is imposed (for example, periodic with time). The two flows (principal and secondary) become superposed in the intersection region. We are now dealing with a case where the velocity field is not stationary, which according to the preceding discussion implies that chaotic trajectories can form. It has been shown in this system that, at the intersection of the canals, a given material line is subjected to a succession of folding and stretching characteristic of chaotic regimes.

This stretching and folding intervenes a finite number of times (one, two, or three times in the intersection, depending on the values of the parameters controlling the principal flow and the periodic perturbation). It is thus a chaotic system, but at 'finite times.' We observe that, despite the small number of stretching and folding carried out at the intersection, the system mixes effectively (Fig. 3.16). Generally speaking, this mixer can develop a substantial number

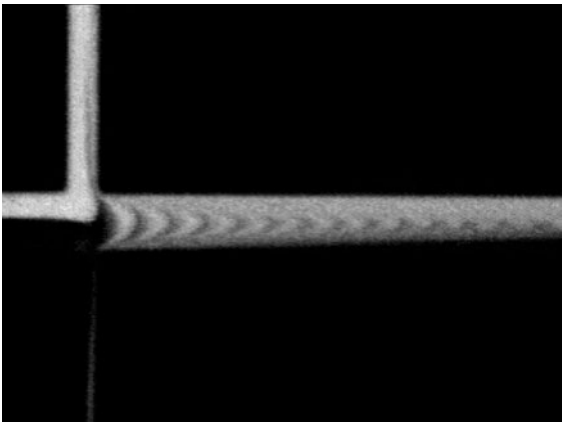

Figure 3.16 Micromixer made at UCLA, by Y.K. Lee *et al*. [23]. The two fluids arrive from the left part of the figure. Initially unmixed, they become mixed after crossing the intersection across which a perturbation is applied. The canals are etched in silicon, and have cross-sections 400 μm square.

of folding and stretching actions in an intersection, leading to a significant increase in the amount of surface of exchange. We can thus consider that such a mixer functioning under optimal conditions can provide a mixing length L_m such that:

$$L_m \approx w,$$

where w is the width of the intersection. This dimension can be small, suggesting excellent effectiveness of the micromixer, though that would require use of an exterior source and fine tuning of the flow conditions. A mixer of this type was also proposed by [24].

3.7.5 **The herringbone micromixer**

This mixer, developed by [25], is a passive chaotic mixer: it is not necessary (contrary to the preceding micromixer) to use an external source of perturbation. The mixer consists of a canal along which a series of herringbone-shaped grooves have been placed. These hollows force the fluid to circulate obliquely with respect to the direction of the principal flow. Due to conservation of mass, return flows are developed. In the end, we obtain a helically-shaped movement of the fluid. Figure 3.17 represents such a system, which is made in PDMS using 'soft lithography,' which will be explained in Chapter 6.

The herringbones do not form a homogeneous motif along the canal. The pattern changes drastically every five herringbones. This translates kinematically to a displacement of the centers of the fluid helices. This variation of the helical structure along the canal can be seen as a time-dependent modification of the flow, passing from a stationary regime to a non-stationary regime, which is conducive to chaos. Chaos is shown to be created in Fig. 3.17 by a succession of folding and stretching of the dye placed in the system. The mixing length L_m was estimated in the article [25]:

$$L_m \approx w \log(Pe),$$

where w is the channel width, and Pe is the Peclet number calculated for the width of the canal and the average flow. In practice, this estimation, confirmed by experiment, leads to mixing lengths several tens of times larger than the distance w, for Peclet numbers on the order of 10^5 [25].

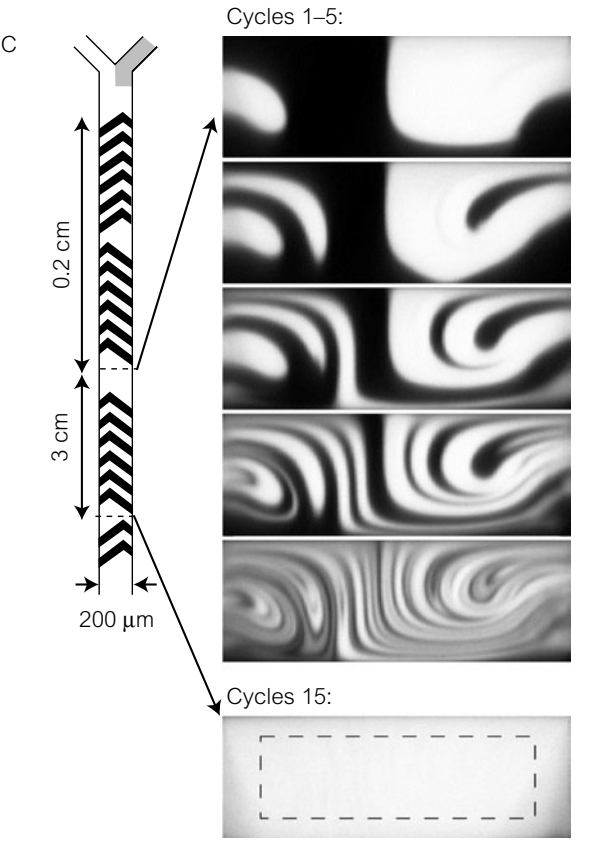

Figure 3.17 Micromixer created by Strooke *et al*. [25]. Grooves of differing shapes along the flow are etched in a microcanal with a rectangular cross-section, fabricated using PDMS-based soft lithography (see Chapter 6). This system leads to chaotic mixing under conditions where the Reynolds number is much smaller than one (image published with the permission of A. Stroock *et al*. [25]; © American Association for the Advancement of Science).

3.8 **Adsorption phenomena**

3.8.1 **Generalizations**

Adsorption is the phenomenon of the accumulation of a substance at the interface between two phases (solid-gas, liquid-liquid, etc.). In physical terms, these substances accumulate at the interface because they are retained by attractive intermolecular forces, a few examples of which were given in Chapter 1.

For an interface/solvent system, there will be adsorption if molecules have attractive interactions that are stronger for the surface than for the solvent. If the molecules 'like' the surface more than the fluid, the surface exposed to the solvent

will find itself covered in a molecular film. This preferential mechanism is a bit like one of Archimedes' principles: depending on the value of the solid/liquid density ratio, the solid body will rise to the surface of the water or it will fall to the bottom. Here, it is a matter of knowing whether the molecules prefer to stay in the liquid or cover the surface. An illustrative example of this preferential effect is that of hydrophobic molecules immersed in water: they hate water, and if the energetic conditions are favorable, they will tend to cover interfaces. This covering is not necessarily complete. The rate of covering depends on the statistical equilibirum between the interior of the fluid and the surfaces exposed to the fluid: due to thermal agitation, adsorbed molecules are subjected to collisions (at a rate equal to the frequency of collisions, typically 10 THz), and tend to return to the fluid. This is where the analogy with the simpler principle of Archimedes has its limits. We will later describe this type of statistical equilibrium.

We have given an example of adsorption phenomena in Chapter 2, for both liquid/solid and liquid/liquid interfaces: the example involved amphiphilic molecules possessing a hydrophobic tail and a hydrophilic head. We showed that energetically, these molecules prefer to reside at interfaces: their behavior is thus brought about by a phenomenon of adsorption.

We distinguish between the two main types of adsorption : physisorption, where the adsorbant is retained at the surface by intermolecular forces, and chemisorption, where the adsorbant undergoes a chemical reaction to fix itself on the interface. One example of physisorption involves amphiphilic molecules, and one example of chemisorption involves oxygen molecules oxidizing a metal surface. The former process is reversible, and the latter process generally is not. Microfabrication often uses one or the other of these two mechanisms for depositing films or layers on silicon. We will see several examples of this in Chapter 6. It is important to understand the phenomena of adsorption in the context of microsystems. They are essentially a matter of surface phenomena, and as we noted in Chapter 1, miniaturization tends to exacerbate interfacial phenomena due to the augmentation of the surface area to volume ratio[12]. Generally speaking, the idea of adsorption comes up several times in this book, in sections dedicated to surfactants, separation methods (we will see this later), and microfabrication (Chapter 6). It is thus useful to have an elementary and intuitive understanding of these phenomena.

[12] We note, however, that the surface area to volume ratios accessible to microsystems are still less than those in systems commonly used for adsorbing substances with the goal, for example, of purifying a given environment: active charcoal, which consists of a network of nanometric-sized pores, has surface area to volume ratios on the order of 1000 m^2/g, which is far greater than values characteristic of microcanals. We will return to this point in the section discussing chromatography.

3.8.2 **Law of Langmuir**

We present here an important theory proposed in 1912 by Langmuir describing the statistical equilibrium between the adsorbant (i.e. the adsorbing surface) and the molecules in solution that have a certain affinity towards the exposed surface. This theory is described in several works, of which [26, 27] are two examples. The process of adsorption described by this theory is schematically represented in Fig. 3.18.

A molecule fixes itself on the surface and stays there for a certain interval of time. Even if the adsorbed molecules found themselves in an energetically favorable state, they would not be able to stay anchored to the surface. Thermal agitation, which favors the homogenization of concentrations, will tend to detach them from the surface. We will see that an equilibrium will eventually be established. The theory of Langmuir relates the flux of molecules J_1 adsorbing on the surface and the bulk concentration C of the same molecules near the surface in consideration. This theory assumes that one single molecular layer is adsorbed: molecules are retained (temporarily) on the bare areas of the surface, but are warded off by areas that are already covered. The flux J_1 of incident molecules is proportional to the local concentration C, and to the area uncovered by the adsorbed monolayer. Calling ϕ the fraction of surface covered by the adsorbant, we can write:

$$J_1 = k_1 C(1 - \phi),$$

where k_1 is a coefficient. Moreover, the evaporation flux of the adsorbed atoms, represented by J_2, is proportional to the covered area:

$$J_2 = k_2 \phi,$$

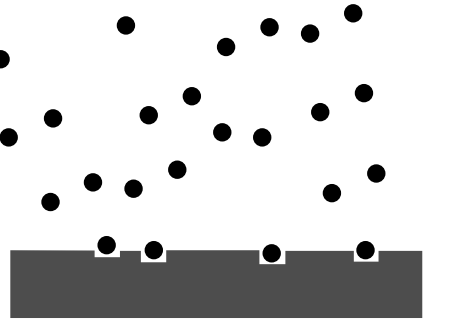

Figure 3.18 Process of adsorption: molecules are temporarily trapped on the surface, which becomes covered with a film (monomolecular in Langmuir theory), characterized by a rate of covering ϕ.

where k_2 is a second coefficient. At equilibrium, the two fluxes are equal. We deduce:

$$\phi = \frac{C}{k_2/k_1 + C}.$$

From this expression, it is possible to determine the flux at equilibrium $J = J_1 = J_2$. We obtain:

$$J = \frac{J_0 C}{K + C},$$

where J_0 and K are constant. This law is called the adsorption isotherm of Langmuir (Fig. 3.19). At high concentrations, the flux saturates, which corresponds to the limit at which the surface is entirely covered by a monomolecular film.

This law is also applicable to gases, in the case of chemisorption (because here, the hypothesis of having only one single adsorbed layer is well verified). Its principal deficiency comes from the fact that it neglects phenomena of diffusion within the surface layer and the interactions of the adsorbant with itself. The law of Langmuir was completed with more complex laws, taking into account more adsorption layers, and empirical relations allowed the inevitable representation of the physico-chemical complexity in several real situations. We thus distinguish between several cases of adsorption, represented in Fig. 3.19, in a graph of $J = f(C)$.

– If the function $J = f(C)$ is concave (near the origin of C), the situation is known as 'favorable.' Even at very small concentrations, the flux is substantial. Thus, in the domain of chromatography, it would be easy to trap traces of

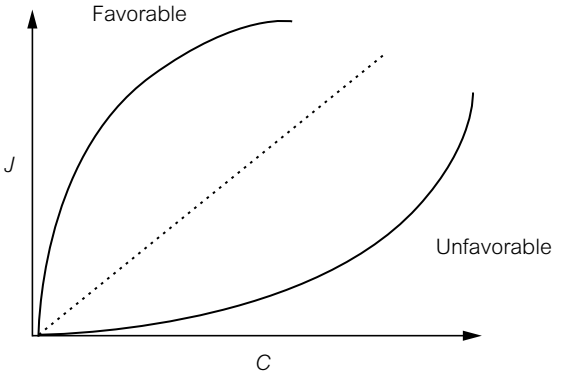

Figure 3.19 Flux of a given species adsorbed onto a surface, as a function of the concentration in solution of the species.

substances on the surface to eventually reconcentrate after elution, in order to perform analyses under more accessible conditions. The law of Langmuir is one of these 'favorable' cases.

– The other situation (convex) is known as 'unfavorable'; at low concentrations, the adsorption flux remains low. However, flux becomes significant at high concentrations, which indicates that interactions between adsorbed layers play a favorable role. One example is that of a wetting liquid film deposited on a surface.
– Between these two extreme cases, there is a linear curve of the form: $J = kC$ that is neither favorable nor unfavorable.

Many laws have a name. We have seen that the law of Langmuir is written:

$$J = \frac{J_0 C}{K + C},$$

where J_0 and K are constants. The law of Freundlich is written:

$$J = KC^a,$$

where K and a are constants (though a is not necessarily an integer). The law of Freundlich, though not theoretically justified, is the most commonly used law in practice for solid/liquid interfaces.

Statistical models of adsorption

In an approach identical to the diffusive processes presented in this chapter, we can examine the phenomenon of adsorption from a microscopic point of view by representing the process with statistical models of walkers. This representation has the advantage of taking into account the phenomena of diffusion and translation in regions close to the surface. One possible walker model for adsorption is a line of traps along which a walker progresses, and is retained between each jump for a certain time at the surface. This model is shown in Fig. 3.20.

In each trap, the walker is retained for a time τ, a quantity characterized by a probability $p(\tau)$. We assume here that the progression is systematic: the walker never steps

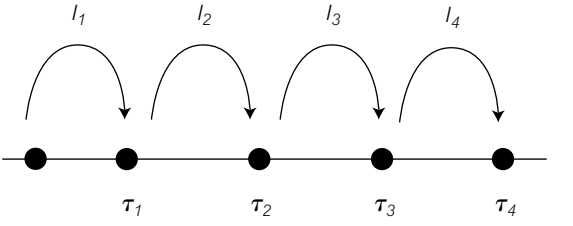

Figure 3.20 Statistical model of adsorption, for which a walker progresses along a line and is subjected to the effects of trapping on each site.

(Continued)
backward s, and the distance L that it travels is written:

$$L = nl,$$

where n is the number of traps that it has passed after time t, and l is the average distance between two consecutive traps.

We assume we are in a 'normal' case, that is to say where the distribution τ is narrow, and that all statistical moments of this quantity are well defined. In this case, the time t is defined by the total time passed between n traps:

$$t = \sum_{1}^{n} \tau_i \approx n\langle\tau\rangle,$$

where $\langle\tau\rangle$ is the average trapping time. We deduce the migration velocity V:

$$V = \frac{l}{\langle\tau\rangle}$$

a result that we could have written intuitively.

As the migration velocity depends on the trapping time, it is possible to use this fact to separate different species according to their affinity for the surface.

REMARK ON THE TRANSPORT OF SOLUTES IN CHROMATOGRAPHY

We will present in a later section the powerful techniques of chromatography, which allow for the fine separation, and then precise identification, of unknown (or poorly known) components of a sample. Here we will investigate the process of separation by adsorption by calculating the velocity of displacement of a group of molecules carried by a flux of velocity U along an adsorbant matrix. In this case, we consider the adsorption process to be reversible. The problem of transport of a solute along an adsorbant matrix is not, in fact, very simple. If we take the advection-diffusion equations again, we must place ourselves in non-stationary conditions and solve the following equations:

$$\frac{\partial C}{\partial t} + U\frac{\partial C}{\partial x} = D\left(\frac{\partial^2 C}{\partial z^2} + \frac{\partial^2 C}{\partial x^2}\right),$$

with the following boundary conditions:

$$\delta J = D\frac{\partial C}{\partial z},$$

where δJ is the difference between the incident flux and flux of evaporation. This quantity is written:

$$\frac{\mathrm{d}C_S}{\mathrm{d}t} = \delta J,$$

(Continued)
where C_S is the surface concentration. These equations are rather complicated to deal with, especially when the non-linearities of the adsorption isotherms must be taken into account. We are far from a simple advection-diffusion problem. In fact, we can obtain close solutions in the form of concentration fronts migrating along the matrix at a velocity dependent on the characteristics of the adsorption process. One of the pertinent parameters in this problem is the partition coefficient k, defined by:

$$k = \frac{C_{Seq}}{C_{eq}},$$

where the index 'eq' signifies that the quantity was estimated under conditions where equilibrium has been obtained. We refer to the work of Cussler [6] for a more detailed treatment of these solutions. A more direct way to understand these regimes used for separation is based on the usage of statistical models of adsorption, such as those presented previously. A commonly used model is the 'retention' model [26], where the walkers (representing a particular species contained in the sample) are retained by the matrix for a time τ, then displaced, carried along by the mobile phase, for a time τ', then are retained once more, etc. The image is that of the walker on its way home, taking the time to stop in pubs. It is rather simple to show that the velocity of the walkers V is given by the following expression:

$$V = \frac{\tau'}{\tau + \tau'} U,$$

where U is the velocity of the mobile phase. As the ratio τ'/τ depends on the nature of interactions between the walkers and the matrix, it can be seen that it is effectively possible, in a chromatographic system, to separate a sample into its different components.

3.9 Dispersion with chemical kinetics

3.9.1 Introduction

As already mentioned in the introduction of this chapter, laboratories on-chip perform chemical reactions in microreactors. We return to the problem of mixing discussed previously, but, here, we cover chemical kinetics. This type of situation has been extensively studied in macrometric-sized systems, particularly in the field of chemical engineering. Due to the absence of hydrodynamic instabilities and turbulence, chemical mixing presents itself in a very particular way in microsystems. The objective of this section is to propose a few basic ideas on chemical kinetics. We can refer to the book of Laidler [28], or to reference [27] for a more detailed treatment of this subject. We will also present

a few elementary situations of reaction-diffusion for which microsystems have facilitated experimental study.

3.9.2 A few notions on chemical kinetics

When a reaction of type:

$$\mathrm{A} + 3\mathrm{B} \longrightarrow 2\mathrm{C} \tag{3.6}$$

is carried out, we define different quantities to characterize it. The coefficients 1, 3 and 2 before the reactants A and B and the product (C), are known as the stoichiometric coefficients. If no intermediary is formed, the following equality is always true:

$$\frac{n_{\mathrm{A}}(t) - n_{\mathrm{A}}(0)}{-1} = \frac{n_{\mathrm{B}}(t) - n_{\mathrm{B}}(0)}{-3} \frac{n_{\mathrm{C}}(t) - n_{\mathrm{C}}(0)}{2},$$

where $n_{\mathrm{X}}(t)$ represents the quantity of substance X (reactant or product of the reaction) at the instant t. To describe its kinetics, we define the rate (>0) of formation of product and the consumption of the reactants by the quantities:

$$v_{\mathrm{A}} = -\frac{\mathrm{d[A]}}{\mathrm{d}t}, \quad v_{\mathrm{B}} = -\frac{\mathrm{d[B]}}{\mathrm{d}t}, \quad v_{\mathrm{C}} = \frac{\mathrm{d[C]}}{\mathrm{d}t}.$$

Taking the previous relation into account, we have the equalities:

$$v_{\mathrm{A}} = \frac{1}{3} v_{\mathrm{B}} = \frac{1}{2} v_{\mathrm{C}}.$$

The rate of consumption and formation divided by the stoichiometric coefficients of the reaction are equal. We thus naturally introduce the rate of reaction, generally defined by the quantity:

$$v = \frac{1}{\nu_i} v_i,$$

where ν_i is the stoichiometric coefficient, and v_i the rate of consumption or formation[13]. There exist kinetic models for gas reactions, which often lead to

[13] However, in practice, chemical reactions often involve intermediaries and one single reaction is not sufficient to describe the whole situation. This is the case for the decomposition of acetone, represented by the equation:

$$2\mathrm{CH_3COCH_3} \longrightarrow 2\mathrm{CH_4} + \mathrm{C_2H_4} + 2\mathrm{CO}.$$

In fact, during the reaction, appreciable quantities of ketene $\mathrm{CH_2CO}$ are produced, according to the system:

$$\mathrm{CH_3COCH_3} \longrightarrow \mathrm{CH_4} + \mathrm{CH_2CO}$$
$$2\mathrm{CH_2CO} \longrightarrow \mathrm{C_2H_4} + 2\mathrm{CO}.$$

expressions for the rate of the reaction having the form of monomial products. They are explained in detail in the text of Laidler [28]. The case of reactions in liquid phase is much less clearly described theoretically. In practice, we most often express the rate of reaction in the form:

$$v = k[\mathrm{A}]^{\alpha}[\mathrm{B}]^{\beta},$$

where k, α and β are coefficients that are independent of time. This form, suggested by theories dealing with the gaseous phase, must be understood as empirical for the case of reactions taking place in liquids. The exponent α represents the order of the reaction *for the reactant A*. The order of the reaction is the sum of all the exponents. The units of k depend on the order of the reaction. For a first-order reaction, k is homogeneous at a certain frequency, while for a second-order reaction, the S.I. units of k are $\mathrm{m}^3\ \mathrm{mol}^{-1}\ \mathrm{s}^{-1}$. The orders of magnitude of the kinetic coefficient k vary significantly. At a fixed order of reaction, the values of k span tens of orders of magnitude. The reason for this derives from the fact that, in general, for a chemical reaction to be produced, molecules involved must adopt a specific conformation and a favorable orientation. This condition brings a probability term into play, which typically depends exponentially on an activation energy, a term that can be designated by the 'Arrhenius factor.' Since the domain of the variation of activation energies is very large, there can be considerable variation in the kinetic factor k. The simplest case, but not necessarily the most frequent, is the first-order reaction, which is written:

$$v = k[\mathrm{A}].$$

One example is the decomposition of cyclopropane into propylene. It is also interesting to note that this reaction has an effective kinetics of order one; when the reaction is of order two, one reactant is found in excess.

The most frequent case is that of the second-order reaction, where the rate of reaction is written:

$$v = k[\mathrm{A}][\mathrm{B}].$$

This is the case for the reaction:

$$\mathrm{H_2} + \mathrm{I_2} \longrightarrow 2\mathrm{HI},$$

and for many others.

In terms of kinetics, it would be erroneous to use the approximate reaction that neglects the formation of ketene. In fact, the kinetics of ketene formation can control the kinetics of the whole reaction.

Finally, it is necessary to point out that there are cases where exponents are integers, and others where the rate of reaction can not be decomposed into the form of a product of monomers. In this case, the issue of the order of reaction is not relevant.

3.9.3 Equations of dispersion in the presence of a chemical kinetics

Damkohler number

To describe the evolution of a field of reactants generating a reaction, it is necessary to take the advection-diffusion equation, written for each reactant and product, and add the source and sink terms.

For a reaction of type (3.6), with second-order kinetics, we have the following system of equations (for reactants and the product):

$$\frac{\partial C_A}{\partial t} + \boldsymbol{u}\nabla C_A = D_A \Delta C_A - kC_A C_B \tag{3.7}$$

$$\frac{\partial C_B}{\partial t} + \boldsymbol{u}\nabla C_B = D_B \Delta C_B - 2kC_A C_B \tag{3.8}$$

$$\frac{\partial C_C}{\partial t} + \boldsymbol{u}\nabla C_C = D_C \Delta C_C + 3kC_A C_B. \tag{3.9}$$

Compared to an ordinary advection-diffusion problem, we note that there are a larger number of equations, and, most importantly for the reactions of order greater than 1, the appearance of non-linearities that modify the nature of the equations. These modifications induce all kinds of new behaviors with respect to the non-reactional case, and we will not undertake this subject here.

We can distinguish between two cases, according to the values of the Damkohler number, which is defined by the following expression:

$$Da = \frac{\tau_C}{\tau_M},$$

where τ_C is the characteristic time of the chemical reaction, and τ_M the mixing time (which can be controlled by the hydrodynamics or the diffusion).

– High Damkohler numbers: in this case, the kinetics are much slower than the mixing. After this mixing time has passed, the concentration field

homogenizes itself, and the preceding equations are considerably simplified. We thus have:

$$\frac{DC_A}{dt} \approx -kC_A C_B \tag{3.10}$$

$$\frac{DC_A}{dt} \approx -2kC_A C_B \tag{3.11}$$

$$\frac{DC_A}{dt} \approx 3kC_A C_B. \tag{3.12}$$

This type of regime is used in measurements of chemical kinetics.

– Low Damkohler numbers: in this case, the situation is more complex. The system develops fronts of reaction that are progressively mixed to form a homogeneous ensemble. The regime of evolution towards the completely homogenized situation is complex.

■ Microsystems

How does the Damkohler number vary with miniaturization? Considering a purely diffusive system, we can interpret the mixing time by the expression:

$$\tau_M \sim \frac{l^2}{D},$$

where l is the size of the system, and D the diffusion coefficient of the reactants (we assume here that they have the same order of magnitude). It follows that the Damkohler number is:

$$Da \sim \frac{D\tau_C}{l^2}.$$

We can thus generally consider that the more one miniaturizes, the more one produces elevated Damkohler numbers, suggesting that in microsystems, chemical kinetics tend to be the slower process. This conclusion has a limited scope, however. As we saw above, chemical reactions have a large range of reaction times. Here again, the influence of pre-factors can reverse the direction of the conclusions in a large number of situations. We can thus conclude by saying that, in general, there is not a typical order of magnitude for the Damkholer number in microsystems.

3.9.4 Reaction-diffusion of a front separating two reactants

We have dealt with the case of the diffusion of a front in a unidimensional space. The solution found for the concentration field is an error function, which increases proportionally with the square root of time. Here, we consider the same

problem, but with a second-order chemical reaction. In this case, the equations governing the problem are:

$$\frac{\partial C_1}{\partial t} = D_1 \frac{\partial^2 C_1}{\partial x^2} - kC_1C_2$$
$$\frac{\partial C_2}{\partial t} = D_2 \frac{\partial^2 C_2}{\partial x^2} - kC_1C_2,$$

with initial conditions:

$$t = 0, \quad C_1(x,0) = C_{10} \quad \text{and} \quad C_2(x,0) = 0 \quad \text{for} \quad x \leq 0,$$

and

$$C_1(x,0) = 0 \quad \text{and} \quad C_2(x,0) = C_{20} \quad \text{for} \quad x \geq 0.$$

These equations are normalized by performing the following transformations:

$$x = lx' \quad \text{and} \quad t = \frac{l^2}{D}t' \quad \text{with} \quad D = \sqrt{D_1 D_2}, \quad l = \left(\frac{D}{k\sqrt{C_{10}C_{20}}}\right)^{1/2}.$$

We find that they can be written (omitting the prime symbols):

$$\frac{\partial C_1}{\partial t} = \chi \frac{\partial^2 C_1}{\partial x^2} - \beta^{-1} C_1 C_2 \quad \frac{\partial C_2}{\partial t} = \chi^{-1} \frac{\partial^2 C_2}{\partial x^2} - \beta C_1 C_2,$$

where β and χ are defined by:

$$\chi = \frac{D_1}{D_2} \quad \text{and} \quad \beta = \sqrt{\frac{C_{10}}{C_{20}}}.$$

Contrary to the case of pure diffusion, the exact solution of these equations is not known for the general case. However, there is an appropriate solution valid at very long times, that Galfi and Racz [29] obtained twenty or so years ago. In this type of analysis, we are brought to consider the function 'rate of reaction' R, defined by the following relation:

$$R = C_1 C_2.$$

This function has the shape of a narrow peak. In the asymptotic solution, the width grows with time to the 1/6 power; in the general case where the diffusion coefficients are different, the maximum of R is displaced along the x-axis as $t^{1/2}$, while its amplitude grows as $t^{1/2}$. These are the principal properties of these

solutions, valid at long times. Here, 'long times' signifies 'values of times for which the function R can be considered to be a Dirac function'[14].

3.9.5 Analysis of the reaction-diffusion of a front in a T-shaped microcanal

Thanks to miniaturization, it was possible to study experimentally the broadening of a reaction-diffusion front that was intially very straight, and to compare the results to the solutions of the reaction-diffusion equations presented previously [30]. The experiment is identical in principle to the experiment shown in Fig. 3.4: two reactants, A and B, after leaving a T-shaped intersection, form a diffusion and reaction interface in the principal canal[15]. An image in false colors (Fig. 3.21) represents the zone of reaction, i.e. the region where the fluids are partially mixed [30].

Here, the reaction in question is the fluoresecent labelling of calcium by a protein (calcium green) according to the equation:

$$Ca^{2+} + CaGr \longrightarrow Ca^{2+*},$$

where the symbol * represents the complexing of a calcium ion with a fluorophor. The reaction is assumed to be irreversible and second order, with a rate equal to:

$$v = kC_1C_2,$$

where k is a constant, and indices 1 and 2 corresponding to calcium and calcium green, respectively. The analysis of the concentration field is revealed to correlate with the solutions of the problem of the spreading of the front analysed above, and obtained numerically. Figure 3.21b shows the agreement between the theoretical and experimental profiles.

This fact was exploited in [30] to measure kinetics on the order of the millisecond. This experiment thus shows that miniaturization gives access to rapid kinetics[16] allowing for the manipulation of very small samples. These two aspects

[14] As the peak broadens less quickly than it displaces and than it grows in amplitude, there is a time at which the peak can be considered infinitely narrow with respect to the scales of the problem. Using this fact, Galfi and Racz were able to solve the problem at long times [29].

[15] The advantages in using this geometry to characterize a chemical reaction is explained in Kalmotz *et al.* [31].

[16] The customary technique allowing for the measurement of chemical kinetics in isothermal conditions is the *stopped-flow* technique. This system consists of mixing two reactants injected into cavities using syringes, and then following the evolution of the reaction. The most rapid kinetics accessible using this technique is of a few milliseconds.

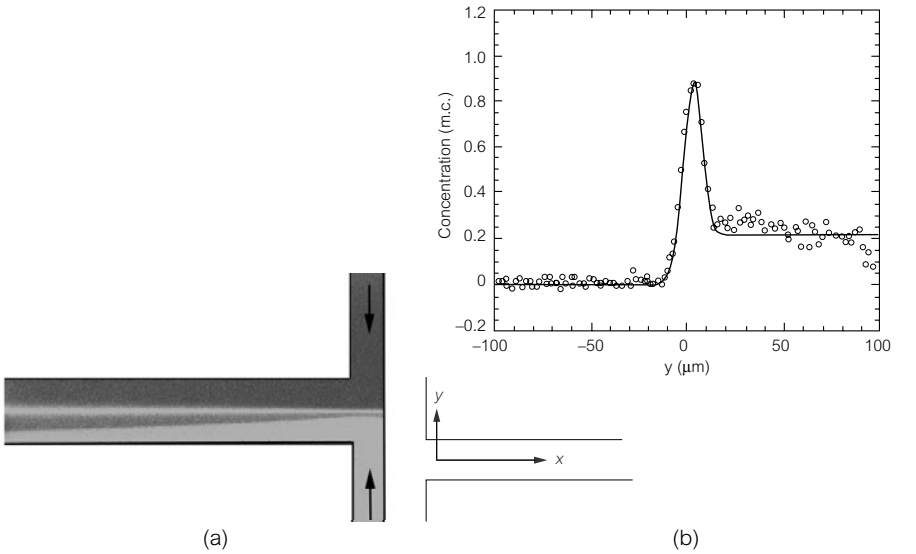

Figure 3.21 (a) Experiment carried out in a T-shaped microsystem, showing the development of a zone of reaction in the collection canal. The two reactants, which circulate from right to left, are a solution of calcium ions (upper arm of the T) and a solution of calcium green (lower arm of the T), a protein that fluoresces when in contact with calcium. The velocity in the (horizontal) branch is 2 cm/s, and the dimensions of the canals are 10 μm high and 200 μm wide [30]. (b) Concentration profiles of Ca green observed and calculated from the reaction-diffusion equations, assuming an irreversible second-order reaction.

are found to be advantageous from a practical standpoint(for example for the formulation of reactions involving rare products).

3.9.6 **Microreactor based on hydrodynamic focusing**

We have seen that hydrodynamic focusing permits the considerable reduction of the size of jets, which allows the attainment of particularly low mixing times, (on the order of ten μs, as shown by Knight *et al.* [20].) This possibility was undertaken by Pabit and Hagen [21] to measure rapid chemical kinetics in a reaction of fluorescent quenching (Fig. 3.22).

The jet is focused in a way that reduces its size, and using diffusion, achieves very low mixing times. One such system was used to measure time constants for fluorescent quenching, and the lower limit obtained was on the order of 400 μs. It would probably be possible to improve the performance of such a system by using, for example, silicon technology. However, this measurement has currently produced the smallest measured kinetic times in microfluidic systems.

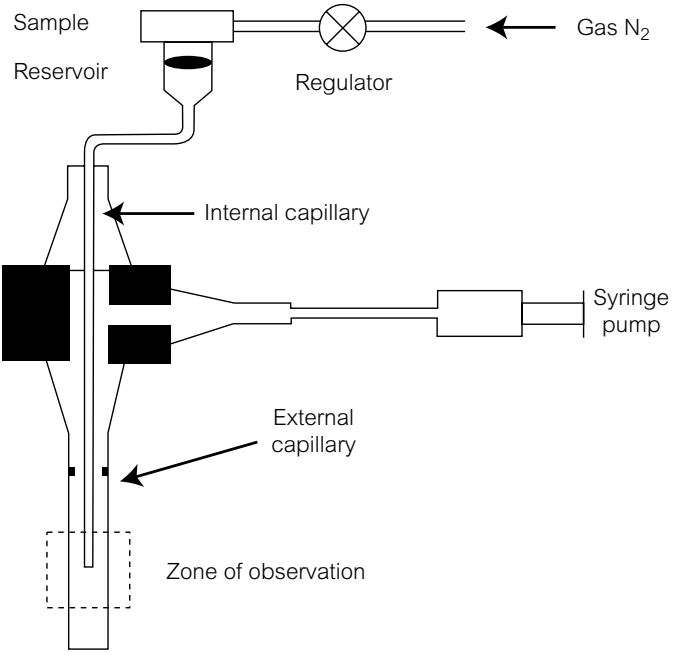

Figure 3.22 Experimental system used by Pabit and Hagen [21] to measure chemical kinetics on the order of 400 μs. The two reactants are put in motion towards the region of observation (bottom of the figure), where they form two jets, circulating from side to side, and mix by diffusion. The flow velocities can be adjusted in such a way that the central jet has a very small width, which favors a rapid mixing time between the two reactants.

3.9.7 **Other examples of microreactors**

We have just emphasized that miniaturization permits the simplest analysis of the characteristics of a chemical reaction, the main reasons being the possibility of having good flow control, and the implementation of extremely small diffusive mixing times. We can mention in this context an experiment [32] permitting the analysis with infrared spectroscopy of the kinetics of a chemical reaction where the reactants are also mixed with diffusion. However, in the domain of microfluidics, most microreactors created today have the function of producing a chemical reaction in a short time (if chemical kinetics allows it), without necessarily analysing it, nor even finely controlling the reaction itself. As examples of such microreactors, we note the micromixers described in the preceding section, which were all conceived for use as microreactors. We refer the reader to the corresponding references for more detail. Many other microreactors have been developed that are based on principles that we present here and are integrated onto chips. Reference [2] gives some examples of these.

3.10 Chromatography

3.10.1 Introduction

Chromatography is a powerful chemical analysis method that attempts to separate molecules, particles, or ions that were initially mixed in a solvent. The discovery of chromatography dates to 1903 by a Russian botanist named Twett, who revealed the constituents of raw chlorophyll. His experiment consisted of putting a spinach leaf in a solution of toluene, then using capillarity to transport the whole system through an adsorbant filter. He observed the spontaneous formation of distinct color zones corresponding to chlorophyll (green), xantophyll (yellow), and carotene (red). The name 'chromatography' is not really appropriate today, and comes from this very experiment, where the separation of molecules was identified using the separation of colors. The method of chromatographic separation was rediscovered in the 1930s and never ceased to evolve and become more and more refined; it was particularly stimulated by the explosion of molecular biology in the 1950s. The success of chromatography comes from the fact that it has a large power of resolution (in theory, it is possible to separate one sample into a hundred or so fragments); it is also possible to work with fragile molecules at ambient temperature, which is crucial for biology. From this standpoint, other methods of separation (such as distillation), are less advantageous than chromatography. Today, the field of chromatography is vast and well established. Chromatographic methods have been diversified and considerably enriched. They are exploited today by thousands of laboratories and companies. There are several journals and numerous studies that take methodological principles and construct, concretely, a separation experiment, often assuming the knowledge of very elaborate protocols. References [33, 34] are examples of works on this subject. There is also an excellent website, which clearly presents the principles of chromatography in liquid phase [35].

We will see that chromatography makes use of fluid flows circulating in geometries possessing a high surface area to volume ratio. It is logical that microfluidics, which operates in the same range of scales, might be a source of interesting structures and configurations for chromatography, and might offer the possibility of integration onto a laboratory on-chip. It is true that microfluidics is currently inducing a revolution in the domain of separation by capillary electrophoresis, which we will deal with in the following chapter. In the domain of non-electrophoretic chromatography (based on finely divided environments, such as powder or gels, without an electric field), which we concentrate on in this chapter, microfluidics also offers very tempting possibilities

conceptually; however, from a practical standpoint, microsystems currently have surface area to volume ratios inferior to those necessary for exclusion chromatography (which we will describe later)[17]; furthermore, microfluidics only offers a modest variety of treatments for exposed surfaces, a diversity that is much less than that of affinity chromatography, for example. A significant research effort is currently being implemented to answer these questions, and we will describe a few specific studies here; despite all the drawbacks, the possibilities offered by microfluidics are significant, and it is thus useful to understand the basic foundation on which the field rests in order to understand the effort currently being taken. This is the objective of this section. The presentation here is very succinct; the text will concentrate only on the basic principles, and on systems without an applied electric field (systems using electric fields will be presented in Chapter 4.)

3.10.2 **Principle of chromatography**

The principle of chromatographic separation is shown in Fig. 3.23, and a high-performance chromatographic device is depicted in Fig. 3.24.

Separation takes place in a chromatographic column. This column is filled with particles whose interactions with the surrounding fluid are known. This collection of particles, confined in the chromatographic column, is called the matrix. It constitutes the 'stationary' phase of the system, while the mobile phase is formed by the solution that circulates through the column. The sample to be separated is an unknown mixture that can be analysed by separating its components, and is initially deposited at the top of the column. We will see that there are several physical mechanisms that allow this separation to take place. Here, we consider the case where separation is based on adsorption, known as adsorption chromatography.

To begin a separation process, a solution that transports the sample is circulated towards the bottom of column, and then progressively desorbed. The adsorption/desorption phenomena, as we have noted in this chapter, depends on the partition coefficient of the molecular species in question. We will thus have selective transport velocity that differs from one species to another. In this way, distinct bands will appear progressively along the column over the course of time, each band containing species with the same partition coefficient. As time

[17] For a system formed of cylindrical canals of radius r, the ratio of surface area-to-volume, which is called χ, is $2/r$. Considering porous particles containing pores of radii 50 nm, we obtain χ values on the order of 4×10^7 m^{-1}. For a capillary canal with a square cross-section of side b, χ has a value of $4/b$. To obtain a value of χ comparable to a chromatographic system using particles of 5 μm, it would be necessary to have canals with sides of 0.1 μm. We will see in Chapter 6 that the fabrication of such canals is beyond the standard possibilities achievable with silicon technology.

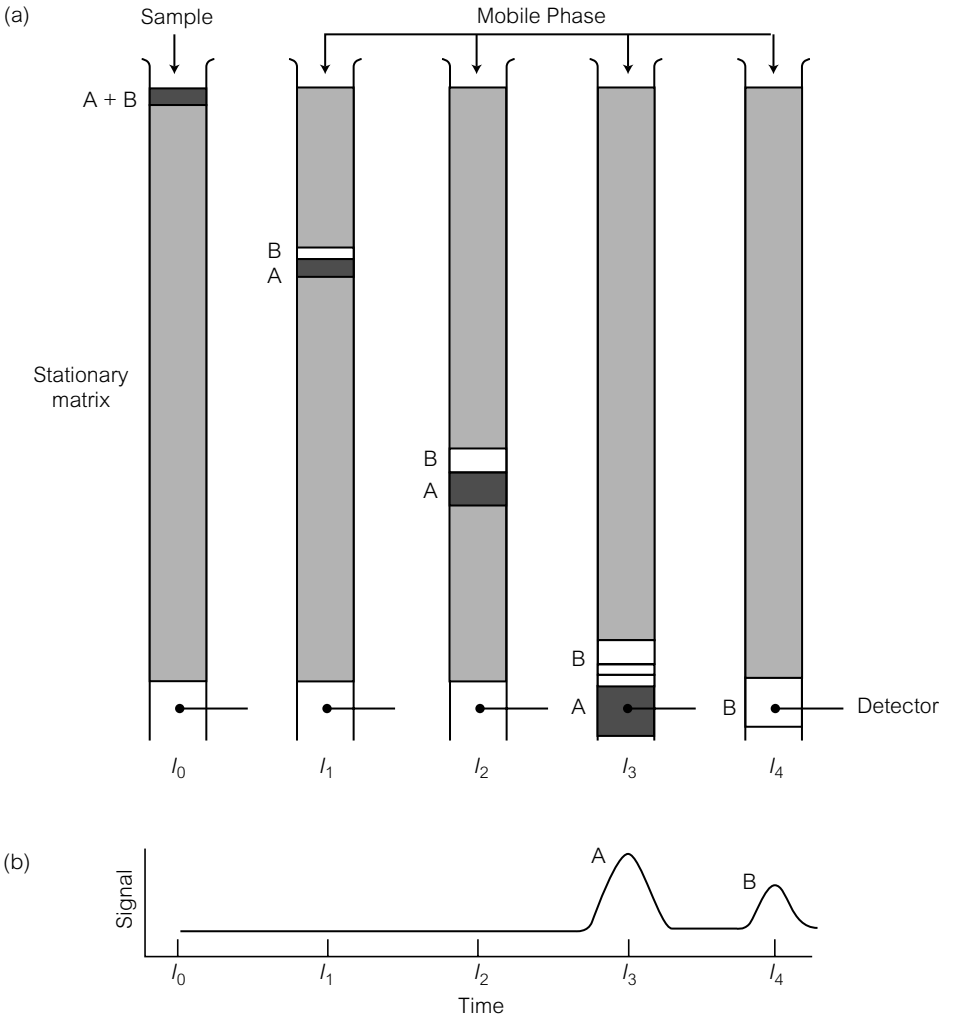

Figure 3.23 Evolution along a column of the two elements A and B present in the sample, and migrating along a column at different speeds.

goes by, a detector placed at the bottom of the column records a temporal signal (Fig. 3.25).

The signal is made up of a series of peaks. It allows the measurement of the time of passage of each band before the detector. From this are deduced the migration velocities, the corresponding partition coefficients, and, exploiting the calibration data or other associated information, the different components of the sample. The chromatographic signal can also, from the measurement of the area under each peak, determine the concentrations for each component. It is remarkable that the method finds its efficacy in an effect of the amplification

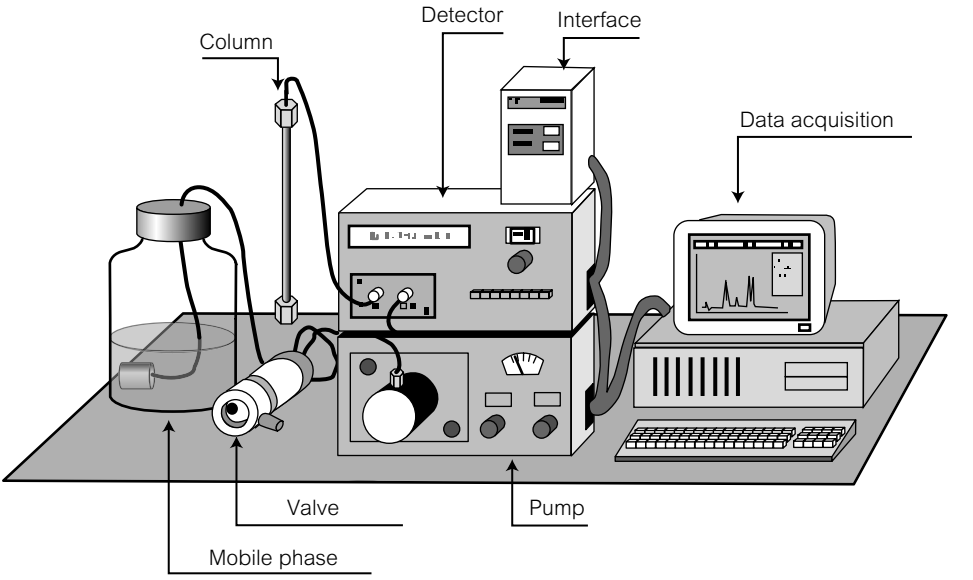

Figure 3.24 Typical equipment for chromatography.

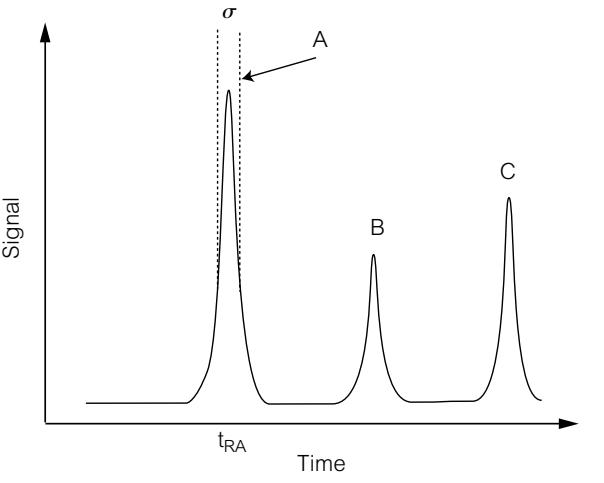

Figure 3.25 Chromatographic signal schematically represented. The peak is characterized by the time of passage in front of the detector (known as the retention time t_{RA}) as well as by its width (characterized by its standard deviation σ).

of small differences: small disparities in the partition coefficients of different consituents of the sample are effectively amplified by repeated passages through the grains forming the matrix.

The minimal amount of equipment to implement the separation process consists of a flask, fluids, and filter paper. Today, separation is most often carried

out using more developed and complex equipment (Fig. 3.24). A pump, an eluant reservoir, the chromatographic column, a detection module, and a computer for data analysis, are all distinguishable in the figure. One of the possibilites offered by microfluidics and microtechnologies is to transform this platform into a portable system. Researchers have already taken the first few steps in this direction.

The characterization of a separation process is based on several different quantities. The first is the retention time t_R, defined in Fig. 3.25. This is the time a component of the sample takes to traverse the column and pass before the detector. The second quantity is the standard deviation of the peak corresponding to a given component (Fig. 3.25). It is of course advantageous to reduce this quantity as much as possible (if not, two successive peaks could be difficult to resolve). This quantity is notated as σ. The 'efficiency' of the column is characterized by a number N, known as the 'number of theoretical plates'[18]. This number is by definition[19]:

$$N = 16\frac{t_R^2}{\sigma^2}. \tag{3.13}$$

Over the course of time, the different bands (corresponding to each species present in the sample) spread according to the law:

$$X \sim \sqrt{D_{\text{eff}} t},$$

where X is the width at time t of a band progressing in the column, and D_{eff} is an effective diffusion coefficient for the species in question. In all matrices formed from particles or gels, the coefficient D_{eff} is not simply the molecular diffusivity of the species: it is necessary to incorporate the effect of dispersion related to the inevitable inhomogeneities of the sizes of the pores or particles constituting the stationary phase. This inhomogeneity results in hydrodynamic shear of the flow in the pores or between particles, leading to the phenomenon of Taylor–Aris dispersion, which we have already discussed in this chapter. The effect of this dispersion is obviously to increase the width of the peaks of the chromatographic signal detected at the base of the column, implying, after the formula (3.13), a diminishing of the number of theoretical plates. This problem is a significant limitation in chromatographic methods.

[18] The term 'theoretical plates' was introduced by analogy with distillation vocabulary.

[19] There is no strong reason to take the square of this value; in fact, we consider in the domain of chromatography that it is more pertinent to work with the variance than the standard deviation. In practice, to get an idea of the maximum number of identifiable components in a sample, it is necessary to take the square root of N. We thus see that N is an important quantity.

It is possible to formalize the effect of dispersion: multiplying the numerator and denominator of equation (3.13) by the square of the typical migration velocity of the bands, we find that the number of theoretical plates N is equal to:

$$N \sim \left(\frac{\text{distance reached by the band}}{\text{width of the band}} \right)^2 .$$

Denoting U as the velocity of the displacement of bands along the column, we have:

$$N \sim \frac{L^2}{D_{\text{eff}}(L/U)} \sim \frac{UL}{D_{\text{eff}}}. \tag{3.14}$$

The number of theoretical plates is in a way representative of the Peclet number of the system. The smaller the D_{eff}, the higher the number of plates, and the larger the velocity and the length of the column, the more the separation is 'efficient.' We find that results conform to intuition. This expression will be useful for the evaluation of N in certain situations.

Once the bands have migrated to the base of the column, we proceed to the detection phase. In chromatographic systems, this problem is crucial, especially when the component in question exists only in trace amounts (this is frequently the case in biology and the environmental sciences). Nevertheless, there are a wide variety of detectors available that use, for example, fluorescence (an extremely sensitive method), thermal conductivity, electrical conductivity, photon adsorption, etc. To conclude this presentation, we will go over a few orders of magnitude: for liquid phase chromatography (LPC), columns are typically 20 cm long and 4 mm in diameter, with particles of 20 μm and applied pressures increasing to several bars or tens of bars. The quantities being analysed are on the order of the milligram, and the efficiency varies between 100 and 1000 theoretical plates. The typical minimum detection for this type of column is on the order of the picogram. The retention time obviously depends on several parameters, but to illustrate, we can say that they are typically on the order of ten or several tens of minutes. The versatility and the richness of chromatographic methods leads us to believe that it is possible to find a solution to whatever analytical problem that may arise.

3.10.3 **Different types of chromatography**

Without entering into the details, the most common methods of liquid-phase chromatography currently being used will be described succinctly here. They are

based on specific interactions between the matrix and the solution, and are represented schematically in Fig. 3.26a and 3.26b.

• **Adsorption chromatography:** This type of chromatography was previously described in Section 3.10.2.

• **Partition chromatography:** the column contains a liquid film covering each sphere making up the stationary phase. Certain components of the sample end up dissolving in this film.

• **Ion-exchange chromatography:** the matrix is made up of charged spheres that retard the displacement along the column (under the effect of a pressure gradient) of ions of the opposite sign. The most common matrices are gels of cellulose. The effect of the retardation of the displacement can be controlled and optimized by modifying the pH of the solution.

• **Exclusion chromatography:** the matrix is electrically neutral and made up of porous spheres. Small molecules frequently visit the interior of these spheres by molecular diffusion. As a consequence, they progress to the base of the column

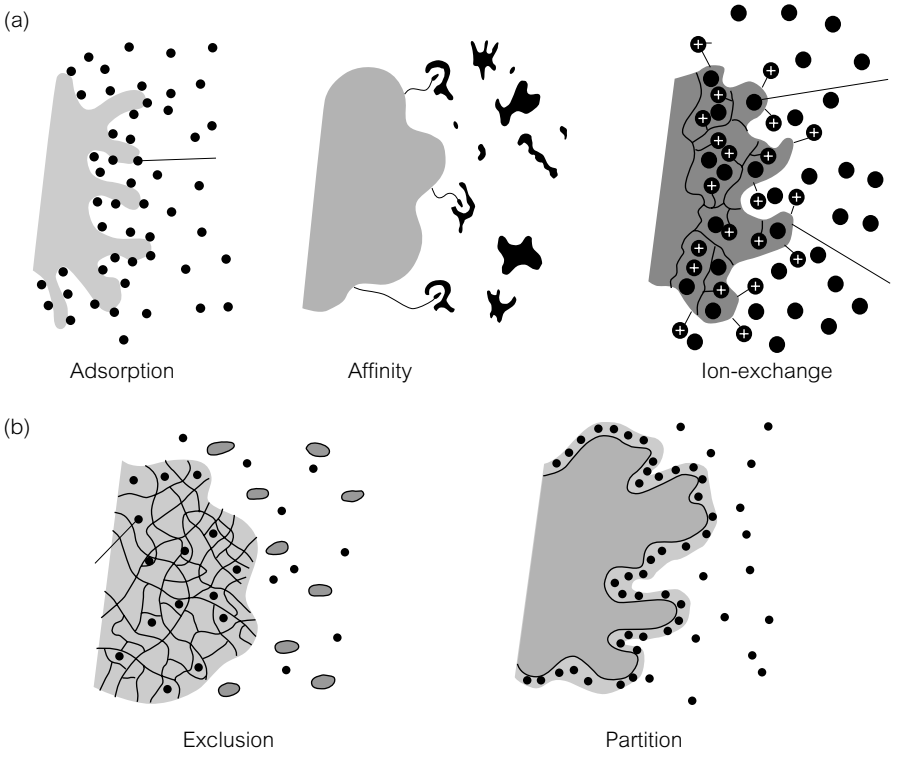

Figure 3.26 Differents types of chromatography: (a) adsorption, affinity, ion-exchange; (b) exclusion, partition.

more slowly than large molcules do: we thus have an effect of separation 'by exclusion.' The spheres used can be, for example, agarose beads, which possess a large diversity of porosities.

• **Affinity chromatography:** in this case, the spheres of the matrix are functionalized by molecules possessing a high affinity for certain components of the solute (for example, antibodies specific to the protein to be isolated are deposited on spheres of the matrix). The molecule in question becomes fixed to the matrix, and can be then eluted by circulating a solvent through the matrix.

We clarify here that two chromatographic modes can be distinguished: a 'normal' and an 'inverse' phase. This distinction emphasizes of the important role played by polarity in chromatographic systems.

• Normal-phase chromatography corresponds to the case where the stationary phase is polar (e.g. silicon gel) and the mobile phase is non-polar (e.g. *n*-hexane). The polar elements of the sample will be retained on the silicon grains but the others will not.

• Inverse-phase chromatography is precisely the inverse of the preceding situation: the stationary phase is non-polar, and the mobile phase is polar. In this case, the non-polar material will be preferentially retained by the matrix.

3.10.3.1 HPLC (high-performance liquid chromatography)

In the pursuit of the amelioration of the performance of chromatographic systems in liquid phase, scientists were led to diminish the size of the matrix grains. The advantage of such a diminution can be understood by examining the formulas presented in the preceding section: by roughly estimating the diffusion coefficient by the Taylor–Aris formula (see Section 3.5.2), we obtain the following estimation for the number of theoretical plates:

$$N \sim \frac{t_R D}{b^2},$$

where, we remember, t_R is the retention time, D is the molecular diffusion coefficient for the species in question, and b is the typical size of the space between grains or pores[20]. We deduce from this that at fixed retention times, reduction of grain size leads to an increase in the efficiency of the column, i.e. that is to say its capacity to separate a sample into a large number of constituents. However, by reducing the size of the grains, the pressure drop across the column tends to

[20] A more detailed discussion including dispersion phenomena in the matrix must be taken into account. We will only perform a rough estimation here, founded on the idea that the principal origin of dispersion is due to the shear of the flow between grains.

increase. The order of magnitude of the pressure drop ΔP across the length of the column is:

$$\Delta P \sim \frac{L^2 \mu}{b^2 t_R},$$

where L is the length of the column. Thus, the diminution of b, with everything else equal, leads to the growth of ΔP; ΔP varies as the inverse of b^2, which is substantial effect. The reduction of the size of the grains, associated with the augmentation of the column length, has led to a group of chromatographic techniques known as 'high-performance liquid chromatography,' or HPLC. It is not a specific type of chromatography, but a refinement of preceding techniques, resulting in very highly resolved, high-throughput separations (i.e. with a significant production of analytical results). Typically, the matrices of HPLC systems are made of monodisperse molecules of very small size (between 3 and 10 μm), the column is long and operates at high pressure (hundreds of bars). With this type of system, hundreds of thousands of theoretical plates can be obtained. This type of equipment is now often used; HPLC is a point of reference for all new systems trying to improve current chromatographic techniques.

3.10.4 The miniaturization of chromatographic systems

In a general manner, the effort currently being taken to miniaturize chemical analysis systems have covered all aspects of the analysis: acquisition of the sample, extraction, injection, micromanipulation, pre-concentration and separation. We refer the reader to [2, 3] for a documented survey of work being done at this point in time. We will concentrate on the separation step itself, that is, the chromatographic step, in the sense that we have defined above.

3.10.4.1 Pros and cons of miniaturizing in non-electrokinetic systems of separation

Why miniaturize chromatographyic systems? There are three main reasons:

– sample volumes can be reduced with respect to ordinary systems,
– possibilies for integration are opened up (μTAS or lab-on-a-chip),
– possibilites for parallelization, leading to high throughput also exist.

These advantages must, however, be mentioned alongside a certain number of difficulties and limitations.

• One difficulty comes from the fact that it is difficult to produce, using MEMS technology, surface-to-volume ratios greater than that of the matrices

formed using microparticles or gels. This point is illustrated in Fig. 3.14; this microsystem, which is particularly advanced, was used by He *et al.* [36] to form a chromatographic column. A separation effect was effectively obtained. However, even in this case, the surface-to-volume ratio was much smaller than that of standard silicon particles, covered with pores of 20 nm in diameter. New ideas involving the introduction of nanopillars in microcanals in order to obtain elevated specific surfaces were recently proposed [37, 38]. It remains that at this point in time, the reproduction of nanometric scales encountered in chromatographic columns is associated with various microfabrication difficulties.

• To guarantee elevated specific surfaces, one possibility is to insert stationary matrices (gels or particles) into microcanals. In this case, miniaturization, if it does not involve electrokinetic effects (which we will discuss in the following chapter), is not accompanied by a gain in analytic performance. To illustrate, we take the estimation for the number of theoretical plates, given by:

$$N \sim \frac{t_R D}{b^2},$$

where t_R is the retention time, D is the molecular diffusion coefficient for a given species, and b is a typical size for the space between grains or pores. At a fixed retention time, miniaturization of the column is not accompanied by a gain in efficiency. A reduction of analysis time (inherently desirable in microsystems) actually leads to a diminution in the efficiency of the column.

It thus seems that the miniaturization of non-electrokinetic chromatographic systems present a whole collection of pros and cons. We will see later that the situation changes once we use a separation method based on electrokinetics.

3.10.4.2 One example of a microsystem incorporating a matrix

We have noted that obtaining high specific surfaces requires the use of microparticles analogous to those used by 'ordinary' chromatographic columns. It is necessary to add that the insertion of particles has the benefit of capitalizing on a large variety of surface treatments available as well as being able to implement established and time-honored separation techniques.

Different techniques are currently used for incorporating a matrix into microcanals: inducing a sol-gel transition, inserting particles, and photopolymerizing a matrix, to name a few. Figure 3.27, taken from [39], shows an example of the formation of a chromatographic column using an obstruction of functionalized particles in a pocket created along a microcanal. This type of technique is often used to form chromatographic microcolumns or microcolumns of extraction.

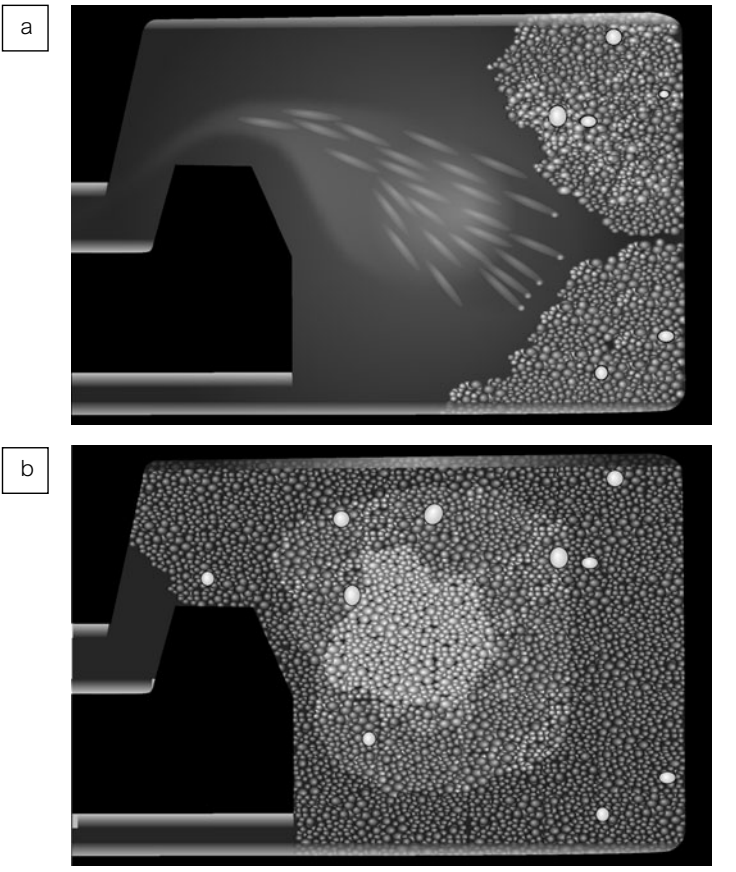

Figure 3.27 Method of the formation of a chromatographic column in a microsystem created using MEMS technology [39]. The particles contained in the cavity are silicon particles between 1.5 and 4 μ in diameter, functionalized with ODS (Octadecylsilane). The cavity is 1 μm wide and opens out to the end of a canal at the lower left of the figure, which allows a flux to come through.

In the experiment of [39], silicon particles 1.5 and 4 μm in diameter are functionalized with ODS (octadecylsilane). The cavity, which is about 1 μm high and 30 μm wide, opens up to the end of a canal at the lower left of the figure, which allows the fluid flux to pass through. The authors showed that the microcolumn allowed for the separation of molecules such as BODIPY and fluorescein[21].

3.10.4.3 The first miniaturized system of separation was created in 1975

The first miniaturized chromatographic column was made in silicon in 1975 [40], more than 25 years ago. This system was remarkable: it consisted of an injection

[21] The method of separation used here is capillary electrochromatography, which will be described in Chapter 4.

valve and a separation column 1.5 m in length. Detection was based on a thermal sensor, fabricated on a plate of associated silicon, and fixed onto the chip. As emphasized in the review of Reyes *et al.* [2], this high-quality precursor work did not create any significant waves in the separation science community. Today, the number of miniaturized *non-electrokinetic* chromatographic systems using MEMS or plastics technology is modest. This situation remains in contrast with capillary electrophoresis, which is based on the implementation of electrokinetic effects, which has been developed into a multitude of miniaturized versions, and has even resulted in several successful commercialized systems.

At the moment, one kind of chromatographic techniques presented in this chapter can be miniaturized. We can mention, by way of example, ion-exchange chromatography, whose miniaturized version is shown in Fig. 3.28 [41]. Here also, functionalized beads are introduced into a microcanal using a restriction. In [41], this system was used to separate proteins BSA and IgG in about a hundred seconds.

3.10.4.4 Miniaturization inspired the invention of new chromatographic methods

The attraction of miniaturization has led to the conception of new methods of separation. One of these proposed new methods was 'hydrodynamic chromatography' (Fig. 3.29) [42, 43]: large molecules circulate, on average, in the central portion of the canal (for steric reasons). Small molecules on average traverse the whole cross-section. It follows that the large molecules, on average, go faster than the small molecules. There is thus a separation based on hydrodynamics and diffusion, and not based on interaction with a surface. In practice, this separation

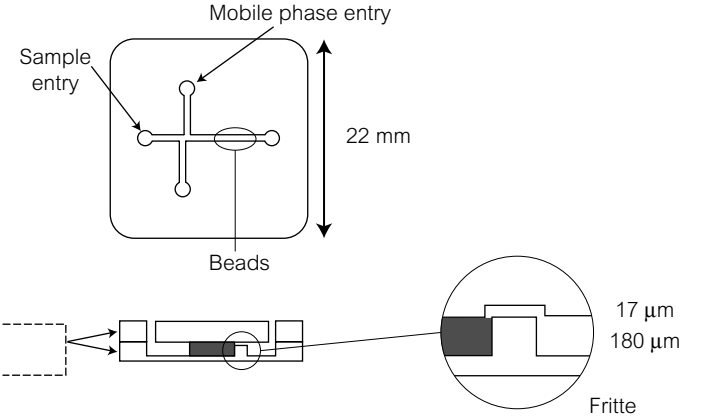

Figure 3.28 A miniaturized system, operating under the principal of ion-exchange microchromatography; the figure represents a network of canals, and the system of an obstruction of functionalized particles (dark zone); these particles are 30 μm in diameter [41].

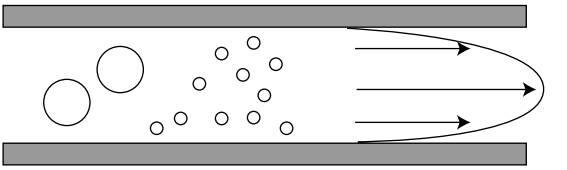

Figure 3.29 Principle of hydrodynamic chromatography, based on the presence of a confinement and a velocity gradient. Large particles circulate more quickly than small molecules, as they tend on average to travel down in the central portion of the canal, where velocities are higher [42, 43].

effect is only appreciable in extremely thin canals, which is why miniaturization has made this technique possible. This principle of this method of separation is evocative of exclusion separation.

These contributions are representative of the research effort currently underway. The history of miniaturization of the separation sciences has not concluded, however. Systems currently being created are still far from being optimized, and the conceptual foundation still needs to be formed. The μTAS conferences attest to the large amount of interest on this subject.

References

[1] A fundamental work explaining chromatographic methods used for the indentification of proteins is *Molecular Biology of the Cell*, B. Alberts, D. Bray, J. Lewis, M. Raff, K. Roberts, J. Watson—3rd edn 1994, Garland Publishing, New York.

[2] D. Reyes, D. Iossifidis, P.A. Auroux, A. Manz, *Anal. Chem.*, **74**, 2623 (2002).

[3] P.A. Auroux, D. Iossifids, D. Reyes, A. Manz, *Anal. Chem.*, **74**, 2637 (2002).

[4] A. Einstein, *Investigations on the Theory of Brownian Movement*, New York, Dover, 1956.

[5] G.I. Taylor, *Proc. Lond. Math. Soc.*, **A20**, 196 (1921).

[6] E.L. Cussler, *Diffusion*, 2nd edn, Cambridge University Press.

[7] C. Jullien, P. Castiglione, P. Tabeling, *Phys Rev E*, E**64**, R35301 (2001).

[8] L. Menetrier, C. Baroud, P. Tabeling, unpublished (2001).

[9] A. Kamholz, P. Yager, *Biophys. J.*, **80**, 155 (2001).

[10] A. Kamholz, P. Yager, *Sens. Actuators B*, **82**, 117 (2002).

[11] G. Batchelor, *Phys. Fluids*, Supp II, **12**, 233 (1969).

[12] G.I. Taylor, *Proc. Roy. Soc.* **A219**, 186 (1953).

[13] H.A. Stone, A.D. Stroock, A. Ajdari, *Ann. Rev. Fluid. Mech.*, **36**, 381 (2004).

[14] Y. Pomeau, P. Bergé, B. Roux, *L'ordre dans le chaos*, Hermann (1984).

[15] *The Kinematics of Mixing: Stretching, Chaos and Transport*, Cambridge University Press (1989), J. Ottino.

[16] A. Lichtenberg, M. Lieberman, *Regular and Stochastic Motion*, Springer-Verlag (1983).

[17] A. Groissman, V. Steinberg, *Nature*, **410**, 905 (2001).

[18] S. Bohm, K. Greiner, S. Schlautmann, S. de Vries, A. Van der Berg, *Proc.* μ*TAS*, 25 (2001).

[19] D.J. Beebe, G.A. Mensing, G.M.Walker, *Ann. Rev. Biomed. Eng.*, **4**, 261 (2002).

[20] J. Knight, A. Vishwanath, J. Brody, R. Austin, *Phys. Rev. Lett.*, **80**, 3866 (1998).

[21] A. Pabit, S. Hagen *Biophys. J.*, **83**, 2872 (2002).

[22] A. Scherer, S. Quake, *Science*, **290**, 1536 (2000).

[23] Y.K. Lee, J. Deval, P. Tabeling, C.M. Ho, *Proc MEMS2001*, Interlaken (2001).

[24] M. Volpert, C. Meinhart, I. Mezic, M. Dahleh, *J. MEMS* (2001).

[25] A. Strooke, A. Ajdari, H. Stone, G. Whitesides, *Science*, March 2002 (2002).

[26] J.F. Richardson, J.H. Harker (with J.R. Backhurst), *Chemical Engineering vol. 2*, Butterworth-Heinemann, 5th edn (2002).

[27] P.W. Atkins, *Physical Chemistry*, Oxford University Press, 5th edn (1994).

[28] K.J. Laidler, *Chemical Kinetics*, Harper and Row (ed.) (1987).

[29] L. Galfi, Z. Racz, *Phys. Rev. A*, **38**, 3151 (1988).

[30] C. Baroud, L. Menetrier, F. Okkels, P. Tabeling, *Phys. Rev E*, **67**, 60104 (2003).

[31] A. Kamholz, B. Weigl, B. Finlayson, P. Yager, *Anal. Chem.*, **71**, 5340 (1999).

[32] P. Hismann, J. Frank, P. Svasek, M. Harasek, B. Lendl *Lab on a Chip*, **1**, 16 (2001).

[33] R.P.W. Scott, *Techniques and Practices of Chromatography*, Marcel Dekker (1995).

[34] V.R. Meyer, *Practical High-Performance Liquid Chromatography*, 2nd edn, Wiley, New York (1994).

[35] Y. Kazakevich, H. McNair, *Basic Liquid Chromatography*, *http://hplc.chem.shu.edu/NEW/HPLC_Book*.

[36] B. He, N. Tait, F. Regnier, *Anal. Chem*, **70**, 3790 (1998).

[37] M. Baba, T. Sano, N. Iguchi, K. Iida, T. Sakamoto, H. Kawaura, *Proc.* μ*TAS 2002*, Nara, Japan, 763 (2002).

[38] A. Pepin, P. Youinou, V. Studer, A. Lebib, Y. Chen, *Microelectron. Eng.*, **61/62**, 927 (2002).

[39] R. Oleshuk, L. Shultz-Lockyear, Y. Ning, D. Harrison, *Anal. Chem.*, **72**, 585 (2000).

[40] S. Terry, J.H. Jerman, J. Angell, *IEEE Trans. Electron. Devices*, **ED-26**, 1880 (1979).

[41] M. Seki, M. Yamada, R. Ezaki, R. Aoyama, J. Hong, *Proc.* μ*TAS 2001*, Monterey (USA), 48 (2001).

[42] M. Blom, E. Chmela, J. Gardenir, R. Tijssen, R. Elwenspoek, A. van den Berg, *Transducers 01*, Munich (Germany), 794 (2001).

[43] M. Blom, E. Chmela, J. Gardenir, R. Tijssen, R. Elwenspoek, A. van den Berg, *Sens. Actuators B*, **82**, 111 (2002).

[44] D. Evans, D. Liepmann, A.P. Pisano, *Proc. MEMS 97*, Nagoya, Japan, 96, (1997).

FOUR

The electrohydrodynamics of microsystems

4.1 Introduction

We have seen in Chapter 1 that miniaturization easily allows the production of intense electric fields. It is thus not surprising that researchers in the domain of microsystems have tried during these last several years to profit from electrohydrodynamics (that is, the coupling between an electric field and moving particles or fluids) to act on the flow of fluids or the movement of charges in miniaturized systems. Many types of miniaturized electrophoretic separators, dielectrophoretic microcytometers, and electro-osmotic micropumps have thus been created. A few of these systems were successfully commercialized: this was the case, for example, of the electrophoretic separation systems of DNA and proteins produced by Caliper/Agilent. One could imagine that tomorrow, these electrokinetic phenomena will be at the heart of future *lab-on-a-chip* technology, and will be used to achieve separation, pumping or trapping. This is where the importance of electrokinetics in the domain of microfluidics enters, and it is to these phenomena that this chapter is dedicated.

The general classification of electrokinetic phenomena is the following:

- **Electro-osmosis**: the movement of an ionized fluid under the effect of an electric field.
- **Électrophoresis**: the movement of charged particles by an electric field in a resting fluid.
- **Streaming Potential**: the inverse of electro-osmosis: an electric field is induced by the circulation of an ionized fluid.
- **Sedimentation Potential**: the inverse of electrophoresis: an electric field is created by the movement of charged particles in a fluid.

• **Dielectrophoresis**: the movement of neutral particles by the application of an electric field.

Today, three of these effects make up a considerable portion of the domain of microfluidics.

Electro-osmosis: is used for the pumping of electrolytes and buffers in microsystems. It consists of a pumping mode that is difficult and not very useful for macrometric systems, but simple and elegant to use in miniaturized systems. We will see that one of the advantages of electro-osmosis is the ability to displace fluids as a 'plug' flow, that is to say, with a spatially homogeneous velocity field along the canal. The consequence of such a property is that it becomes possible to transport objects without the effect of hydrodynamic dispersion (of the Taylor–Aris type). This advantage is particularly beneficial in the field of separation, introduced in Chapter 3. Electro-osmotic pumping has been integrated in the first commercialized lab-on-a-chip device, and is often included in miniaturized electrophoretic separation devices.

Electrophoresis: This domain was born after the discovery of electrophoresis (Linder and Piction 1892). The subject expanded considerably, notably due to the work of Jorgenson and Lukacs [1] and Hjerten [2]. One of the principal uses of electrophoresis is to separate ionized molecules, which are made to migrate at different velocities along a capillary. This technique is called 'capillary electrophoresis,' and its success over traditional systems is based on its favorable separation conditions, specifically its particularly low separation volumes and times. Capillary electrophoresis is so well established as a separation technique that it is currently used by French judiciary bodies for DNA tests[1]. Today we use it for genotyping, paternity tests, microwell identification, and the identification of GMOs (genetically modified organisms). There are journals on the subject (e.g. the *Journal of Capillary Electrophoresis*), and there are regularly organized specialized conferences. Capillary electrophoresis, coupled with mass spectrometry, has been called upon to play an important role in the rising field of proteomics (i.e. the analysis of proteins in a given system). Thus, capillary electrophoresis is one of the domains where miniaturization actually induced a revolution. This technique will be described in some detail in this chapter.

Dielectrophoresis: can be exploited to manipulate neutral particles in microcanals, to induce the movement of cells, to trap or select cells [4, 5], or to pump a fluid [6]. It is also worthy to mention the chaotic electrohydrodynamic mixer, which mixes neutral dielectric particles [7]. Finally, it was shown

[1] Capillary electrophoresis was used in 1997 for the DNA analysis of a hair in a criminal matter [3].

very recently that it is possible to manipulate dielectric particles using valves and pumps[2] [8].

We are thus going to describe in this chapter all the principal electrohydrodynamic effects involved in microfluidic systems, concentrating more closely on the three major effects. This chapter is only an introduction to the rich and complex domain that is currently the focus of a significant research effort. The reader can refer to reference [9], which develops some of these subjects in relation to microsystems.

4.2 Brief review of electrokinetics

4.2.1 Movement of charged particles in an insulating fluid, submitted to an electric field

An isolated particle placed in an insulating medium (i.e. where no mobile charges exist), and subjected to an electric field $\boldsymbol{E}$, is acted on by the Coulomb force $\boldsymbol{F}$, whose expression is:

$$\boldsymbol{F} = q\boldsymbol{E},$$

where q is the charge. One of these particles obeys the following equation (in the absence of Brownian motion):

$$q\boldsymbol{E} - \boldsymbol{F}_{\mathrm{v}} = m\frac{\mathrm{d}\boldsymbol{V}}{\mathrm{d}t} \approx 0,$$

where $\boldsymbol{F}_{\mathrm{v}}$ is the viscous friction force applied on the moving particle and is given by Stokes' Law:

$$\boldsymbol{F}_{\mathrm{v}} = 6\pi R\mu\boldsymbol{V},$$

where R is the radius of the particle, μ is the viscosity of the fluid, and $\boldsymbol{V}$ is the velocity of the particle. In the preceding equation, the inertial term can be neglected right away; this simplification is equivalent to the Stokes approximation for moving particles in a fluid at low Reynolds numbers. One can verify that in practice this term is many orders of magnitude less than the viscous terms in typical microfluidic situations. From the two preceding equations, we deduce

[2] Although in this particular case the manipulation of dielectric particles is achieved using a laser and not electrodes, the nature of the forces allowing the micromanipulation of particles is identical to the one discussed in the text.

the migration velocity of the particle:

$$\boldsymbol{V} \approx \frac{q\boldsymbol{E}}{6\pi R\mu}.$$

This result can be rewritten by introducing an 'electrophoretic mobility,' represented here by μ_e so that it is not confused with dynamic viscosity, which is represented by μ in this book. The definition of the mobility is established from the relation:

$$\boldsymbol{V} = \mu_e \boldsymbol{E}.$$

One deduces that for an isolated charge, the electrophoretic mobility equals

$$\mu_e = \frac{q}{6\pi R\mu}. \tag{4.1}$$

This formula is very important for the process of electrophoretic separation. We can ask ourselves whether equation (4.1) should be reconsidered when the particle is immersed in an electrolyte. In this case, the mobile charges of the electrolyte redistribute themselves around the charged particle, and they must be taken into account in the mobility calculation. We deal with this situation later in the text. We can, however, predict that even in the presence of an electrolyte, equation (4.1) is more or less applicable.

4.2.2 **Electrokinetic equations**

Electric current measures the displacement of charges, and this displacement can have several sources.

– Charges can be displaced by diffusion, that is to say by the action of a charge density gradient. This process is analogous to the ordinary diffusion process, and is governed by Fick's Law, which we saw in Chapter 3. This law is written:

$$\boldsymbol{J}_m = -D\nabla C,$$

where $\boldsymbol{J}_m$ is the mass current (i.e. the mass crossing a surface element per unit time), C is the mass charge concentration, and D is the molecular diffusion coefficient of the charged species in consideration. This relation must be rewritten to adapt it to the electrical terminology we are using here. Dividing the two sides of the equation by q/m (where q is the charge of the species in question and m is its mass), we obtain the relation:

$$\boldsymbol{J}_D = -D\nabla \rho_e, \tag{4.2}$$

where $\boldsymbol{J}_{\mathrm{D}}$ is the current with a diffusive origin, and ρ_{e} is the charge density, i.e. the electric charge per unit volume.

– The charges can be displaced by an ensemble translation (for example a flow). The current induced by this effect is written:

$$\boldsymbol{J}_{\mathrm{T}} = \rho_{\mathrm{e}} \boldsymbol{V},$$

where $\boldsymbol{V}$ is the velocity of the translation of the charges.

– Finally, the charges can be displaced by an electric field. In this case, we have the relation:

$$\boldsymbol{J}_{\mathrm{e}} = \sigma \boldsymbol{E},$$

where σ is the electrical conductivity.

Adding up these three contributions, we arrive at the equation:

$$\boldsymbol{J} = -D\nabla\rho_{\mathrm{e}} + \rho_{\mathrm{e}}\boldsymbol{V} + \sigma\boldsymbol{E}. \tag{4.3}$$

It is necessary to add the conservation of charge expression to this equation, which has a structure identical to the conservation of mass equation:

$$\frac{\partial \rho_{\mathrm{e}}}{\partial t} + \operatorname{div} \boldsymbol{J} = 0. \tag{4.4}$$

It is also necessary to take into account the relation of the charge density to the electric field, in a homogeneous medium of permittivity ϵ:

$$\operatorname{div} \boldsymbol{E} = \frac{\rho_{\mathrm{e}}}{\epsilon}. \tag{4.5}$$

Equations (4.3), (4.4) and (4.5) must be completed by the equation governing the flow of a charged fluid. For liquids, this equation is simply the Navier–Stokes equation, amended by the incorporation of Coulombic forces, which are related since locally the fluid possesses a charge, and because the fluid is subjected to an electric field. The latter is written:

$$\frac{D\boldsymbol{u}}{Dt} = -\frac{1}{\rho}\nabla p + \nu\Delta\boldsymbol{u} + \rho_{\mathrm{e}}\boldsymbol{E},$$

where $\boldsymbol{u}$ is the velocity of the species in consideration, and $\boldsymbol{E}$ is the imposed electric field. In the context of microsystems, as we have emphasized in Chapter 2, we can eliminate inertial terms, and restrict ourselves to the following simplified form:

$$-\frac{1}{\rho}\nabla p + \nu\Delta\boldsymbol{u} + \rho_{\mathrm{e}}\boldsymbol{E} = 0.$$

The use of these relations is described in detail below.

4.2.3 **The electrical double layer**

We saw in Chapter 1 that when a dielectric is immersed in an electrolyte, a surface charge often appears. We had presented the example of glass immersed in an aqueous solution that becomes negatively charged. As mentioned previously, the origin of this phenomenon comes from the fact that the silane terminals Si–O–H, located at the surface of the glass, become protonated in the presence of an aqueous solution. The electrical potential associated with these charges at a pH of 7 is on the order of −100 mV. Thus, it is appropriate to take into account the surface charges for the flow of an electrolyte or a buffer solution in a confined system. We will also see that due to the high surface-to-volume ratio, these charges play an important role in miniaturized systems[3].

When one isolated surface carrying an 'acquired' charge is immersed in an electrolyte, the mobile charges of the liquid organize themselves and form a double layer near the immersed surface, giving rise to a remarkable structure (Fig. 4.1).

The first layer is a molecular film of counter-ions, which are fixed at the level of the solid/liquid interface under the effect of attractive forces developed by the charged solid surface. This first layer is known as the 'Stern layer.' It is bonded to the solid by an electrostatic interaction. The second layer is not bonded to the crystalline network (ordered or disordered) of the solid: it is diffuse. The structure of this second layer results from a statistical equilibrium between thermal agitation (which tends to homogenize a charge distribution)

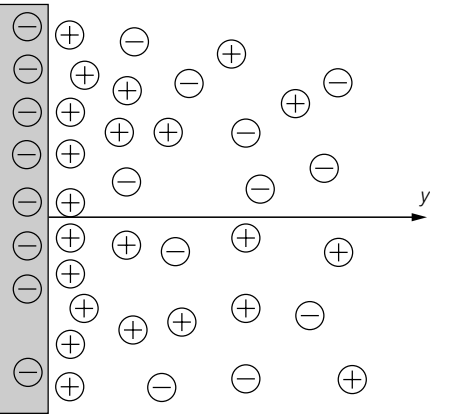

Figure 4.1 Structure of a Debye–Huckel double layer, formed from a molecular film bonded to the surface (called the Stern layer) and a diffuse layer where the ions, erratically fluctuating in the space due to thermal agitation, have an inhomogeneous distribution.

[3] Note that we have already mentioned in Chapter 1 the presence of surface charges for solids exposed to electrolytes. Here, we are interested in the experiments carried out by surface-force apparatuses, which revealed the structure of electrostatic forces in play. We are also interested in the hydrodynamic consequences of the presence of these charged layers.

and electrical forces (which tend to displace charges of the same sign towards the surface, thus breaking the homogeneity). The characteristics of this layer are obtained by using statistical physics, but one can also come to the same conclusions by manipulating the electrokinetic equations presented previously, completed by the Poisson equation. We consider an infinite slab, where z represents the co-ordinate normal to the plane. As the surface is isolated and in a stationary regime, and depends only on z, we deduce from equation (4.4):

$$J_z = 0.$$

We then project equation (4.3) on the axis z:

$$0 = \sigma E_z - D\frac{\mathrm{d}\rho_e}{\mathrm{d}z}.$$

We introduce the electrical potential Ψ defined by:

$$E_z = -\frac{\mathrm{d}\Psi}{\mathrm{d}z}.$$

We thus have the relation near constant:

$$\Psi = -\frac{D}{\sigma}\rho_e.$$

Furthermore, the Poisson equation for the electrostatic potential ψ is written:

$$\frac{\mathrm{d}^2\Psi}{\mathrm{d}z^2} = -\frac{\rho_e}{\epsilon},$$

where ϵ is the dielectric constant of the liquid medium. These equations lead us to:

$$\frac{\mathrm{d}^2\Psi}{\mathrm{d}z^2} - \frac{\sigma}{\epsilon D}\Psi = 0.$$

This equation is solved simply, noting that the potential of the surface at infinity is zero. We obtain as a solution:

$$\Psi(z) = \zeta \mathrm{e}^{-z/\lambda_D},$$

where ζ is the potential when $z = 0$, and λ_D is the Debye–Huckel length, defined by the relation:

$$\lambda_D = \sqrt{\frac{D\epsilon}{\sigma}}. \tag{4.6}$$

This is the characteristic length scale of the problem. The order of magnitude of this number is a few tens of nanometers for a solution of water and salt at 1 μM. In practice, it is difficult to obtain much higher Debye–Huckel lengths.

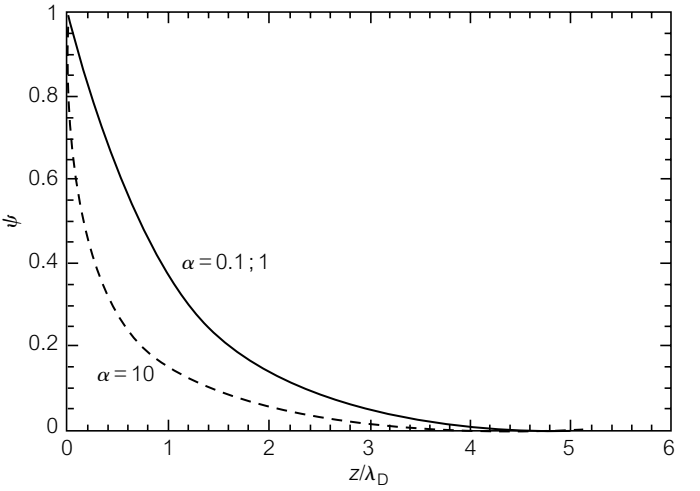

Figure 4.2 Profile of the electric potential Ψ in the Debye–Huckel double layer as a function of the coordinate z, which gives the distance to the surface. Beyond several Debye–Huckel lengths λ_D, the potential is constant, and thus the electric field created by the surface charge density is practically zero. There is thus a screening effect.

Reducing the electrical conductivity of the electrolyte is difficult because, for a solvent like water, the inevitable presence of dissolved ions gives rise to a substantial electrical conductivity[4]. The evolution of the potential Ψ is traced in Fig. 4.2: for a planar surface, the potential and the charge density become nearly zero once the distance to the surface is longer than one Debye–Huckel length.

What is the value of the potential ζ? It appears as a boundary condition of the problem. It is in fact the electrical potential *at the boundary of the Stern layer*. We gave in Chapter 1 the measurements of potential ζ with surface-force apparatuses. In terms of orders of magnitude, the typical values of potential ζ fall between -100 mV and $+100$ mV.

It is interesting to note that the potential ζ can be related to the surface charge density by a conservation relation:

$$\int_0^L \rho_e(z)\mathrm{d}z = -\sigma_e = -\frac{\sigma\zeta\lambda_D}{D}.$$

We thus deduce:

$$\zeta = \frac{\sigma_e D}{\sigma\lambda_D}.$$

[4] The Debye length is close to 1 μm in pure water; however, as just noticed, this value is difficult to achieve practically.

The surface charge σ_e is the sum of the charges frozen in the Stern layer and those appearing at the solid side of the interface the moment it is submerged in the electrolyte. However, it is difficult to estimate from the type of solid and the solution what the surface charge σ_e will be.

4.3 Electro-osmosis

4.3.1 Electro-osmosis produces plug flows in microsystems

Electro-osmotic flow (often called EOF) is a phenomenon produced in a fluid when an electric field is applied parallel to the surfaces in the presence of an established double layer. In such a situation, the double layer is moved by the effect of Coulomb forces, and it follows that the rest of the fluid is pulled with it. This occurs due to viscous forces, which, as reviewed in Chapter 2, transfer the quantity of movement from one layer to another. The word *electro-osmosis* is used to express the fact that the phenomenon of the electrical double layer, localized to the surface, exerts an influence or induces a synergy in all of the fluid.

In the context of the Stokes approximation, the movement of the fluid subjected to the electro-osmotic effect is governed by the following equation:

$$0 = -\nabla p + \mu \Delta \boldsymbol{u} + \rho_e \boldsymbol{E},$$

where p is the pressure, $\boldsymbol{u}$ is the velocity of the fluid, μ is the viscosity of the fluid, ρ_e is the electrical density of ionic charges, and $\boldsymbol{E}$ is the electric field. The density ρ_e is determined from the preceding paragraph. We consider here the case of a flow between two planes along the direction x, the length of which is developed from the double layers. In this context, the preceding equation simplifies and becomes:

$$0 = -\frac{\partial p}{\partial x} + \mu \frac{\partial^2 u}{\partial z^2} - \epsilon E_x \frac{\mathrm{d}^2 \Psi}{\mathrm{d}z^2},$$

where ψ represents, as in the preceding paragraph, the local electrostatic potential. An important situation must be considered: the case where the pressure gradient along the length of the canal is zero. Under these conditions, after integrating the preceding equation, we have:

$$u(z) = \frac{\epsilon E_x}{\mu}(\Psi - \zeta).$$

Within the Debye–Huckel layer, the potential Ψ is zero, and the velocity of the flow is expressed by:

$$u(z) = u_{\mathrm{p}} = -\frac{\epsilon\zeta}{\mu}E_x.$$

This velocity is called the Helmholtz–Smoluchowski velocity. It plays a very important role in electro-osmotic and electrophoretic phenomena. We see that the fluid is pulled at a constant rate outside the double layers, at a velocity precisely equal to u_{p}. Remarkably, at a fixed exterior field, this velocity is independent of scale: this property is very important for moving liquids around in ultraminiaturized systems. In typical situations where the double layer is very thin, we can consider that a plug flow was generated. We often introduce the notion of electro-osmotic mobility μ_{EOF}, which is defined by the expression:

$$u_{\mathrm{p}} = \mu_{\mathrm{EOF}}E_x.$$

Rearranging and substituting, we obtain:

$$\mu_{\mathrm{EOF}} = -\frac{\epsilon\zeta}{\mu}.$$

For a slab of glass immersed in water, the electro-osmotic mobility is positive. The flux will thus go in the direction of the electric field, that is, towards the negative electrode. The mixed case where a pressure gradient also exists $G = -\mathrm{d}p/\mathrm{d}x$ is solved in the same way. We tackle the following velocity field in the case where the flow exists between two parallel planes separated by a distance b:

$$u(z) = \frac{Gb^3}{8\mu}\left(1 - \left(\frac{2z}{b}\right)^2\right) + u_{\mathrm{p}}\left(1 - \frac{\Psi}{\zeta}\right).$$

In this case, the velocity profile is no longer a plug, but a superposition of a parabolic Poiseuille profile and a plug profile. We note that in these calculations, we assumed that the surfaces are ideally planar and that the charge densities are well defined. In practice, the control of the surface charges on a non-prepared surface can be difficult to the point that surface treatment is often necessary to control electro-osmotic flows. Otherwise, problems concerning charge stability at the surface arise. Certain materials, such as glass, are relatively stable. However, materials such as PDMS (polydimethylsiloxane—a material frequently used in microfluidics, as explained in Chapter 6), typically have mediocre stability as their charges evolve with time in a way that is difficult to control.

4.3.2 Electro-osmosis in nanocanals

A recent experiment performed by Jacobson *et al*. [10] allowed the access (albeit indirect) to a measurable quantity that is directly related to the thickness of the Debye–Huckel layer. This work consisted of circulating a weakly conducting electrolyte through a canal whose width varied between 98 nm and 10.4 μm. The fluid used was a solution of 0.20 to 15 mM sodium tetraborate, methanol 50% v/v, and water[5]. The thickness of the Debye layers varied between 21.5 nm (for the weakest concentration) and 0.78 nm. The measurement of the transport of rhodamine B, a neutral dye, permitted the comparison of theory and experiment. This comparison between the theoretical expression—established in the general case or the case of a Debye layer of a given thickness—and the experiment allowed the inference of an estimation of the thickness of the Debye layer. This indirect measure of thickness is only possible when operating under conditions where the Debye layer has a thickness comparable to the thickness of the width of the canal, which for typical concentrations implies the use of nanometric-sized canals. In the end, the comparison of these measurements with equation (4.6) lead to good agreement.

4.3.3 It is possible to introduce all types of flows by adjusting the surface density charge

Ajdari [11] showed that by adjusting surface charges, it is possible to produce all types of electro-osmotic flows: vortices, recirculating flows, etc. By concentrating more on the effect of asymmetry, an average amount of motion can be obtained, which gives rise to continuous pumping [12]. One example is the recirculating flow produced by a surface charge gradient showed in Fig. 4.3.

The surface is treated in such a way as to develop positive surface charges on one side and negative surface charges on the other. Due to the non-irrotational

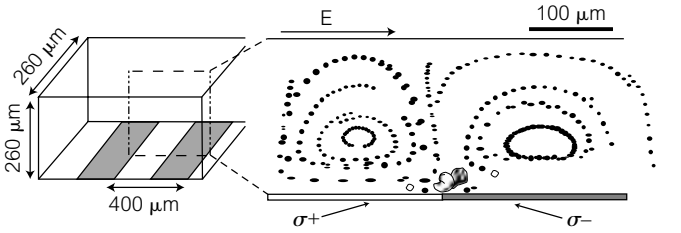

Figure 4.3 In this microsystem recirculating flow is produced by a heterogeneity of surface charge [13].

[5] % v/v denotes the concentration, in volume and percentage, of one liquid in another.

character of the forcing and also to mass conservation, rolls of fluid develop when in the presence of an electric field. These rolls can be used for pumping or for mixing. Several projects of this type have been carried out recently; we refer the reader to reference [14] for a review on this subject.

4.4 Electrophoresis

4.4.1 Mobility of a charged particle in an electrolyte

When a charged particle is immersed in an electrolyte, it can no longer be considered to be an isolated charge: in fact, this particle develops a local electric field and reorganizes mobile ions around itself. This behavior establishes a double layer, whose structure is analogous to the one that spontaneously forms near a charged surface (see Fig. 4.4). The thickness of this double layer is again the Debye–Huckel length:

$$\lambda_{\mathrm{D}} = \sqrt{\frac{D\epsilon}{\sigma}}.$$

As we have seen above, this length is roughly ten nanometers for an isolated particle immersed in an electrolyte. Two cases can be present: either the charged particle is larger than λ_{D} (in the case of cells or beads), or the particle is much smaller (in the case of ions). We examine here these two situations.

Case of small particles: 'Small' signifies a size small with respect to the Debye–Huckel length. In this case, we can consider the particle to be immersed in an insulating medium. Thus, the mobility for eqn (4.1) is:

$$\mu_{\mathrm{e}} = \frac{q}{6\pi R\mu}.$$

This situation corresponds to ions (Na^+, Ca^+, ...), small ionized proteins and small strands of DNA in solution.

Case of large particles: In this case, the particle is enclosed in the Debye–Huckel double layer, which is much thinner than the particle itself. It is rather like an atmosphere on a planet. We find ourselves in the electro-osmotic situation of the preceding section. By changing the frame of reference (we are now working here in the frame of reference of the resting fluid), the migration velocity of the particle is:

$$\mu_{\mathrm{e}} \sim \frac{\epsilon\zeta}{\mu}.$$

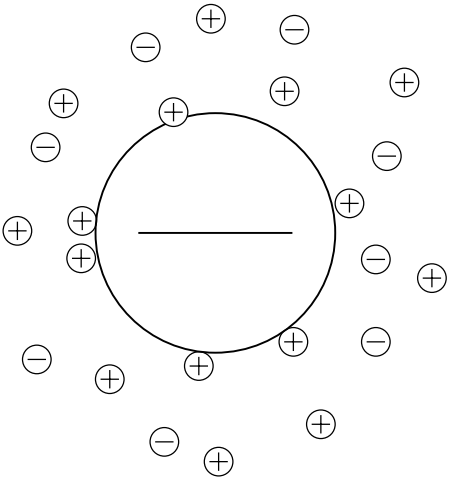

Figure 4.4 Negatively charged particle placed in an electrolyte. A diffuse layer forms around it with a thickness equal (by order of magnitude) to the Debye length; this layer tends to screen the electric field produced by the particle.

Here, the velocity is proportional to the potential ζ associated with the particle. The case of large molecules is rather complex and necessitates a separate analysis that we will not carry out here.

Electrophoresis is defined as the phenomenon of moving ions, particles, bacteria, macromolecules, or more generally, *charged* objects distributed in a solution in the presence of an imposed electric field. This displacement is made with a mobility μ_e that depends, as we have previously noted, on the characteristics of the charged object in question. Subjecting the sample to an electric field, we can thus obtain a separation effect on the charged components contained in a sample: this is electrophoretic separation. In a large number of situations, the Debye layer is larger than the size of the molecule, and the separation is made according to the value of the charge/size ratio. The case of DNA is particular: when subjected to a field, DNA stretches and acquires a mobility that only weakly depends on size. It is thus in theory difficult to separate fragments of DNA using differences in mobility. DNA separation systems use a gel to achieve separation on a subtle principle: basically, the small fragments explore the numerous parts of the gel and migrate more slowly along the matrix than fragments with a larger size. The mechanisms of DNA separation in gels briefly described here are described in more detail in the review of Viovy [15].

4.4.2 **Free solution capillary electrophoresis (FSCE)**

Free solution capillary electrophoresis (FSCE) is an electrophoretic separation technique of ions confined in a capillary, or (in the miniaturized version) in a microcanal (Fig. 4.5).

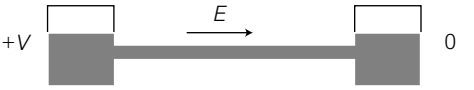

Figure 4.5 Capillary electrophoresis. Ions in the solution with the same electrophoretic mobility will migrate at the same velocity in the canal, forming a spot that can be detected at the exit of the canal.

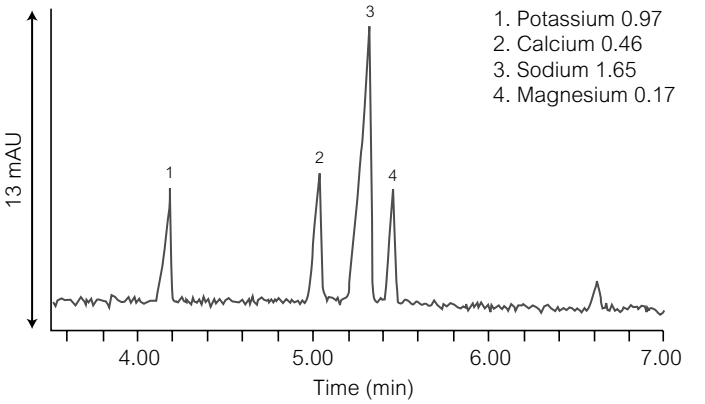

Figure 4.6 An example of the temporal reading obtained in an capillary electrophoretic separation system. Each peak corresponds to a particular molecule, identifiable based on its mobility relative to the others. Here, the ions of magnesium, sodium, potassium and calcium were identified [16].

An electric field is imposed along the capillary by two electrodes submerged in external reservoirs. The field has two effects: it induces an electro-osmotic flow that displaces the whole fluid at the same velocity, and it also separates charged particles that migrate at different velocites. Globally, in a typical capillary electrophoretic system, the electro-osmotic currents are sufficiently large so that the charged objects are all displaced from the left to right in the figure above, but at different velocites depending on their size/charge ratio. As a result, the objects will pass under the detector at different instants. A reading from the detector of capillary electrophoresis for a sample containing a collection of ions is shown in Fig. 4.6.

Each peak corresponds to the passing of a group of particles that had the same electrophoretic mobility. From the analysis of Fig. 4.6, we can deduce the migration velocities, and can then identify the different solutes present from associated information (for example, prior calibration). Figure 4.6 shows that the ions of magnesium, sodium, potassium and calcium were identified in this particular system.

Detection is more often based on fluorescence. This method of detection, which is very sensitive, requires that the biological molecules we want to separate are marked by a fluorescent marker. If we wish to separate simple inorganic

ions (like Na^+, Cl^-, etc.), the solution could be made to be fluorescent instead, and in this case we would detect the non-fluorescent molecules in a homogeneously fluorescent medium. This inversed situation is, however, less sensitive. Fluorescence is an important method in the domain of capillary electrophoresis in 'free solution,' but other methods are currently equally used: e.g. conductivity, absorption, etc.

Limitations

What are the limitations of FSCE? The first limitation is related to molecular diffusion: when the spot migrates along the canal, molecular diffusion acts to enlarge its size. The spreading of δX of the spot can be estimated by the following expression:

$$\delta X \sim \sqrt{Dt},$$

where D is the diffusion coefficient of the ions contained in the spot, and t is the time. The smallest band can thus be formed by its length:

$$W_{\min} \sim \sqrt{\frac{DL}{U_b}},$$

where L is the distance between the injection region and the detection region, and U_b is the velocity of the migration of the band. This velocity can be decomposed into two components:

$$U_b = U_{EOF} + U_{el},$$

where U_{EOF} is the electro-osmotic velocity and U_{el} is the electrophoretic migration velocity.

The number of theoretical plates $N(t)$ (a measure of efficiency) that this method can achieve can be determined by using the formula established in Chapter 3 (equation (3.14)):

$$N \sim \frac{UL}{D},$$

where U is the velocity of the transport of the bulk (that we relate to the EOF velocity), L is the capillary length, and D is the molecular diffusion coefficient (because here, there is no dispersion effect due to the presence of a divided medium, or of a Taylor–Aris-type phenomenon). We thus obtain:

$$N \approx \frac{\mu_{EOF} EL}{D} \approx \frac{q\Delta V}{k_B T},$$

where μ_{EOF} is electro-osmotic mobility, E is the electric field, ΔV is the applied potential difference along the column, q is an ionic charge, k_B is the Boltzmann constant and T is the temperature. Taking $q = 1$ e and $\Delta V = 6000$ V, we obtain:

$$N \approx 2 \times 10^5,$$

which is a very high number with respect to non-electrokinetic methods of separation.

The previous formula shows that in order to obtain thin spots and a large number of theoretical plates for separations, we must work with strong electric fields and long microcanals (which can obviously be difficult when systems are miniaturized). In traditional systems, the capillary is a silicon tube with a circular section, from 25 to 50 μm in diameter, and 20 or so cm long. In terms of orders of magnitude, the applied voltages in capillary electrophoresis are of several thousand volts. It is instructive to note that, in spite of its attractive aspects, FSCE was handicapped in the 1980s by the non-reproducibility of its surface states. This difficulty was eventually overcome, however; today, there are protocols for robust surface treatments, allowing for excellent surface charge stability.

With respect to non-electrophoretic systems exploited in divided media (gel, porous media, paper, etc.), capillary electrophoresis offers a gain in analysis time of about one order of magnitude: retention times are on the order of tens of minutes (instead of several hours). The origin of this increase comes from the fact that it is possible with FSCE to apply a significant electric field, leading to substantial migration velocities and short analysis times. Heating is caused by the passing of an electric field, and it is easier to drain the heat by the surfaces of a capillary with a small diameter, which is the case with FSCE systems in current use[6]. We will detail this argument later for miniaturized systems.

4.4.3 **Micellar capillary electrophoresis**

If capillary electrophoresis permits the separation of charged particles in the solution configuration (FSCE), neutral particles are simply displaced in a uniform manner and pulled by the electro-osmotic flow (EOF). There is an elegant method for separating these neutral particles: *micellar electrokinetic chromatography*) or MEKC (Fig. 4.7).

[6] In gel electrophoresis, Joule heating is more difficult to dissipate. Joule heating is induced by convection movements, which blur the separation; it is thus not possible in gel electrophoresis to apply an intense electric field, and the system is forced to operate under slow migration velocities. This important advantage had been proved by Jorgenson and Lukacs [1] in the 1980s. This subject is often emphasized in the literature.

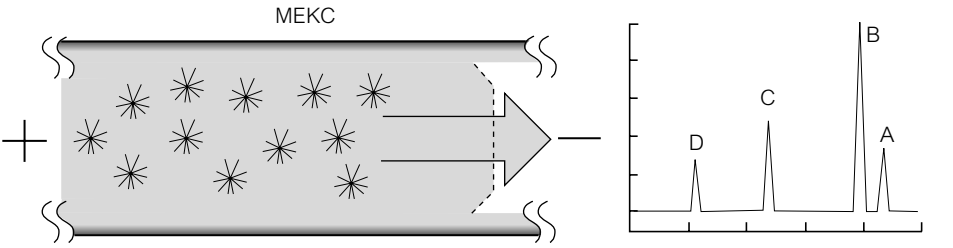

Figure 4.7 The stars in this figure represent micelles that capture particles or neutral molecules, and are transported by an EOF towards the electro-osmotic detector.

The principle of MEKC consists of introducing charged micelles into the system to be analysed, which these are obtained by adding a surfactant to the sample. An example of a commonly used surfactant in this case is SDS (sodium dodecyl sulfate). Under the CMC (see Chapter 3), micelles form spontaneously. In the case of SDS, micelles are negatively charged. These charged micelles tend to trap certain molecules as a function of the molecules' solubility: thus, solutes that are less soluble in water will be preferentially incorporated into the micelles. One example is that of hydrophobic molecules in solution in water. Incorporated into the micelle, the neutral particle finds itself at the border of a charged vehicle, and thus migrates with it under the effect of an electric field. Passing under the detector, the particle will emit a signal that permits its identification.

4.4.4 **Capillary electrochromatography**

This technique combines chromatography and capillary electrophoresis. One basic experimental set up of capillary electrochromatography (also known as CEC) consists of a capillary filled with a matrix (e.g. silicon particles) subjected to a longitudinal electric field. In this case, the ion sample placed at the head of the capillary will be able to be analysed, because the different ions will migrate along the canal at different velocities depending on their interactions with the matrix and their potential ζ (as previously noted, a quantity related to the charge and size of the ion). We see that by combining these different effects, we have at our disposal a powerful method of separation.

The principal role of the electric field is to ensure global displacement of the solution and of the solutes using the EOF. Compared to ordinary chromatography, even 'high-performance liquid chromatography' (HPLC) that uses a pressure gradient to move fluids, CEC considerably reduces the chromatographic band dispersion by eliminating Taylor dispersion caused by EOF. CEC leads to resolutions superior to ordinary chromatographic techniques. This characteristic is extremely valuable for the separation of DNA and proteins, and thus CEC

has seduced a considerable number of users in the biomedical world and is used in thousands of hospital centers and biological laboratories.

4.4.5 The miniaturization of electrophoretic systems of separation

4.4.5.1 The virtues of miniaturization

Why miniaturize separation systems like FSCE or CEC? There are several advantages:

- the ability to manipulate samples of very small volumes,
- integration possibilities,
- parallelization possibilities, allowing high-throughput analysis,
- much shorter analysis times, at set efficiency.

The first three advantages are applicable to miniaturization in general. The fourth advantage is justified in the following manner: we take the expression of the number of theoretical plates given in Section 4.2. We have:

$$N \sim \frac{\mu_{\mathrm{EOF}} EL}{D},$$

where μ_{EOF} is the electro-osmotic mobility, an intrinsic property at the solid/liquid interface. The formula shows that it is advantageous to work at elevated electric fields. The electric field strength is limited by Joule heating, due to the electric current crossing the solution containing ions we want to analyse. We have the following equality, by order of magnitude:

$$Q \sim \sigma_{\mathrm{e}} E^2 l^3 \sim \Delta T l,$$

where Q is the heat produced by the Joule effect in the microsystem, l is the characteristic scale of the system, and ΔT is the temperature difference between the microsystem and the exterior. From this equality, we obtain the following estimation for the maximal electric field that is possible to apply wihtout excessive heating, that is to say at a fixed ΔT:

$$E \sim l^{-1}.$$

Thus, miniaturization allows one to work at an elevated electric field. The reason for this comes from the fact that dissipation by the Joule effect towards the exterior is more easily achieved: a general property of miniaturized systems that was emphasized in Chapter 1. This scaling law leads to the following estimation

for the number of theoretical plates:

$$N \sim l^0.$$

Thus, the effectiveness of a chromatographic column is not affected by miniaturization. The retention time in the column is estimated by the relation:

$$t_r \sim L/U \sim l^2.$$

Time diminishes with the square of the size of the system, at a fixed efficiency. This is the key advantage of miniaturization of electrokinetic systems of separation: a huge reduction in the analysis time, coupled with significant efficiencies. Using the obtained scaling law, the drop in analysis time is of several orders of magnitude. To illustrate this point, we refer the reader to the work of Jacobson *et al*. [17], who managed to separate a sample of two components along a microcanal of 200 μm in a time of 800 μs. For the same type of separation, traditional gel-based methods would take several hours.

4.4.5.2 Capillary electrophoretic microsystems

As there are several advantages to miniaturizing, microtechnologies seized the opportunity to use capillary electrophoresis during the years 1991–1992 [18, 20]. This gave rise to an abundant body of literature, and a number of commercial achievements as well. The structure of microcanals widely used for sample injection is represented in Fig. 4.8.

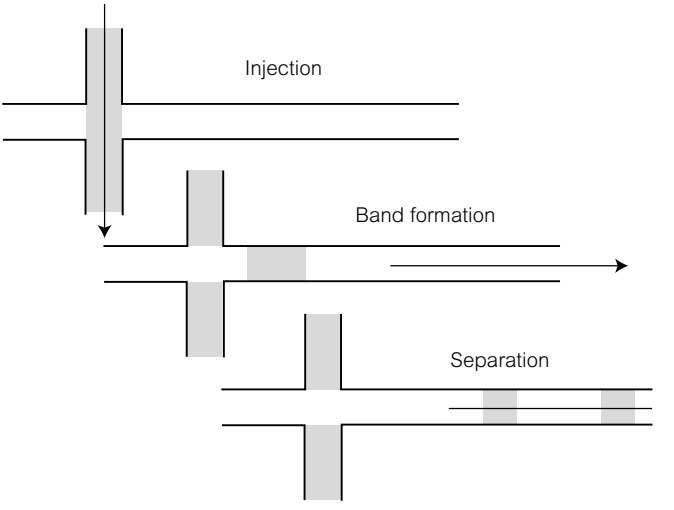

Figure 4.8 Injection method of a small-volume band in an on-chip capillary electrophoretic system.

The two lateral reservoirs contain the volume of the sample. This volume is displaced towards the principal canal by an electro-osmotic flow, applied between the two reservoirs. Once the sample reaches the principal canal, forming a well-defined plug, the applied electrical voltages are equilibrated along the injection canal. Then the principal canal is subjected to an electric field and capillary electrophoresis is put into use. Thus, the plug can split into different bands depending on the mobilities of the ions in the sample. In practice, this protocol necessitates a control of electrical voltages and hydrostatic pressures at the level of the four inlets (the injection canal and the separation canal).

One example of a commercial product of this system is made by Caliper Technologies Corp. [21] (Fig. 4.9). The system is etched in glass. Detection is made using fluorescence. The electric field is about 1 kV/cm and the length of the electrophoretic microcanal is a few millimeters; the obtained separation time is tens of seconds, with several thousand theoretical plates. There are appreciable advantages of this system over traditional systems. The idea of parallelization, which leads to high throughput, is illustrated in Fig. 4.10 [22]. This system enables the high-throughput analysis of DNA. Samples are placed in the 384 wells situated at the periphery of the system. An electric field is applied, leading to their migration and separation along the radial canals, which are filled with a gel. The detection system is based on fluoresence, confocality, and scanning, and allows for the detection of the bands. The number of theoretical plates has been evaluated to be 4×10^6 for this system, and complete analysis of 384 samples lasts for about 6 min.

To conclude, we mention that the miniaturized version of methods such as CEC [23] and MEKC [24, 25] have already been around for several years: the first devices were made in 1994 and 1995, respectively.

4.4.5.3 Capillary microelectrophoresis with entropic traps

A remarkable system[7] developed by the Craighead group [26, 27] is represented in Fig. 4.11.

The canal consists of a succession of 1 μm-wide cavities with thin 90-nm wide passages. A longitudinal electric field allows for the migration of ions. The principle of separation is based on entropic trapping: an ionized polymer reaches a cavity and adopts an equilibrium conformation in the shape of a ball. It must stretch itself out to penetrate and displace itself along the thin passages. There is thus an unfavorable change of conformation from an entropic point of view. As a result, the cavities behave as entropic traps. Intuitively, we see that the longer the molecule, the larger its radius of gyration, and the more

[7] But rather anecdotal in that it is currently not yet widely used in laboratories.

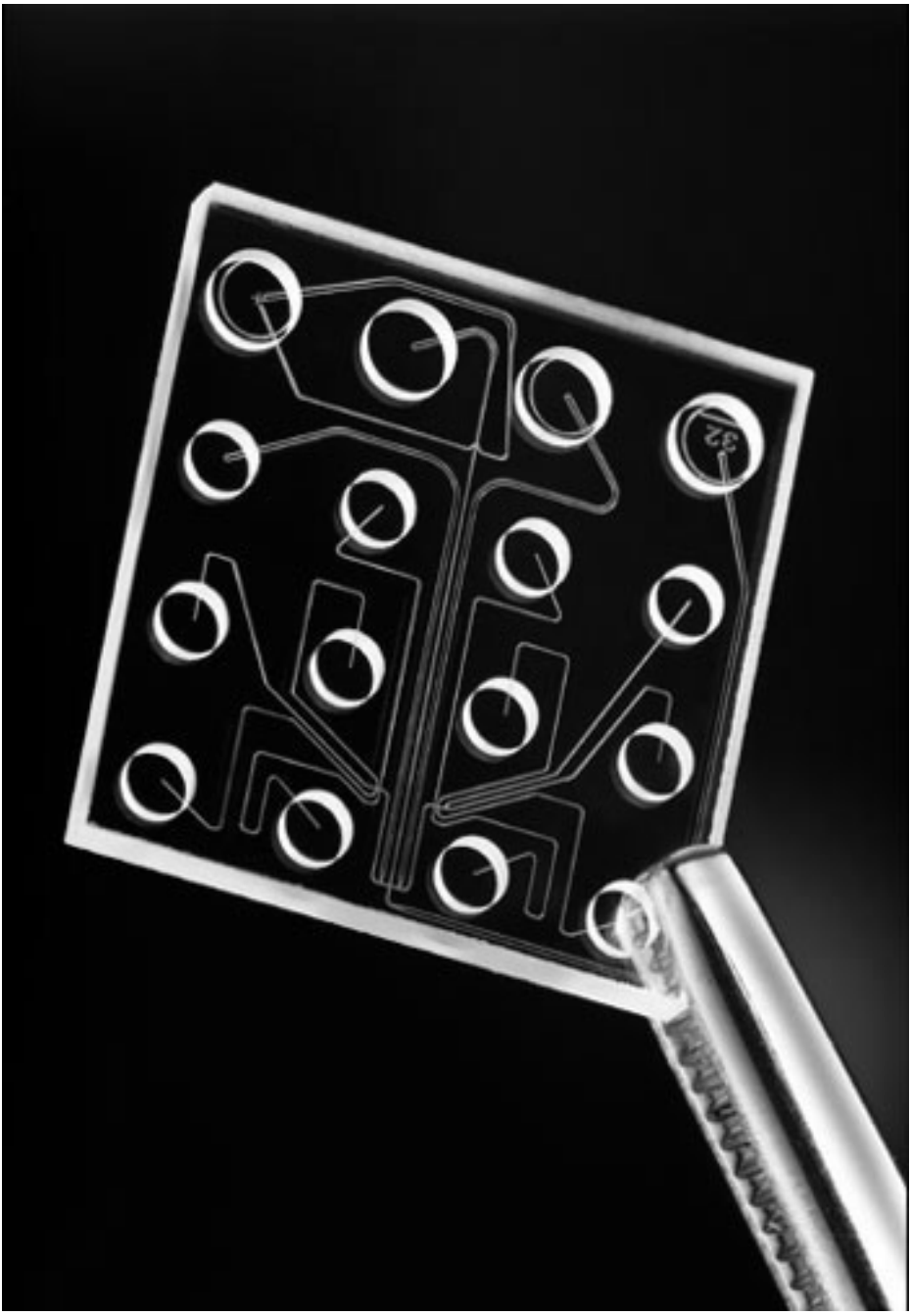

Figure 4.9 Chip that performs electrophoretic separation, commercialized by the company Caliper Technologies Corp. The microcanals are filled with a colored liquid for visualization.

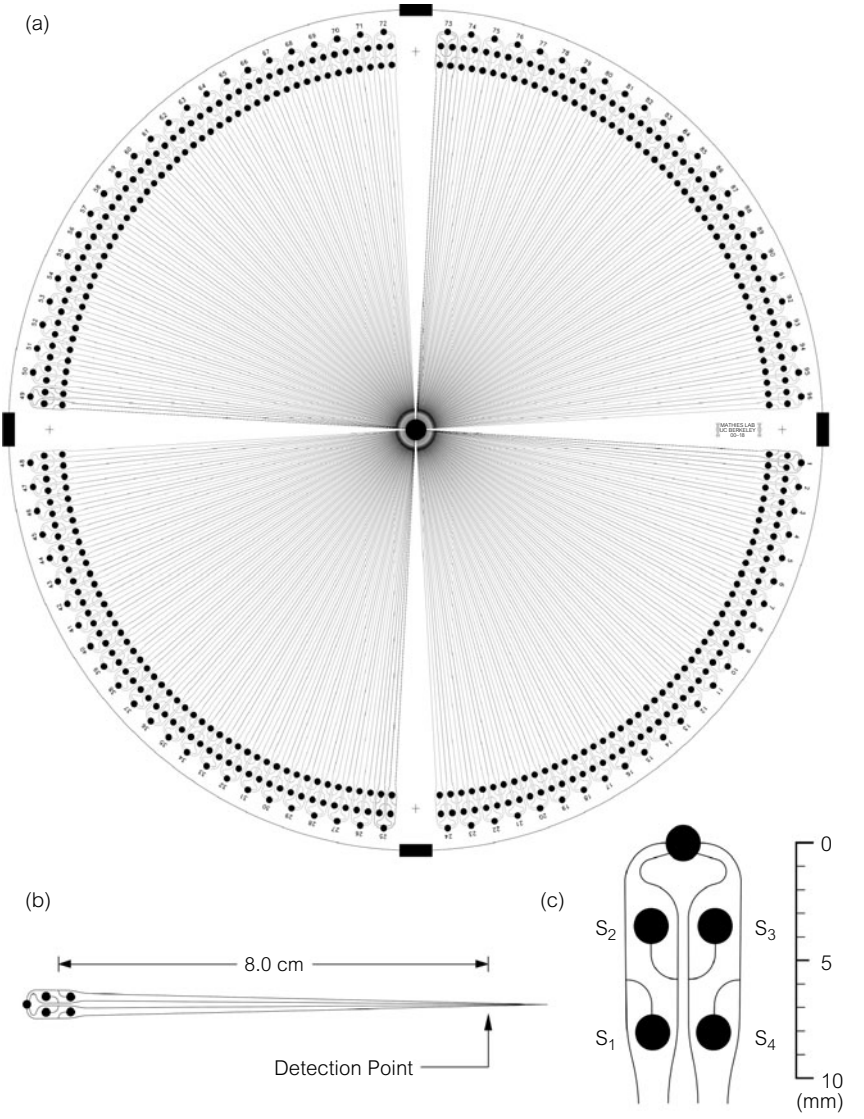

Figure 4.10 384-well system that analyses DNA samples in just a few minutes. a), b) and c) represent different views of the system.

Figure 4.11 Basis of this experiment of Craighead *et al*. (1999). DNA molecules migrate from left to right in a system consisting of 1-μm wide cavities and 90-nm wide restrictions. The molecule must lose entropy to get through these restrictions; this system is thus known as an 'entropic trap.'

easily it is trapped in the cavities. Thus, in such a system, we would expect that larger molecules would migrate more slowly than smaller ones. However, this experiment shows that in fact the converse is true: larger molecules move more quickly than smaller molecules! The reason is due to the effect of 'collision section efficiency': the larger molecules have a larger probability of displacing the smaller molecules from their cavities! Nevertheless, the fact remains that a separation effect still exists.

4.5 **Dielectrophoresis**

In the case where the particle is neutral, the previously calculated Coulomb force is zero. However, a force appears once the particle is immersed in an electrical field gradient. This force is called the dielectrophoretic force, a name proposed by Pohl [28]. The physical origin of this force is illustrated by Figs. 4.12 and 4.13.

We consider the case of a neutral particle placed in a vacuum. This particle encloses all charges of opposite signs, and the global charge is zero. A dielectric particle encloses dipoles that, in the absence of an exterior electric field, are oriented randomly in space. In the presence of an exterior electric field, as shown in Fig. 4.12, the dipoles orient themselves parallel to the lines of the field, and the particle acquires a non-zero dipole: i.e. the particle is now 'polarized' by a mechanism mentioned in Chapter 1 (though in a different context). If the field is non-uniform, a force will appear that is oriented in such a way that the particle

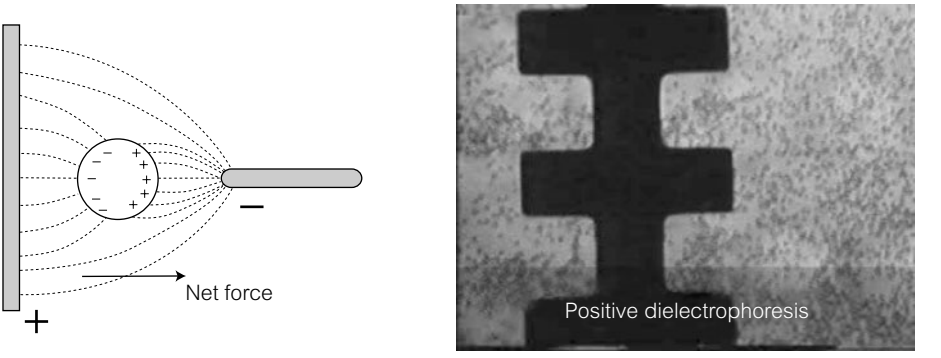

Figure 4.12 (Left) Schematic distribution of charges induced by a neutral particle submitted to an electric field in a vacuum. (Right) an experiment carried out in a microsystem showing that positive dielectrophoresis leads to an accumulation of particles in the regions where the field is at a maximum. Here, that maximum lies around the electrodes.

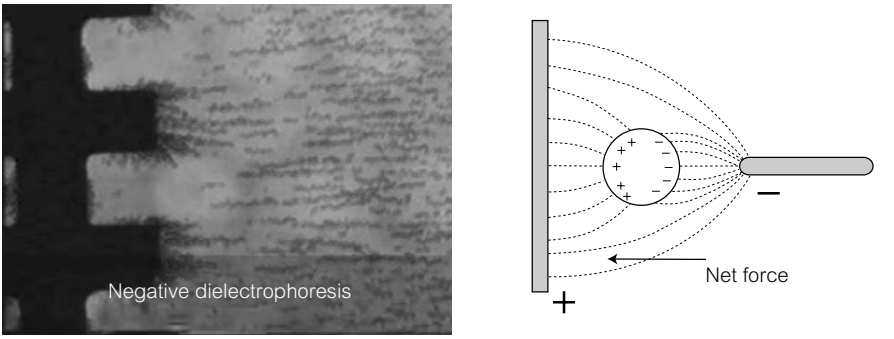

Figure 4.13 Schematic distribution of charges induced in a neutral particle that has been placed in an electric field in a solution that is more polarizable than the particle. Instead, there is an accumulation of particles far from the regions where the field is maximal.

will displace itself towards the maximum of field. This is positive dielectrophoresis. In the case where the particle is placed in a polarizable solvent, one can have the situation shown in Fig. 4.13, which leads to negative dielectrophoresis.

This situation is produced when the liquid is more polarizable than the particle. In this case, the dipoles localized in the fluid are the ones that will move the particle towards the minimum of the electric field. This principle is somewhat like the principle of Archimedes, only in this case the difference in polarizability is playing the role of the difference in densities.

One amazing consequence of dielectrophoresis is that the free particles in a solution tend to increase the maxima or minima of the electric field depending on the nature, i.e. positive or negative of the dielectrophoresis. The preceding figures show such phenomena (Fig. 4.13). This effect can be used to trap all sorts of objects, such as latex particles or biological cells. Whether dielectrophoresis is positive or negative, the force is independent of the direction of the applied electric field (we can convince ourselves of this by inversing the electric field in Figs. 4.12 and 4.13).

The expression of the force for a sphere immersed in a given fluid and subjected to a continuous electric field is:

$$F = \frac{1}{2}\alpha \nabla E^2,$$

where α is the polarizability. The sign of α can be positive or negative depending on the nature of the particle and its environment. When an alternating electric field with pulsation ω is applied, it is necessary to introduce the idea of complex dielectric permittivity, defined by:

$$\epsilon = \epsilon_{\mathrm{R}} - i\frac{\sigma}{\omega},$$

where σ is the electric conductivity. The force exerted on the dielectric particle is thus written:

$$F = 2\pi a^2 K \nabla E^2,$$

where K is the Clausius–Mosotti factor, which depends on the frequency and on the components of the complex dielectric constant. We have the following expression:

$$K = \mathrm{Re}(\epsilon_\mathrm{m})\mathrm{Re}\left(\frac{\epsilon_\mathrm{m} - \epsilon_\mathrm{p}}{\epsilon_\mathrm{m} + 2\epsilon_\mathrm{p}}\right).$$

Here, Re denotes the real part and the indices m and p denote the medium in which the particle is immersed and the particle itself, respectively. The amplitude and sign of K depend on the applied electric field. Alternating fields are more commonly used in microsystems than continuous ones so that it is easy to adjust the sign of the dielectrophoretic effect, and avoid the phenomena of electrophoretic demixing.

The neutral particle, subjected to a dielectrophoretic force, is moved through the fluid. Its movement is governed by the equation:

$$m\frac{\mathrm{d}\boldsymbol{V}}{\mathrm{d}t} \approx 0 = \boldsymbol{F}_\mathrm{DEP} - \boldsymbol{F}_\mathrm{Drag},$$

where m is the mass of the particle, $\boldsymbol{V}$ is its velocity, $\boldsymbol{F}_\mathrm{DEP}$ is the dielectrophoretic force, and $\boldsymbol{F}_\mathrm{Drag}$ is the drag force made by the fluid on the particle. We can immediately neglect inertial forces as in preceding sections. In practice, as for charged particles, this approximation is satisfied as precisely as the Stokes approximation in microsystems.

The viscous drag force is given by Stokes law, and is expressed:

$$\boldsymbol{F}_\mathrm{v} = 6\pi R\mu\boldsymbol{V},$$

where μ is the viscosity of the fluid and R is the radius of the particle. From the preceding equation, it is possible to obtain the relationship between the velocity of the particle and the different magnitudes characterizing the applied electric field and the fluid medium. Here, we consider the case where the applied electric field is sinusoidal with time. We obtain, after taking a time average:

$$\boldsymbol{V} = \frac{R^2\epsilon_\mathrm{m}\mathrm{Re}(K(\omega))\nabla E^2_\mathrm{rms}}{3\mu},$$

where E^2_rms represents the average quadratic value of the applied electric field. The velocity of the particle is deduced to be proportional to its area, and thus proportional to the square of the gradient of the electric field. To obtain substantial

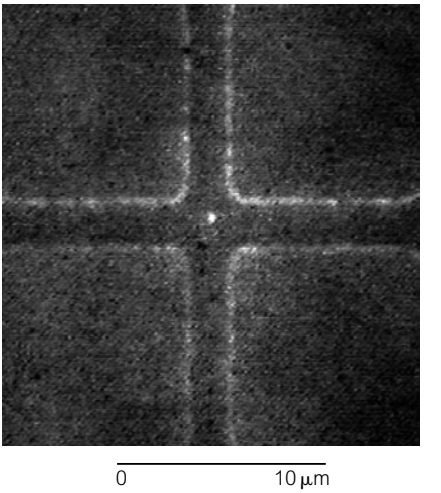

Figure 4.14 Dielectrophoretic trap localized between four electrodes, allowing a 93-nm particle to be trapped and immobilized. In the absence of an electric field, it is feverishly agitated in the fluid due to Brownian motion [4, 5, 30]. Photo printed with permission of H. Morgan and G. Green.

forces, it is important to miniaturize the electrodes in order to have large electric field gradients available. A typical dielectrophoretic device consists of evaporated electrodes[8], in canals of size less than 10's of micrometers.

One example of the use of dielectrophoretic forces is the trapping of particles. Figure 4.14 shows an example of a device where a 93-nm particle is trapped in a field produced by 4 electrodes [4, 5]. Here, the electrodes are constructed in such a way that the electric field has a pronounced maximum, thus consituting a trap of substantial width, and allowing the immobilization of even very Brownian particles. For more information on work done in the last few years on the subject of dielectrophoresis, see the reviews of [29], Ramos *et al.* [30] and the text of Jones, *Electromechanics of Particles* [31].

References

[1] J.W. Jorgenson, K.D. Lukacs, *Anal. Chem.*, **53**, 1298 (1981).

[2] S. Hertjen, *J. Chromatog.*, **347**, 191 (1985).

[3] E. Marchi, R.J. Pasacreta, 'Capillary electrophoresis in court: the landmark decision of The People of Tennessee versus Ware', *J. Cap. Electrop.*, **4**, 145 (1997).

[4] G. Green, H. Morgan, *J. Bioechem. Biophys. Methods*, **35**, 89 (1997).

[5] G. Green, H. Morgan, *J. Phys. Chem.*, **103**, 41 (1999).

[6] T. Muller, W.M. Arnold, T. Schnelle, R. Hagedorn, G. Fuhr, and U. Zimmermann, *Electrophoresis*, **14**, 764 (1993).

[8] These are made by depositing a metallic layer on a substrate using a plasma. Deposition techniques are discussed in Chapter 6.

[7] J. Deval, Y.K. Lee, P. Tabeling, C.M. Ho, *Proc. MEMS Conf.* (2001).

[8] A. Terray, J. Oakey, D. Marr, *Science*, **296**, 1843 (2002).

[9] H. Girault, *Electrochimie physique et analytique*, Polytechniques and Universitaires Romandes Presses.

[10] S. Jacobson, J. Alarie, J. Ramsey, *Proc.* μ *TAS*, 608 (2002).

[11] A. Ajdari, *Phys. Rev.*, **E53**, 4996 (1996).

[12] A. Ajdari, *Phys. Rev.*, **E61**, 45 (2000).

[13] A. Stroock, M. Weck, D. Chiu, P. Kenis, R. Ismagilov, G. Whitesides, *Phys. Rev. Lett.*, **84**, 3314 (2000).

[14] H.A. Stone, A.D. Stroock, A. Ajdari, *Ann. Rev. Fluid. Mech.*, to appear.

[15] J.L. Viovy, *Rev. Mod. Phys.*, **72**, 813 (2000).

[16] Y. Kazakevich, H. McNair, *Basic Liquid Chromatography*, *http://hplc.chem.shu.edu/NEW/HPLC_Book*.

[17] S. Jacobson, C. Culbertson, J. Daler, J. Ramsey, *Anal. Chem.*, **70**, 3476 (1998).

[18] A. Manz, D. Harrison, E. Verpoorte, J. Fettinger, A. Pausus, H. Ludi, H. Widmer, *J. Chromatogr.*, **593**, 253 (1992).

[19] D. Harrison, K. Fluri, K. Seiler, Z. Fan, C. Effenhauser, A. Manz, *Science*, **261**, 895 (1993).

[20] S. Jacobson, R. Hergenroder, L. Koutny, R. Warmack, J. Ramsey, *Anal. Chem.*, **66**, 1107 (1994).

[21] Refer to company website: www.caliper.com

[22] C. Emrich, H.. Tian, I. Medintz, R. Mathies, *Anal. Chem.*, **74**, 5076 (2002).

[23] S. Jacobson, R. Hergenroder, L. Koutny, J. Ramsey, *Anal. Chem.*, **66**, 2369 (1994).

[24] A. Moore, S. Jacobson, J. Ramsey, *Anal. Chem.*, **67**, 4184 (1995).

[25] F. Von Heeren, E. Verpoorte, A. Manz, W. Thormann, *Anal. Chem.*, **68**, 2044 (1996).

[26] J. Han, S.W. Turner, H.G. Craighead, *Phys. Rev. Lett.*, **83**, 8, 1688 (1999).

[27] S.W. Turner, A.M. Perez, A. Lopez, H.G. Craighead, *J. Vac. Sci. Technol. B*, **16**, 6, 3835 (1998).

[28] H.A. Pohl, *Dielectrophoresis: The Behavior of Neutral Matter in Nonuniform Electric Fields*, Cambridge University Press (1978).

[29] M. Washizu, T. Jones, *J. Electrostatic.*, **37**, 121 (1994).

[30] A. Ramos, H. Morgan, N. Green., A. Castellanos, *J. Phys. D: Appl. Phys.*, **31**, 2205 (1998).

[31] T. Jones, *Electromechanics of Particles*, Cambridge University Press, New York City, NY, (1995).

FIVE

Microfluidics and thermal transfers

5.1 Introduction

The preceding chapters have discussed the phenomena of thermal exchanges in microsystems. It was shown that miniaturization facilitates thermal exchange: the characteristic thermal diffusion times are shorter in miniaturized systems and the heat flux exchanges at a fixed temperature difference are larger (see Chapter 1). This property is advantageous for controlling exo- or endothermic chemical reactions, as well as for the implementation of biological processes requiring thermal cycling (one important example is PCR[1], for the amplification of DNA). On the other hand, it is difficult to impose a temperature difference in the middle of a microsystem. It is thus hard to conceive of microturbines with a high Carnot efficiency, or the measurement of chemical kinetics using the temperature jump, or T-jump technique[2].

In this chapter, the first question that we will investigate involves the foundation of the transport equation of ordinary heat used to calculate thermal fluxes in macrometric systems. Is this equation applicable to microsystems? Or is it necessary to resort to a different microscopic description of thermal exchange? We will see that the macroscopic approach can generally apply to microsystems, since their characteristic sizes are effectively much larger than the mean free path of particles or quasi-particles that allow for heat transport in fluids and solids. We will also see that despite the increase of the surface-to-volume ratio in

[1] PCR stands for 'polymerase chain reaction' and is a technique invented in the 1980s for the large-scale replication of DNA fragments. This technique is vital for the treatment of DNA samples, as the amplification of initial material facilitates analysis. Miniaturized systems have been shown to be capable of carrying out one amplification cycle in 10–20 s, which is an order of magnitude faster than traditional systems. This gain in time is due to the reduction of thermal inertia [1].

[2] The T-jump method consists of imposing an abrupt variation in local temperature in an equilibrated chemical system, and then measuring how long it takes for the system to return to equilibrium. This relaxation time gives information on the chemical kinetics of the system in question.

miniaturized sytems, the thermal resistance of the boundary (known as Kapitza resistance) can most often be neglected. The second question that we will examine regards the thermal phenomena induced by the flow of gas in a microcanal under conditions where the Knudsen number (introduced in Chapter 2) is no longer small. We will see that there are effects analogous to hydrodynamic slip at the surface: most notably, a discontinuity in temperature spontaneously appears. We will mention several consequences of this effect. Subsequently, we will consider the ordinary heat transport equation to be applicable. In this framework, we will study the matter of heating produced by a heat source in a microsystem and we will calculate in detail the characterstics of extremely simple heat exchangers. This section ends with a difficult problem: the issue of heat transfers in the presence of a phase transition (for example, a change of state from liquid to vapor). The liquid–vapor phase transition can be advantageous in conventional exchangers for two reasons: the transition absorbs energy, and it creates energetic movements of the liquid, which favors heat transfer. Researchers are currently examining how to exploit this phenomenon to improve the performances of microheat exchangers, but at this time, there is still very little knowledge on this subject. We will thus content ourselves to present a simplified introduction in the framework of this book. Finally, in the last section of this chapter, we will discuss the issue of how to cool the next generation of microprocessors. These microchips dispel more and more power densities, and this power must be dissipated with the aid of microheat exchangers. The industrial concern regarding this problem is considerable, and these systems are currently the focus of intense research in dozens of academic and industrial research teams.

5.2 Conduction of heat in gases, liquids, and solids

Heat-conduction phenomena were studied a great deal in the last century, and we will give an extremely brief history here. The reader can consult works such as that of Kittel [3] for a thorough presentation of the subject. For gases, the origin of thermal conduction stems from the random movement of molecules. The molecules, subjected to Brownian motion, transport and transfer thermal energy within the system. For systems with much larger mean free paths λ (which, as the reader may recall, is about a hundred nanometers at ambient temperature), kinetic theory gives the following expression for the thermal conductivitiy K of a gas:

$$K \approx \frac{1}{3}\rho C_{\mathrm{p}}\lambda u, \tag{5.1}$$

where ρ is the density of the gas, C_p is the heat capacity, and u is the agitation velocity of the gas molecules. This expression works well for perfect gases. For systems that are about the same size or smaller than the mean free path λ, some of the collisions will take place not between molecules, but between molecules and surfaces. In this case, the expression of thermal conductivity must be amended, and more generally, the hypotheses leading to the establishment of the macroscopic laws of heat transport must be re-examined. We will return later to this question.

For solids, it is necessary to distinguish between metals and insulators: for insulators, heat is transported by the internal modes of vibration in the crystal lattice [2]. These modes are quantized, and one can treat them as quasi-particles known as phonons (quasi indicates that they do not have an automonous existence independent of the crystal lattice that supports them). These quasi-particles undergo collisions between each other, producing an erratic agitation movement that resembles movement prevalant in ordinary gases. Just as for an ordinary gas, the mean free path λ_p can be defined. Practically speaking, λ_p ranges from 1 to 100 nm at ambient temperature. The table below gives some values of the mean free paths of phonons for quartz and an ionic crystal. The velocity of the phonons is equal to that of the propagation of sound.

Some values of λ_p and K_p for solids

Material	Temperature (°C)	λ_p(nm)	K_p (cal/cm °c s)
quartz	0	40	0.03
quartz	−190	540	0.12
NaCl	0	23	0.17
NaCl	−190	100	0.064

Applying the kinetic theory of gases, it is thus possible to estimate the thermal conductivity K_p for insulators of size greater than λ_p. We thus obtain:

$$K_p \approx \frac{1}{3}\rho C_{ph}\lambda_p u_p, \tag{5.2}$$

where C_{ph}, is the heat capacity of phonons, and u_p is the speed of sound. Some values of K_p are shown in the above Table[3]. This line of reasoning is only applicable for systems of sizes greater than λ_p. For systems smaller than λ_p, the calculation is more complicated, and would take us beyond the scope of this book. The study of systems of sizes smaller than λ_p is one of the topics of nanothermal phenomena, a field that has stimulated much research work.

[3] In the table, C_{ph} is estimated using the law of Dulong and Petit: this law approximates C_{ph} as $3R$, where R is the universal gas constant.

For pure metals, electrons are the principal carriers that transport heat. These electrons undergo collisions with phonons, and also contribute to the thermal exchanges in the system. Although they have tiny mass, electrons have significant agitation velocities, and the kinetic energy exchanged during electron–phonon collisions is actually greater than that exchanged during collisions between just phonons, which is why, they are the principal carriers of heat in metals. At ambient temperature, the mean free paths and agitation velocities involved in such a process are on the order of 100 nm and 10^3 km/s, respectively. Just as for insulators, the conduction of heat in these nanometric-sized metallic systems is currently an active area of research. Lastly, in the case of disordered solids (and thus for liquids as well), phonons and electrons are involved in the process of heat transport to a varying extent. In general, macroscopic theories are no longer valid at scales below 100 nm.

Today there are numerous experiments carried out in nanometric-sized systems that prove the deviations from macroscopic heat transport theory. One example is an experiment completed at Caltech, where the phenomena of thermal conduction were studied in a wire just a few nanometers in diameter (see Fig. 5.1). This type of work is examined in a recent review (Cahill *et al.* [2]).

Another aspect of miniaturized systems to take into account is the existence of thermal resistance at interfaces. The experiments of Kapitza [4] near the end of the 1930's showed that interfaces possess an intrinsic thermal resistance that is now known as the Kapitza resistance[4]; however, the physical description of such a resistance has not yet been established. We understand it as the result of an acoustic scattering of phonons as they traverse the two media [9], or of their diffuse reflection at the interface. A detailed description of these phenomena would take us far from the central subject of this book; however, a reader interested in learning more about these issues can consult reviews such as Swartz and Pohl [5]. Be that as it may, miniaturization makes phenomena at the interfaces more important, and one can ask if the Kapitza resistance ends up having a prominent role in heat transport for micrometric systems. The length scale that is naturally introduced in this problem is given by the expression:

$$l = \frac{K}{\sigma_{\mathrm{K}}},$$

where σ_{K} is the Kapitza conductance, and K is the ordinary thermal conductivity. This scale is interpreted as the thickness of a film with a Kapitza resistance equal to its own thermal resistance. In practice, at ambient temperature Kaptiza

[4] This discovery required manipulations at low temperatures, because at temperatures on the order of a few degrees Kelvin, the thermal resistance of materials becomes extremely weak compared to resistances due to interfaces. Moreover, Kapitza used superfluid helium, which has zero thermal resistance.

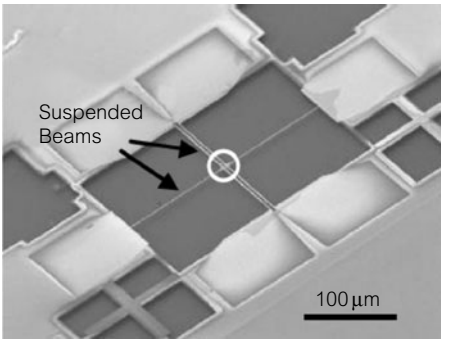

Figure 5.1 Calorimetry experiment on a 40-nm wide silicon wire. The wire was used to study deviations from Fourier's Law of heat conduction, which makes up a part of macroscopic heat transport theory. Reprinted with permission from Cahill *et al. Journal of Applied Physics,* **93**, 793(2003). Copyright 2003, American Institute of Physics.

conductivities are on the order of 10^8 W m^{-2} K^{-1}. Taking into account typical values of thermal conductivities of solids (on the order of 1 W K^{-1} m^{-1} for plastics and greater than 100 W m^{-1} K^{-1} for a semiconductor), one can conclude that for the Kapitza resistance to be significant, the system would have to be on the order of tens of nanometers. Therefore, this resistance can be neglected in mircosystems.

5.3 Gas flows at moderate Knudsen numbers

We have emphasized in the preceding section that for gases, the macroscopic laws of heat transport are not applicable once the mean free path of the fluid λ is smaller than the size of the system. We can introduce, as we did in Chapter 2, the Knudsen number *Kn* defined by:

$$Kn = \frac{\lambda}{l},$$

where l is the characteristic size of the system. Just as in Chapter 2, we find that it is possible to obtain deviations from macroscopic laws of heat transport when the Knudsen number has moderate values. For values of *Kn* roughly between 0 and 0.2, a thermal regime analogous to the slip regime appears. In such a regime, the equations of heat and of the quantity of macroscopic movement are still applicable; however, the boundary conditions acting on the velocity and on the temperature must be modified. The general expression of the boundary conditions in this particular context had been obtained by von Smolukowski in 1898 [12], and are the following:

$$u = \frac{2-\sigma}{\sigma}\lambda\frac{\partial u}{\partial z} + \frac{3}{4}\frac{\mu}{\rho T}\left(\frac{\partial T}{\partial x}\right) \quad \text{and} \quad T - T_{\mathrm{p}} = \frac{2-\sigma_{\mathrm{T}}}{\sigma_{\mathrm{T}}}\frac{2\gamma}{\gamma+1}\frac{\lambda}{Pr}\left(\frac{\partial T}{\partial z}\right), \tag{5.3}$$

where σ is the correction factor of the velocity at the surface, μ is the viscosity of the fluid, ρ is the density, σ_T is the correction factor of the temperature, γ is the ratio of specific heats, and $\mathrm{Pr} = \nu/\kappa$ (where ν is the kinematic viscosity of gases), a quantity known as the Prandtl number. In these relations, z is the co-ordinate normal to the surface, and x is oriented in the direction of flow. Two modifications appear in the boundary conditions with respect to isothermal systems (see Chapter 2).

– In the condition concerning velocity, a term known as the thermal ramp appears. This term indicates that a variation of temperature along the surface drives a flow in the direction of the gradient, i.e. towards higher temperatures. This effect points to the possibility of creating a thermal pump (known as a Knudsen pump) that would be devoid of any moving parts. However, practically speaking, a pump like this would only function at high Knudsen numbers.
– In the condition concerning temperature, a discontinuity appears. This discontinuity depends on the thermal correction factor σ_T, the analog of σ for the temperature. In reality, values of σ_T range between 0 and 1, depending on the nature of the gas/solid interface.

Calculations of thermal and hydrodynamic fields, including having the complete boundary conditions, are possible in simpler geometries. We will not carry out these calculations here, but the reader can refer to reference [8] for more. We indicate that in general, the discontinuity of temperature appears at the surface, which stems from the fact that a moderate Knudsen number tends to increase thermal fluxes between the fluid and the surface. At the present time, this type of situation has not been studied in detail experimentally.

5.4 Convection-diffusion heat equation and properties

5.4.1 Fourier's Law

We have placed ourselves here in the case where the mean free paths of the particles ensuring heat conduction (molecules, phonons, or electrons) are much smaller than the size of the system. In such a case, and for most physical systems that we will consider there, the local heat fluxes $\mathbf{q}$ are related to the temperature gradients ∇T by Fourier's Law, which is written:

$$\mathbf{q} = -K\nabla T, \tag{5.4}$$

where K is the thermal conductivity. The physical origin of this law is related to the diffusional nature of the heat transport process for gases, solids, and liquids, as underscored in the preceding section. The units of K are $\mathrm{W\,m^{-1}\,K^{-1}}$. An important quantity to introduce is the thermal diffusivity, denoted by κ, and defined as:

$$\kappa = \frac{K}{\rho c_{\mathrm{p}}}, \tag{5.5}$$

where ρ is the density of the gas and c_{p} is its specific heat. It is important to note that for perfect gases, all diffusivities (mass, thermal, or kinetic) are equal. A few values of K and κ for different gases, liquids, and solids are given in the table below:

System	K ($\mathrm{W\,m^{-1}\,K^{-1}}$)	κ ($\mathrm{m^2/s}$) $\times 10^{-6}$
water	0.6	0.14
silicon	150	80
glass	1.4	0.34
copper	401	113
aluminum	237	98
air	2.41×10^{-2}	22

5.4.2 **Convection-diffusion equation and boundary conditions**

The equation governing the internal energy of a flowing fluid is obtained using the first law of thermodynamics. The reader can refer to the work of Batchelor for a detailed derivation of this equation [6]. The equation for the internal energy is written:

$$\frac{De}{Dt} = \frac{\partial e}{\partial t} + \mathbf{u}\nabla e = -pdiv\mathbf{u} + \epsilon - \mathbf{divq} + \mathbf{s}(\mathbf{x},\mathbf{t}), \tag{5.6}$$

where $e(\mathbf{x},\mathbf{t})$ is the volumetric internal energy of the fluid, $\mathbf{x}$ is the position vector, t is the time, $u(\mathbf{x},\mathbf{t})$ is the local velocity, ϵ is the viscous dissipation, q is the conduction heat flux and $s(\mathbf{x},\mathbf{t})$ is a heat source or sink. In this equation, the term $-pdiv\mathbf{u}$ represents the work due to pressure forces. This equation is complicated, but it is considerably simplified in the important case of incompressible Newtonian fluids governed by Fourier's Law. Neglecting variations in thermal conductivity, the following equation is obtained:

$$\rho C_{\mathrm{p}} \frac{DT}{Dt} = \rho C_{\mathrm{p}} \left(\frac{\partial T}{\partial t} + \mathbf{u}\nabla T \right) = K\Delta T + \epsilon + s(\mathbf{x},\mathbf{t}), \tag{5.7}$$

where $T(\mathbf{x}, \mathbf{t})$ is the local temperature and ρ is the density of the fluid. Here, the expression of viscous dissipation is written:

$$\epsilon = \frac{\mu}{2}\left(\frac{\partial u_i}{\partial x_j} + \frac{\partial u_j}{\partial x_i}\right)^2,$$

where μ is the viscosity of the fluid. In this equation, the summation is systematically taken over the repeated indices. It is necessary to relate both the Navier–Stokes equation and the conservation of mass equation with the equation above. The Navier–Stokes equation incorporating Archimedes' principle is written:

$$\rho\frac{D\mathbf{u}}{\mathrm{d}t} = -\nabla p + \rho\mathbf{g} + \mu\Delta\mathbf{u}, \tag{5.8}$$

where $\mathbf{g}$ is gravity. Finally, the continuity equation is written:

$$div\mathbf{u} = 0.$$

Recall that eqns (5.7) and (5.8) assume that the density of the fluid is constant. We can investigate the validity of such an approximation in the case of non-isothermal flows: temperature variations in these flows will clearly induce density variations. This complication was discussed by Boussinesq in the nineteenth century. In the Boussinesq approximations, the density varies little with temperature and the equations remain unchanged from those for incompressible flows. In this framework, the density can be replaced by an average density, with the exception of the buoyancy term. In the majority of situations, the phenomena of thermal convection are handled this way. For the temperature boundary conditions, we saw that the macroscopic point of view is applicable once the size of the system exceeds about a hundred nanometers. In this situation, the thermal boundary conditions separating the two media 1 and 2 is written:

$$T_1 = T_2, \quad K_1\frac{\partial T}{\partial z} = K_2\frac{\partial T}{\partial z}, \tag{5.9}$$

where the indices 1 and 2 represent which medium the corresponding values refer to. Here we have expressed the continuity of temperature and of the thermal flux at the interface between media 1 and 2.

5.4.3 **The thermal exchange coefficient**

A very useful quantity to introduce in thermal problems is the thermal exchange coefficient, usually denoted by h. This coefficient is generally defined by the

following relation:

$$h = \frac{Q}{A\Delta T},$$

where Q is the thermal power passing through the system, over a surface of area A, under a temperature deviation ΔT. One example is a radiator functioning at fixed temperature heating up a room: in this case, the temperature difference is defined as the difference between the radiator and room temperatures, A is the area of the radiator and Q is the thermal power output. The units of the coefficient h are $\mathrm{W\,m^{-2}\,K^{-1}}$. It incorporates all the mechanisms (natural convection, forced convection, radiation, conduction) participating in the thermal exchange. The higher the h, the more the thermal output exchanged by the system (at fixed temperature) will be important. The table below, taken from reference [7], represents some orders of magnitude of h, useful for characterizing the performances of common systems.

Type of transfer	Fluid	h ($\mathrm{W\,m^{-2}\,K^{-1}}$)
natural convection	gas	5–30
	water	100–1000
forced convection	gas	10–300
	water	300–12 000
phase transition (water)	boiling	3000–60 000
	condensation	5000–110 000

5.4.4 Common orders of magnitude for thermal phenomena in monophasic microsystems

We now study situations in which the equations developed in the preceding section can be applied. These equations encompass a considerable variety of phenomena: natural convection, forced convection, heat diffusion, and heating due to the presence of heat sources. In the framework of miniaturized systems, this diversity can be reduced by exploiting the scaling laws presented in Chapter 1.

First, we showed in Chapter 1 that heat exchanged by conduction for a system of size l under influence of temperature difference ΔT is:

$$Q \sim Kl\Delta T, \tag{5.10}$$

where K is the thermal conductivity. In addition, the quantity of heat Q produced by a volumetric source (such as the one represented by the term $\mathbf{s}$ in

equation (5.6)), or lost by a sink, has the value:

$$Q \sim l^3.$$

Thus, heating produced by a source (or cooling produced by a sink) increases with the square of the size of the system. We will see using a detailed calculation that this scaling law applies well in the case of an exo- or endothermic chemical reaction taking place in a microcanal. Generally speaking, in microsystems, it is acceptable to neglect the contribution of volumetric sources and sinks. Internal heating of the fluid produced by its own viscosity (represented by the term ϵ in equation (5.7)) can generally also be neglected: in effect, ϵ being independent of the size of the system, the quantity of heat produced in a system of size l will be proportional to l^3, which is much smaller than the amount of heat transferred by conduction. Losses related to blackbody radiation (often important in macrometric-sized systems) can also be estimated: the radiation output is given by Stefan's law:

$$P = \sigma T^4 \times A$$

where σ is the Stefan–Boltzmann constant, T is the temperature of the microsystem, A is the emission area, and χ is the emissivity. The result is a term proportional to the square of the size of the system; it can thus be neglected with respect to the thermal output transferred by conduction that varies with the size l.

We now examine the phenomena of thermal convection: they are governed by the Navier–Stokes equation, completed by the buoyancy term (representing the force of Archimedes), that was discussed above (see equation (5.8)). The Archimedes force is:

$$F \sim \rho g \Delta T l^3,$$

where ρ is the density of the fluid and g is gravity. This force must be compared to viscous forces F_μ that are:

$$F_\mu \sim \mu u l \sim \mu l^2.$$

It thus can be seen that in a microsystem, the Archimedes forces are typically weaker than the viscous forces. This physically signifies that movement due to natural or forced convection is substantially damped by the effect of viscosity; we may therefore expect them to be weak. This remark may raise a concern over the efficiency of systems such as micro heat pipes, which aim to extract a heat flux by forcing convection inside a microcavity.

In equation (5.8), it would be tempting to neglect the inertial terms just as we had in preceding chapters. However, in microexchangers it is possible to

have moderate or even high Reynolds numbers (up to a few hundred). As we will see later, this condition is necessary to be able to extract substantial heat fluxes using a flow. We will thus keep the inertial terms in the equation to keep the following presentation as general as possible. Following this discussion, it is interesting to consider a situation where one can neglect the contribution of thermal sources and of viscous dissipation in the diffusion-convection equation, as well as the Archimedes principle in the Navier–Stokes equation. In this case, the two equations (5.6) and (5.8) can be written:

$$\frac{DT}{Dt} = \frac{\partial T}{\partial t} + \mathbf{u}\nabla T = \kappa \Delta T, \tag{5.11}$$

$$\rho \frac{D\mathbf{u}}{\mathrm{d}t} = -\nabla p + \mu \Delta \mathbf{u}. \tag{5.12}$$

The velocity field here is imposed independently of the temperature field. In contrast, the latter is not decoupled from the flow. In general, one can write:

$$Q = f(\kappa, U, l, \Delta T, \rho, c_\mathrm{p}).$$

We have here 7 variables and 4 dimensions. We can thus write this equation in the form:

$$\frac{Q}{\kappa \rho c_\mathrm{p} l \Delta T} = f\left(\frac{Ul}{\kappa}, \frac{c_\mathrm{p}\Delta T}{U^2}\right).$$

At small ΔT, we assume that the heat flux Q to be proportional to ΔT. The only way to reconcile this hypothesis with the preceding formula is to write the following approximation:

$$\frac{Q}{\kappa \rho c_\mathrm{p} l \Delta T} \approx f\left(\frac{Ul}{\kappa}\right),$$

which can be written in the form:

$$Nu = f(Pe_\mathrm{th}),$$

where Pe_th is the thermal Peclet number, defined by:

$$Pe_\mathrm{th} = \frac{Uw}{\kappa},$$

and Nu is the Nusselt number Nu defined by the expression:

$$Nu = \frac{Q}{lK\Delta T}.$$

The expression of the Nusselt number is also written using the exchange coefficient h introduced above:

$$Nu = \frac{hl}{K}.$$

The Nusselt number characterizes the efficiency of the exchanger. The higher the Nusselt number, the more thermal fluxes are exchanged at fixed ΔT. This dimensionless parameter allows the comparison of the performances of different exchangers.

How large is the thermal Peclet number? As the velocity varies with l, the thermal Peclet number varies as l^2: this suggests that it is small in microsystems, which might tempt us to neglect the role of flow in microsystems. This would lead us to the conclusion that it is pointless to use a flow in a microsystem to transport heat. This conclusion is, however, exaggerated, because in microexchangers it has been shown to be possible to extract heat using micrometric flows. These systems in fact operate at high thermal Peclet numbers, obtained with the implementation of flows on the order of a few m/s, which is much higher than those used in preceding chapters. Taking into account common values for thermal and kinematic diffusivities, we may note that a high Peclet number is most often associated with a moderately high Reynolds number. To get an idea of orders of magnitude, for a heat microexchanger with a typical size of 100 μm and with velocities on the order of m/s, the thermal Peclet number for water is on the order of 10^3 and under the same conditions, the Reynolds number is about one hundred. This value does not imply microexchangers are operating in the turbulent regime, as a Reynolds number on the order of several thousand would be necessary to have turbulence.

One may thus conclude that the thermal Peclet number and the Reynolds number cannot be generally considered small in microsystems dedicated to heat exchange. Such systems remain in the domain of laminar flows, but often evade the Stokes description (see Chapter 3). From a hydrodynamic standpoint, these characteristics reveal a major difference between the microheat exchangers and the lab-on-a-chips that we presented in preceding chapters.

5.5 Thermalization of a heat source in a microsystem

In the preceding section we neglected the contribution of volumetric heat sources in the heat diffusion-advection equation. The reason for doing this was based on

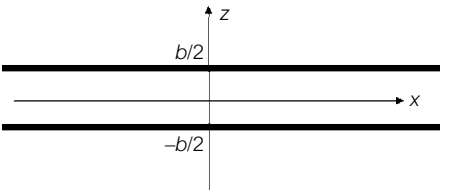

Figure 5.2 Geometry of the problem of a microcanal filled with a resting fluid, subjected to internal heating characterized by a source s_0.

a comparison between the scaling laws governing the conduction term and those associated with the volumetric heat source. We will make this argument clearer by completely calculating the temperature field induced by a permanent heat source that is confined in a microcanal where the fluid is at rest. We will consider a very simple geometry, where the system is bidimensional and unchanging along the direction of the canal. This problem can be seen as similar to that of the monitoring of exo- or endothermic chemical reactions taking place along the length of a microcanal. The geometry of the system is represented in Fig. 5.2.

We assume a stationary regime, and the simplicity of the geometry of the flow allows us to say that the temperature T only depends on z. Following these assumptions, the form of the equation governing the problem is thus:

$$0 = \kappa \frac{\partial^2 T}{\partial z^2} + s_0. \tag{5.13}$$

The thermal boundary conditions for surfaces maintained at fixed temperature T_p are:

$$z = \pm \frac{b}{2}, \quad T = T_\mathrm{p}. \tag{5.14}$$

After integrating, we find:

$$T(z) = T_\mathrm{p} + \frac{s_0}{\kappa}\left(\frac{b^2}{8} - \frac{z^2}{2}\right).$$

The maximum heating is situated at the center of the canal. The temperature difference ΔT_max between the center of the canal and the surface is given by:

$$\Delta T_\mathrm{max} = \frac{s_0 b^2}{8\kappa}. \tag{5.15}$$

Just as the scaling laws predicted, we thus have heating ΔT that increases with the square of the transverse dimension of the canal. We can thus expect a small increase (or decrease if s_0 is negative) of the temperature of the fluid. This signifies that these sources are easily maintained at constant temperature using simple thermal diffusion.

5.6 Heat transfers in the presence of flows in microsystems

5.6.1 The thermal boundary layer

The thermal boundary layer is an important concept in transfer problems with open geometries. A thermal boundary layer appears once a fluid flows along a surface maintained at a temperature different from that of the upstream fluid. A very simplified flow geometry is shown in Fig. 5.3, where we have implicitly assumed that the Prandtl number, defined by:

$$Pr = \frac{\nu}{\kappa}$$

is much smaller than 1. In this case, the hydrodynamic boundary layer developing along the plane is very thin, and the flow can be considered to be uniform[5].

We are thus considering here the problem of heating along an infinite slab maintained at fixed temperature T_p. The velocity field is assumed to be uniform, and far from the slab the fluid is at temperature T_0. Under these conditions, the temperature field $T(x, z)$ is given by the equation:

$$U\frac{\partial T}{\partial x} = \kappa\frac{\partial^2 T}{\partial z^2}, \tag{5.16}$$

where U is the velocity of the flow. The boundary conditions are:

$$x \geq 0, \quad z = 0, \quad T = T_\mathrm{p}; \qquad z \to \infty, \quad T = T_0. \tag{5.17}$$

Equation (5.16) is a diffusion equation; the solution is a Gaussian centered around $z = 0$ whose standard deviation represents the width δ of the boundary layer. This quantity is written:

$$\delta(x) = 2\sqrt{\frac{\kappa x}{U_0}}. \tag{5.18}$$

Thus, the thickness of the thermal boundary layer grows with the square root of the distance from the edge of the slab.

[5] This assumption will be justified at the end of the calculation: it will be possible to infer, once the characteristics of the laminar boundary layer are known, that the ratio of the thickness of the hydrodynamic boundary layer and the thermal boundary layer is on the order of the square root of the Prandtl number.

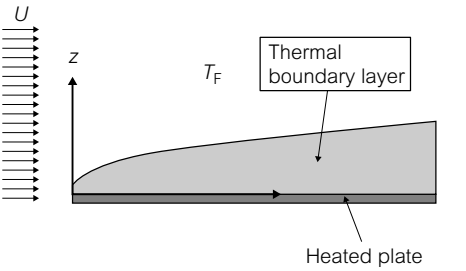

Figure 5.3 Thermal boundary layer for small Prandtl numbers (in this case, the flow can be considered uniform above the slab).

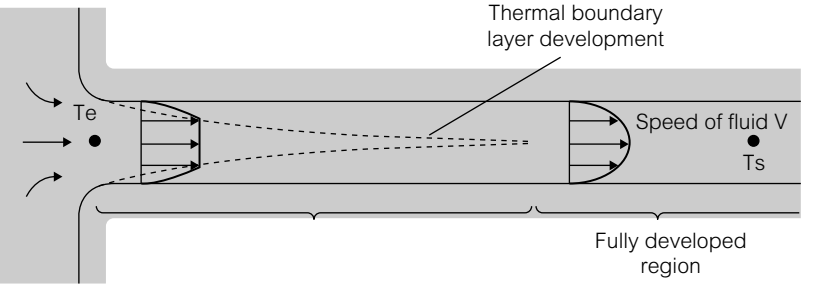

Figure 5.4 Length of the thermal entrance denoting the distance beyond which the temperature field 'forgets' its initial temperature.

5.6.2 **Thermal transfers in microcanals with flows**

5.6.2.1 Thermal entrance length for a microcanal

Consider the diagram in Fig. 5.4. Here we suppose that the walls of the canal are maintained at a uniform temperature T_p that is different from the temperature of the fluid, which is designated by T_f.

The fluid penetrating into the microcanal will gradually adopt the temperature of the walls of the canal. The thermal length L_e is defined as the distance beyond which the thermal boundary layer invades the width of the microcanal. Beyond L_e, the fluid penetrating the canal forgets its initial temperature. This length can be easily calculated from the expression for the thermal boundary layer given above. Assuming that the flow is uniform (which corresponds to the limit of small Prandtl numbers), and imposing the condition $\delta = b/2$, we express the invasion of the canal by the thermal boundary layers. We thus obtain the relation:

$$L_e \approx \frac{1}{16}\frac{Ub^2}{\kappa},$$

where U is the velocity of the vluid, κ is the thermal diffusivity, and b is the height of the canal. Another way to obtain the expression of the thermal length is to note that the temperature field has a temperature equal to $b^2/4\kappa$ to diffuse

over half the height of the canal. During this time, the field is transported by the flow a length of $Ub^2/4\kappa$. We thus again find the expression for L_e.

The thermal length L_e can be rewritten in the following form:

$$\frac{L_e}{b} \approx \frac{1}{16} Pe_{th},$$

where the thermal Peclet number again appears, and is defined for this particular geometry by the formula:

$$Pe_{th} = \frac{Ub}{\kappa}.$$

In practice L_e does not exceed ten times the width of the canal. Beyond this thermal entrance length, we enter into a region known as the fully developed region. In this case, the equations become simplified, and it is possible to solve the problem exactly. We will treat this problem in the following subsection.

5.6.2.2 The fully developed region

We consider the problem of the temperature field produced by a homogenous heat flux q_0 crossing the surface of a Poiseuille flow. The geometry of this problem is shown in Fig. 5.5.

The fluid is confined between two infinite planes separated by b, the direction of the flow is along x, and the corresponding Poiseuille profile is given by the expression:

$$U(x, z) = U_0(1 - 4z^2/b^2),$$

where U_0 is a characteristic velocity and z is the co-ordinate normal to the planes. The temperature field, assumed stationary, only depends on x and z. The energy equation (5.6) simplifies and reduces to:

$$U_0(1 - 4z^2/b^2)\frac{\partial T}{\partial x} = \kappa \frac{\partial^2 T}{\partial z^2}. \tag{5.19}$$

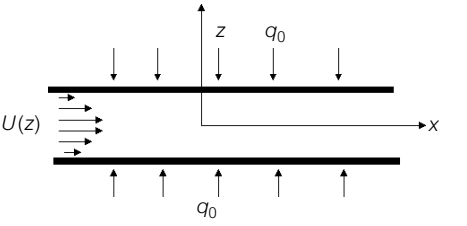

Figure 5.5 Geometry of the problem of a flow in the presence of a fixed thermal flux q_0.

The thermal boundary conditions at the walls $z = \pm\frac{b}{2}$ are given by the equations:

$$z = \pm\frac{b}{2}, \quad K\frac{\partial T}{\partial z} = \mp q_0, \tag{5.20}$$

where K is the thermal conductivity of the fluid and q_0 is the fixed thermal flux (see Fig. 5.5).

We now place ourselves far from the entrance to the canal in a region known as the thermally developed region, and we look for a general solution of the form:

$$T(x, z) = Ax + F(z),$$

where A and $F(z)$ are the values to be determined. The form of the solution we are seeking corresponds to a linear increase in temperature along the canal subjected to the thermal flux. The structure of the temperature profile in this solution is invariant along the canal. By identification, we find the following expression for the function $F(z)$:

$$F(z) = \frac{AU_0}{\kappa}\left(\frac{z^2}{2} - \frac{z^4}{3b^2}\right) + B,$$

where B is a constant. Then, considering the boundary conditions (5.20), we obtain the relations:

$$A = \frac{3q_0}{\rho C_\mathrm{p} b U_0}. \tag{5.21}$$

Now we only have to determine B. The difficulty in doing this is that the solution we will find corresponds to an asymptotic solution far from the entrance to the canal. However, it is not necessary to connect the entrance region to the fully devleoped region in order to completely solve this problem. To determine B, it is enough to use a relation of conservation of thermal flux. This relation is established by twice integrating (with respect to x and z) equation (5.19), and using (5.20). The conservation relation is written:

$$\rho C_\mathrm{p} \int_{-b/2}^{b/2} U(z) T(x, z) \mathrm{d}z = 2q_0. \tag{5.22}$$

After performing all the calculations, we find:

$$B = -\frac{39}{280}\frac{q_0 b}{k}.$$

The final solution of the problem is written:

$$T(x,z) = \frac{3q_0}{\rho C_p b U_0} x + \frac{3q_0 b}{2K}\left(\frac{z^2}{b^2} - \frac{2z^4}{3b^4}\right) - \frac{39}{280}\frac{q_0 b}{k}. \tag{5.23}$$

It is of interest to calculate a few global values. The temperature difference ΔT along the microcanal is equal to:[6]

$$\Delta T = \frac{3q_0}{\rho C_p b U_0} x. \tag{5.24}$$

It can also be seen that the exit temperature T_S is related to the inlet temperature by the relation:

$$T_S = \frac{3q_0}{\rho C_p b U_0} L + T_E. \tag{5.25}$$

The average temperature, defined by the relation:

$$T_b(x) = \frac{\int_{-b/2}^{b/2} U(z)T(z)\mathrm{d}z}{\int_{-b/2}^{b/2} U(z)\mathrm{d}z} \tag{5.26}$$

has the expression:

$$T_b(x) = \frac{3}{2}\frac{xq_0}{K}. \tag{5.27}$$

In conclusion, it is advantageous to calculate the exchange coefficient h of this system and its associated Nusselt number. For the problem being considered, we define the exchange coefficient between the wall and the fluid with the help of the following relation:

$$h = \frac{2q_0}{\Delta T}, \tag{5.28}$$

where ΔT is the temperature difference between the wall and the average temperature of the flow, which is defined above as $T_b(x)$. After carrying out all the calculations, we find the following result:

$$h = \frac{140K}{17b}. \tag{5.29}$$

The Nusselt number is calculated similarly, and we find the following result:

$$Nu = \frac{2bq_0}{K\Delta T} = \frac{140}{17}. \tag{5.30}$$

[6] This relation would have been directly obtainable by writing that $2q_0 wx$, the quantity of heat injected into the canal, is carried away by the flow. This quantity is thus equal to $2U_0/3wb\rho C_p \Delta T$.

This number is thus constant, showing that the more one miniaturizes, the smaller the temperature difference between the center of the microcanal and the walls. In other words, the exchange coefficient is inversely proportional to the size of the system. This characteristic will be exploited later in a section dedicated to the issue of cooling of microprocessors.

5.7 Evaporation and boiling

5.7.1 The phenomena of evaporation and boiling

The phenomena of evaporation and condensation take place, for liquids, in the presence of their vapor. At equilibrium, the liquid/gas interface is the site of continuous phenomena of condensation/evaporation at the microscopic scale. If the system is taken out of equilibrium (e.g. by heating the system or lowering the pressure), the liquid evaporates until it once again reaches thermodynamic equilibrium: this is the phenomenon of evaporation. It is useful to recall the Clausius–Clapeyron equation, which provides a relation between the temperatures and the corresponding vapor pressures:

$$LogP/P_s = \Delta H_{vap}/R * (1/T_s - 1/T) \tag{5.31}$$

where R is the universal gas constant, ΔH_{vap} is the heat of vaporization, T and T_s are two temperatures, and P, P_s are the corresponding vapor pressures.

The phenomenon of boiling implies the crossing of a liquid–vapor phase transition: one example is the microcanal of water crossing a system having a temperature greater than 100 °C. Boiling is indicated by the appearance of gas bubbles in the liquid, the result of a subtle process of nucleation. In all cases, the transformation of the liquid to gas is accompanied by an absorption of energy L_v (latent heat). The table below gives a few values of latent heat.

System	L_v (10^4 J kg^{-1})
water	100
silicon	150
glass	1.4

The appearance of gas bubbles in a liquid flow does not necessarily mean that it is boiling. We have seen in Chapter 2 that liquids can make bubbles appear

by the effect of dewetting, or by the expansion of gas bubbles already dissolved in the liquid. We now estimate useful orders of magnitude in the context of microsystems. Consider a vaporization front of size l, moving at a velocity u. For such a front, the amount of heat per unit time that is in play during the vaporization process is:

$$Q \sim \rho L_{\mathrm{v}} l^2 u,$$

where ρ is the density, L_{v} is the latent heat of vaporization, u is the typical velocity, and l is the scale. Q_v can be compared to the transfer of thermal output by conduction, estimated by equation (5.10). The dimensionless ratio between these two terms is given by:

$$S = \frac{\rho L_{\mathrm{v}} l u}{K \Delta T}. \tag{5.32}$$

Considering that u is proportional to the length scale l, we find that S is proportional to l^2, which suggests that the latent heat can be neglected in microsystems. This argument works well for small microsystems. For example, for a flow of water circulating at 1 cm/s in a system of 10 μm, operating under a temperature difference of 50 °C, and developing a liquid vapor front, this number would have a value of 10^{-1}. However, for microsystems several hundred micrometers large, S can achieve values much higher than 1. In the preceding case, we find that this number can reach almost 100 for a system 100 μm in size. Despite the favorable scaling laws, we thus cannot always neglect the contribution (or absorption) of energy related to the transformations of gas to liquid (or liquid to gas). The rough approximation that we have just made suggests that it is possible to use a liquid–vapor phase transition to extract a portion of the energy dissipated in 'large' microsystems.

5.7.2 Temperature field in a microcanal in the presence of a liquid–vapor transition front

The structure of flows carried by boiling along a heated canal has been studied extensively in macrometric systems. A review of these phenomena can be found in books such as the one by Hetsroni [10]. Simplifying the phenomenonolgy, we can say that the liquid begins by flowing in a temperature field increasing along the flow. The liquid ends by crossing a threshold of boiling, where a diphasic regime appears that carries both bubbles of vapor and liquid. Farther along in the flow, the continuously penetrating heat flux transforms an increasing amount of liquid into gas. Bubbles grow larger and larger and, and in the end they fling liquid up onto the walls, forming an annular regime. Finally, the liquid evaporates

completely, leaving in its place a monophasic gas flow. As long as there is a liquid/vapor interface, the heat carried by the flow is integrally used to transform the liquid into vapor, and the temperature of the flow remains constant. We thus see a plateau in the temperature forming along the canal. When the fluid is a pure liquid or a gas, the temperature of the fluid increases linearly along the flow, as indicated by the solution (5.23) obtained previously for a monophasic fluid flow in a canal that has a fixed heat flux passing through. For microsystems, we still do not have a very good idea of the succession of regimes appearing along a microcanal when it is taken above the boiling temperature of the working liquid. This subject is the goal of much current research. We will be satisfied here to explore the consequences of the appearance in a microcanal of a liquid–vapor front. We are inspired by the work of Peles *et al*. [11], who worked within a very simple framework: the problem is taken to just one dimension, which allowed them to prove several physical mechanisms and to introduce several important dimensionless numbers. When a liquid–vapor front appears in a microcanal, the flow regime adopts a structure like the one represented in Fig. 5.6.

Upstream of the front, the fluid is a liquid, and downstream of the front, the fluid is a gas. Assuming a one-dimensional system, the only contributing variable in the system is the x coordinate, oriented along the direction of flow. In this framework, the heat flux q_0 is replaced by a volumetric source s_0 that we will determine below. Taking the position of the front as the origin for our axes, the temperature $T(x)$ is governed by the equation:

$$U\frac{\mathrm{d}T}{\mathrm{d}x} = \kappa\frac{\mathrm{d}^2T}{\mathrm{d}x^2} + \frac{s_0}{\rho C_\mathrm{p}}, \tag{5.33}$$

where κ is the thermal diffusivity of the gas or of the liquid, and U is the velocity of the phase in consideration. The boundary conditions at the level of the front are:

$$x = 0, \quad K_\mathrm{L}\frac{\mathrm{d}T_\mathrm{L}}{\mathrm{d}x} = K_\mathrm{G}\frac{\mathrm{d}T_\mathrm{G}}{\mathrm{d}x} - \rho_\mathrm{L}L_\mathrm{v}U_\mathrm{L} \;\; \textit{and} \;\; T_\mathrm{L} = T_\mathrm{G} = T_\mathrm{S}, \tag{5.34}$$

where the indices L and G indicate the liquid or the gas, respectively, T_S is the vaporization temperature of the liquid at the pressure P_S of the front and ρ_L is

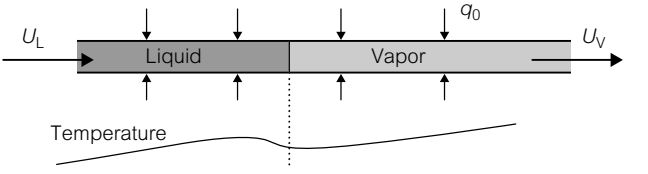

Figure 5.6 Liquid–vapor vaporization front in a flow of a microcanal, and the associated temperature profile plotted along the flow.

the density of the liquid. Taking into account the high ratio between liquid and gas thermal conductivities, one could envisage that it is possible to neglect the contribution from the gas conductivity, and write for $x = 0$:

$$x = 0, \quad K_{\mathrm{L}} \frac{\mathrm{d}T_{\mathrm{L}}}{\mathrm{d}x} \approx -\rho L_{\mathrm{v}} U_{\mathrm{L}} \ \textit{and} \ T_{\mathrm{L}} = T_{\mathrm{G}} = T_{\mathrm{S}}. \tag{5.35}$$

In the liquid, equation (5.33) associated with the condition imposing $T_{\mathrm{L}} = T_{\mathrm{S}}$ on the front, allows us to come up with the following solution[7]:

$$T_{\mathrm{L}}(x) = T_{\mathrm{S}} + \frac{s_0}{\rho C_{\mathrm{p}} U_{\mathrm{L}}} x + A \left(\exp \frac{xU}{\kappa} - 1 \right), \tag{5.36}$$

where A is a constant of integration. By comparison with the expression for the temperature field in a microcanal, in the fully developed regime (see equation (5.24)), the relation between s_0 (the volumetric source that must be introduced to treat this problem in one dimension) and the heat flux q_0 that is subjected to the flow can be written:

$$s_0 = 3 \frac{q_0}{b}.$$

Using the boundary conditions at the level of the front, the following relation is obtained:

$$K_{\mathrm{L}} \frac{s_0}{\rho C_{\mathrm{p}} U_{\mathrm{L}}} + A K_{\mathrm{L}} \frac{U_{\mathrm{L}}}{\kappa} = -\rho L_{\mathrm{v}} U_{\mathrm{L}}. \tag{5.37}$$

This allows us to determine the integration constant A:

$$A = -\frac{L_{\mathrm{v}}}{C_{\mathrm{p}}} - \frac{s_0 \kappa}{\rho C_{\mathrm{p}} U_{\mathrm{L}}^2}. \tag{5.38}$$

We can rewrite the solution (5.36) using the following dimensionless numbers:

- The Jakob number, defined by $Ja = L_{\mathrm{v}}/C_{\mathrm{p}} T_0$, where T_0 is a reference temperature (or temperature difference).
- The thermal Peclet number, defined by $Pe_{\mathrm{th}} = U_{\mathrm{L}} b/\kappa$
- a dimensionless number characterizing the heat flux that is subjected to flow, defined by

$$\theta = \frac{s_0 b}{\rho C_{\mathrm{p}} U_{\mathrm{L}} T_0}.$$

[7] The integration can be carried out assuming that the physical characteristics of the fluids are constant. This hypothesis can be made if the pressure variations in the flow are not too large.

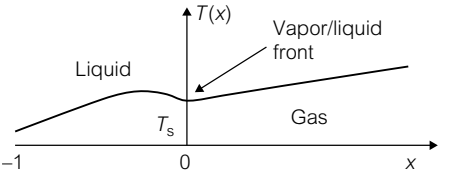

Figure 5.7 Temperature profile along a canal in the presence of a liquid–vapor vaporization front localized around $x = 0$. The solution is obtained using a one-dimensional model.

Using these dimensionless numbers, the solution (5.36) can be written:

$$T(x) = T_S + T_0(\theta x/b - (Ja + \theta/Pe_{th})(\exp(Pe_{th}x/b) - 1)). \tag{5.39}$$

The temperature profile has a curve shown in Fig. 5.7.

The temperature increases linearly with the coordinate x in the liquid. At the approach of the vaporization front, $T(x)$ ceases to grow linearly, but curves and decreases until it reaches the liquid–vapor equilibrium value T_S. This behavior is related to the absorption of latent heat at the level of the front, and to the specific conditions of thermal conduction induced by the presence of a liquid/gas interface. If T_S is the vaporization temperature of the liquid, the curve in Fig. 5.7 indicates that ahead of the front, there are regions where the liquid has a temperature higher than T_S. This is a metastable region, an important source of nucleation of new gas bubbles. We will not discuss this region's stability here. Using equation (5.39), it seems that the contribution of latent heat can be measured using the relation:

$$P = \frac{JaPe_{th}}{\theta} = \frac{\rho U_L^2 L_v}{s_0 \kappa} \tag{5.40}$$

How does one estimate such a quantity for microsystems? In terms of scaling laws, we have the following estimation[8]:

$$P \sim l^3.$$

This scaling law suggests that the contribution of the latent heat is very weak for microsystems. However, the dimensionless number P has a large range of values, roughly between 10^{-4} and 10^2. In practice, we find the same conclusion as the preceding section: heat absorbed during a liquid–vapor transition is weak (here compared to heat convection) in small microcanals; however, the amount of heat can become substantial for large microsystems, i.e. systems with a size of a few hundred or so micrometers. In conclusion, remember that when considering

[8] Just as in previous chapters, we assume here that the velocity U_L is proportional to the size of the system.

the complexity of these phenomena, using order of magnitudes provides useful guidelines, which can then be compared with experimental data.

5.8 Microexchangers for electronic components

5.8.1 The necessary miniaturization of cooling systems for the next generation of processors

Since the invention of the integrated circuit, the course of the integration of transistors onto the chips of microcomputers, or onto CPU units of servers, has proceeded with vigor. In 1971, the operating units of computers contained around 2000 transistors. Today, this number has been multiplied by 25 000, approaching 60 million transistors for the 3 GHz Pentium IV. In five years, the projected number of transistors hits a billion, operating at a frequency of 20 GHz. This increase in the density of transistors is accompanied by an increase in the number of commutations operated by the chip, and the amount of consumed power. It is obviously necessary to dissipate this heat for the transistors to function at a stable temperature between 80 and 95 °C. Figure 5.8 shows the evolution by years of the size of radiators coupled to microprocessors, which allow the functioning temperature of the chip to remain constant.

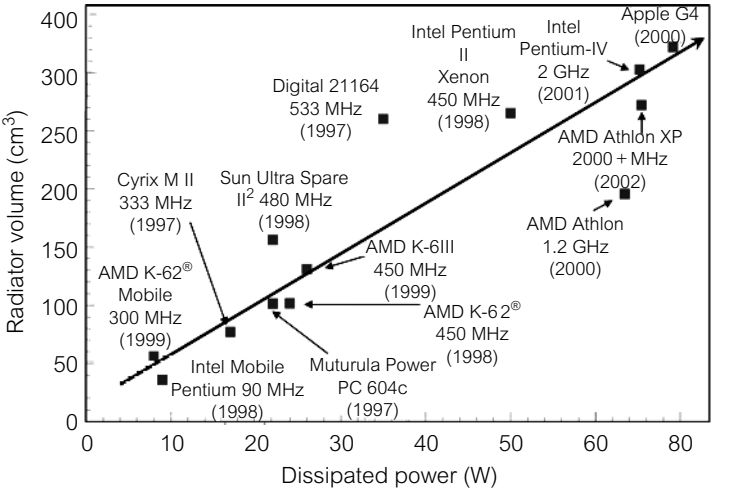

Figure 5.8 Temporal evolution of the size of radiators designed to maintain the temperature of microprocessors in the range between 80 and 95 °C. This curve emphasizes the existence of an inexorable evolution towards the production of high output.

The curve shows that the volumes of radiators increases linearly over time; one can conceive that this trend will pose long-term problems, in the conception, for example, of portable microcomputers. Currently, radiators are fabricated using an excellent heat conductor (copper), ventilated, or traversed by minicanals covered by liquid coolant. The pioneer work of Tuckerman and Pease [13] showed that the usage of microcanals placed directly on or in good thermal contact with the chip allows the extraction of the heat dissipated by the chip, with exchange coefficients much higher than those achieved by using traditional methods. This work had an important impact: it stimulated the activity of dozens of research teams. The analysis of these particular microexchangers, carried out in this chapter, will provide a new example of the virtues of miniaturization.

5.8.2 **Traditional method**

The method that prevailed until now consisted of dissipating the heat source produced in the electronic component by installing a radiator cooled by forced or natural convection (i.e. with or without a fan). The general layout is shown in Fig. 5.9.

The heat flux q extracted by such a system is given by the equation:

$$q = \frac{P}{A} = h\Delta T, \tag{5.41}$$

where h is the exchange coefficient characterizing the radiator, ΔT is the temperature difference between the component and the exterior, P is the power produced by the component, and A is the exchange surface. For a radiator cooled by natural convection of air, and a microprocessor functioning at 90 °C, the maximum value of q is on the order of 10^3 W m^{-2}. The exchange coefficients in this case are on the order of ten or so W m^{-2} K^{-1}. The usage of fans improves performance, increasing these coefficients by an order of magnitude.

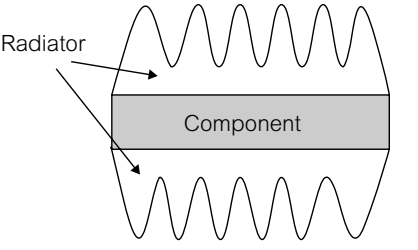

Figure 5.9 Structure of a traditional radiator, possessing cooling fins intended to increase the surface area of exchange with the cooling source.

5.8.3 Optimization of a microexchanger

The principal motivation leading to the replacement of a traditional system with a microexchanger was given in this chapter: effectively, for a microcanal, the thermal exchange coefficient h given by equation (5.29) increases when the width b decreases. By miniaturizing, higher exchange coefficients are favored. In terms of orders of magnitude, for a fluid like water in a microcanal 100 μm high, equation (5.29) gives values of h on the order of 10^5 W m^{-2} K^{-1}, which is many orders of magnitude higher than traditional systems[9]. The contribution of Tuckerman and Pease [13] demonstrated that such an advantage can be implemented experimentally.

A schematic view of a microexchanger etched in a substrate is given in Fig. 5.10.

This microexchanger consists of a canal of width b, total length L, crossing the substrate, and following a pattern forming a sort of accordion. The substrate produces thermal power P, and the heat flux acting on the microexchanger is thus (for very thin microcanals):

$$q = \frac{P}{wL},$$

where w is the width of the microcanal, and is assumed to be much larger than the height b. In the preceding section we calculated the temperature differences in the fluid in the transverse direction (ΔT_z) and the longitudinal direction (ΔT_x) as, respectively:

$$\Delta T_z = \frac{q_0 b}{2K} \quad \text{and} \quad \Delta T_x = \frac{3 q_0 L U_0}{\rho C_\mathrm{p} b}. \tag{5.42}$$

One increases with increasing thickness, the other decreases. An optimized microexchanger would be one in which the two values are equal, thus giving the condition on optimization (substituting in the thermal Peclet number):

$$Pe_\mathrm{th} = \frac{U_0 b}{\kappa} = \frac{L}{b}. \tag{5.43}$$

For an optimized microexchanger, the temperature difference between the fluid and the wall is comparable to the temperature difference between the inlet and the outlet. The exchange coefficient h, given by order of magnitude by K/b, can thus be used to evaluate the maximum heating *throughout* the fluid. It would be useful to decrease b, but it is still necessary to increase the power of the pump assuring circulation in the microexchanger occurs in such a way that the conditions for equation (5.43) are satisfied. The pressure difference is given

[9] Also see the table of exchange coefficients presented above.

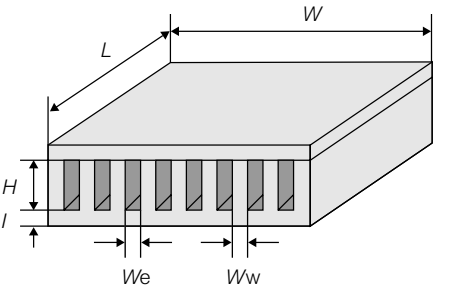

Figure 5.10 Diagram of a microexchanger forming a portion of a collection of parallel microcanals organized in such a way to form a sort of accordion. This structure is one option for the cooling of microprocessors.

by the expression (for very thin microcanals)

$$\Delta P = \frac{12\mu L U_0}{b^2}, \tag{5.44}$$

where μ is the viscosity of the fluid. At the fixed maximal ΔP, one can deduce that the thickness of the microcanal can not be reduced below a minimal value. Thus, the problem of the pump is critical. In the last several years, there has been much research seeking to replace traditional pumps with electroosmotic pumps in order to produce high ΔPs (on the order of several bars) [14]. These subjects are still currently a hot area of research.

5.9 **Conclusion**

This chapter is an introduction to the study of thermal phenomena taking place in microfluidic systems. Emphasis was given to the specific problem of cooling of microprocessors. Obviously, being able to control thermal phenomena is also an issue in miniaturized systems in the domains of biology and chemistry as well. However, in these cases, the situation appears simpler, because it is often a matter of heating a system in a controlled way, a situation where miniaturization is highly efficient. Extraction of heat fluxes rests on the ambivalent usage of the reduction of scale, and appears to be a more delicate problem. All of these issues are currently the subject of a great deal of research, and undoubtedly in the next several years, we will see that highly capable microexchangers will be a standard component in a large number of miniaturized systems.

References

[1] M.A. Northrup, M.T. Ching, R.M. White and R.T. Watson, *Proc. Transducers (IEEE), 93*, Yokohama, Japan, 924 (1993).

[2] D. Cahill, W. Ford, K. Goodson, G. Mahan, A. Marjumdar, H. Maris, R. Merlin, S. Philipot, *J. Appl. Phys.*, **93**, 2, 793 (2003).

[3] C. Kittel, *Introduction to Solid State Physics*, Wiley, New York (1953).

[4] P.L. Kaptiza, *J. Phys.* (Moscow), **4**, 181 (1941).

[5] E.T. Swarz, R.O. Pohl, *Rev. Mod. Phys.*, **61**, 605 (1989).

[6] G. Batchelor, *Introduction to Fluid Dynamics*, Cambridge University Press.

[7] J. Taine, J.P. Petit, 3rd edition, "Transferts Thermiques", Dunod, Paris (2003).

[8] *Microfluidique traité EGEM*, S. Colin (ed.), Hermès Science (2003).

[9] I.M. Khalatnikov, *Sov. Phys. JETP*, **22**, 687 (1952).

[10] G. Hestroni, *Handbook on Multiphase Flows*, Oxford University Press (1982).

[11] Y. Peles, L. Yarin, G. Hestroni, *Int. J. Multiphase Flows*, **27**, 577 (2001).

[12] M. Von Smoluchowski, *Annal. Phys. Chemie*, **64**, 101 (1898).

[13] D.B. Tuckerman, R.F. Pease, *IEEE Electron Device Lett.*, **EDL-2**, 5, 126 (1981).

[14] L. Jiang, J. Mikklsen, J. Koo, L. Zhang, D. Huber, S. Yao, A. Bari, P. Zhou, J. Santiago, T. Kenny, K.E. Goodson, Proceeding of Thermal Challenges in Next Generation Electronic Systems, THERMES 2002, Santa Fe, New Mexico, USA, 133 (2002).

SIX

An introduction to microfabrication

6.1 Introduction

In this chapter we introduce the most common techniques of microfabrication used in microfluidics today. The chapter is just an introduction, offering a simplified presentation of the implementation of these processes. The reader will note that in this chapter, we devote several pages to silicon technology. There are several reasons for this: first, the range of microfabrication possibilities available using this method is very large. Also, silicon microfabrication is often an unavoidable step in many other technologies. Finally, this technology is an immense resource of know-how, and expertise from which all alternative technologies can benefit.

In addition, soft technologies (based on plastics and polymers) are also described in this chapter, taking into account the large role they play today in the domain of microfluidics. This chapter does not intend to be exhaustive. The reader can refer to specialized literature, abundant for silicon technology and rapidly expanding for soft technologies, for more detailed information. We recommend in particular the text entitled *Fundamentals of Microfabrication* [1], or *Handbook of Microlithography, Micromachining and Microfabrication* [2].

6.2 Current situation of microtechnologies

6.2.1 Different scales and their associated fabrication techniques

Figure 6.1 gives different fabrication techniques according to the size of the given objects.

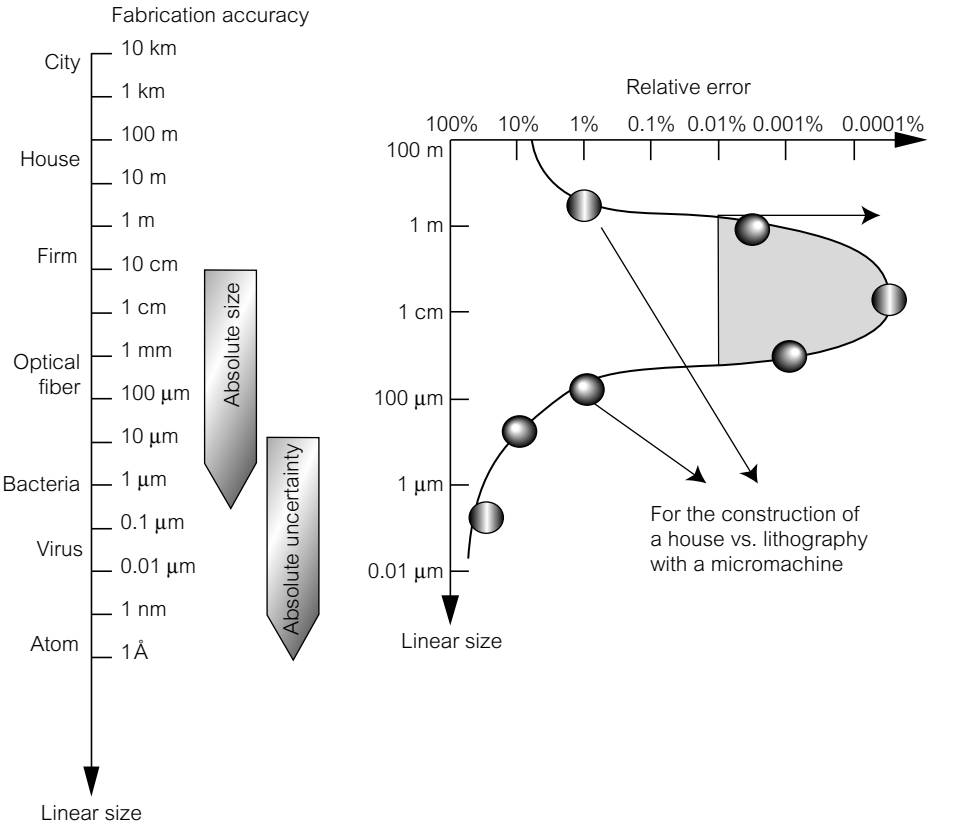

Figure 6.1 Absolute and relative precision of different fabrication techniques.

– Ordinary fabrication or machining techniques produce objects of a size between 1 mm and a few decimeters. We have entered the domain of traditional mechanical machining, whose precision is on the order of tens of µm. However, there are special machines that allow for the production of metallic objects with a precision of tens of nanometers. These machines represent a great technological achievement. One example, presented during the MEMS 2001 conference [3], is shown in Fig. 6.2a. The machine has five degrees of freedom ((3 in translation, 2 in axial rotation). Its displacement precision is of 1 nm, and its angular precision is of $(10^{-5})°$. Figure 6.2b shows an example of the use of such a machine: a micromask of Buddha, machined with nanometric precision.

The fact that these machines are dedicated solely to use on metals reveals a significant limitation: it is difficult, for example, to make use of an electric field under the conditions described in Chapter 4; nor is metal an appropriate material for analytical chemistry or biology, fields that prefer chemically inert

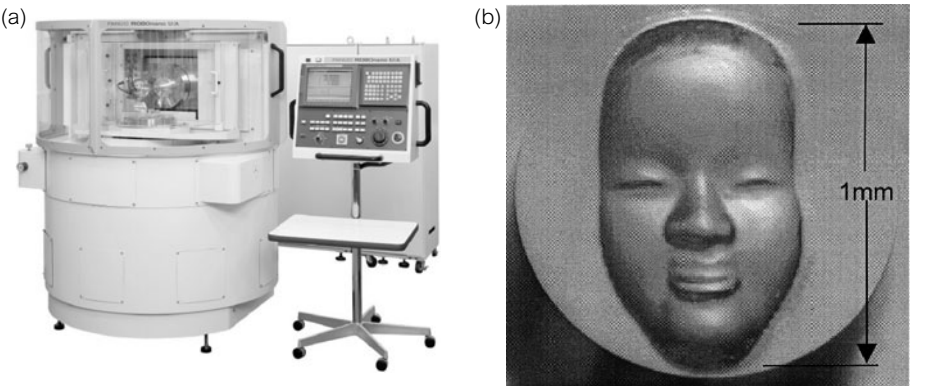

Figure 6.2 (a) Machine ROBOnano-Ui. It has 5 degrees of freedom (3 in translation, 2 in axial rotation). The displacement precision is of 1 nm, and its angular precision is of $(10^{-5})°$. (b) Mask fabricated by traditional machining, using the machine ROBOnano-Ui (photos by Pr Takenchi, University of Electro-Communications, Osaka).

materials such as teflon, glass, or plastic. In addition, these machines are obviously unable to make deposits or to perform surface treatments. They are thus not very useful considering they also have an extremely high price tag. It is thus necessary to appreciate these machines as great technological feats, the crowning achievement of traditional methods, but with unfortunately a very limited usage in practice.

– The domain of microfabrication involves scales such as a fraction of a micrometer and the millimeter. These technologies can be divided into two categories: silicon technologies and 'soft' technologies, which use materials like elastomers or plastics.
– Nanometric scales can currently be obtained using a variety of rapidly developing techniques. We know today how to isolate molecules and to use them to achieve a specific function. Nanomanipulation techniques constitute the base for the approach known as *bottom-up*, which consists of producing complex systems from molecular scaffolding. These molecular constructions, among other things, will be called upon to form the high-density microprocessors of tomorrow. We will not tackle this vast subject here, and will limit ourselves only to micrometric scales and the associated fabrication methods.

6.2.2 **Hard, plastic, and soft microtechnologies**

Figure 6.3 shows different types of microtechnologies currently used in microfluidics.

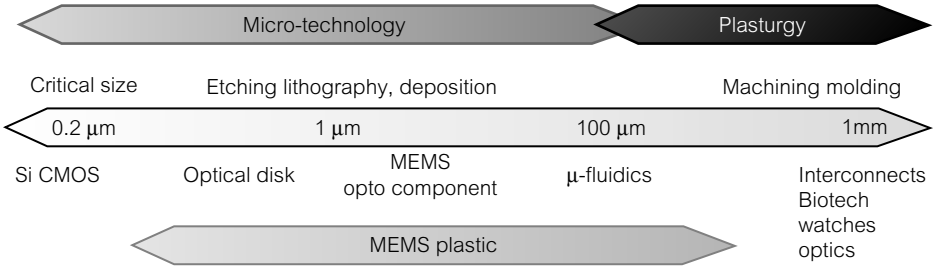

Figure 6.3 Differents types of microtechnologies.

– Technologies based on etching/lithography/deposition can be applied in the range of scales between 0.2 and 500 micrometers. These are the 'hard' technologies, because they use hard materials such as glass or silicon. The combination of etching, lithography, and deposition techniques makes it possible to obtain complex microfluidic devices that are open or closed, contain evaporated electrodes, and allow access to the exterior.
– 'Plastic MEMS' occupy a domain between 0.5 and 500 μm. These are the 'soft technologies' or 'plastic technologies'. As materials they use elastomers such as PDMS or plastic materials like PMMA (polymethylmethacrylate). Depending on the material, plastic MEMS are made using a direct method (for example, laser ablation) or by replication methods. The latter consists of the use of a mold before being fabricated elsewhere. Today there exists an abundance of techniques. Those that have achieved the largest industrial success are a result of the adaptation of well-mastered techniques from the field of plastics.

We note that while 'silicon' technology is mature, microfabrication technologies based on plastics and polymers have only appeared more recently and are still evolving. Plastic technologies are attractive from the standpoint of cost: by unit weight, current plastics are about 100 times less expensive than silicon. The question of price intervenes when it is necessary to produce a large number of miniaturized elements that may eventually be disposible, at a small cost. Soft technologies are also attractive because of the possibility of rapid prototyping. Some of them allow the development of a microfluidic circuit in just a few hours[1], while silicon technologies require times typically on the order of about one week. Other aspects (surface effects, transparency, diversity of materials, etc.) also contribute to the interest of using soft technologies. Microfluidics was considerably transformed by the appearance of plastic and soft technologies. These technologies accelerated the development of microfluidics by making microfabrication

[1] Beebe *et al*. [4] showed that it is possible to reduce these few hours to 5 min by using an *in situ* polymerization.

of microcanals more accessible. This situation is analogous to the role played by microcomputing in reference to computer science in the 1970s.

6.3 The environment of microfabrication

Microfabrication based on silicon is carried out in an extremely clean environment known as a clean room. Standard particles have a micrometric size, and tend to adsorb onto surfaces; considering the scales used in microfabrication, it is clear that it is difficult to carry out the series of procedures leading to the fabrication of a microfluidic system if the environment is dusty. What is a clean room? It is an environment that is temperature regulated (around 20 °C), humidity regulated, and permanently traversed by a flux of air. The air is filtered, allowing for the elimination of particles and gas that are inevitably introduced into the work space due to the human presence and chemical processes at work. The quality of the clean room is classified by the number of particles of a size less than 4 μm contained in a volume equal to a cubic inch[2]. Typical clean room classes for MEMS microfabrication are 1000 to 10 000. For microelectronics, the level of cleanliness of the room tends to be higher and thus class number of the room is reduced. In industry, it is no longer rare to find large rooms classed at 10 or 1 that are dedicated to fabrication of microprocessors that have low failure rates. For a class of 1000 to 10 000, it is necessary to wear specialized clothing, to cover hair, and to put on gloves and shoecovers to preserve the cleanliness of the room. These precautions are not necessary for rooms of higher classes (i.e. less 'clean').

6.4 Photolithography

6.4.1 Introduction

One process that plays a central role in microfabrication is photolithography. It consists of lighting through a mask[3], a photosensitive resist that has been deposited on a substrate. Since the work of Niepce—the inventor of photography—different types of energy sources have been used, giving rise to several families of lithography: X-ray, electron, and photon. There seems to be

[2] Recall that an inch equals 2.56 cm.

[3] We clarify that in the domain of microfabrication, use of the mask results in an object by protecting certain parts of a resist from the illumination of a chemical reactant. This term can sometimes lead to confusion.

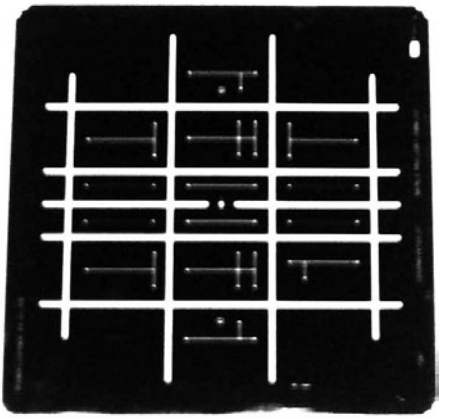

Figure 6.4 Mask for optical photolithography. The black areas correspond to metallic deposits made using electronic microscopy.

an obvious advantage to using small wavelengths, to achieve higher micromachining precision. However, in practice most of the main technologies are based on optical lithography, which exploits a spectral band between 300 and 450 nm. In this chapter we deal with this particular type of lithography, which for the moment is by far the most widespread[4].

6.4.2 **Photolithography masks**

Masks are generally plates of quartz on which deposits of chrome forming a pattern are made (Fig. 6.4).

It is obviously not possible to microfabricate an object with a geometric precision superior to that of the mask. Masks are thus often made using electron beams with a precision on the order of a fraction of a micrometer. This is essentially an electronic lithography technique that will not be described in detail here. If submicrometric precision is not required, other methods are used (based on a gel, or a high-quality printout on a transparency, etc.).

6.4.3 **Deposition of the photosensitive resist**

After making the mask, it is placed on top of a substrate covered by a photosensitive polymer; the substrate is then put under a uniform beam. In this way dark and light regions appear on the polymer, forming the same pattern that had been designed on the mask. This step is known as the 'transfer' step of the

[4] That is, with the exception of the fabrication of the masks themselves, which for silicon technology most often involves electronic lithography. We note that LIGA technology, based on X-rays, can be used to obtain devices of submicrometric lateral precision. This technology could eventually play an important role in the domain of microfluidics, considering its remarkable performance capabilities. However, at this time it still has only limited applications.

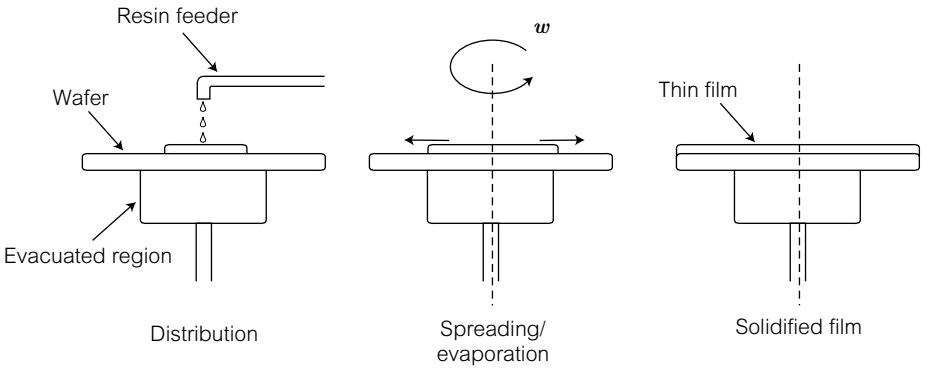

Figure 6.5 Deposition step of the resist on a spincoater (spin coating).

pattern. The photosensitive polymer is deposited in a thin layer on a solid substrate of silicon or glass. The deposit is made using a spincoater, as depicted in Fig. 6.5. This piece of equipment consists of a disk that turns at high velocities (typically between 1000 rpm and 10 000 rpm) and allows for the spreading of a drop of liquid initially deposited at the center of the disc. The thickness h of a film obtained in this way is uniform (to about several tens of nanometers); the following empirical expression accurately models the height:

$$h = kC\left(\frac{\mu}{\omega^2}\right)^{1/3},$$

where C is the initial concentration of polymers in solution, k is a constant, ω is the angular rotation velocity, and μ is the viscosity. An equilibrium thickness is achieved at long times; in practice this takes a few minutes. If the resist exhibited Newtownian behavior, the film would thin out progressively over time, and an equilibrium thickness would not exist. However, in the case of photosensitive resists, the flow behavior is characteristic of a non-Newtonian fluid. Notably, the viscosity of the fluid increases with time due to the evaporation of the solvent, which leads to pre-reticulation of the polymer[5]. At the end of the deposition process, the film no longer has a liquid structure, but is more like a glass. This leads to the notion of an equilibrium thickness, given by the preceding formula, whose justification (not provided here) is rather complex.

The typical film thickness to make dry or humid etching masks (defined below) for silicon is 2 μm. We will see that the precision of the pattern decreases

[5] The solvent evaporates rapidly because during spreading, the surface-to-volume ratio increases considerably, which favors the evaporation process. This effect can be considered as a sort of consequence of the reduction in scale of the deposition. This phenomenon was already mentioned in another context in Chapter 2. The evaporation of the solvent results in an increase in the resist concentration, which favors the activation of the polymerization process.

when the thickness of the mask increases, which is why thin deposits are favored. On the other hand, depositions cannot be too thin, because they are attached chemically by reactants in the chemical etching phases. These lead to a compromise of photosensitive polymers being deposited in thicknesses on the order of a micrometer to a few micrometers. Over the last few years, highly photosensitive polymers such as SU8 or AZ-series resists have been selected not to form molds, but to create structures on glass or silicon (for example, canals whose surfaces are made of a polymer material, or microgears made from resists). In this case, polymer layers several tens of micrometers thick are deposited. The difficulty here is not in spreading the layers, but, as we will see later, in assuring the homogeneity of the luminous flux during the exposure phase.

While the resist spreads on the substrate, the solvent evaporates, and the film ressembles a soft solid. However, once the step is over, the resist still typically consists of about 15% solvent. If this solvent is not removed, cracks or fissures appear once the film is completely reticulated. To completely eliminate the solvent, the resin is heated slightly (at 70 °C for a few minutes), before the exposure step.

6.4.4 **Exposure**

After performing a light rebake, the photosensitive polymer and its substrate are placed in an aligner whose precision is on the order of 5 μm. The film is thus exposed to a luminous flux produced by a source crossing the photolithographic mask. The source is most often a mercury vapor lamp that delivers substantial luminescent power (10 to 20 mW in strength), in wavelengths between 300 and 450 nm[6]. Basically, the luminous flux initiates physico-chemical reactions in the polymer, which modify the solubility in certain solvents. There are two types of resists, positive and negative.

– **Positive resist:** the light zones become soluble in a particular solvent, while other zones remain insoluble.
– **Negative resist:** the light zones become insoluble in a particular solvent, while the other zones can be dissolved in that same solvent.

Thus, for positive resists, insolation (radiation) across a photolithographic mask defines the zones that will, after development (that is, after immersion in a solvent), form holes in the resist film, leaving the other parts of the film permanently polymerized. We will return to the physico-chemical composition of the most commonly used resists. Physically speaking, the resist must be sufficiently

[6] *g*- and *i*-lines are used at 436 nm and 365 nm, respectively.

transparent to allow the illumination of the whole thickness of the deposited layer, and sufficiently sensitive to the light to induce chemical reactions. This delicate equilibrium limits the thickness of a large number of photosensitive resists. In this respect, the invention of SU8 by IBM several years constituted a small revolution in the field, as SU8 is a resist with high photosensitivity and can also be deposited in thick (tens of micrometers) layers. During the exposure (or insolation) step, several phenomena limit the precision of the definition of a pattern exposed on the resist. There is the half-light effect: as shown in Fig. 6.6, a parallel beam of finite size crossing a mask produces lit portions as well as portions left in the dark. However, some portions are in the half-light of the mask, and are thus subjected to a flux of an intermediate intensity between darkness and light. Another phenomenon limiting the precision of the transfer of a pattern from the photolithographic mask to the resist is diffraction. We do not present here the calculation that allows for the estimation of the limit of the corresponding precision. The important point is that at the level of the resist, the size of the zone δ in which diffraction phenomena are developed is not on the order of the wavelength of the light (as a single reasoning would conclude), but is much higher. The estimation of such a region is given by the following formula:

$$\delta \approx 3\sqrt{\lambda s},$$

where λ is the wavelength of the luminous flux (assumed to be monochromatic), and s is the thickness of the polymer film. This formula is obtained assuming that the distance between the photolithographic mask and the upper surface of

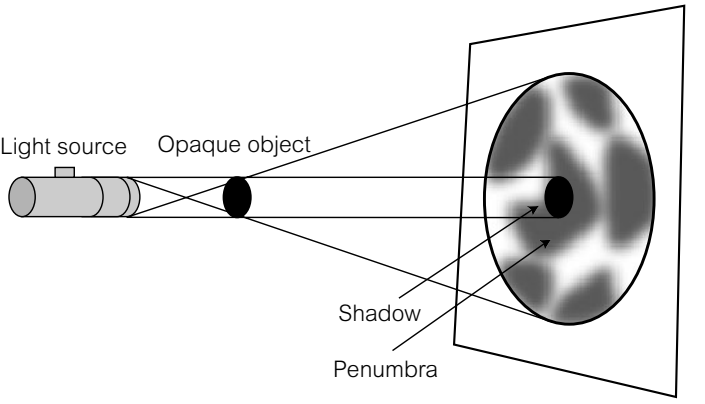

Figure 6.6 Half-light effect. There is a light zone and a dark zone, but between the two regions lies a half-light zone that tends to reduce the spatial resolution of patterns defined by the mask. The effect is essentially due to the finite size of the light source.

the resist is much higher than the wavelength[7]. Inserting typical values, the size δ calculated using the preceding formula is on the order of 3 μm. This steers researchers to work with resists of limited thicknesses and short wavelengths.

6.4.5 **Commonly used resists and the development step**

We now properly discuss resists. Resists used for photolithography must possess the following characteristics:

1. A large contrast between the solubilities of the exposed and unexposed parts.
2. High photosensitivity.
3. High resistance to certain classes of chemical agents.

The solutions used for photolithography are composed of a photosensitive resist, a solvent (that reduces the viscosity of the solution, allowing the spreading on a spincoater), and an additive (in order to control the kinetics of the photoreaction). For positive resists, the light breaks or weakens the internal bonds of the resist, and induces a rearrangement of the molecule to a more soluble form. For negative resists, the action of the light is to induce the formation of covalent bonds between principal or secondary chains, making them soluble by a process we will not describe here. Examples of 'positive' resists include PMMA(polymethylmethacrylate), DQN (a mix of diazoquinone with the resist phenoline novolak), and AZ. These resists are soluble in highly basic solutions such as KOH, TMAH, ketones and acetates. As an example we cite the negative resists KTFR (a polyisoprene elastomer produced by Kodak), and most importantly SU8, a fairly new resist that we have already mentioned above. SU8 can be used as a mold, but can also form structures with a high aspect ratio[8].

With regard to microfabrication, the choice between positive and negative resists is not trivial: negative resists adhere better to the substrate than positive resists, and tend to be more chemically resistant. However, the contrast of the photosolubility of negative resists is weaker than those of positive resists. These characteristics are all factors in the refinement of the microfabrication process. After the insolation step comes the development step. This step consists of immersing the system in a solvent. This step must be carried out at a carefully controlled temperature[8]. It is necessary to remember that the relevant processes during the development phase are physico-chemical, and thus in general have a

[7] Mask aligners generally have two positions: contact (the mask is in contact with the resist) and proximity (the mask is 10 μm above the resist). The second mode is more often favorable because the first carries the risk of the resist, which is still in a sticky state, adhering to the mask.

[8] The solvents used in this phase of development for resists have a xylene base.

high temperature dependence. Then, either the exposed part (for positive resists) or the unexposed part (for negative resists) is eliminated. The photolithographic process concludes by the final polymerization of the resist, incubating the system above the glass transition temperature typically for tens of minutes.

An example of a protocol for the fabrication of an SU8 mold

To clarify, I give here an example of a detailed protocol for the photolithographic fabrication of an SU8 mold. This mold will then be used to create structures in PDMS (discussed later).

Suppose that the resist, the optical aligner, spincoater, and a silicon or glass substrate are all available. The substrate must be cleaned and dried, which is achieved in two steps. The first step consists of immensing the wafer in acetone (to dissolve organic residue), in an ultrasound bath, and then drying. The second step consists of performing the same operation but with alcohol. The substrate must then be placed on a hotplate at 120 °C for 5 min for dehydration. It is necessary to have a substrate with no traces of contaminant whatsoever. Then the resist is spread on the wafer with a spincoater. The system is then heated to 65 °C for 60 s, then at 95 °C for 180 s, which serves both to eliminate the violent nature of the residual solvents and also as a first hardening step. It is after the exposure step that the baking step known as *post bake* (PBM) takes place. To encourage the progressive rearrangement of material during thermal deformation, heating is achieved in two steps: the wafer is heated to 65 °C for 60 s, and then to 95 °C for 120 s. The system is now ready for the development step. The system is dipped in a developing solution for 180 s. The SU8 is a negative resist, so the exposed motives stay, and the non-exposed motives are dissolved. The whole system is then rinsed with alcohol and dried with nitrogen gas. To finish the protocol and obtain a stable mold, the whole system is heated to 200 °C for 2 h.

6.5 Microfabrication methods for silicon and glass MEMS

6.5.1 Silicon as a micromachining material

6.5.1.1 The benefits of using silicon

The use of monocrystalline silicon is justified for the following reasons:

1. The ready availability of the material, and the considerable documentation of its properties.

2. The large number of well-established microfabrication processes, which allow for the fabrication of devices with greater than submicrometric precision.
3. Anisotropy advantageous for microfabrication.
4. The possibility of integration with electronic circuits.
5. Its physico-chemical characteristics are compatible with a large number of processes.

Germanium is not a viable alternative to silicon: in effect, germanium, the native dioxide GeO_2 is soluble in water, making it inconvenient for photolithography. Glass is a particularly favorable material for chemical and biological uses of microfluidic systems. The principles of silicon microfabrication that we present here can apply for the most part to glass as well.

6.5.1.2 Characteristics of silicon

Silicon is delivered in the form of wafers that constitute (almost) a monocrystal[9]. Silicon is produced by a well-controlled crystalline growth process carried out in a very clean environment (around class 1 or 10). The growth process, developed by Czochralski, consists of slowly pulling a crystal from an ultrapure bath of silicon while the whole ensemble rotates. A cylindrical crystal is obtained, from which slices hundreds of micrometers thick are cut. This is followed by the atomic polishing phase. All this leads to the fabrication of a wafer, quasi-atomically smooth on the polished surface, whose crystallographic orientation is identified by two planes.

From a crystallographic point of view, silicon is a cubic crystal, whose structure is the same as that of diamond (Fig. 6.7).

We recognize two cubic networks with overlapping centers, resulting in a two interpenetrating face-centered cubic structure. The side of one cubic face is 5.43 Å. Each tetravalent silicon atom belonging to a given network is at the center of a tetrahedron, whose points are made of atoms of the partner network, as shown in Fig. 6.7. The highest-density planes are the (111) planes, which form an angle of 54.74° with respect to the (100) planes[10]. We will later see that these planes play an important role in the wet-etching process. The table below characterizes certain mechanical, electrical, and thermal properties of silicon. One remarkable fact is the practically perfect elastic behavior of the material in the range of stretching between 0 and 2×10^{-3}. This property is important for making resonators with a high quality factor (see Chapter 2). Note that the higher values currently obtained for such a factor are on the order of 10^8.

[9] The word 'almost' signifies that there are defects; it is interesting to note that the density of defects is lower for silicon wafers oriented along the direction (111).

[10] Examining the elementary cell, this angle is seen to be arctan $\sqrt{2}$.

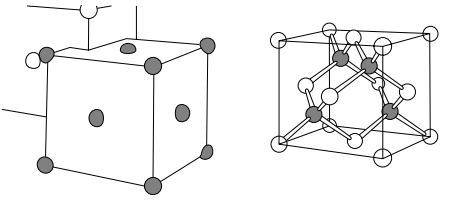

Figure 6.7 Crystallographic structure of silicon. Wafers are practically monocrystals of silicon.

Table 6.1 Physical characteristics of monocrystalline silicon

Physical size	Value	Units
Rupture strength	7	GPa
Young's modulus	190	GPa
Density	2.33	g/cm^3
Thermal conductivity	2.33	W/cm K
Thermal dilation	2.33×10^{-6}	K^{-1}
Electrical permittivity	11.9	F/m
Electrical field breakdown	3×10^5	V/cm
Electrical resistivity	2.3×10^5	Ω cm
Thermal diffusivity	0.9	cm^2/s
Specific heat (at constant pressure)	0.7	J/g K
Fusion temperature	1415	K

Another important point is that the Young's modulus of silicon is comparable, by order of magnitude (regardless of the crystallographic orientation), to those of conducting metals such as stainless steel. This value stays the same for a certain number of silicon-based materials, such as weakly doped silicon. The Young's modulus of polysilicon (a material composed of silicon atoms in a structurally disordered state) is 160 MPa[11]. This value remains comparable to the value shown in Table 6.1.

Silicon is a fragile material, rather similar to glass[12]. This signifies that there is no plastic zone. Beyond the elastic deformation zone is the mechanical rupture zone. This limit coressponds to a bound of 7 GPa (and thus a maximal strain of about 3.5%).

As for its electrical properties, it is necessary to note that non-doped silicon is an insulator at ambient temperature. Otherwise it is an excellent piezo-resistor, which means that when subjected to a deformation, the electrical resistivity changes markedly. However, silicon has poor piezoelectric properties. (this

[11] As we will see later, polysilicon can be evaporated on a substrate of silicon to make microstructures. It is a fundamental material in the field of MEMS.

[12] Glass and silicon can be compared from a mechanical behavior point of view, but structurally the two materials are very different: silicon is an ordered crystal in the minimum energy state, while glasses are disordered and metastable systems.

effect is interesting when making sensors) Finally, silicon's thermal properties are important to consider as well. It is a good heat conductor (comparable to a metal) and will thus favor the heating of miniaturized systems, all the more since miniaturization intensifies heat exchanges (see Chapters 2 and 5). Thermal expansion of silicon is weak: in the range of temperatures around 300 K, the corresponding coefficient is equal to 2.33×10^{-6}, a value comparable to glass. This coefficient varies significantly with temperature: it decreases with temperature, and becomes negative around 100 K. In fusing operations at high temperature, it is difficult to avoid the presence of residual constraints, which present a certain number of problems. We will return to this point in a section dedicated to anodic bonding.

Native silicon dioxide SiO_2 adheres well to a substrate, is thermally stable, has an excellent resistance to certain reactants important for etching, and is not soluble in water (unlike germanium dioxide); we will see that silicon dioxide is an appropriate material to make masks for dry and wet etching.

Currently, silicon wafers can be delivered with one or both sides polished, the location of the crystallographic orientation (defined by two planes) marked, and with different diameters and thicknesses. To get an idea of typical sizes, the 4-inch wafer is frequently used because current machines in the field of MEMS have adopted this format, though the trend is going towards increasing these sizes. The reason for this is a practical one: the larger the wafer, the more microsystems in parallel are able to be constructed, the more the production costs are cut, and thus the more the success of creating a given process is assured. Note that there is at this time a disparity between the field of microelectronics, which currently often uses 8-inch and 12-inch wafers, and that of microfabrication, which does not yet even use 6-inch wafers. Typical thickness for a wafer is 500 μm, but other thicknesses are available on the market. It is interesting to mention SOI systems(*Silicon on insulator*): these wafers possess three layers, two made from silicon and one made from silicon dioxide. They facilitate the fabrication of a certain number of devices, notably those employing the use of sacrificial layers.

6.5.2 **Wet etching of silicon and glass**

6.5.2.1 Introduction

Wet etching consists of subjecting an object, on which certain parts have been protected by a mask, to a chemical attack in liquid phase. This type of process is not new, and was already in use as early as in the fifteenth century to decorate armor. To accomplish this, the armor was covered with wax, the parts destined for exposure to chemical attack were cut out, and then it was all dipped into

a reactive bath for a determined period of time. When the armor was taken out of the liquid bath and the wax was eliminated by heating, and an etched or hollowed-out pattern was obtained with a controlled depth. The discovery of photosensitive materials and their usage by Niepce, the inventor of photography, resulted in the evolution of this technique. The microelectronic revolution of the 1950s caused an extraordinary refinement in the technique of wet etching, associated with photolithography. We now have a large amount of data on etching velocities in different conditions, which allow us to control the geometry of the etched object to just a few micrometers.

6.5.2.2 Isotropic and anisotropic etching

An important distinction must be made between isotropic and anisotropic etching. Isotropic etching is carried out equally in the three spatial directions, and can be used for forming structures such as spherical cavities; examples include fluoric acid in glass and EDP in silicon. Anisotropic etching consists of a chemical attack that is carried out preferentially along one of the crystallographic planes. It is possible to create cavities that have facets, which can be useful. This type of etching is not possible in glass, since it is an amorphous solid. Figure 6.8 illustrates these two types of etching for silicon. In the first case (left figure), EDP is used for isotropic etching, while in the second case (right figure), the base KOH is used to etch anisotropically, which is carried out along the planes (111).

6.5.2.3 Isotropic etching of silicon and glass

Isotropic etching generally implies the use of acids: a commonly used system for silicon is composed of HNA, which is a mix of $HF/HNO_3/CH_3COOH$. For glass,

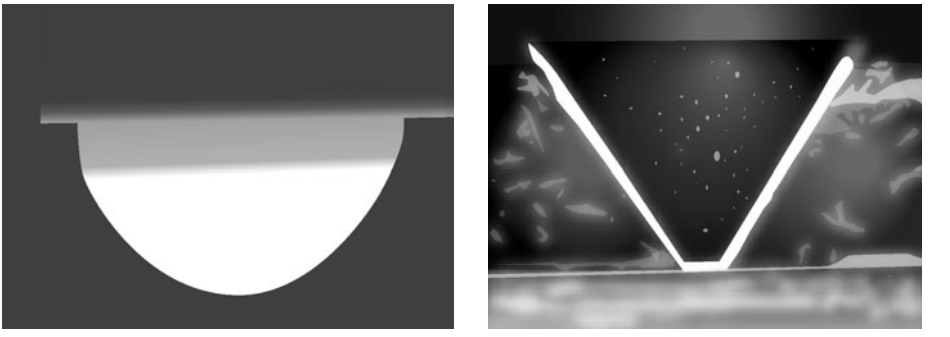

Figure 6.8 (Left) Isotropic wet etching using EDP and (right) anisotropic wet etching using KOH lead to rounded or faceted forms, respectively.

a commonly used system is fluoric acid. In these two cases, the etching is carried out at ambient temperature, with etching velocities of tens of micrometers per minute. The attack is accomplished in four steps: the transport of the reactant towards the surface, the local development of chemical reactions, the formation of a cavity, then the evacuation of the product. The transport steps are controlled by the mixing of the reactants in the bath in which the material is submerged. As the etching velocities are high (in comparison to the velocities of the evolution of the diffusion fronts), it is important to mix well to assure the homogeneity of the concentrations of reactive chemicals in the volume of the system. Chemically speaking, the attack of the reactant is in fact a subtle process. For example, the action of HNA on silicon makes use of the following global reaction:

$$\mathrm{Si} + \mathrm{HNO_3} + 6\mathrm{HF} \longrightarrow \mathrm{H_2SiF_6} + \mathrm{HNO_2} + \mathrm{H_2O} + \mathrm{H_2}\ (\mathrm{gas}).$$

Simplifying the reaction model, we can consider the action of HNA to essentially consist of breaking the covalent bonds of the crystal, and producing a fluoride compound of silicon (H_2SiF_6) that is soluble in fluoric acid. The reader can refer to the work of Marc Madou [1] for a detailed presentation of this process, including several steps initiated by the formation of holes in the valence band of silicon. Since we are dealing with a chemical reaction, the temperature of the bath must be maintained constant in order to control the depth of the etching. Typically, regulation to a few tenths of a degree is necessary to guarantee precision on the order of 10% of the depth. The state of the surface is also an important issue: physically, to obtain smooth surfaces, it is useful to place the system in the regime where diffusive processes (which tend to make reactive concentrations uniform) are quicker than the chemical kinetics. This regime is chosen by controlling the temperature of the system. The corresponding conditions are now known, and are just one of several parameters defining microfabrication protocols. It is useful here to refer to the specialized literature. In an ideal situation, the mask is not attacked by the reactant. In practice, however, there is a chemical attack of rates on the order of a few per cent of those in the intended process itself. For example, silicon is used as a mask for HNA, but it itself is also attacked by HNA, although at a rate 80 times slower than that of silicon. It is thus important to work with thick masks (hundreds of nanometers) to ensure that the masked part remains covered during the entire etching step. However, it has also been shown that the thicker the mask, the less geometric precision is achieved when the pattern is transferred from the lithographic mask to the photosensitive resist. A compromise must thus be reached. As a final point, it is important to note that the chemical reactant etches not only the volume of the exposed part, but also under the mask. This phenomenon can be elegantly used to form original

structures, such as planes fixed on rounded supports, or to make tips for atomic force microscopy (AFM).

6.5.2.4 Anisotropic etching of silicon

Anisotropic wet etching of silicon is a very common technique in the field of MEMS because it allows the formation of flat surfaces, such as wells or canals with flat walls (but with a trapezoidal cross-section, as we will later see). Here, the reactants that are used are alkanes at high concentrations (several moles per liter); unlike isotropic etching that uses acids, the medium in which the object to be etched is immersed is strongly basic.

The principle of anisotropic etching is based on the diagram shown in Fig. 6.9.

The etching rate thus depends on the crystallographic orientation that the chemical attack follows. The velocity of etching is slow along the planes (111) (on the order of 13 μm per hour), and faster along other orientations. The corresponding ratio of etching velocities is on the order of 60. The consequence of such a contrast is that the silicon crystal immersed in base will make the cut-out forms appear spontaneously along the planes where the etching is the slowest, i.e. along the planes (111). An analogous process occurs during the phenomenon of faceted growth, where the visible facets are those associated with the slowest growth velocities, which also happen to be the highest-density planes. It is this process that causes cubic crystals such as salt to have an orthorhombic form (constructed from the planes (111)), and no longer cubic. Unlike isotropic etching,

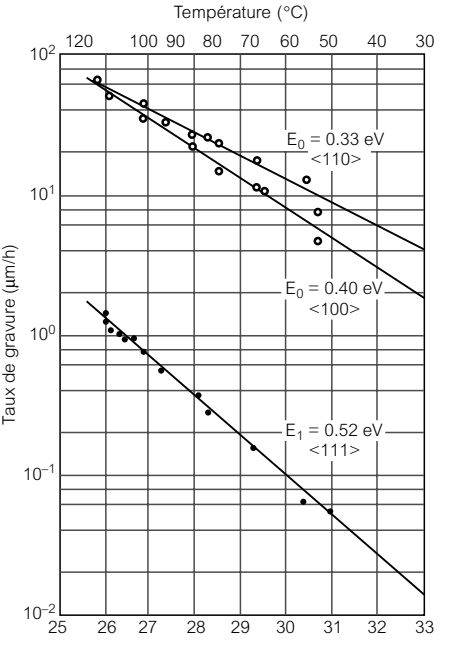

Figure 6.9 The evolution of the etching speed with respect to temperature for different crystallographic orientations (anisotropic etching). The lowest velocities seem to correspond to the densest planes. The contrast between slow and fast orientations is significant.

the process of anisotropic etching is not completely understood in all its detail today. There are several concurrent models that describe the various mechanisms in play. The reader can refer to specialized literature for a description of these models. As for the state of the surface, anisotropic etching theoretically allows for the production of an atomically smooth surface formed from terraces. In fact, in the common case of silicon etching by KOH, the production of hydrogen bubbles introduces local fluctuations in concentration of the chemical reactants, inducing inhomogeneities in the etching velocities, and thus leading to more roughness in the surfaces. These perturbations can be reduced by using moderately elevated temperatures (thus reducing the flux of bubbles, which raises the temperature), and thorough mixing of the bath. In a standard well-tuned process, the surfaces have a local roughness on the order of 20 nm.

It is not always simple to guess the shape produced by anisotropic etching. Figure 6.10 illustrates a few examples, which are at times unusual. The general rule is: etching will take place along the rectangle circumscribing the pattern defined by the mask.

6.5.3 **Dry etching of silicon**

6.5.3.1 Introduction

Dry etching is the attack of a substrate by an ionic species contained in a gaseous or plasma phase. This method of etching is very rich: depending on the etching conditions, the shapes obtained can be anisotropic or isotropic, with an anisotropy controlled by the system and not by the crystalline structure of the etched object (for example, square canals in glass can be obtained). The diversity and refinement of these dry-etching techniques have progressed significantly in the last 30 years due to innovation in the microelectronics industry, and, to a lesser extent, to MEMS research. Today there is all sorts of equipment for performing dry etching, and it is difficult for a technology platform dedicated to microfabrication to operate without the minimal

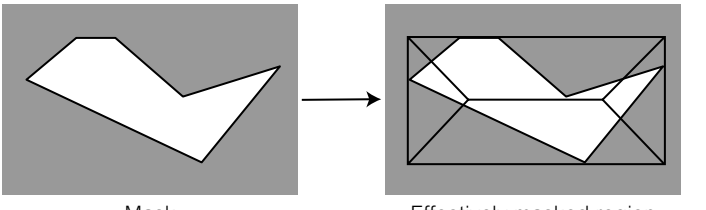

Figure 6.10 Different shapes obtained by anisotropic etching. The general rule is: etching will take place along the rectangle circumscribing the pattern defined by the mask (taken from M. Madou [1]).

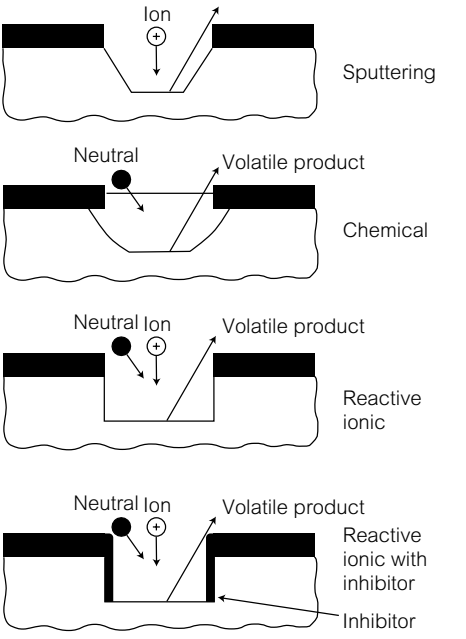

Figure 6.11 Different types of dry etching for silicon (from top to bottom): physical, chemical, physico-chemical, and physico-chemical with inhibitor [1].

equipment necessary to access these techniques. We will limit ourselves here to a very simplified presentation of the methods and principles of dry etching. The interested reader can easily find the details in the specialized literature [1]. We begin by a general classification: Fig. 6.11 represents the four most common types of dry etching, which are obtained by adjusting the nature of the plasma containing the ions.

- **Physical etching.** Here, ions are accelerated in an electric field and bombard the surface of a target (the object to be etched). An etching effect is produced by the physical action of the flux of incident ions. We will see that this type of etching is anisotropic and not very selective.
- **Chemical etching.** Chemical species migrate towards the surface of the target under the action of an electric field, and chemical reactions occur on the surface, thus producing volatile species and holes.
- **Physico-chemical etching.** The two preceding actions are combined. This type of etching is the most commonly used type in the field of microfabrication.
- **Physico-chemical etching with inhibitor.** This sophisticated process consists of depositing a protective layer along the sides of the etched cavities while the bottom of the cavity continues to be attacked both physically and chemically. This type of process enables the formation of geometries with high aspect ratios.

We describe in detail in this section the four techniques favored in the field of microfluidics. The reader will find some basic notions on cold plasmas discussed in a text box at the end of the chapter: these systems are often mentioned in the following descriptions.

6.5.3.2 Physical dry etching

The action of a plasma on a target placed at the cathode (Fig. 6.12) in the chamber where the plasma is created depends on the kinetic energy of the ions accelerated toward the target, a quantity controlled by the voltage between the electrodes. For kinetic energies less than 10 eV, ions are not sufficiently energetic to eject material from the substrate by collision. For energies between 10 eV and 5000 eV, ejection of material is produced, resulting in physical etching of the target. For energies between 10 and 20 keV, ions penetrate the depth of the target, and we enter into a domain of ionic implantation, useful for the doping of semiconductors.

Physical dry etching can only be carried out at low pressures (typically a few mTorr). Incident ions on the target must be ballistic to undergo substantial acceleration, and the ejected material must be able to be transported far from the target so that it does not redeposit. All this points a low pressure working environment and conditions under which the movement of ions is ballistic. The simplest configuration (Fig. 6.12) is known as *sputtering*. The most commonly used machines are based on the coupling of the target (what we want to etch) and the electrodes producing the plasma. The target receives ions produced by the plasma; the ions are then redirected by a magnetic field towards the target, for example, and can be placed on a substrate independent of the cathode. Here it is useful to refer to the ionic machining technique of *ion milling*, and its associated acronyms: IBE (*ion beam etching*) and MIE (*magnetron-enhanced ion etching*).

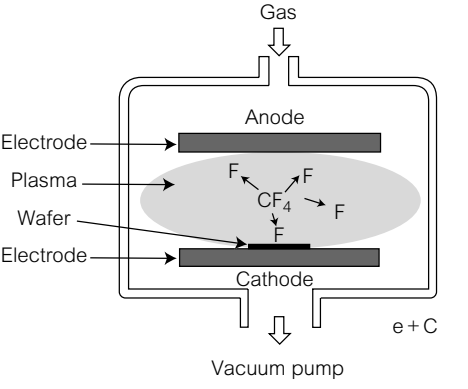

Figure 6.12 Setup for sustaining a plasma for etching silicon.

The etching rates are on the order of 100 to 3000 Å/min (or 0.6 to 18 μm per hour for most materials used for microfabrication (silicon, metals, oxides, etc.)). The selectivity of this technique is particularly poor, which must be taken into consideration when fabricating masks for this technique.

6.5.3.3 Chemical etching of silicon

In chemical etching, the object to be etched is in contact with reactive components contained in a gas or a plasma. The principle of this method can be decomposed into five steps, as indicated in Fig. 6.13.

Chemical etching consists of the following five steps.

- Diffusion of reactive species towards the target.
- Adsorption of the target.
- Reaction with the material making up the target and the formation of a volatile component.
- Desorption of the component.
- Diffusion in the gas or plasma.

Unlike physical etching, the movement of reactive molecules or ionic species near the target is diffusive (and not ballistic). It is thus useful, for purely chemical etching, to increase the density of chemical species acting on the target surface: substantial etching velocities are thus obtained. On the other hand, using a ballistic regime would give rise to the coupling of chemical and physical effects, which will be described below (this becomes physico-chemical etching). Chemical dry etching is carried out under pressures on the order of 10^{-1} to

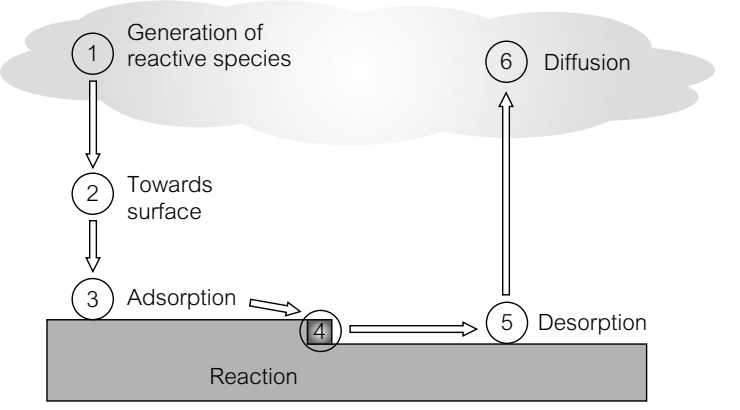

Figure 6.13 Physico-chemistry of dry etching on silicon: the etching is carried out in five steps: diffusion of reactive species, adsorption, chemical reaction, desorption of the component, diffusion in the plasma [2].

1 Torr, which is higher than pressures used for physical or physico-chemical etching. The simplest example of chemical dry etching does not use a plasma to produce reactive species, but uses a system in which a component (XeF_2) contains a strongly electronegative element (in this case, the fluoride ion) that is sublimated. XeF_2 spontaneously reacts with silicon according to the equation:

$$2XeF_2 + Si = 2Xe + SiF_4 \text{ (volatile)}.$$

The volatile components are SiF_4 and xenon, which desorb. This technique leads to isotropic etching with etching rates on the order of a few μm/min. However, the etched surface is rough (the roughness is on the order of a micrometer, which is large for the MEMS standards). The most sophisticated and best-controlled (in terms of roughness) systems of chemical etching involve the formation of a cold plasma, whose role is to produce reactive species from a gas that is not spontaneously reactive with silicon. This is the case for systems based on CF_4. This tetrafluoride of carbon does not attack silicon, but CF_3^+ ions, as well as the species CF_3 and F created by the plasma, are reactive towards silicon.

There are several phenomena in play in the process of chemical etching (the effect of charge, the bullseye effect, etc.) The reader can find descriptions of them in the specialized literature.

6.5.3.4 Physico-chemical dry etching: RIE (reactive ion etching) systems

Another etching technique consists of favoring the reaction by using radiofrequency heating, which raises the temperature of the set up, and also by the bombardment of ions activating the reaction and allowing the etching to take place. This technique is known as RIE (*reactive ion etching*). It is very widespread in microfabrication centers. The basic configuration is rather simple: the object to be etched (i.e. the target) is placed on the cathode of a cold plasma, which is made up of reactive species. As described previously, the movement of the ions is ballistic at low pressures, and the target is bombarded by ions accelerated in the electric field localized near the cathode. An etching rate on the order of 1000 Å/min is achieved, much higher than the 100 Å/min typical of physical etching. The presence of an ion flux leads to anisotropic etching. Taking the etching velocities into account, RIE in its simplest versions is the type of etching most often used for etching not silicon, but silicon oxide, covered with a mask made from a photosensitive resist. This procedure allows the transfer of the pattern from the photolithographic mask to the silicon mask, which is useful for wet etching for example.

6.5.3.5 Physico-chemical etching with inhibitor

In the case of physico-chemical etching with inhibitor, the surface reaction creates non-volatile components that, under the action of the ion flux, are ejected from the exposed surface. These ions adsorb on the neighboring vertical surfaces, forming a polymerized protective film. This subtle process reinforces the anisotropic effect of the etching. An inhibitory film is generated in an RIE process with plasma products from CCl_4 and $CF_2 2CL_2$.

This phenomenon has been coupled for several years to highly energetic plasma sources (known as ICP: *ion coupling plasma*). This system gave rise to a technique known as DRIE (*deep RIE*), and also to a sophisticated piece of equipment allowing the etching of very deep structures (on the order of 500 μm). This technique allows structures with aspect ratios on the order of 30:1 to be made. One spectacular example is given in Fig. 6.14. The associated machine, developed specifically for MEMS, had a notable impact in the field, as it allowed for the deep etching of forms more easily usable than those based on the planes (111) of a symmetric cubic crystal. In the context of microfluidics, DRIE is often exploited to pass through silicon wafers, and to put in fluidic access holes on the front surface (thus permitting easy access to visualization windows).

6.5.4 **Techniques of deposition onto silicon and glass**

6.5.4.1 Introduction

Deposition is a procedure that plays an important role in almost all processes of microfabrication. There are currently a large variety of deposition techniques that allow for the deposition of all types of materials: metals, insulators,

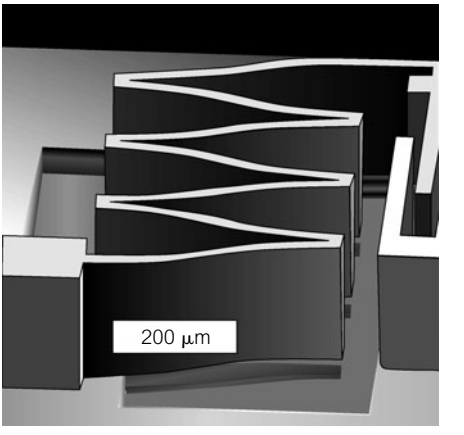

Figure 6.14 A remarkable microfabricated structure obtained by DRIE. It consists of a spring linked to a small mass and reveals the potential of deep etching.

semiconductors, polymers, proteins, etc. Again, this text will present here the principles without delving into the detail. Most deposition techniques fall into one of two main categories.

1. PVD: *physical vapor deposition*. In this case, the object (or target) is put into contact with a holding gas; certain species in the gas adsorb, forming a layer that constitutes the deposit.
2. CVD: *chemical vapor deposition*. In this case, species in contact with the target react with the surface, forming components that are chemically bonded to the object.

In this section both approaches will be described, as well as the different techniques that have arisen from these deposition methods.

6.5.4.2 PVD: physical vapor deposition

Thermal evaporation

In this case, the material to be deposited is placed in a container and positioned facing the target; the entire setup is then placed in a chamber maintained at a low pressure. Next, the system is taken to high temperature and sublimated. The sublimation produces an atom flux that adsorbs on the target surface. The deposition of the desired material takes place simultaneously with other molecules contained in the chamber; it is thus necessary to work at low pressures (on the order of 10^{-8} Torr) to avoid unwanted parasite deposition.

Due to its simplicity, the technique of thermal deposition is commonly used in laboratories. The velocities of deposit are slow (a few Å per second), and the method is mostly used for metallic deposits.

Sputtering

For this it is necessary to create a cold plasma. This method is often preferred over the thermal method because it is possible to deposit a larger variety of materials, and also because it results in better adhesion between the deposited layers. *Sputtering* uses a method of deposition similar to physical dry etching. The difference comes from the fact that the target is placed on the anode, and not the cathode. The container with the material destined for deposition is placed on the cathode. The cathode is then subjected to an elevated energetic flux, and there is ejection of material. The ejected material then deposits on the target. In practice, ionic kinetic energies are in the region of 0.3 to 2 keV for the bombardment of the material in the container. Energetic ions collect at the level of the target, and

they penetrate one or two of the molecular layers of the substrate. In this way, good adhesion between the layer and the substrate is made.

■ CVD: ***chemical vapor deposition.***

In this case, the substrate is put into contact with a gas containing reactive species. There are two possibilites:

– the reaction takes place in the gas. The products of the reaction are adsorbed onto the surface of the target, resulting in a homogeneous reaction;
– the reaction takes place at the surface of the target, resulting in a heterogeneous reaction.

Most equipment for CVD are based on heterogeneous reactions, since the adherence of the film produced is superior to that of the homogeneous case. Figure 6.15 represents the mechanism in the heterogeneous case.

CVD is highly versatile; it allows for the deposition of insulators (for masks or electric insulation), and of polysilicon (for surface micromachining). The deposition rates in all cases are slow (on the order of μm per hour), and this is a problem for the microfabrication of thick structures. Because of this slow deposition speed, many polysilicon structures (e.g. motors, beams, etc.) reproduced

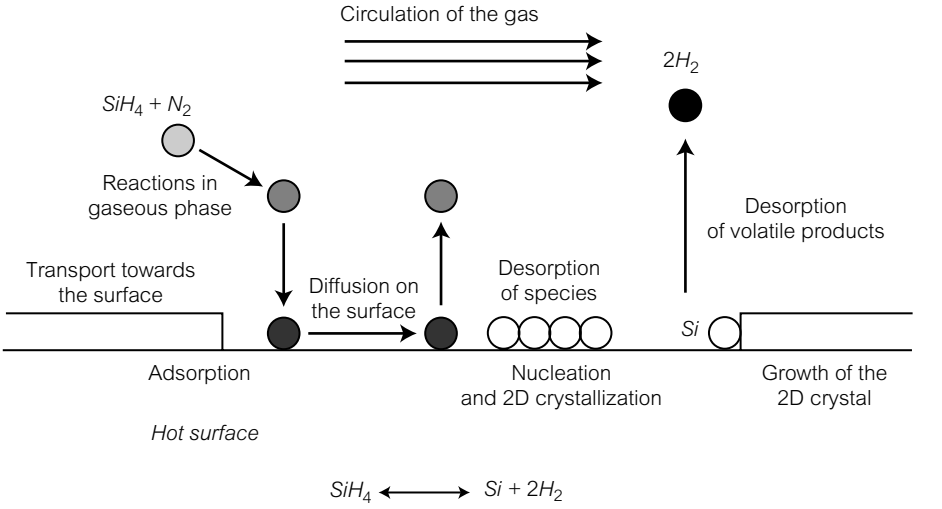

Figure 6.15 Chemical deposition in the vapor phase is the product of a succession of steps, which are, in order: the adsorption of species, their diffusion on the surface, and their aggregation leading to the formation of a film, which constitutes a bidimensional crystal with a very low defect density.

in the literature are only a few micrometers high[13]. We note that refinements have been developed in these last few years; in the particularly important case of polysilicon, these improvements have pushed the thickness limit by an order of magnitude. Here I describe briefly the techniques of CVD most commonly used for MEMS and microfluidics. In the field of MEMS, there are basically three types of CVD.

LPCVD (***low-pressure chemical vapor deposition***)**.** Deposition takes place at low pressure (1 Torr). This is used for polysilicon, a fundamental material for MEMS. Deposition speeds are in the order of 1 μm/hour.

APCVD (***atmospheric-pressure chemical vapor deposition***)**.** In this case, the deposition takes place at atmospheric pressure.

PECVD (***plasma-enhanced chemical vapor deposition***)**.** This technique deals with systems for which thermal activation is not sufficient to allow heterogeneous chemical reactions. A plasma is thus used, whose role is to activate chemical reactions at the target surface using ionic bombardment.

Evaporating a material on a pre-existing relief does not necessarily lead to uniformly thick layers. Two cases must be defined: conformal and non-conformal deposition (Fig. 6.16):

– conformal deposition: in this case, the deposited film has a constant thickness at all points on the target
– non-conformal deposition: in this case, the film does not have constant thickness, and possesses rolls and crevices.

Physically, to obtain conformal deposition, the incident particles must be sufficiently energetic to diffuse to the target surface before forming chemical bonds. This type of situation depends on the initial energy of the incident particles and on the mean free path. It is advantageous to work with a high mean free path (which is reached at low pressures). From this point of view, LPCVD systems are more useful than APCVD systems. Thus, we try to work at low pressures for PECVD systems.

The special case of the deposition of silicon dioxide

Silicon dioxide is a very important material for microfabrication. It is used as a mask for the components etching silicon, and is also used to electrically insulate

[13] The problem with small thicknesses lies in the fragility of the object, its sensitivity to the presence of particles, and the need for precision during fabrication. These characteristics are all drawbacks in the industrial world.

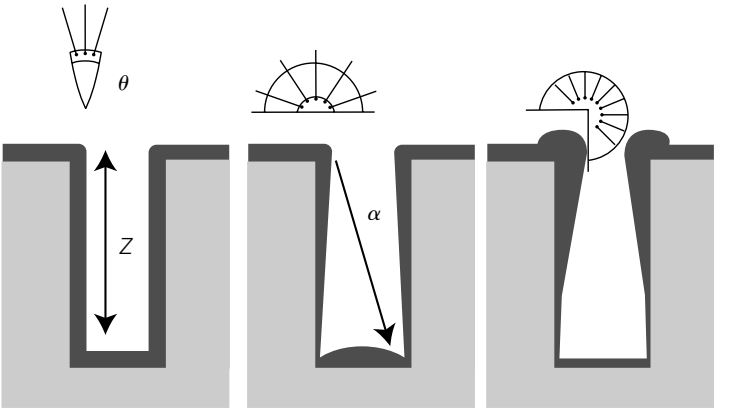

Figure 6.16 Conformal and non-conformal deposition. Conformal deposition (left) takes the form of the substrate, while non-conformal deposition (right) develops forms different from those of the substrate (From [1]).

metallic structures. It is thus often necessary to deposit silicon dioxide (SiO_2) onto a silicon or metal substrate.

When forming a silicon dioxide film on a silicon substrate, the simplest method uses oxidation. A silicon wafer exposed to ambient air is covered in a layer of silicon dioxide about 2 nm thick: this oxide is known as the 'native' oxide of silicon. However, this layer is too thin to serve as a mask. We thus proceed to thermal oxidation at high temperatures (650 °C) in the presence of an oxygen/nitrogen mix; typical thicknesses obtained by this method are on the order of a micrometer.

It is important to note that the surface of silicon is covered with a layer of the silane Si-OH. We saw in the chapter describing electro-osmosis that the H^+ ions are freed in aqueous solution, causing the appearance of negative charges on the surface, which in turn allows the electro-osmotic effect to take place.

Electrolytic deposition

This section concludes with a discussion on additive microfabrication methods using electrolytic deposition. When a metallic current is put through a solution of metallic salt (such as $CuSO_4$), metallic ions migrate towards the anode, capturing electrons there, and forming molecules that adsorb onto the electrode. The reduction reaction is written:

$$Cu^{2+} + 2e^- \longrightarrow Cu.$$

There is thus a metallic deposit on the anode. At the same time, there is generally some production of hydrogen bubbles, which commercialized systems avoid by including chemical additives.

6.5.5 **Sealing**

6.5.5.1 Introduction

We presented in the preceding paragraphs etching techniques that allow structures such as microcanals and microcavities to be made in materials such as glass and silicon. Once the etching step is completed, we have grooves carved onto a wafer, and must now cover them with something else in a watertight manner in order to make microfluidic canals. Thus, a sealing step is necessary. Sealing is not necessarily an easy procedure; to ensure the watertightness of a microfluidic system, adhesion must be applied on all surfaces brought into contact with one another. If the sealing is poorly done, the pieces in question will have defects in their flatness, and interstitial spaces form. These defects will cause hydrodynamic fluxes, and often render the system unusable. To make seals between glass-silicon, glass-glass, or silicon-silicon, fusion techniques are most often used, with or without an electric field[14]. We describe these techniques below.

6.5.5.2 Anodic Bonding

Anodic bonding is a technique that allows for the adhesion of glass onto a metal or semi-metal such as silicon. We are interested here in the case of glass-silicon sealing. A schematic diagram of an anodic sealing system is shown in Fig. 6.17. The electric field induces the migration of Na^+ ions in the glass to the glass-silicon interface. Trapped at the interface, they produce an intense local electric field. Physico-chemically speaking, sealing is assured by the interpenetration of atoms at the glass-silicon interface. This mix of atoms is made possible by an elevated temperature (400 °C) to which the system is raised, and by the intense local electric field reduced the sodium trapped for the interface. In the absence of the electric field, the system should be brought to 1000 °C so that the sealing can be carried out (this is sealing by simple fusion). Typical voltages used to assure anodic sealing are on the order of 1 kV (Fig. 6.17). An important contribution to the success of this method is the minimization of relative thermal deformations between glass and silicon. This means that the choice of glass should have a thermal expansion coefficient near that of silicon. One example of a commonly used glass is Pyrex Corning 7740. The conditions of cleanliness at the interface

[14] It is obviously not recommended to use a liquid glue as the glue tends to fill and block the microcanals.

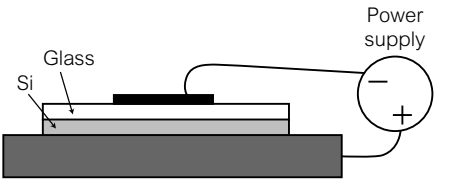

Figure 6.17 Anodic Bonding. A voltage is applied between the glass and the silicon. A charge density appears at the interface, locally producing a very intense electric field that favors the adhesion of the two materials.

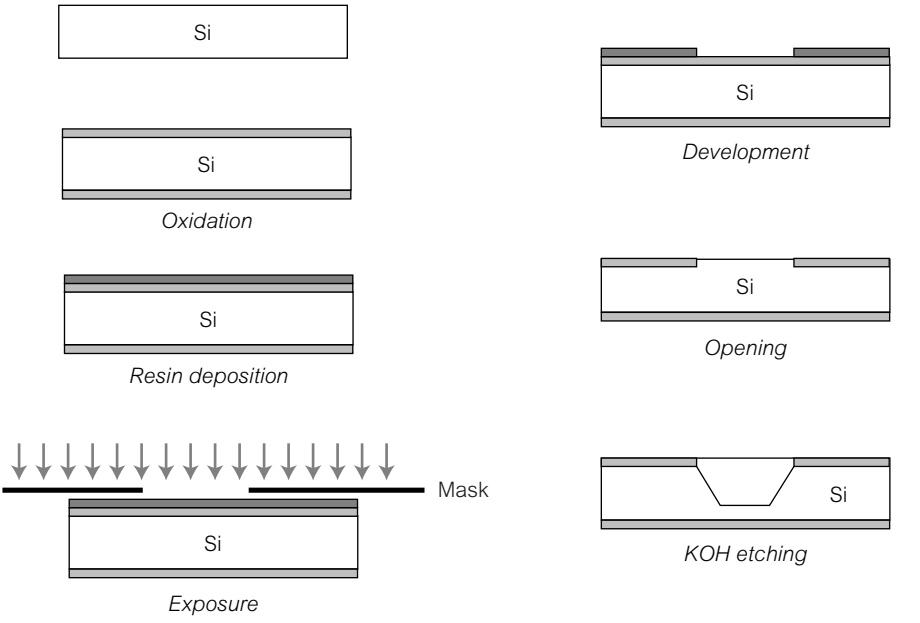

Figure 6.18 Obtaining a silicon membrane by KOH wet etching. 7 steps and 1 mask are necessary for this device.

are also critical for the success of the sealing. It is thus recommended to carry out the sealing process in a clean room. When performed well, it results in perfectly watertight systems that are capable of withstanding very high pressures (about a hundred atmospheres for a microcanal etched in glass and covered with a plane of silicon by anodic sealing).

6.5.5.3 Fusion bonding

It is possible to seal two pieces of silicon or glass by fusion bonding. Physically, thermal agitation causes the reorganization of silicon atoms at the interface, establishing a small amount of interpenetration that ensures bonding. Depending on the material, temperatures used range between 600 and 1100 °C. The adhesion in this case is particularly robust.

6.5.6 One example: fabrication of a membrane

To apply the preceding ideas, the steps leading up to achieving a membrane on a silicon wafer will be presented here schematically.

The first step consists of depositing a silicon dioxide layer (SiO_2) on a silicon wafer. Then, a layer of photosensitive resist is deposited on the insulating wafer. After this is the exposure step, which partiallly illuminates the resist leading to the modification of its physico-chemical properties. After development, the exposed portion of the resist is dissolved, leaving the exposed layer of SiO_2. This layer can be made to disappear with a chemical attack. The silicon is thus partially exposed, or by using a new selective chemical attack, it is possible to form a cavity. In this way, it is (theoretically) possible to microfabricate a membrane with a controlled thickness.

6.6 Methods of fabrication of plastic MEMS

6.6.1 The three principal methods of replication

The three current methods of replication are presented in Fig. 6.19.

We have:

• **molding**: a mix containing a catalyst and a polymer is poured on a mold and heated. After reticulation, the structure is peeled off the mold and it contains the pattern of the mold, though in 'negative' form;

• **casting**. The mold is pressed into a heated deformable material. After cooling and separation, a structure is obtained that also represents the negative of the mold;

• **microinjection**. The heated plastic is injected in a liquid state into a mold. After separation, the negative of the mold shape is obtained.

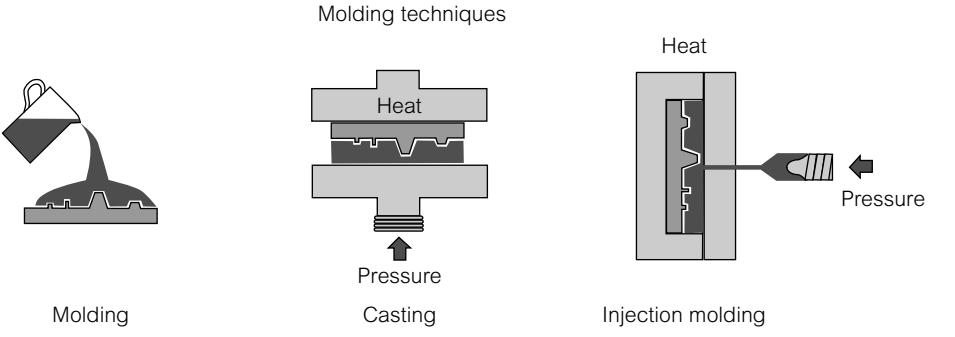

Figure 6.19 Three replication techniques commonly used for plastic or polymer MEMS: molding, casting, and microinjection.

The molds are generally fabricated using the technologies described previously in this chapter. For the molding technique, polymer molds are suitable. For the techniques of casting and microinjection, temperature and pressure constraints generally require metallic molds, often made by electrodeposition. Traditional micromachining methods can also be used. In this case, the precision of microfabrication, as we indicated at the start of this chapter, is on the order of tens of micrometers.

6.6.2 **PDMS-based molding**

In the domain of microfluidics, molding based on PDMS (polydimethylsiloxane) plays a very important role. Numerous articles include many details on these technologies, which is particularly advantageous for rapid prototyping (see, for example [5–7]).

PDMS belongs to a family of polymers that notably contain silicon oils. The formula of PDMS is $(–Si(CH_3)_2O)–$. The semi-structural formula is shown in Fig. 6.20.

These polymers, when taken beyond their polymerization temperature and put in the presence of a reticulating agent, form an elastomer whose principal properties are shown in Table 6.2 (from [5]).

To form a structure like a microcanal, replication by a molding method is used. There are essentially three steps (Fig. 6.21).

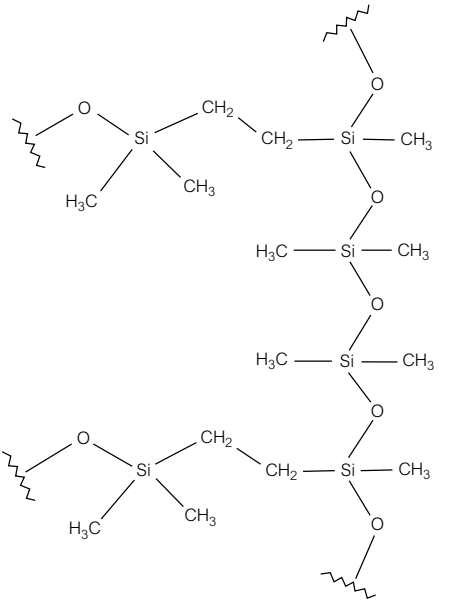

Figure 6.20 Semi-structural formula of PDMS.

Table 6.2 Physico-chemical properties of PDMS

Property	Characteristic
Density	Around 0.9 kg/m^3
Optical	Transparent, between 300 nm and 2200 nm
Electrical	Insulating, breaking field 20 kV/cm
Mechanical	Elastomeric, Young's modulus ~750 kPa
Thermal	Insulating, thermal conductivity ~0.2 W/m/K
Interfacial	Low surface energy (~20 mN/m)
Permeability	Permeable to gas, apolar organic solvents, nearly impermeable to water
Reactivity	Inert, oxidizable by a plasma
Toxicity	Non-toxic

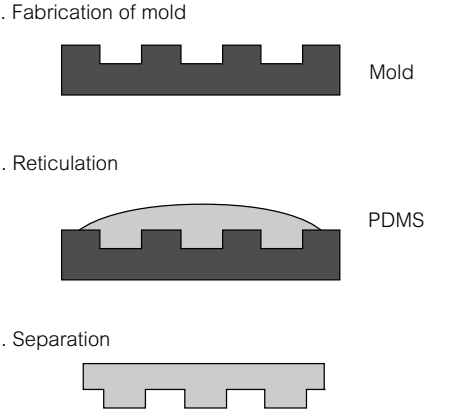

Figure 6.21 Soft lithography of PDMS. (a) Mold made from a hard material; (b) pouring of the PDMS + reticulating agent mix. The ensemble is taken to the polymerization temperature of PDMS; (c) peeling off the PDMS.

A mold made from a hard material is used, and this mold is made separately. The mold material can be silicon, an electrodeposited metal or a reticulated polymer such as SU8 that we described above. The fabrication of the mold requires the use of a clean room. However, the molding step can be carried out in an ordinary environment as long as the temperature and hygrometry are carefully controlled. A mix of PDMS and a reticulating agent is poured onto the mold. The system is taken to a moderately elevated temperature (on the order of 70 °C). During this phase, the PDMS polymerizes, reticulates, and the mix becomes solid. After peeling off the PDMS an object representing the negative of the mold structure is obtained.

The precision of the structures obtained this way is surprisingly high. Whitesides *et al*. [6] showed that it is possible to obtain structures (canals, electrical contacts, etc.) with submicrometric precision. However, taking into account the elastomeric character of the materials as well as aging phenomena,

the dimensions of microcanals best suited to the characteristics of PDMS lie between 5 and 500 μm. In the same vein of thought, it is possible to make geometries with high aspect ratios. However, due to the deformability of PDMS, most microfluidic structures give rise to aspect ratios that are, for example for microcanals, greater than 1/10.

With respect to microfabrication, the specific properties of PDMS deserve a few remarks.

- Its transparency in the visible spectrum allows for the visualization of flows.
- The Young's modulus of reticulated PDMS varies considerably depending on the ratio between PDMS/reticulating agent; the value given in Table 4.35 is a higher-end value.
- It is important to emphasize the considerable advantages of the mechanical properties of reticulated PDMS. Its elastomeric quality facilitates the watertightness of microfluidic connections, tightly hugging the shape of fluid pathways. The elasticity of the material allows the fabrication of valves and pumps using membranes, as we will see in Chapter 7. Taking these facts into account, PDMS offers an elegant solution to the management of fluids in laboratories on-chip. Moreover, most complex lab-on-a-chip systems today are made of PDMS.
- Untreated (native) PDMS is hydrophobic, and becomes hydrophilic (temporarily) after the oxidation of the surface by oxygen plasma or after immersion in a strong base. The plasma causes the appearance of silanes by the oxidation of methyl groups. Oxidated PDMS adheres by itself to glass, silicon, or polyethylene, as long as those surfaces were themselves exposed to an oxygen plasma.
- Its permeability to gas facilitates filling (it is theoretically no longer necessary to unblock canals)[15]. However, its permeability to non-polar organic solvents makes PDMS unsuitable for many uses.
- Its weak surface energy is advantageous, as it facilitates the process of peeling off the mold from the substrate.
- However, we note that the properties of reticulated PDMS are not stable with respect to time. There are aging effects that can be difficult to anticipate. Also, the exposure of PDMS to water vapor can substantially modify the hydrophobicity of surfaces. PDMS is a productive material, but it has more unpredictable properties than glass or silicon.

[15] This signifies that it is possible, in principle, to fill an obstructed canal (that is to say, a canal with an entrance but not an exit). The bubble of air trapped in the canal during the filling process escapes by migrating through the material, possible because of the permeability of PDMS.

It is also important to note that it is not possible to evaporate metallic electrodes on PDMS due to its adherence properties and the elevated temperature needed for deposition. PDMS structures can nevertheless be placed on a silicon wafer, made up, for example, of evaporated electrodes. We thus define a 'hybrid' technology that has a large amount of potential.

6.6.3 **Casting**

The most commonly used casting material is PMMA (polymethylmethacrylate), which resembles a transparent plastic like Plexi-glass when in its solid state. When raised to a moderately elevated temperature (on the order of 170 °C), and subjected to a pressure of tens of bars, the material can deform considerably. In this way, it is possible to impose a pattern of structures by pressing with a press onto a slab of PMMA at a controlled temperature. The pattern produced is the negative of the one on the mold. The principle of this technique is simple and is shown in Fig. 6.22.

For microfabrication, the mold is made with a rigid material such as silicon or a metal. It is generally fabricated using the silicon technology described in this chapter. The materials used for the technique of casting are not limited to PMMA, but include other plastics such as PC, etc. PI, PE, PET, PVC, PEEK, ... The patterns that are obtained can have a remarkable precision, typically on

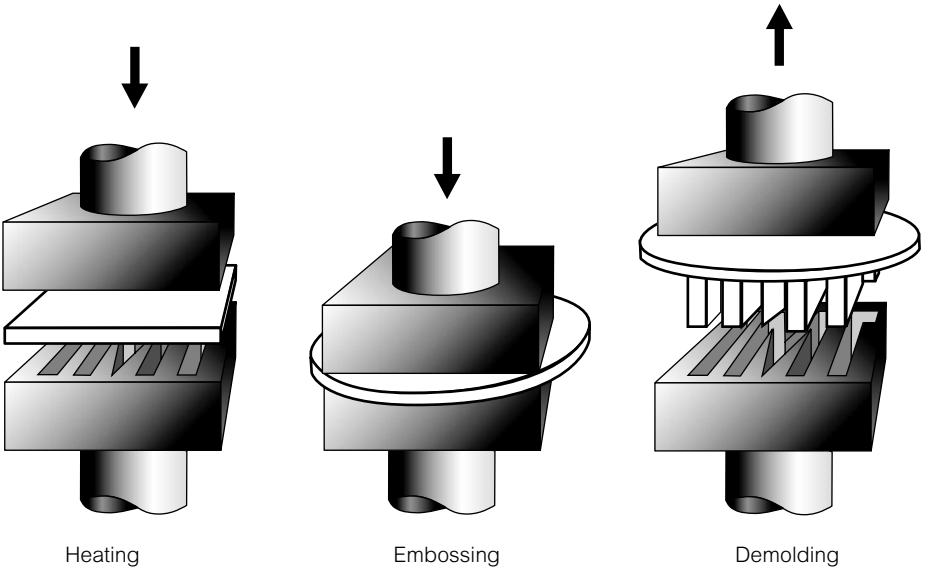

Figure 6.22 Technique of casting.

the order of tens of nanometers. The thickness of these structures has a large range (from a few nm to mm), and the forming factors can be very high (several hundred). This technique is well adapted to prototyping and productions of average series, and benefits from a significant body of knowledge that has been acquired in the field of plastics for decades.

6.6.4 **Microinjection**

Microinjection is a technique taken from the field of plastics. It is shown schematically in Fig. 6.23.

The method can be broken down into three phases:

- The liquid plastic material is injected into a mold under a vacuum and pressure, at a temperature greater than the glass transition temperature T_g of the plastic.
- The system is cooled down below the glass transition temperature.
- After taking off the mold, a structure is obtained that corresponds to the negative of the mold.

The technique is slow, the molds are delicate to make, and the optimization of the technique is complex. Nevertheless, this technique is advantageous from an

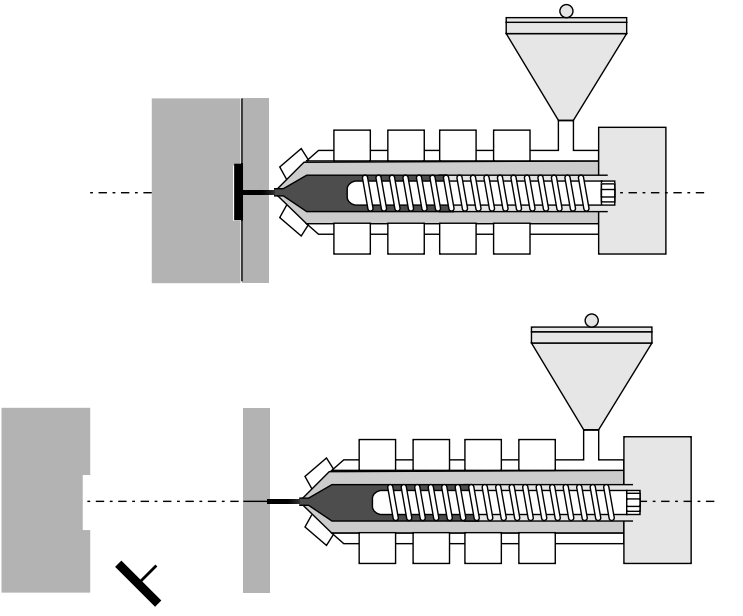

Figure 6.23 Technique of microinjection.

industrial standpoint for serial production. It also benefits from all the important work done in the field of plastics, and in several cases, existing machines need only be modified slightly to be adapted to mass production. Several companies such as Aclara, Weidmann, Corning, etc., already use this method.

6.6.5 **Direct micromachining of plastics**

Plastic can be directly micromachined. Today there are an abundance of techniques that allow this type of micromachining to be carried out, a few of which we will briefly mention here.

– μ-*Stereolithography*. Here, photosensitive resists are polymerized, layer after layer, by applying a spot of UV laser. The micromachined materials are epoxy resins and acrylics. A remarkable example of the use of this technique is shown in Fig. 6.24.

  The technique of stereolithography is complex to use, and necessary equipment includes sophisticated control of the movement of a beam. The precision of this technique is on the order of a few micrometers. Nevertheless, it is the most accomplished tridimensional method of microfabrication today.

– *Laser ablation*. Here, plastic is sublimated by the local application of an intense laser beam. Examples of its use are shown in Fig. 6.25.

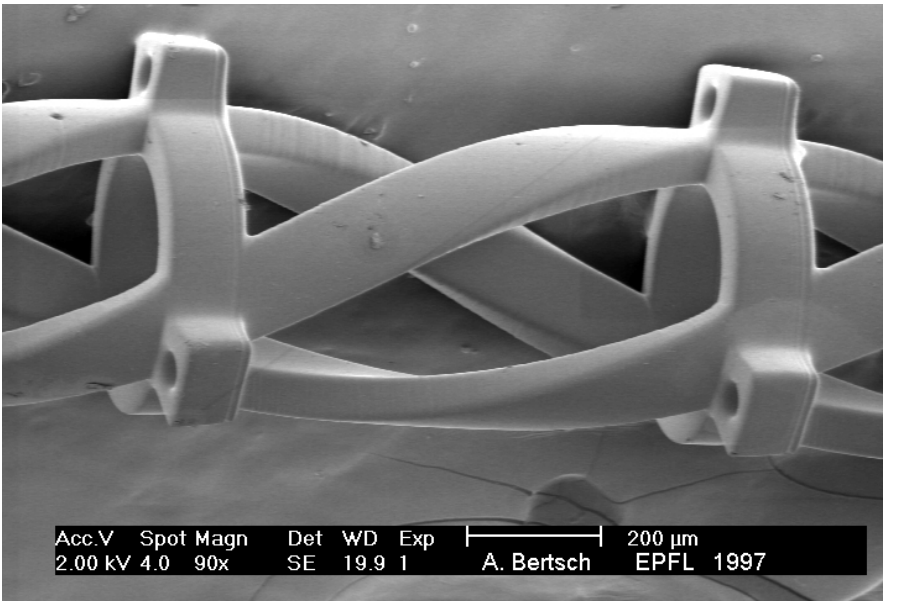

Figure 6.24 Example of a structure made by stereolithography (photo: EPFL-FSTI-LMI4, Lausanne).

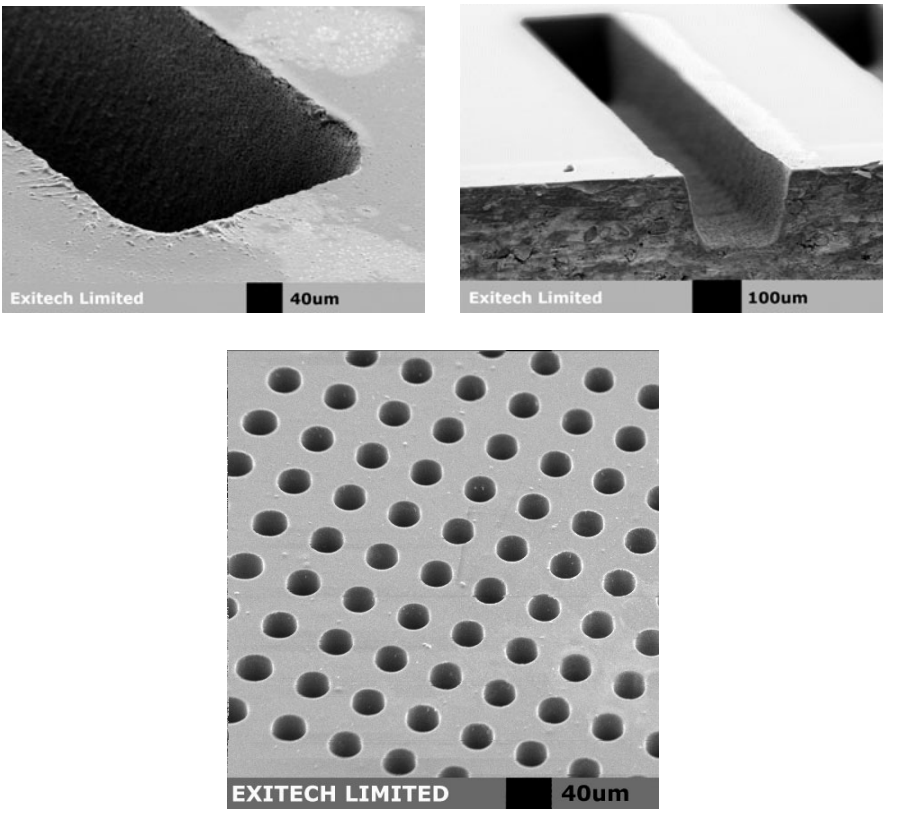

Figure 6.25 Examples of structures made using laser ablation.

UV and femtosecond lasers are used for this technique. The micromachining precision is mediocre (a few micrometers), and the roughness of the surfaces is on the order of 200 to 500 nm. However, micromachining by laser ablation is quite versatile. It allows for control of wetting properties of the surface and charges at the surface. Also, there is no difficulty in assuring access to the microcanals from the exterior world.

– *Other methods.* Other methods exist, such as oxygen plasma etching, particle jet ablation, and microelectro-erosion. We refer the reader to the specialized literature for more information about these techniques.

References

[1] M. Madou, *Fundamentals of Microfabrication*, CRC Press (2000).

[2] R. Choudhury, *Handbook of Microlithography, Micromachining and Microfabrication*, Vols 1 and 2, SPIE Press, Bellingham, WA (1997).

[3] T. Kawai, K. Sawada, Y. Takeuchi, Proc. MEMS 2001, Interlaken, 22–25 (2001)

[4] D.J. Beebe, G.A. Mensing, G.M. Walker, *Ann. Rev. Biomed. Eng.*, **4**, 261 (2002).

[5] J. McDonald, G. Whitesides, *Accounts of Chemical Research*, **35**, 7, 491 (2002).

[6] E. Kim, Y. Xia, G.Whitesides, *Nature*, **376**, 581 (1995).

[7] G. Whitesides, A. Stroock, *Physics To-Day on line*, June 2001.

SEVEN

Some microfluidic devices

7.1 Introduction

When this book was written, many microfluidic devices were in existence. Some of them have already been mentioned briefly in preceding chapters; but it seems instructive to be more precise. The goal of this chapter is to describe in detail some typical microfluidic systems, either available on the market or published in research articles. One can hope, judging from the rate at which this field is progressing, that this chapter will rapidly become obselete.

This chapter does not try to propose a review on the subject, but presents, rather eclectically and very arbitrarily, a few examples. For a more comprehensive treatment of this field, the reader can refer to recent articles (2002) [1, 2] that cover several hundred references.

Thus, several characteristics of microcanals made using different microfabrication techniques mentioned in detail in the previous chapter will be described here. The chapter will conclude with a description of recurring problems in microfluidics: connections, valves and pumps.

7.2 Examples of microfluidic structures

7.2.1 Microcanals made from silicon or glass

'Silicon' technology allows for the microfabrication of objects to submicrometric precision. Figure 7.1 presents an example of a sequence of operations resulting in the fabrication of microcanals in glass.

We have the following sequence of operations.

a. Deposition of a chrome layer as a mask for fluoridic acid.
b. Definition of the width of the canal by lithography.

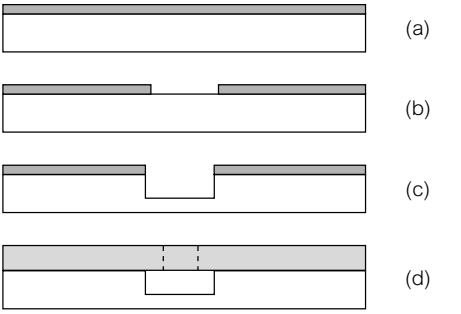

Figure 7.1 Steps of microfabrication permitting the creation of a microcanal etched in glass, and covered by a wafer of silicon.

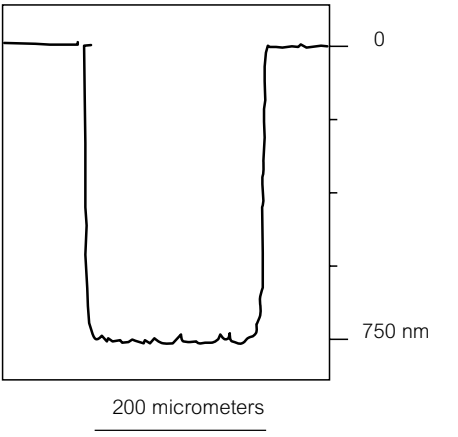

Figure 7.2 Profile of a rectangular microcanal of 0.75 μm, etched in glass after the series of operations presented above. Image courtesy of ESIEE, Marne la Vallée (France).

c. Wet etching using HF.
d. Anodic adhesion of a silicon wafer, pierced with two holes beforehand (with DRIE), permitting access to the exterior world.

We can interchange materials and obtain canals etched in silicon instead of glass. Silicon etching can be dry, wet, isotropic, or anisotropic. In all cases, the covering is achieved using anodic adhesion, which maintains excellent watertightness even under high pressures, as we have emphasized in the preceding chapter. When canals are produced in glass or silicon, canals are very well defined geometrically. Figure 7.2 shows that the canal is defined to about 20 nm in width (which represents the order of magnitude of the roughness) for a canal 0.75 μm wide, etched in glass with the series of operations presented above. Figure 7.3 shows the cross-section of a canal 20 μm wide etched in glass using isotropic etching, and confirms that this type of method results in exceptionally parallel canal surfaces.

Figure 7.4 shows a three-dimensional analysis carried out by an interferential microscope of a canal 1.14 μm wide etched in glass and covered with a silicon wafer [3].

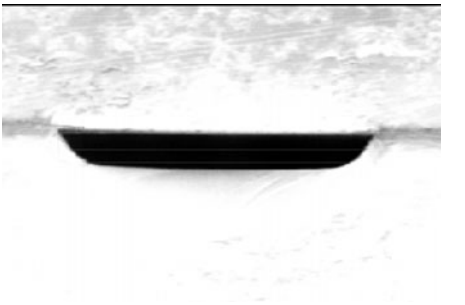

Figure 7.3 Cross-sectional view from a scanning microscope of a canal 20 μm high and 100 μm wide, etched in glass and covered with a silicon wafer (the system was microfabricated by ESIEE, and the photo taken at the Laboratory de Physique des Solides at ESPCI).

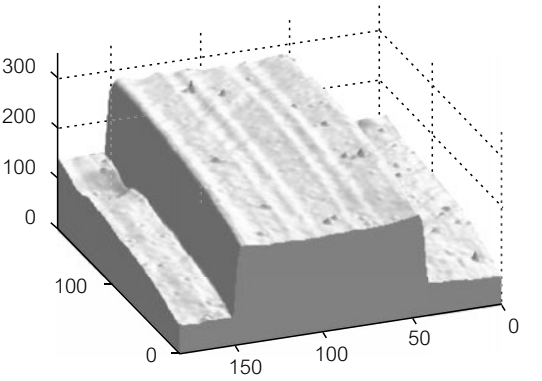

Figure 7.4 Interferometric image of a canal wet etched in glass, with dimensions 1.14 μm high and 100 μm wide. The horizontal scale is in micrometers, and the vertical scale is in nanometers. The width of the canal is obtained by adding an integer 2π times an effective distance. It can be seen in the figure that the geometric characteristics of the canal are well defined (to about 20 nm). Image courtesy of the Laboratory of Optical Physics at ESPCI.

This figure confirms the preceding characteristics of having excellent geometric definition of the canal. It is now possible, thanks to the interferential microscope, to obtain a precise estimation of the average height of the canal. The absolute precision is 20 nm. These characteristics recently allowed the measurements of the subtle effects of the slip phenomenon in gas [3]. The process presented in Fig. 7.4 shows that it is possible to create canals etched in glass and covered by a silicon wafer (or in silicon, if the materials are interchanged). There are also other solutions for the microfabrication of the canals. For example, canals of nanometric width can be made by etching a silicon layer deposited on a wafer and covering the ensemble with a plate of Pyrex. Figure 7.5 illustrates another example, though slightly atypical, used by the group of Craighead to create submicrometric electrophoretic canals.

Figure 7.5 represents the image from a scanning electron microscope of the cross-section of a canal created in silicon nitrate, using silicon as a sacrifical layer.

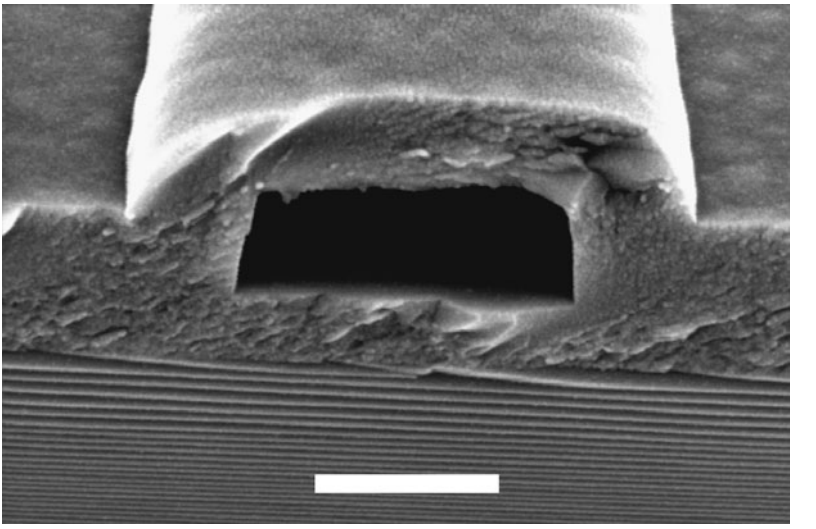

Figure 7.5 Cross-section of a canal bounded by surfaces in silicon nitride. The horizontal bar represents 500 nm [4]. Photo by Prof. H.G. Craighead, Cornell University.

This canal is about 250 nm high and 750 nm wide. This method, which leads to objects that are geometrically less well defined than that of Fig. 7.1, nevertheless presents the particularity of being able to expose the surfaces of silicon nitride to the working fluid.

7.2.2 **Microcanals made from PDMS**

Soft lithography, based on the material PDMS, is well adapted for rapid fabrication (a few hours) of microcanals. Aspect ratios are generally limited to no lower than 1/10, due to the deformability of the elastomer[1].

The technological process leading to the microfabrication of PDMS canals is reproduced in Fig. 7.6. In this particular case, there are two perpendicular canals creating an intersection, a typical geometry in miniaturized capillary electrophoresis. We first have available a mold fabricated by lithography, which has the form of a simple parallelepiped. A volume of PDMS flows in this structure, and the whole device is placed in an oven for reticulation of polymer as we have presented in Chapter 6. The process can be finished in one day.

[1] It is necessary to note that the deformation of a surface of a microcanal does not only depend on the aspect ratio, but also on the thickness of the layers in play. The recommendation to work with aspect ratios greater than 1/10 must be understood as a sort of rule of thumb.

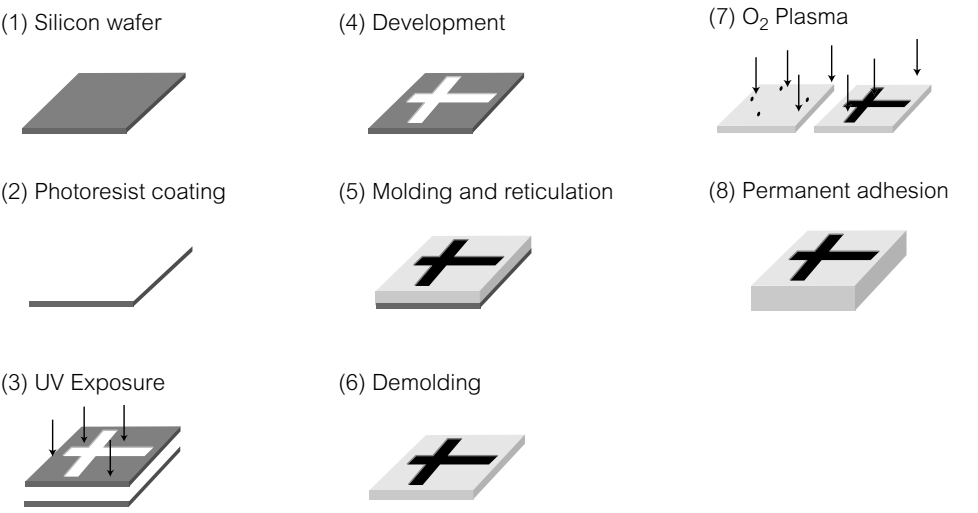

Figure 7.6 Series of steps leading to the fabrication, by molding, of microcanals in PDMS.

7.2.3 Polyimide microcanals covered with a laminated film and incorporating electrodes

Polyimide is a polymer that boasts excellent thermal and chemical stability, and it also absorbs very little water. It has been used by Goll *et al*. [5] for creating microcanals. A group from EPFL recently enhanced this approach [6] by creating covered structures in polyimide, which resolves the tricky problem of integration of electrodes for plastic MEMS (Fig. 7.7).

The polyimide PI2732 is evaporated on a substrate (which can be silicon), either on the substrate itself or on a pre-deposited metallic layer. In the first case, the integrated canals are maintained on a rigid support, while in the second, it is possible to obtain supple microcanals after dissolving the metallic layer. It is possible to deposit (by a metallic evaporation method similar to *sputtering*) electrodes and a second layer of polyimide as shown in Fig. 7.7c). After this comes the preparation of the cover of the canal and the resolution of the tricky problem of the adhesion of different parts. To obtain good adhesion, Metz *et al.* [6] used the technique of lamination (Fig. 7.7e), associated with a chemical treatment. The polyimide constituting the cover was previously mixed with an additive that slows down polyimization. Lamination is carried out between layers not yet completely polyimized, which favors good adhesion.

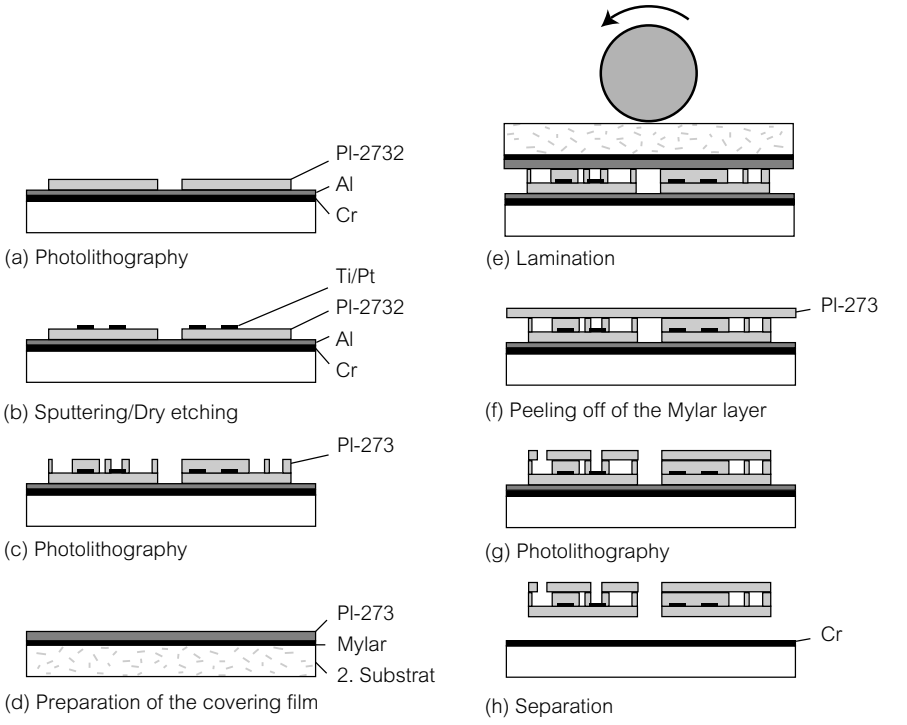

Figure 7.7 Process allowing incorporation of electrodes into microcanals, covered with a laminated film [6].

7.2.4 **Microcanals fabricated using a photocopier**

Tan *et al*. [7] showed that it is possible to fabricate microcanals with PDMS, and canal intersections as well, by using a mold created using a simple photocopier. This technique is unconventional but instructive and elegant.

A photocopier allows the deposition on paper of layers of ink whose thickness is on the order of ten or so micrometers and a minimal width of 20 to 50 micrometers. An ink deposit/transparency system can create a mold for fabricating canals and systems of canals in PDMS, following the method exposed previously. An example of a Y-shaped canal seen from below, and fabricated in PDMS from a CANON photocopier, is presented in Fig. 7.8.

The cross-section of the canal is not geometrically well defined [8], and the topography of the sides are perturbed. We again find here the obvious limits of this fabrication method, which works with very low-resolution (around 20 or so micrometers) molds. Despite these limitations, it is possible, as the photo showing an intersection of microcanals seen from below indicates, to microfabricate a microfluidic network. Tan *et al*. [7] succeeded in circulating fluids in

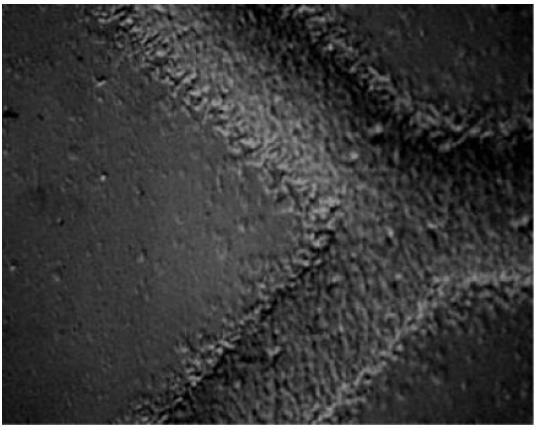

Figure 7.8 View of the bottom of a microcanal that has not yet been covered, fabricated in PDMS from a mold created with a photocopier [8].

these systems. The spectacular result of the study of these authors is to succeed in fabricating microcanals in very short times (on the order of an hour) from a method using office material (we note, however, that it is necessary to have an oven, a balance, and a plasma cleaner to obtain the final structure in PDMS).

7.3 A ubiquitous microplumbing problem: connections

Microfluidic connections have the function of communicating between the microfluidic system and the exterior world, and are a recurring problem in the field. In research laboratories, a multitude of solutions, robust and flimsy, general and specific, have been proposed. Figures 7.9 and 7.10 show two examples of microfluidic connections created in the laboratory, one in silicon and the other in PDMS.

For silicon, it is possible to put into place slack tubes made from metal or plastic, adhered by epoxy resin at the level of the entrance holes of the microcanals. These tubes can be fixed onto a rigid structure, to a standard connector. This type of setup, in the shape of an oil platform, is robust.

For PDMS, microfluidic connections can be carried out by inserting a tube into a cylinder pierced into PDMS using a calibrated tool. Taking the elasticity of PDMS into account, water tightness is assured. However, this type of connection proves to be rather fragile. It is often interesting to flow PDMS around an entrance hole to stabilize the connection.

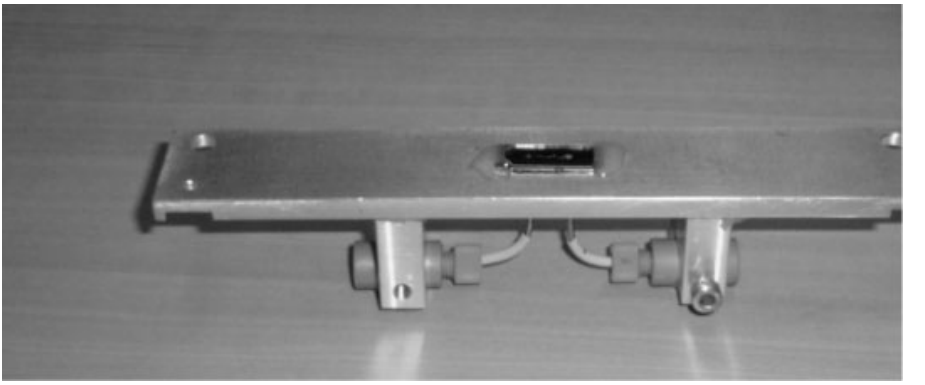

Figure 7.9 Microfluidic connection for silicon, watersealed by epoxy glue [9].

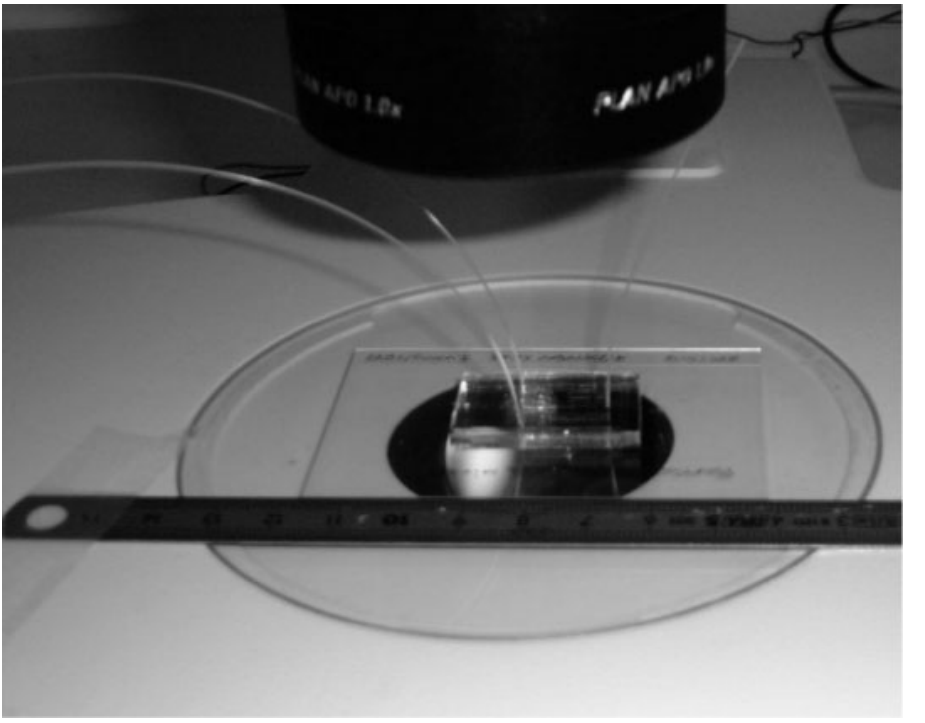

Figure 7.10 Elegant connections using the elasticity of PDMS [9].

From an industrial perspective, the problem of microfluidic connections is open, and there is currently no definitive and universal solution. It is interesting to note that, in this context, the connection between the microsystem and the exterior world can take complex forms, particularly when high throughput is sought. One example is presented in Fig. 7.11.

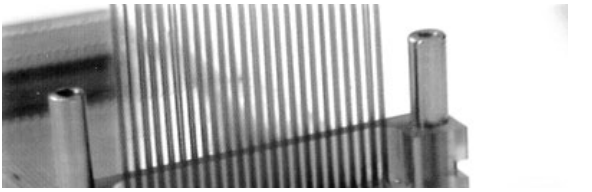

Figure 7.11 An example of a microfluidic connection developed by LETI-CEA and the company Radiall.

In Fig. 7.11, a microfluidic system is connected to an on-chip analysis device. We look here to 'standardize' the connection. In this case, the fluidic connector evokes SCSI plugs for computers. Only the future will tell if the comparison will lead to the success of the connector.

Another type of standardized connection that we can mention here, even for millimetric scales, is that of thermal microexchangers mentioned in the introduction of this book. Here, we use a classical technique based on toric joints.

These two examples shown the eclecticism of methods currently used to assure communication between the fluid and the exterior world. It is likely that this type of subject will evolve significantly in the future.

7.4 Examples of microfabricated valves and pumps

7.4.1 Different approaches to the problem of microfluidic actuating

■ **Valve**

The problem of controlling the movement of fluids has not yet received a definitive solution. One first control element is the valve. Here, a multitude of solutions have been proposed, and the reader will be able to refer to two reference articles [1, 2] for detailed information on this subject. Out of the proposed solutions, we cite:

– mechanical systems, sometimes tricky to microfabricate: some examples are parylene membranes closing an orifice, and systems of flaps connected to springs;
– systems based on hydrogels, whose mechanical properties vary with the pH;
– electrokinetic systems, where, by actuating the flows, fluxes can be forced to pass or not to pass through a microcanal;

– bubble-based systems, generated electrolytically;
– systems based on non-Newtonian behaviors;
– systems based on hydrophilic/hydrophobic behaviors, on rapidly rotating disks, which were presented in Chapter 2;
– fluid valves, designed to function at high Reynolds numbers.

Pumping

Pumping is also an important problem to consider in microfluidics; there are several mechanical and non-mechanical solutions.

– Of the non-mechanical systems, we can mention electrokinetic pumping, described in Chapter 4. This mode of pumping is currently used in separation microsystems, and generally constitutes a valuable option in microfluidic systems.
– Mechanical solutions use an assembly of valves or membranes associated with valves to induce a peristaltic effect.

In this section, we describe two devices, one made using silicon technology, the other made using replication technology based on PDMS molds, constituting remarkable structures of valves and pumps. In a more eclectic way, a system of valves and pumps, made using the control of microparticles, is also presented.

7.4.2 Debiotech's silicon pumps

The company Debiotech, in collaboration with EPFL (École Polytechnique Fédérale de Lausanne), created a micropump using silicon technology (Fig. 7.12). This pump can be held with the tip of a finger, as shown in Fig. 10 (p. 10). The pump was presented in several conferences[2]. A rather detailed report on this device is found in the proceedings of the 2001 MEMS conference [11].

The pump is made of one membrane and two valves. It is a three-layer structure, and each layer is supported by a plate of silicon or glass, and the closing of the system is achieved via anodic bonding. The microfabrication techniques involved include SOI, DRIE, and the sacrificial layer, all described in the preceding chapter. The dead volume is 158 nl; this pump functions at flow rates reaching 2 ml per hour under pressures of -100 to $+100$ mbar. One significant difficulty intervening in the creation of this pump is the stiction phenomenon (the valves have a tendancy to stay stuck to their bases). This difficulty was

[2] It is interesting to note that the micropump was also used in flights in space [10].

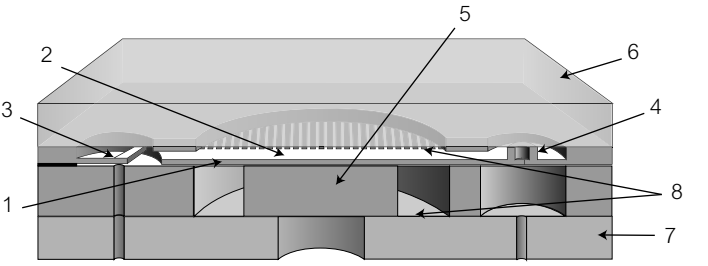

Figure 7.12 Cross-section of the Debiotech micropump (the diagram is not to scale); 1: membrane; 2: actuator; 3 and 4: valve; 5: support; 6: glass support; 7: glass base; 8: electrodes.

resolved by minimizing the solid-solid area of contact [11]. This necessitated a meticulous microfabrication process for the system. One could deduce that this pump is expensive. On this subject, the authors argue that it is feasible to create a hundred micropumps on just one 4-inch wafer, which would evidently diminish the cost. At this point in time, the use envisioned for this pump is to deliver medication. Specifically, this pump is destined to be taped to the skin, and allow the distribution of insulin to diabetics.

7.4.3 **PDMS valves and pumps**

The group of S. Quake have developed during these last few years elegant techniques for fabricating pumps and valves in PDMS [12]. The method uses MSL (or *multilayer soft lithography*), presented in Fig. 7.13. The technique is described in detail in [12], and this section will only present a simplified description. The reader interested in the fabrication of valves by multilayer lithography will find it useful to study this reference, which contains several crucial details for the success of the fabrication.

Two rectangular-shaped molds are used to form two canals placed perpendicularly with respect to one another. PDMS is poured on the molds, resulting in two independent canals. One, designated the working canal, is where the working fluid circulates and is also the canal that experiences a deformation. The other canal is the command canal. In the system of [12], the working canal has a height on the order of 40 micrometers. This canal has a very thin surface (on the order of 10 micrometers), which deforms under the effect of pressure variations. The command canal is molded in a thick layer of PDMS (around 300 μm just to illustrate) and possesses non-deformable surfaces. To create the valve, the working part and the command part are integrated; adhesion is obtained by oxygen treatment of the contact surfaces, followed by rebaking and the diffusion of reticulant [12]. We thus obtain, in cross-section, a system of two layers Fig. 7.14.

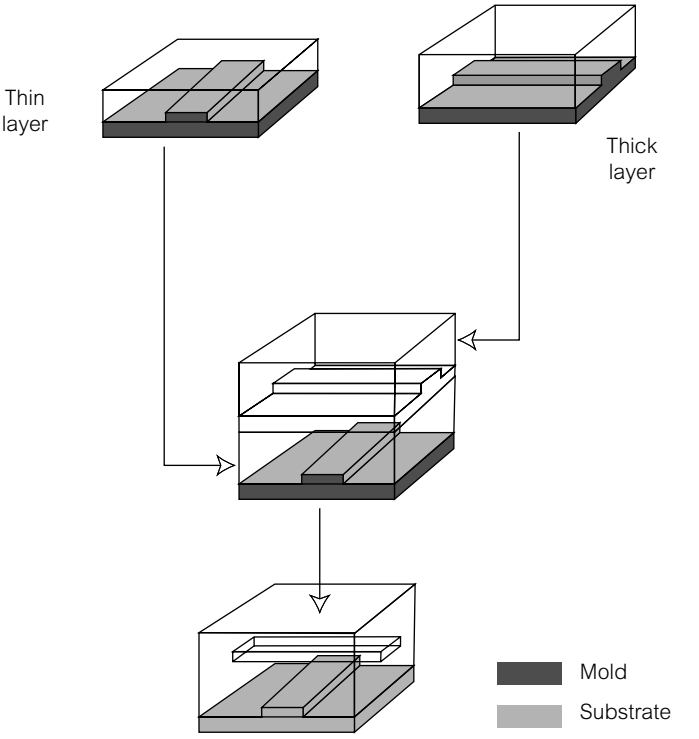

Figure 7.13 Fabrication of a valve according to the technique developed by the group of S. Quake [12].

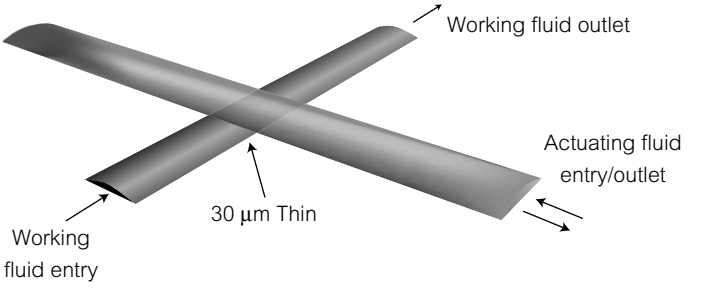

Figure 7.14 Diagram of the principle showing two superposed canals: the command canal (upper canal) and the working canal (lower canal). When pressure is applied in the command canal, the thin surface separating the two canals is deformed, and the working canal is closed.

The upper canal (command) is filled with gas and submitted to a controlled pressure. The lower canal (working) is filled with the working fluid. In the absence of imposed pressure in the upper canal, the working fluid can circulate freely. To obstruct the fluid circuit, pressure is applied on the command canal. The membrane separating the two fluid circuits is deformed and, due to its elasticity, contacts the bottom of the lower canal, thus obstructing flow. An acceptable

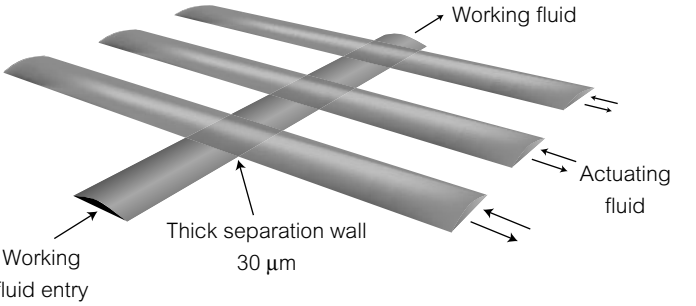

Figure 7.15 Peristaltic pump, created from three valves placed in series and activated sequentially.

level of watertightness is assured by working with canals possessing a rounded rectangular cross-section [12]. When the pressure is turned off, the membrane returns to its initial state. Typical pressures imposed are on the order of a fraction of a bar. The time constants for the opening and closing of the valve are about a few milliseconds long, and the functioning of the valves is stable over several million operations.

A peristaltic pump can be fabricated using three valves put in series along one such canal, and actuated sequentially (Fig. 7.15). The same principle is applied to a circular pump, that we mentioned in Chapter 4. These systems are particularly useful to introduce in the conception of architectures of laboratories on-chip[3]. A model has recently been proposed for these pumps [15].

7.4.4 **Valves and pumps using microparticles**

We conclude this chapter with an astonshing recent creation: Terray *et al.* [13] fabricated valves and pumps using functionalized silicon particles 1.5 μm in diameter. The different phases of functioning of a valve made using these particles are represented in Fig. 7.16. The particles forming the active element of the valve are trapped in a laser beam, then'glued' using a photosensitive agent fixed on the surface. The reported flow rates are on the order of 2 nl/h. The values are implemented in PDMS canals that are 3 μm high and 11 μm wide. These actuators are spectacular and conceptually interesting. We mention that similar actuators, using magnetic particles, have been recently developed [14].

[3] We note that it is necessary to have a pressure reservoir, electrovalves, and a command for the functioning of the peristaltic pump. At this time, all these elements are situated outside the chip, and occupy a substantial amount of space. This aspect may constitute a difficulty if the end goal is total integration of the system.

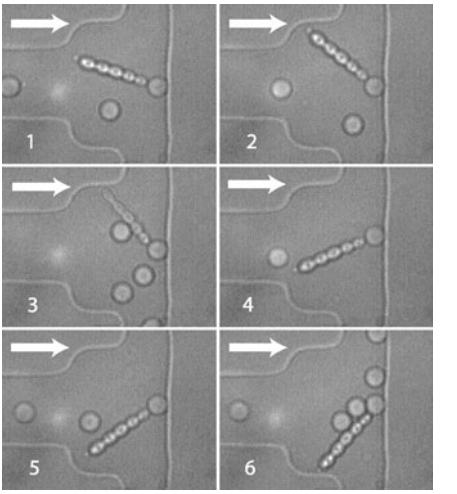

Figure 7.16 Valve fabricated by Terray *et al*. using dielectric particles manipulated in a laser beam (photo published with the permission of Terray *et al*. [13]).

References

[1] D. Reyes, D. Iossifidis, P.-A. Auroux, A. Manz, *Anal. Chem.*, **74**, 2623 (2002).

[2] P.A. Auroux, D. Iossifids, D. Reyes, A. Manz, *Anal. Chem.*, **74**, 2637 (2002).

[3] J. Maurer, P. Joseph, H. Willaime, P. Tabeling, *Phys. Fluids*, **15**, 9 (2003).

[4] H.G. Craighead, *Proc MicroTAS 2001*, (ed.) J. Ramsay and A. Van den Berg, Kluwer Academic Publishers, 40 (2001)

[5] C. Goll, W. Bacher, B. Bustgens, D. Maas, W. Menz, and W.K. Schomburg, *J. Micromech. Microeng.*, **6**, 77 (1996).

[6] S. Metz, R. Holzer, P. Renaud, 'Polyimide-based microfluidic devices', *Lab on a Chip*, **1**, 29 (2001).

[7] A. Tan, K. Rodgers, J.P. Purrihy, C. O'Mathuna, J.D. Glennon, *Lab on a Chip*, **1**, 7 (2001).

[8] Picture taken at MMN (ESPCI, France) by T. Juès, R. Prunières, E. Brunet, P. Tabeling (not published) (2002).

[9] These photos were taken by the laboratory Microfluidics, MEMS, Nanostructures (ESPCI) (www.mmn.espci.fr).

[10] This is the result of work carried out at IMT (Neuchatel, Switzerland); information given by A. Dodge (private communication).

[11] D. Maillefer, S. Gamper, B. Frehner, P. Balmer, H. van Lintel, P. Renaud, *Proc. MEMS 2001*, Interlaken, 414–417 (2001).

[12] M. Unger, H. Chou, T. Thorsen, A. Scherer, S. Quake, *Science*, **288**, 113 (2000).

[13] A. Terray, J. Oakey, D. Marr, *Science*, **296**,1843 (2002).

[14] S. Biswal, A. Gast, *Proc.* μ*TAS*, Nara, Japan, 760 (2002).

[15] J. Goulpeau, D. Trouchet, A. Ajdazi, P. Tabeling, *Jour. Appl. Physics*, **97**, 1 (2005).

Conclusion

Microfluidics is still rapidly evolving, and the obvious risk in writing a book devoted to this subject is to appear out of date. This field did not, however, appear out of nowhere: a good part of it depends on established concepts in physics and chemistry. One of the objectives of this work was to go over these concepts and to present them from a particular perspective. In this respect one may think that there is an enduring element in this text.

As in all applied sciences, microfluidics will grow in tempo with the successes of its applications. The economic future of this domain of activity is very promising, and both the economic and industrial stakes are substantial, but, as for all human endeavors, its advancement is fraught with hazards. Today, on the short term, the situation seems favorable: a considerable number of both small and large companies have launched research projects in microfluidics and it is likely that in the next several years new industrial products that exploit the potential of microfluidics will appear. In the long term, lab-on-a-chip-type systems will still be perceived as harbingers of significant socio-economic impact, and will probably remain on the horizon of this field for many years to come. In this context, it is useful to highlight the fact that a roadmap, analogous to that pertaining to microprocessors, is currently being developed for microfluidics as well. These questions obviously still remain open, and, taking into account the degree of industrial and economic investment, it is not surprising that there exist international conferences dedicated almost entirely to this subject.

On the scientific plane, the dynamism of the current research gives much hope for the attainment of remarkable progress. Each year, research teams go beyond limits deemed difficult to overcome, producing astonishing systems and implementing new approaches with obvious potential. The field is pluridisciplinary and the subjects evolve quickly: in this type of dynamic, the field of microfluidics has little chance of remaining focused on static questions. In the future, nanofluidics will certainly become an important subject. The premise of this field was seen in the 2003 μTAS 2003 conference, where two sessions were dedicated to nanofluidics. The work presented involved, for example, multiphasic fluids circulating in decananometric canals, or the manipulation of attomoles in nanocavities. Nevertheless, the micrometric world still holds much to be explored, notably when it is paired with complex situations, and research will probably concentrate itself on this aspect over the next several years.

If one examines the progression of microfluidics over the period of several years, one has the feeling that the foundation for an important building is being constructed. This building is still far from being completed, and does not have the refined appearance of mansions of the past, nor does it have the imposing beauty of cathedrals ; and yet, it already possesses the charm of houses found on the borders between two countries which are somehow able to harmoniously combine many different architectural styles.

This page intentionally left blank

Index